

Metamorphosed carbonates and fluid behaviour
in the Dalradian of S.W. Argyll, Scotland.

Kenneth Muir Greig



Thesis submitted for the degree of
Doctor of Philosophy
Edinburgh University

1984

'Call me Ishmael.'

Moby Dick, Herman Melville.

Abstract

The Dalradian rocks of Knapdale, SW Argyll, Scotland, consist of a thick sequence of quartzites, semi-pelitic schists, phyllites and metabasite lavas and sills, which represent the exposed root zone and lower limb of the Tay Nappe. Included in this sequence are rare, thin limestone horizons, containing a wide variety of calc-silicate mineral assemblages, which by dint of their well constrained P-T- X_{CO_2} conditions of formation, allow much of the metamorphic fluid history of Knapdale to be determined.

These metacarbonate assemblages can be divided into Primary low grade, Primary high grade and Secondary in nature, primary low grade being typically: calcite + quartz + muscovite + rutile (+)albite \pm biotite \pm chlorite \pm dolomite, primary high grade consisting of some combination of: calcite, quartz, grossular, clinozoisite, diopside, amphibole, Kfeldspar, biotite, muscovite, sphene and albite, and secondary being typically: dolomite + quartz + Kfeldspar + muscovite + albite \pm rutile \pm chlorite.

Primary high grade assemblages formed at roughly 8kb, 450-550°C, during infiltration of an $\text{H}_2\text{O}-\text{CO}_2$ fluid of composition $X_{\text{CO}_2} \ll 0.1$, with a fluid:rock ratio of the order of 9.0 (relative to 1000cm³ rock); this large volume of fluid probably formed by regional dehydration of metabasite sills at the garnet isograd. The small (cm) scale distribution of different assemblages seen may be the result of either heterogeneities in fluid flow, or local bulk compositional constraints, but both point to pervasive infiltration of fluid, probably through microcracks, driven by a fluid pressure gradient. Non-equilibrium thermodynamic modelling of this transfer process suggests that fluid velocity was high (0.009 - 0.09 m.sec⁻¹)

Secondary assemblages are found in discrete zones within primary assemblages, and probably formed at <6kb, <450°C, in equilibrium with a more CO_2 -rich fluid ($X_{\text{CO}_2} > 0.15$).

The clear distinction between stable isotope

compositions of primary: $\delta^{18}\text{O} = +9$ to $+19$ per mil(SMOW), $\delta^{13}\text{C} = -4$ to $+8$ per mil(PDB), and secondary metacarbonates: $\delta^{18}\text{O} = +24$ to $+30$ per mil(SMOW), $\delta^{13}\text{C} = -1$ to $+5$ per mil(PDB), is good evidence for a secondary fluid infiltration event. Lack of an obvious source for this secondary fluid within Knapdale, and its apparent channelling and lack of equilibration with much of the sediment pile through which it passed, suggests that it was derived from outside the system.

Index

Chapter 1: Introduction	1
1.1 Fluids in metamorphism	1
1.2 The Knapdale metamorphic system; scope of this project	7
Chapter 2: The geological framework of Knapdale	11
2.1 Introduction	11
2.2 Rock types and stratigraphy	14
2.2.1 Meta-sedimentary	14
2.2.2 Meta-igneous	22
2.3 Structure and deformation	24
2.3.1 Large scale structures	24
2.3.2 Small scale deformation	27
2.4 Metamorphism	29
2.4.1 Introduction	29
2.4.2 Non-calcareous metasediments	30
2.4.3 Metabasites	38
2.4.4 Metacarbonates	43
2.4.4.1 Lower grade localities	43
2.4.4.2 Higher grade localities	45
2.4.4.3 Conclusions	52
Chapter 3: Equilibrium thermodynamics	53
3.1 Introduction	53
3.2 Equilibrium	53
3.3 Components and the Phase Rule	55

3.4 Thermodynamic formulation and data	62
3.5 Geobarometry and geothermometry	70
3.6 Conclusions	78
Chapter 4: Evolution of the South Bay metacarbonates	81
4.1 Introduction	81
4.2 Mineral assemblages and mineral reactions	81
4.2.1 Shapes of T-X-(CO ₂) paths	81
4.2.2 Textural evidence for fluid compositions	84
4.2.3 Sequence of reactions, possible assemblages	101
4.3 Bulk compositional control	106
4.3.1 Theoretical assemblages	106
4.3.2 Real assemblages	110
4.3.3 Paths to grossular formation	112
4.4 Fluid:rock ratio	112
4.4.1 Calculation of fluid:rock ratio	112
4.4.2 Fluid:rock ratios from South Bay metacarbonates	114
4.5 Conclusions	117
Chapter 5: Stable Isotopes	119
5.1 Introduction	119
5.2 Isotopic notation	120
5.3 Analytical methods	120
5.4 Isotope fractionation effects	121
5.5 Results and interpretation	124
5.5.1 Isotopic variations: a three fluid model	124
5.5.2 The primary fluids	128
5.5.3 The secondary fluid	134
Chapter 6: Fluid transfer processes in metamorphism	137
6.1 Introduction	137
6.2 The framework of rock mechanics	138
6.3 Metamorphic processes involving fluid transfer	140

6.3.1 Diffusion metasomatism	140
6.3.2 Infiltration metasomatism	141
6.4 Fluid pathways	142
6.5 Porosity and permeability	144
6.6 Permeability and time	145
6.7 Rates of transport processes	149
6.8 Conclusions	152
Chapter 7: Non-equilibrium thermodynamics	154
7.1 Introduction	154
7.2 The framework of non-equilibrium thermodynamics	154
7.3 Fluid transfer processes in metamorphism	157
7.3.1 Simplifications	157
7.3.2 Estimation of parameters	159
7.3.3 General conclusions	160
7.4 Fluid transfer through microcracks	162
7.4.1 Theory - derivation of equations	162
7.4.2 Application - the South Bay infiltration	164
7.5 Conclusions	166
Chapter 8: Conclusions - The fluid history of Knapdale	167
Acknowledgements	171
References	172
Appendix A: List of symbols	188
Appendix B: Graham I(et al.) (1983)	190
Appendix C: Probe data compilation	(enclosure)

C H A P T E R 1: Introduction

1.1: Fluids in metamorphism

Metamorphism can be defined as the processes by which changes are brought about in natural physico-chemical systems within the Earth's Crust, by the agencies of pressure, temperature and chemically active fluids. These natural systems are rocks, which are complex, multicomponent porous media, made up of mineral phases.

The high pressures and temperatures in metamorphic systems generally imply that volatile phases present are supercritical, that is, they lie above subcritical regions where the division between liquid and vapour phases is rigidly defined. Because the densities of metamorphic volatiles more closely resemble liquids, and because volatiles show evidence of having flowed through rocks during metamorphism, the term metamorphic *fluid* is preferred (Holloway, 1977).

Ferry & Burt (1982) have defined five lines of evidence for the existence of a fluid phase in rocks during metamorphism. These are as follows:

- a) the common occurrence of fluid inclusions in metamorphic minerals, which are believed to represent trapped metamorphic fluids.
- b) the fact that whole-rock chemical analyses of high grade metamorphic rocks are depleted in volatile components relative to their low grade equivalents.
- c) the fact that prograde mineral reactions commonly involve devolatilization, and that the volatiles lost from the rock are believed to form a fluid phase.
- d) the presence of hydrates, carbonates, sulphides etc. in metamorphic rocks, implying that the partial pressures of

volatiles are non-zero, and in addition, the fact that their sum often closely approaches the lithostatic pressure.

e) the fact that metamorphism in the presence of fluids is taking place in modern geothermal fields, and that directly sampled fluids appear to be in equilibrium with the metamorphic minerals which are forming.

Accepting that, at least in some cases, fluids do exist during metamorphism, the problem becomes one of incorporating the behaviour of these fluids into the relevant models of metamorphic processes. To do this, it may be useful to divide the investigation of fluids in metamorphism into three broad categories, into which specific questions fall, namely:

- (i) generation of fluids: sources?, amounts?, transport processes?
- (ii) compositions of fluids: methods of determination?
- (iii) effects of fluids on rocks: processes involved?

What follows is an attempt to summarise the present level of understanding in each of these categories, primarily with examples of work which deals with systems relevant to this thesis, namely, low to medium grade metamorphism in a regional setting, and H_2O-CO_2 dominated fluids.

1. Sources and amounts of fluid, fluid transfer

Fluids present during metamorphism may be derived from:

- a) meteoric or sea water originally present in pore spaces in the unmetamorphosed sediment,
 - b) the progress of devolatilization reactions within the metamorphic system,
 - c) an external fluid reservoir ,
- or some combination of all three (Rice & Ferry, 1982).

The first, however, can probably be neglected for most low-medium grade metamorphic systems, as by that stage in the evolution of a sediment pile, most, if not all, of the pore fluid will already have been lost, and the porosity will

be of the order of 0.1% (see Section 6.5).

In the second case, the amount of CO_2 and H_2O produced by devolatilization reactions in the metamorphism of an average pelite is equal to roughly 12 vol% of the rock at 5kb and 500°C (Walther & Orville, 1982). Because the porosity of the rock under these conditions is very low, it can be inferred that such fluid must leave the system. The amount calculated here is an average, however, taken over a whole metamorphic episode, so little can be inferred about the rate of volatile escape, or its possible heterogeneity.

Thirdly, external fluid reservoirs may consist of meteoric or magmatic waters, or indeed metamorphic fluids from other systems. One possible mechanism for the production of retrograde H_2O is its release from quartz as a metamorphic terrain cools (Spear & Selverstone, 1983). The decrease in solubility of H_2O in quartz from $700\text{--}400^\circ\text{C}$, with a drop in pressure of around 3kb, would release a minimum of $3 \times 10^{-2}\text{g}$ of H_2O per kg of rock, which is equivalent to roughly 0.1cm^3 per 1000cm^3 rock at 2kb, 400°C (volume data from Burnham *et al.*, 1969). Ponding or focussing of this fluid could result in significant retrograde fluid:rock ratios.

Stable isotope studies of metamorphic terrains have the potential to distinguish possible fluid sources (e.g. Kreulen, 1980; Graham *et al.*, 1983, and Chapter 5, this thesis). However, the wide range of fractionation effects, due to devolatilization reactions, complicates this (e.g. Rye *et al.*, 1976; Jansen *et al.*, 1978). Kreulen(1980) reports $\delta^{13}\text{C}$ values of -7 to 5 per mil (PDB) for metamorphosed siliceous dolomite layers on Naxos, Greece, while co-genetic quartz segregations have values of -13 to -1 per mil (PDB). This emphasises the need for consideration of the several fluid environments which may exist in one terrain.

The mechanisms of fluid transfer are poorly understood. The problem involves identification of a) fluid pathways and b) driving forces, the nature of which must depend on such factors as composition and amount of fluid, magnitude of fluid pressure, temperature and chemical potential gradients, and structural constraints imposed by the various

mechanical responses of different rock types. A spectrum of fluid pathways, from grain boundaries to open fractures, and on a range of scales, can be envisaged. The recognition of which particular pathway dominated in a metamorphic episode will be the result of a combination of mineralogical, structural, isotope and fluid inclusion data, and few such studies have been undertaken (see Table 1.1). A complete description of the possible mechanisms of fluid transfer is presented in Chapter 6, along with conclusions on the sort of process which operated during prograde infiltration of fluid into the high grade metacarbonates of Knapdale.

A more difficult problem in the study of fluid transfer is the determination of the rates of such processes. The assumption of a local equilibrium between the amount of fluid introduced into a rock, and its incorporation into solid phases allows comparison of the rates of different processes (Fisher, 1977,1978; Fisher & Lasaga, 1981), but truly non-equilibrium models of metamorphic processes have yet to be developed. The value of such models cannot be overestimated, and they represent a logical next step in the understanding of fluid processes. Application of non-equilibrium thermodynamics to the high grade metacarbonates of Knapdale forms the subject of Chapter 7 in this thesis.

2. Compositions of fluids

Ferry & Burt(1982) have also defined three general ways in which the composition of a metamorphic fluid may be determined. These are:

- a) Direct sampling of waters from modern active geothermal fields (e.g. Salton Sea, Bird & Norton, 1981; Iceland, Sveinbjornsdottir, 1983).
- b) Analysis of fluid inclusions. This may be achieved by extraction and direct analysis of the liquids (e.g. Roedder, 1972; Kreulen & Schui ling, 1982), or by laser Raman spectroscopy (e.g. Rosasco & Roedder, 1979), but is usually

Author	Area	Terrain	Rock type	P,T	X _{eq}	X _{eqn}	Fluid:rock ratio	Stable isotopes	Fluid inclusions
Melson(1966)	Montana, USA	contact	sil. dolomite	-	>0.5	>0.75			
Greenwood(1967)	B.C., Canada	contact	lst, pelites	1-2kb, 450°C	0.1	1.0			
Guidotti(1970)	Maine, USA	regional	pelites	3-5kb, 575-630°C	0.0	0.0			
Chatterjee(1971)	W. Italian Alps	regional	pelites, volcanics	7kb, 350-520°C	0.0-0.77	0.57			
Crawford(1972)	California, USA	contact	pelites, calc-schists	2-3kb, 340-600°C	<0.06	>0.5			
Ernst(1972)	California, USA	regional	basics	7kb, 300-500°C	<0.1	1.0			
Ghent & DeVries(1972)	B.C., Canada	regional	basics	4kb, 500-600°C	<0.1	0.0, 1.0			
Jones(1972)	B.C., Canada	regional	pelites	4kb, <630°C	<0.19	>0.9			
Trommsdorff(1972)	C. Swiss Alps	regional	sil. dolomite	>5kb, -	<0.5	>0.5			
Cernignani & Anderson(1973)	Ontario, Canada	contact	sil. dolomite	1kb, <500°C	<0.757	>0.75			
Bewitt(1973)	Connecticut, USA	regional	mica lst.	6kb, 510-590°C	<0.1	0.75			
Kerrick et al.(1973)	California, USA	contact	calc-schists	2kb, 400-600°C	<0.1	>0.75			
Evans & Trommsdorff(1974)	C. Swiss Alps	regional	peridotite	7kb, 600°C	0.1-0.5	0.5-0.83			matrix magnesite, XCO2=0.8
Roy(1976)	B.C., Canada	regional	calc-schists	5kb, >600°C	0.25-0.6	0.0-1.0			
Moore & Kerrick(1976)	Utah, USA	contact	sil. dolomite	1-2kb, 400-600°C	<0.2	0.75			
Rye et al.(1976), Jensen et al.(1978)	Naxos, Greece	regional	sil. dolomite	6kb, 350-700°C	<0.1	0.5-0.75			$\delta^{18}O$ rock: 7.3to23.6 per mil, qz segregations, XCO2=0.01-0.66 $\delta^{18}O$ qz seg.: 7.7to23.4 per mil, $\delta^{13}C$ qz seg.: -8to+3.6 per mil
Rice(1977a, b)	Montana, USA	contact	sil. dolomite	1kb, 435-600°C	0.75	0.75			
Suzuki(1977)	Kasuga-Mura, Japan	contact	sil. dolomite	2.5-3.5kb, 465-545°C	0.15-0.95	>0.5			
Rumble(1978)	New Hampshire, USA	regional	psammites, pelites	5-6kb, 485-505°C	0.0	0.0			matrix quartz, H2O-NaCl-CaCl2
Crawford et al.(1979)	B.C., Canada	regional	calc-schists	9kb, <685°C	<0.05	>0.66			
Ghent et al.(1979)	B.C., Canada	regional	calc-schists	6-8.5kb, 570-640°C	<0.23	>0.75			
Ferry(1980, 1983)	Maine, USA	regional	sil. carbonates	3.5kb, 375-575°C	<0.31	>0.75			0.01-3.08 (minerals)
Hoschek(1980, 1981, 1984)	E. Austrian Alps	regional	sil. carbonates	4-6kb, <550°C	<0.25	>0.5			$\delta^{13}C$ matrix: -7to+5 per mil, qz segs, a: XCO2=0.6-0.9 $\delta^{13}C$ qz seg.: -13to-1 per mil, b: H2O c: H2O-NaCl
Kreulen(1980)	Naxos, Greece	regional	sil. dolomite	6kb, 350-700°C	-	-			
Valley & Essene(1980)	Adirondacks, USA	regional	sil. carbonates	6.5-8kb, 650-750°C	<0.1	0.75			
Bucher-Murminen(1981)	S. Italian Alps	contact	sil. dolomite	3.5kb, 700°C	<0.1	1.0			
Erdmer(1981)	Quebec, Canada	contact	pelites, calc-schists	2-3kb, 400-600°C	<0.15	>0.75			
Ferry(1981)	Maine, USA	regional	graphitic schists	3.5kb, 375-575°C	CO2+CH4+H2O H2S+CO2	2.2-5.0 (minerals)			
Grambling(1981)	New Mexico, USA	regional	pelites, psammites	4kb, <540°C	<0.6	0.0			
Sisson et al.(1981)	Ontario, Canada	regional	calc-schists	6.5kb, 600°C	<0.1	>0.66			matrix quartz, H2O+12-20wt%NaCl qz segs, a: H2O+23-24wt%NaCl b: H2O c: CO2 (near pure)
Sivprakash(1981)	C. Highlands, UK	regional	basics	8kb, 500-600°C	<0.1	>0.5			
Williams-Jones(1981)	Quebec, Canada	contact	sil. carbonates	0.5kb, 600-750°C	0.25-0.3	0.75			
Bowman & Essene(1982)	Montana, USA	contact	sil. dolomite	1kb, 400-600°C	0.1-0.6	>0.75			
Rumble et al.(1982)	New Hampshire, USA	regional	calc-schists	3.5kb, 600°C	<0.14	>0.83			1.5-4.0 (minerals), $\delta^{18}O$ +12 per mil 4.0-6.0 (isotopes) up to 9.0 (minerals), $\delta^{18}O$ basics: +8to+12 per mil, matrix qz, H2O(+3-5wt%NaCl?) $\delta^{13}C$ basics: -16to-4 $\delta^{18}O$ carbs1: +9to+19 $\delta^{13}C$ carbs1: -4to+8 $\delta^{18}O$ carbs2: +24to+30 $\delta^{13}C$ carbs2: -1to+5 qz segregations, a: H2O-NaCl b: CR4 c: CO2
Graham et al.(1983), Greig(1984, this thesis)	SW. Highlands, UK	regional	basics, sil. carbonates	1-8kb, 450-550°C 11: 76kb, <450°C	<0.1 >0.15	>0.5 >0.5			
Mesbitt & Essene(1983)	Virginia, USA	regional	pelites, calc-schists	5-7kb, 400-500°C	<0.2	0.0-1.0			
Yardley(1983)	Connemara, Eire	regional	pelites	4-5kb, 640°C					

Table 1.1: Synthesis of published work on fluids in metamorphism, in which fluid composition has been determined. X_{eq} = equilibrium fluid composition, X_{eqn} composition of fluid produced by devolatilization reactions. $\delta^{18}O$ and $\delta^{13}C$ given relative to SMOW and PDB respectively.

inferred by heating/freezing microthermometry. An example of this technique relevant to the problems of fluid behaviour is the work of Sisson et al. (1981). In this study, fluid inclusion compositions from quartz in large segregations, and in metacarbonate 'matrix', in an amphibolite grade regional terrain showed marked differences. The matrix inclusions, though small and not present in large numbers, were pure H_2O with 12-20 wt.% NaCl, whereas segregation inclusions split into two distinct populations, one pure H_2O with 23-24 wt.% NaCl, the other near pure CO_2 . The matrix inclusions are interpreted as representing fluid in equilibrium with the metamorphic minerals, and the segregation inclusions as representing the immiscible parts of a single fluid produced by prograde devolatilization reactions. Kreulen (1980) describes four populations of inclusions in quartz segregations from Naxos. Of these, near pure CO_2 and H_2O -NaCl compositions dominate. Lack of NaCl content for the brine inclusions precludes the interpretation of these results as further evidence for fluid immiscibility.

c) Calculation from the positions of relevant mineral-fluid equilibria in P - T - X_{fluid} space stems from equilibrium thermodynamic treatments of mineral-fluid systems, which use thermodynamic data such as entropies, enthalpies and molar volumes of mineral phases (culled from experimental work), and activities and fugacities of volatile phases (based on P - V - T data and/or equations of state), to quantify the P , T and X_{fluid} positions of mineral reactions, whose relative positions can be established graphically by Schreinemaker's method. The inaccuracies and necessary assumptions in these calculations are many and complex (see Section 3.4). However, many metamorphic systems have been analysed in this way (see Table 1.1), and estimates of P and/or T used to delimit fields of stability of mineral assemblages, which thereby delimit fluid compositions. The majority of rock systems studied have been siliceous carbonates, which is a reflection of the common fluid influence in such systems, and of the potential for recognising and quantifying that

influence which is the result of the diversity and range of P-T- X_{CO_2} stabilities of calc-silicate minerals.

Table 1.1 shows the rarity of studies in which the fluid composition determined by mineral assemblage information is backed up by determination of fluid composition by another method, such as fluid inclusion work, or indeed stable isotope determination. In metacarbonate rocks, small or no deviations of $\delta^{13}C$ from normal marine limestone values, accompanied by a large deviation in $\delta^{18}O$, could imply equilibration of the rocks with an O-rich, C-poor fluid, e.g. H_2O (see Chapter 5).

3. Effects of fluids on rocks

The effects that presence of fluid in a metamorphic system could have on the minerals in that system will depend on the composition and amount of fluid, and the nature of the fluid pathway. Rock volumes subjected to infiltration of large volumes of fluid will evolve along different T- X_{CO_2} paths to those subject only to small amounts of fluid, present as a grain boundary phase. In addition, infiltration of large volumes of fluid will have different effects in cases where fluid is channelled along large, discrete fractures, and where fluid moves pervasively through the rock (see Section 4.2, and Figure 4.1). In the case of large infiltrative volumes, the fluid may dominate the rock chemistry, imposing on it the X_{CO_2} value of the external fluid reservoir. In the case of small volumes, the rock chemistry may dominate, and mineral reactions in the rock control and alter the composition of the fluid. These examples, which are known as 'infiltration' and 'buffering', respectively, represent the end-member cases of a spectrum of processes which occur in real systems. It is possible to quantitatively assess the effects of buffering (Greenwood, 1975), and many studies of real systems have shown it to be an important process, especially in contact metamorphism (e.g. Rice, 1977a,b). However, many studies show that

infiltration is also important. Table 1.1 is an updated and extended version of Table 2 of Rice & Ferry(1982), and lists most of the published studies of fluid-influenced metamorphic systems which have included estimates of fluid composition. The X_{eq} column gives these values in each case. The X_{rxn} column, however, gives the composition of fluid which was released by the relevant devolatilization reactions in each case. Wherever the two values differ, some degree of infiltration is implied (in all documented cases, of a more H_2O -rich fluid), because either the fluid produced by the devolatilization reactions has been immediately removed from the system without equilibrating, which seems unlikely, or else that fluid has been diluted by another, H_2O -rich fluid, to result in the X_{eq} value determined. In all of the cases given in Table 1.1 the X_{eq} values are imprecise, due to the inaccuracies in the positioning of the mineral reactions, but the results show a general pattern which is convincing - infiltration is a common phenomenon.

It is possible to quantitatively assess the effects of infiltration, by calculation of the fluid:rock ratio during the metamorphic event. This can be achieved either by studying the relative amounts of reactant and product minerals in an assemblage (Ferry, 1980), or by calculating the effect of fluid on stable isotope ratios (Rumble *et al.*, 1982). The methods and assumptions of the former approach are described in Section 4.4 of this thesis, where fluid:rock ratios for Knapdale metacarbonates are presented. Table 1.1 also shows the few other published values.

1.2:

The Knapdale metacarbonate system; scope of this project

This thesis presents work done in the Dalradian regional metamorphic terrain of Knapdale, SW Argyll. The area consists of a thick sequence of quartzites, semi-pelitic schists and pelites which represent the proximal parts of

the overturned limb of the Tay Nappe, and these rocks show the typical low to medium grade, chlorite to garnet-bearing, pelitic mineralogies found elsewhere in the Scottish Highlands. However, within these units occur rare, thin carbonate horizons, which contain a wide range of metamorphic calc-silicate mineral assemblages. These offer an excellent opportunity for determining the detailed metamorphic history of the rock system, in particular the evolution and behaviour of the metamorphic fluid phase.

Another metamorphic element in Knapdale is the large number of basic rocks. These formed the basis of a Ph.D thesis by Graham(1973), which together with this thesis, complete the petrological description of Knapdale.

It has been shown above how the problem of fully characterising metamorphic fluid behaviour in any system requires multiple lines of attack. This thesis represents one of the few complete petrological and stable isotope studies of a fluid-dominated system. Fluid inclusion work was attempted during the project the author being responsible for the setting up and calibration of a Linkam TH600 heating/freezing stage at Edinburgh University. The pilot project on this apparatus, however, to study the composition of inclusions from quartz of the 'matrix' of high grade metacarbonates (i.e. not quartz in veins or segregations) was plagued by the small (5 μ m) size, and small number of primary inclusions. The few results obtained did suggest that fluid in the inclusions was pure H₂O, with perhaps 3-5 wt.% NaCl, which supports many of the conclusions made in this thesis.

This study is particularly important because the detailed investigation of mineral assemblages, together with the stable isotope results, has allowed clear identification of two separate and distinct fluid infiltration events in the Knapdale metacarbonate system. Moreover, small-scale mineral assemblage distribution has allowed the primary fluid infiltration event transport process to be determined, and factors controlling that evaluated. Finally, Chapter 7 of this thesis represents a crude, but nevertheless valuable

attempt to use a non-equilibrium framework to model the fluid processes seen in Knapdale. Estimation of parameters in these equations has substantiated earlier petrological conclusions, and led to order of magnitude solutions to the problem of time durations.

C H A P T E R 2: The geological framework of Knapdale

2.1: Introduction

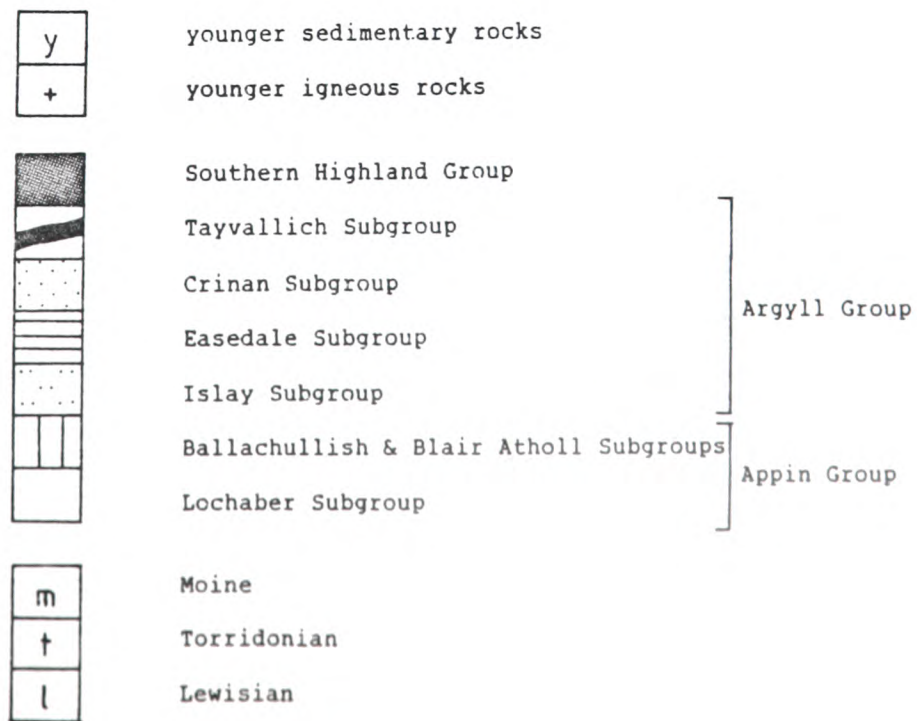
Part of the Kintyre peninsula, at the south-western end of the Scottish Highlands, is described here, namely that part which forms a north-south trending block of land 40km by 20km, bounded by latitudes $56^{\circ}05'$ and $55^{\circ}44'N$, and by longitudes $5^{\circ}23'$ and $5^{\circ}43'W$, and which is known as Knapdale (see Figure 2.1).

Knapdale is of fairly low elevation, the average height of the interior being 200-400m, but the land margins, with the Sound of Jura in the west, and Loch Fyne in the east, are relatively steep, and low-lying coastal areas are narrow. The rounded, poorly drained hills of the interior are largely covered with tussock grass and peat, and exposure of most rock types is very poor.

Three long NE-SW trending sea lochs indent the western coastline (see Figure 2.2). In the north, Loch Sween, with Knapdale forest at its head, separates the land further to the north known as Tayvallich. In the centre of the area, Loch Caolisport divides regions known as North and South Knapdale, and in the south, West Loch Tarbert divides South Knapdale from the remainder of the area described here, and that which is more properly called North Kintyre. The rock exposure along these sea lochs, and along the rest of the coastline, is frequently good, if narrow, and the bulk of the material studied here comes from such exposures.



Figure 2.1: SW Argyll - geology. After Roberts & Treagus(1977).



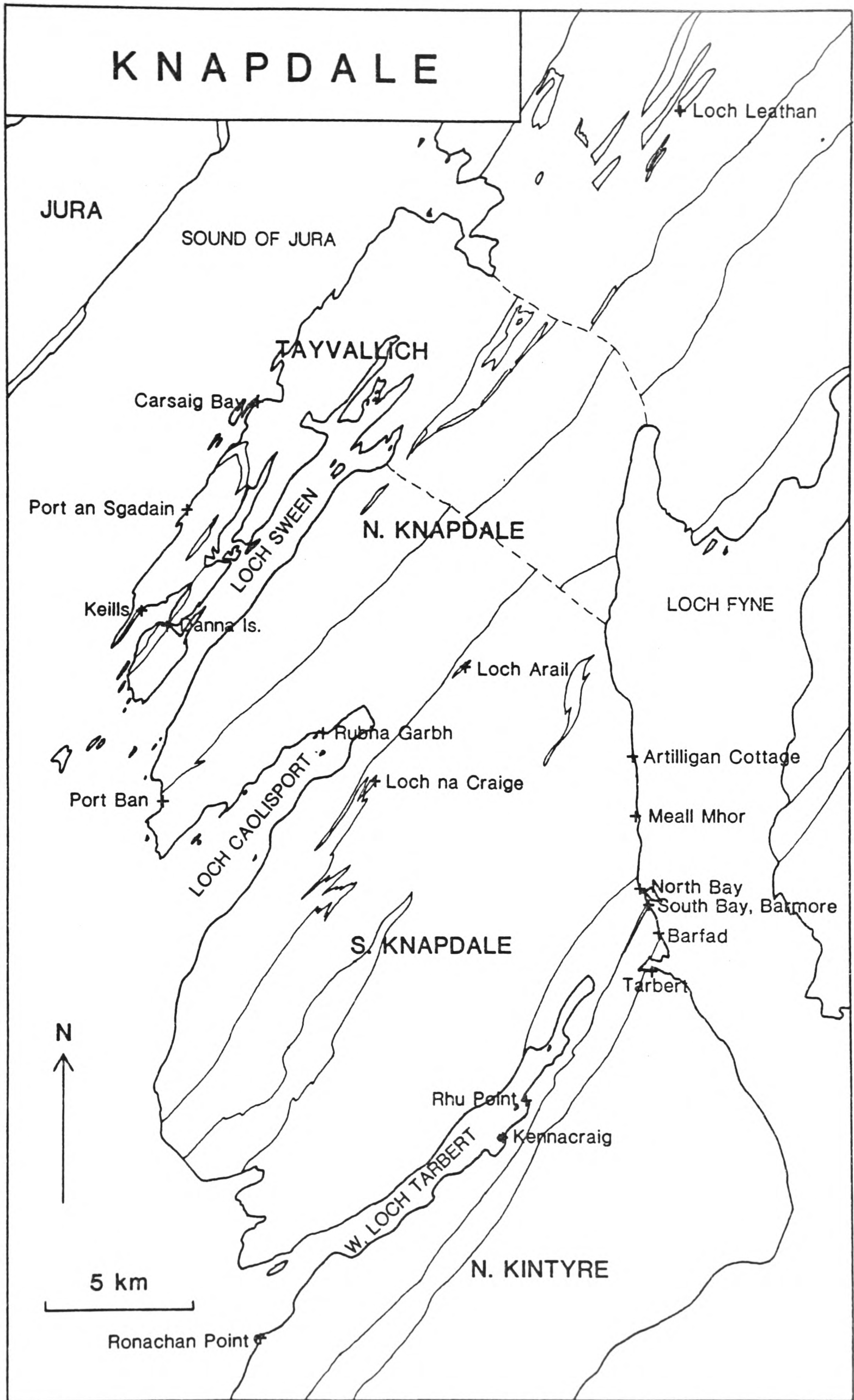


Figure 2.2: Knapdale - localities mentioned in the text.

2.2: Rock types and stratigraphy

The rock types of Knapdale and North Kintyre can be conveniently separated into meta-sedimentary and meta-igneous types.

2.2.1: Meta-sedimentary rocks

The sedimentary sequence consists of pebbly sandstones or grits, finer grained nearly pure sandstones, interbedded sands and silts, and fairly homogeneous silts or muds. Interspersed in these are rare limestones, often interbedded with silty horizons, and occasional sands and silts of a more or less calcareous nature.

Few sedimentary structures are visible, especially in the southern part of the area, and quartz grain-size criteria must be viewed in the light of widespread recrystallisation.

Consequently, division of this broadly homogeneous sediment pile into litho-stratigraphic units is somewhat arbitrary. However, the existing scheme (after Bailey, 1922; Roberts, 1966; see Figures 2.3 and 2.4) is useful for describing the overall predominance of one type of sediment in a particular area, and for the splitting up of the geology of the whole area into digestible units.

All the sedimentary units reflect the simple structural interpretation by outcropping as bands trending NW-SE across the peninsula. The oldest rocks in the area, the Ardrishaig Phyllites, are dark silt or mud-stones, which are homogeneous throughout their extent, which consists of a 4-5km wide central tract containing Loch Caolisport. Apart from good coastal exposures at Port Ban (NR699.742) as described by Roberts(1966), and at Rubha Garbh (NR752.766), these Ardrishaig Phyllites form a strip of land of lower relief and are poorly exposed. Thicknesses of this and other

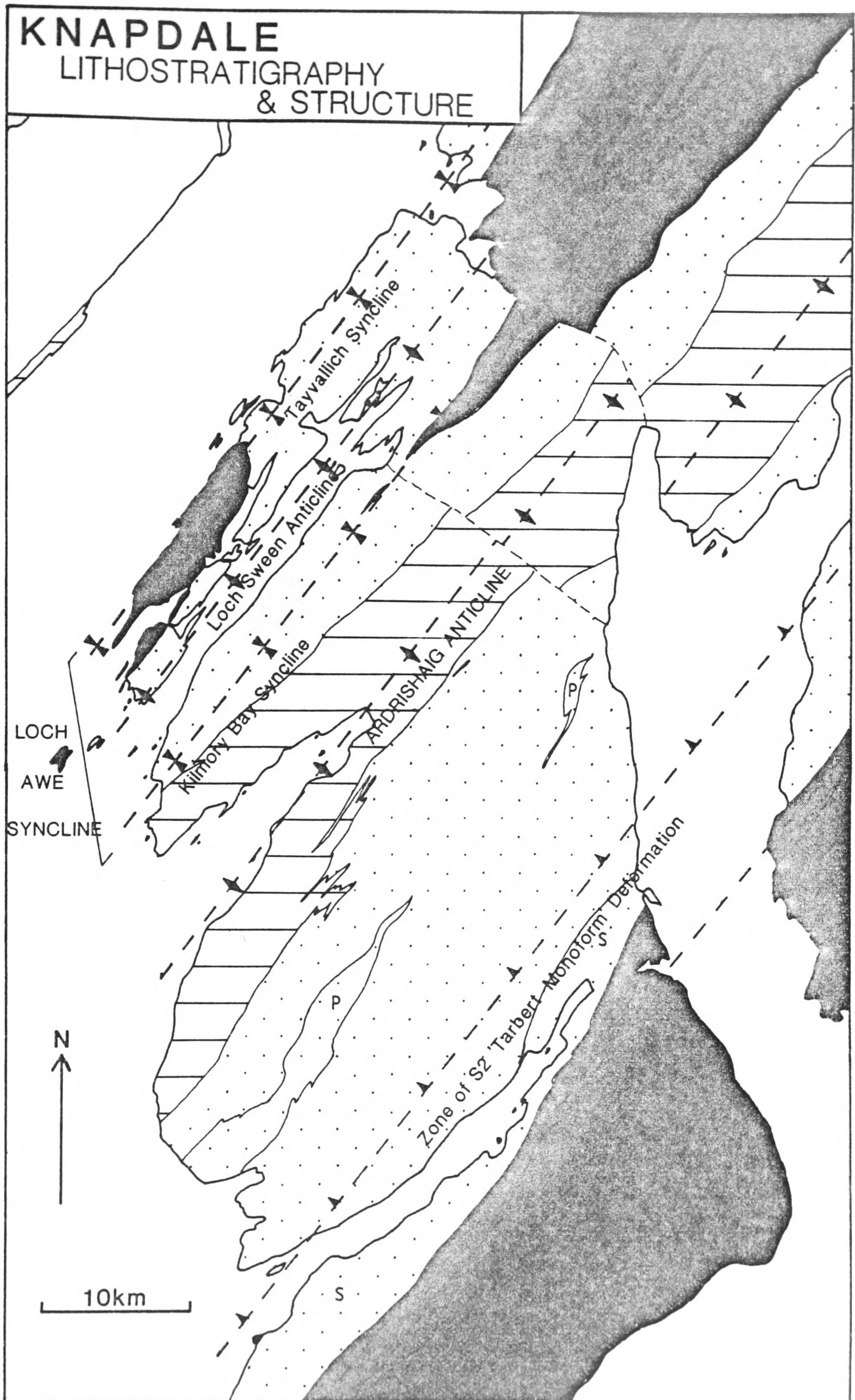


Figure 2.3: Knapdale - lithostratigraphy and structure. Sedimentary units as in Figure 2.4.

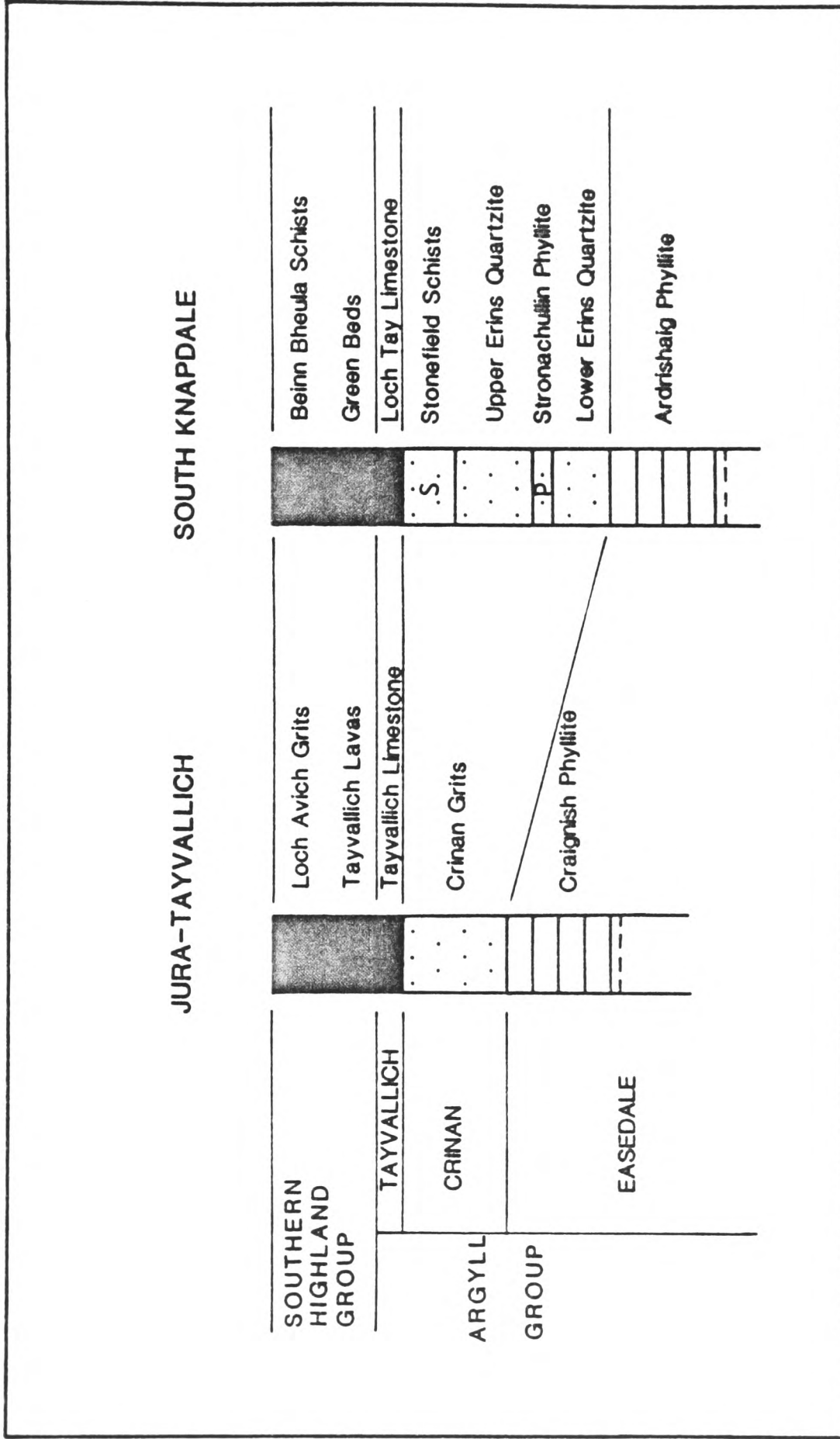


Figure 2.4: Correlation of sedimentary units throughout Knapdale (after Roberts & Treagus, 1979). Note that the Erins Quartzite units in South Knapdale are much thicker than the stratigraphically equivalent Crinan Grits in Jura - Tayvallich.

units are difficult to estimate due to the presence of large numbers of intrusive igneous sills, and possible repetition by folding.

To the north of these rocks the upper part of the stratigraphic sequence comprises the Crinan Grits, overlain by the Tayvallich Limestone.

The Crinan Grits are a much more consistently coarse grained arenaceous rock, often well bedded, with a dominance of pebbly sandstones with clasts of up to 1cm in diameter set in a sandy matrix (see Plate 2.1a). These rocks have formed part of a sedimentological study by Knill(1959,1963) with attention mainly to their provenance. Due to their more resistant nature and the lessening grade of metamorphism to the NW, these rocks are frequently well exposed, notably around Carsaig Bay (NR735.881).

Down the centre of the Tayvallich peninsula, on its western shores at Port an Sgadain (NR711.850) and at its south-eastern tip around Keillmore (NR687.803) various types of limestone and limestone breccia are found. These blue-grey Tayvallich limestones are for the most part deformed and recrystallised, and rather homogeneous, but some relict textures can be seen. Notable is an occurrence from one roadside exposure at Keillmore (NR687.803) of broken and partly recrystallised ooids, set in a matrix of highly deformed calcite (see Plate 2.1b). Another isolated occurrence of very similar rocks just outside the described area to the NE near Loch Leathan (NR867.987), which rocks are correlated as an along strike equivalent of the Tayvallich limestones, may reflect their original patchy and variable nature.

To the south of the outcrop of the Ardrishaig Phyllite Formation, the remaining part of the area described consists of a much thicker sedimentary sequence, split into several litho-stratigraphic units which are roughly correlated in time with those already described. This correlation is as a result of the structural constraints rather than of sedimentological criteria, although well-documented lateral facies changes (e.g. Borradaile, 1973; Knill, 1963; Anderton,

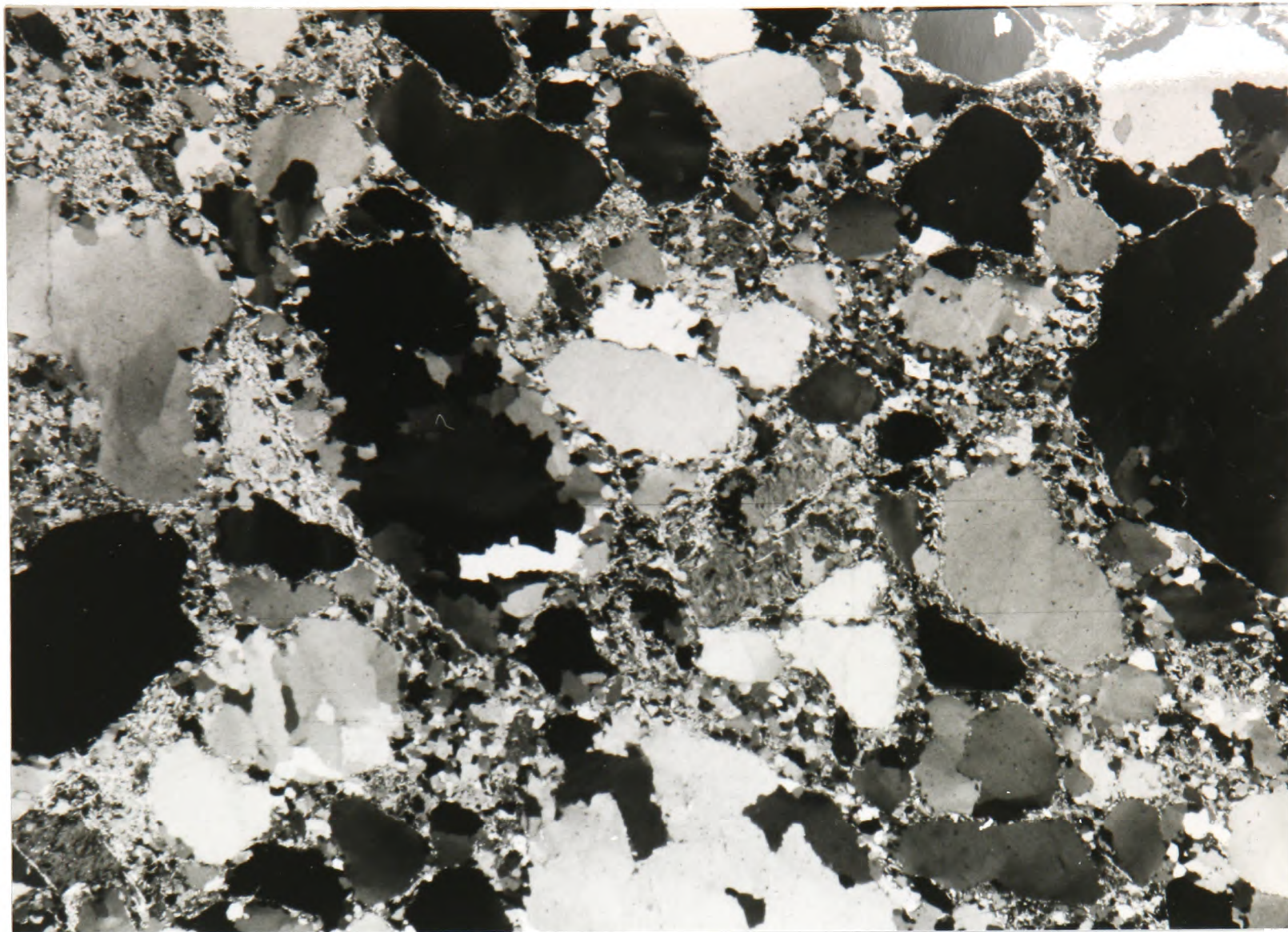


Plate 2.1a: Crinan grit, quartz pebbles in a silty matrix. Deformed quartz exhibits undulose extinction, subgrains, primary recrystallisation. Rock CO, Carsaig. X8, xp.

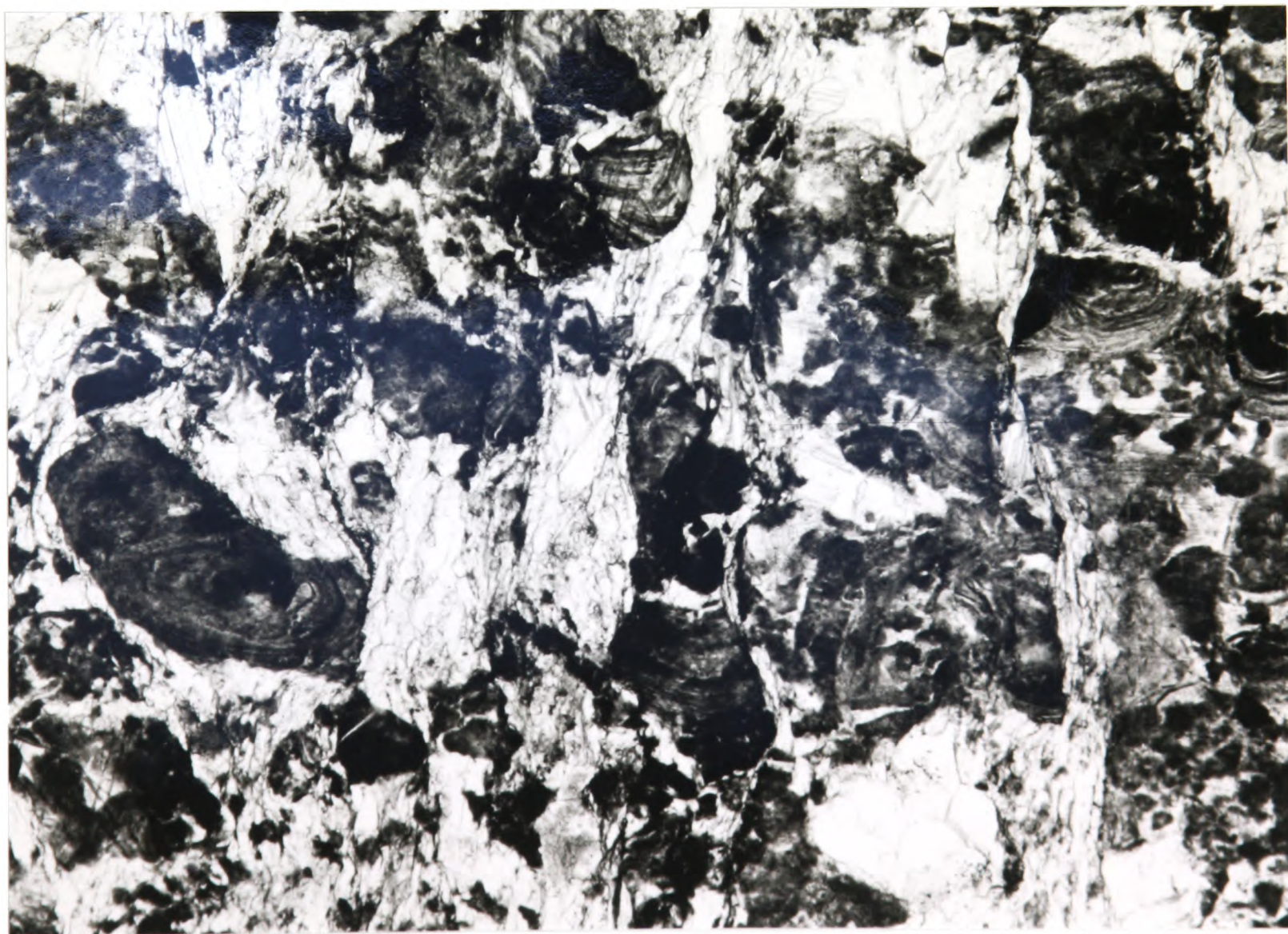


Plate 2.1b: Tayvallich limestone, broken and deformed ooids, set in a matrix of recrystallised calcite. Rock K1, Keills. X16, xp.

1979) would inevitably make the latter proof difficult. However, this thicker southerly sediment pile contains broadly the same elements of sedimentation as the northern area. The stratigraphic divisions are if anything more subtle.

The sediments through the whole of South Knapdale are largely made up of coarse sandstone members, often several metres thick and containing little clay material, and the domination of these now indurated rocks in the sediment pile defines the Erins Quartzite Formation. These rocks are particularly well exposed in the steep, narrow coastal sections along Loch Fyne between Artilligan Cottage (NR860.767) and North Bay, Barmore (NR864.718).

Part of this section, around the small promontary just south of Meall Mhor (NR864.735) shows a typical sequence of white, fairly pure quartzites with thin clayey now mica-rich partings, along with lesser amounts of darker, more pelitic horizons which now contain abundant lenticular quartz segregations on a 1-50cm scale. Also visible in this section are several discrete limestone lenses and occasional zones of carbonate segregations, suggestive of an original patchily calcareous nature to the sediment.

The Erins Quartzite Formation as a whole consists of a structural thickness of 7-8km with only minor local deviations from the general sedimentary theme. The subdivision of this Formation into lower and upper units, separated by a laterally discontinuous fine-grained or phyllitic member, the Stronachullin Phyllite, has been suggested, and generally adopted.

Above the Erins Quartzite Formation to the south, the sediments become even more deformed and metamorphosed, making their original sedimentary character correspondingly difficult to determine. In general though, these are finer grained, more silt or clay-rich rocks, and are dominated less by the thicker and coarser sandstone/quartzite units.

Two fairly coherent and laterally continuous limestone bands are found within these younger sediments, however, the thin, poorly exposed Ashens limestone, and the thicker,

well exposed Loch Tay limestone. This latter Loch Tay Limestone Formation is traceable along strike throughout the Dalradian rocks towards the NE into Central Perthshire, and in Knapdale separates a thin strip of semi-pelite, the Stonefield Schist Formation, from the Green Beds and the Beinn Bheula Schist Formations to the SE.

The Ashens limestone lies within the Stonefield schists and is a bluish-grey, fairly pure marble (NR856.712). A marble in a similar structural position but in the extreme SW of the area, at Ronachan Point ((NR742.555), is a probable lateral equivalent of the Ashens limestone, and as such represents its best exposure.

The Loch Tay limestone is visible in several places, but there are three main well exposed sections: South Bay, Barmore on the Loch Fyne coast (NR867.714), and Rhu Point (NR827.639) and the Islay ferry terminal at Kennacraig (NR819.626) on the south shores of West Loch Tarbert. Of these, which are described in detail in section 2.5.2, the first offers the thickest section (70m including intruded igneous sills), and has been the primary location of study with regard to the metamorphic history of the carbonate rocks of the area, and the behaviour of metamorphic fluids. In terms of original sedimentary character, the Loch Tay limestone is less pure than the Ashens limestone, consisting of variably distributed sandy or silty, now quartz-rich horizons, interbedded with siliceous to fairly pure carbonate beds.

This limestone and the Tayvallich limestone to the NW are tentatively correlated by structural position.

The enigmatic nature of the 'Green Beds', also traceable large distances along strike to the NE and in the south of the Cowal peninsula, has long been the subject of discussion (Phillips, 1930; Roberts, 1966; Van de Kamp, 1970). Thin, metre-thick scale horizons of a now epidote + chlorite + garnet metamorphic assemblage (see Plate 2.2a), suggestive of sediment of a basic or volcano-sedimentary nature, are, while occurring sporadically throughout the whole of Knapdale, more frequent in a roughly 1km thick sequence of



Plate 2.2a: Green Bed *sensu stricto*, a volcano-sedimentary rock now consisting of garnet, biotite, chlorite, epidote, rutile. Rock CA20, South Bay. X20, pp.

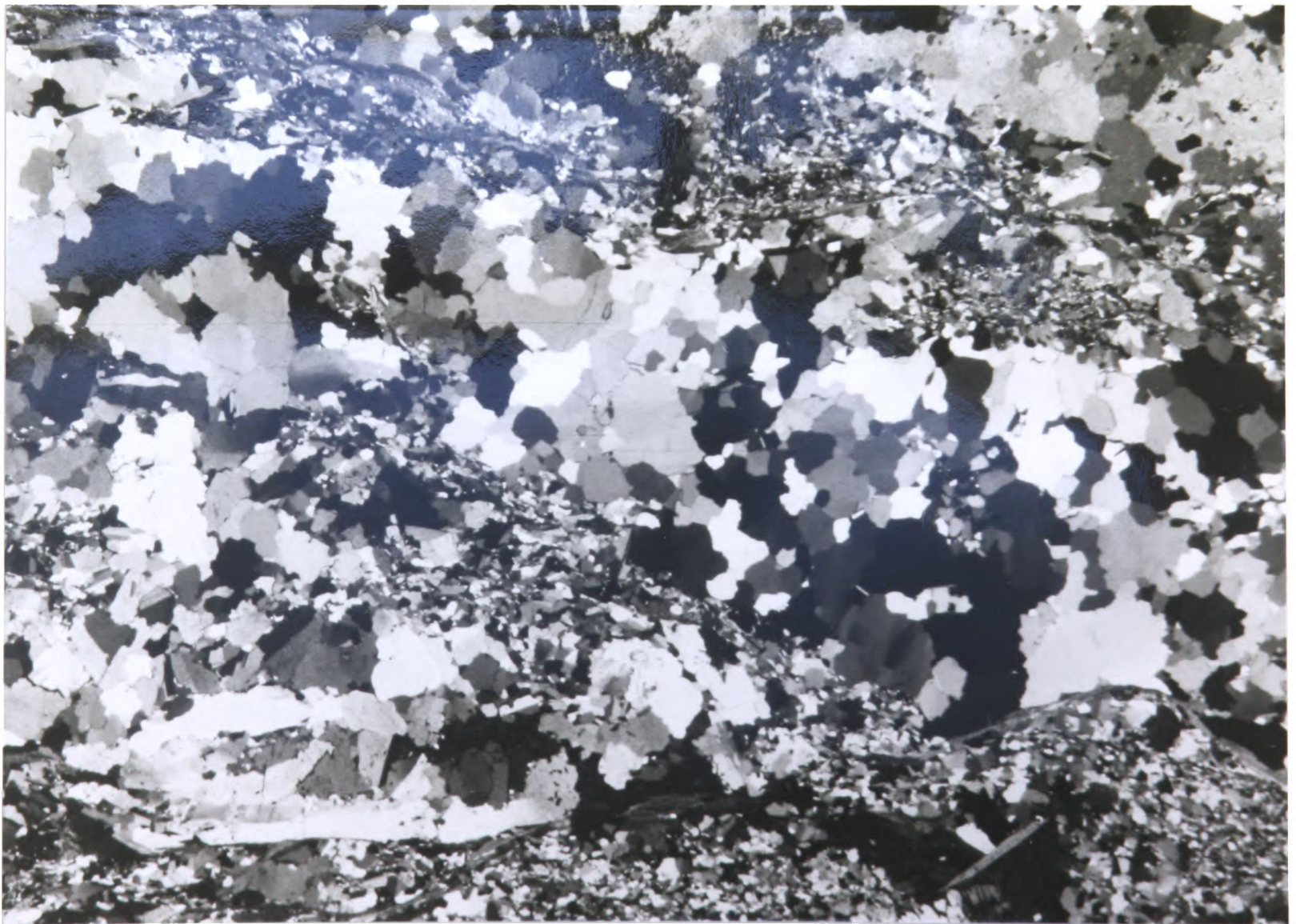


Plate 2.2b: Green Beds semi-pelitic schist, showing quartz deformation features - truncated grains, sutured margins, subgrains, primary recrystallisation. Rock CA26, South Bay. X8, xp.

schists overlying the Loch Tay limestone. Thus, these schists, on the whole indistinguishable in sedimentary character from the preceding Stonefield schists, or from the succeeding Beinn Bheula schists, are separated stratigraphically as the Green Beds Formation. These youngest two Formations are exposed in continuous section in narrow, fairly inaccessible coastal outcrops along Loch Fyne from South Bay, Barmore to Barfad (NR875.695) and at the road end east of the picturesque village of Tarbert.

2.2.2: Meta-igneous

The meta-igneous rocks of Knapdale are without exception basic in nature, and can be divided simply, for the purposes of description, into intrusive and extrusive types.

The whole of the area, from Crinan Harbour in the north to beyond Tarbert in the south, contains a vast number of intrusive igneous sills. These lensing, from metre to hundred metre-scale thick and roughly concordant bodies are inferred to have been emplaced before the first phases of deformation (Graham, 1976). The greater thickness of sills in the NW of the area may be causally linked with its subsequent structural evolution (Graham & Borradaile, 1984). A clear trend in the proportions of sill to country rock can thus be seen on a traverse NW-SE through the area, the ratio decreasing to the SE. Such a traverse would also show the roughly increasing metamorphic grade to the SE, and the increasing degree of deformation. Consequently sills in the NW are relatively less metamorphosed and deformed, and often display relict igneous textures, whereas those in the SE bear little resemblance to their original state (see Plate 2.3a).

All the sills are metamorphosed throughout to a greater or lesser extent, however, and relict igneous mineralogies are rare. The occurrence of plagioclase laths of some composition, orientated in a vaguely ophitic or trachytic way, in a matrix of Fe-Mg minerals, is widely visible in the



Plate 2.3a: Metabasite sill, now epidote, albite, amphibole, stilpnomelane, sphene, showing relict igneous texture. Rock 69-140, Carsaig. X6.3, xp.

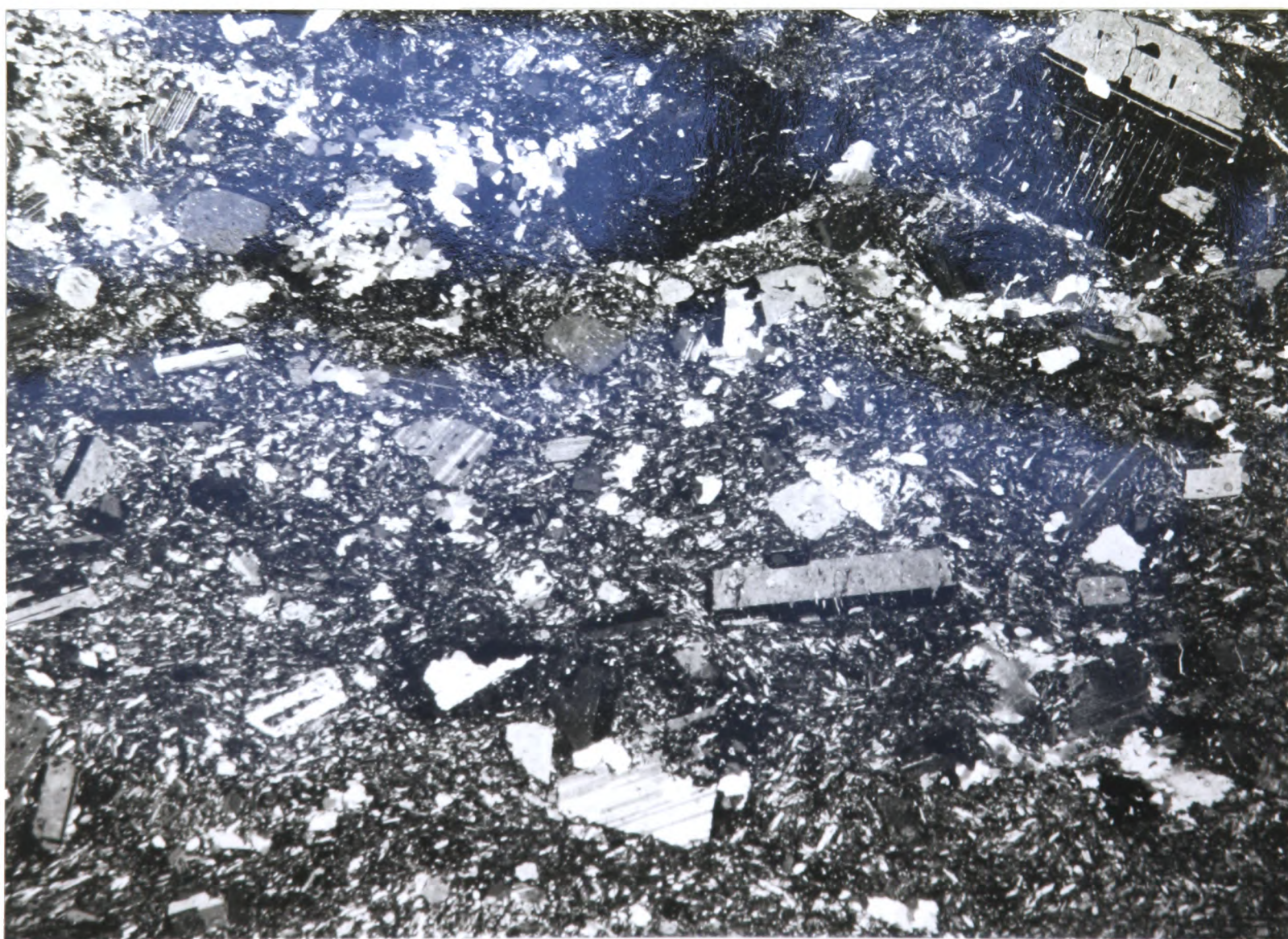


Plate 2.3b: Metalava, showing phenocryst albite in groundmass with clear trachytic texture. Rock K4, Keills. X6.3, xp.

northerly sills, but absent in the south.

Extrusive basic rocks, or lavas, occur only in the Tayvallich peninsula, and are the structurally highest rocks exposed in the whole area. A complicated sequence of lavas and interbedded sediments is visible at Port an Sgadain, on the west side of the peninsula (NR711.850), just south of limestone exposures already mentioned.

The lavas of this section, which is roughly 100m thick, contain extrusive features such as pipe amygdales and vesicle trails, along with some clear, metre-scale pillow structures with vesicular margins, which are surrounded by a between-pillow infill of ashy sedimentary material. In thin section these lavas show obvious fine-grained trachytic textures (see Plate 2.3b).

2.3: Structure and deformation

2.3.1: Large scale structures

The Dalradian outcrop over the whole of the S.W. Highlands takes the form of a SW-NE trending zone bounded to the NW by the Loch Skerrols thrust on Islay, and to the SE by the Highland Boundary fault.

The presently accepted structural interpretations of the Knapdale area are due to Bailey(1922), Roberts(1966,1974,1977), Borradaile(1973) and Roberts & Treagus(1977,1979), and for the most part these interpretations depend on the along strike continuation of more rigorously defined structures around Loch Awe to the NE. In these works, four separate structural phases (D1 to D4) are recognised. This thesis follows a simpler scheme of Primary (S1) and Secondary (S2), which correspond to the dominant D1 and D3 phases of Roberts (1977).

The Central Highland structures are at an inferred structurally lower level than those seen in Knapdale (Thomas, 1979; Bradbury et al., 1979), which represent the highest uneroded levels of the sediment pile. As such the

Knapdale area is interpreted as having a simple, relatively open structure, lacking the complex refolding seen at deeper levels. Due to a lack of exposure, only broad, loosely defined elements of structure can be recognised in the field in Knapdale, and correlated with similar structures to the NE.

Three structural elements can be recognised, the compound Loch Awe Syncline, the Ardrishaig Anticline and the Tarbert Monoform (see Figure 2.3)

Trending NE-SW in the Tayvallich and North Knapdale area, the Loch Awe Syncline is composed of a northerly Tayvallich Syncline and a southerly Kilmory Bay Syncline, separated by the Loch Sween Anticline. The southern part of this structure is visible in Kilmory Bay (NR699.744, as described by Roberts, 1977) where the position of the synclinal axis is inferred from grain size fining-upwards criteria in Crinan Grit sandstone/quartzite units visible at either end of the bay.

The Ardrishaig Anticline is also poorly exposed, but marks the NW edge of a zone of steep inclination (the 'Knapdale Steep Belt') which persists throughout South Knapdale.

Taken together, the Loch Awe Syncline and the Ardrishaig Anticline represent those structural elements interpreted as being primary in origin (Borrodaille, 1973). Further, the Ardrishaig Anticline is seen to represent a zone of divergence of SE and NW facing structures. To the south is the so-called 'Loch Tay Inversion', being essentially the exposed lower limb of a recumbent fold or nappe, the root zone of which is represented by the Ardrishaig Anticline itself, and whose vestigial upper limb is visible in the Loch Awe Syncline (see Figure 2.5).

Thus the North Knapdale and Tayvallich sedimentary sequence is separate from, though roughly synchronous with, the inverted South Knapdale and North Kintyre sequence.

The third structural element visible in Knapdale, the Tarbert Monoform, is designated secondary, and is clearly so. This 'monoform', loosely definable as a zone in which

secondary refolding and crenulation of earlier schistosity occurs, runs NE-SW in a diffuse, roughly 3km wide belt which includes West Loch Tarbert. In the light of more modern views of deformation, it is perhaps more useful to think of 'continuous' processes, or complete models of nappe formation in which some separate phases, or styles can be recognised, rather than to stick with rigidly defined primary and secondary events. In this way, Secondary deformation in Knapdale can be thought of in terms of stress fields evolved as a consequence of late-stage, probably vertical adjustments of the emplaced nappe.

2.3.2: Small scale deformation

Because of the necessarily vague way in which a large-scale tectonic framework is imposed on the area, it is difficult to review the features of small-scale deformation in terms of their different structural positions within that framework. In other words, it is difficult to distinguish stress fields characterising say, the 'Root Zone' or the 'Nappe Lower Limb', and then show how deformation differs in each area. It is really only possible to look over the area as a whole and make some general points about the various deformation styles seen. This implies looking at deformation on outcrop and smaller scales.

Three major observations can be made in this way: firstly, the presence everywhere of one penetrative fabric; secondly, its increasing intensity to the SE; and thirdly, some localised overprinting of that earlier fabric by a later crenulation.

Overall, the particular deformation seen in any one outcrop can be thought of as a kind of 'best solution' to a complicated equation which relates stress fields to the amount and nature of metamorphism, with the additional constraints implied by bulk rock composition, presence or absence of metamorphic fluid, and a host of other rock property and physico-chemical parameters.

1. 1st Fabric

The one penetrative fabric, seen in rocks throughout Knapdale, takes the form of a planar schistosity defined by phyllosilicates, variably developed in the various metasedimentary lithologies at any one particular locality, but increasingly more intensely defined towards the SE of the area. Most rocks show classic deformation textures (see Plate 2.2b), which can be interpreted in terms of both dislocation creep (or intracrystalline plasticity) and diffusive mass transfer. On the one hand all the phases of dislocation motion can be seen in thin section,

- i) easy glide: formation of kink bands.
- ii) work hardening: undulose extinction due to dislocation pile-up and tangling.
- iii) recovery: formation of adjacent sub-grains with low angle mismatch.
- iv) primary recrystallisation: sutured margins, growth of new grains in areas of high dislocation density.
- v) secondary recrystallisation: grain boundary migration and straightening, formation of triple junctions.

On the other hand, diffusive mass transfer on a thin section scale is obvious too, with the segregation, particularly in broadly pelitic rocks, of quartz-rich microlithons separated by anastomosing mica-rich seams (e.g. Robin, 1979). From the evidence presented later on the probable ubiquitous presence of metamorphic fluids during deformation/metamorphism, it seems reasonable to suggest that such diffusive transfer processes were volatile-assisted, i.e. 'pressure solution' operated.

There is also some evidence, particularly around the Tarbert area, for segregation into diffuse quartz-richer and mica-richer zones on a somewhat larger, cm to metre scale. The situation in these areas, however, is complicated by the imposition of the secondary fabric.

2. 2nd Fabric

Within the loosely defined Tarbert Monoform area, early S1 schistose fabrics are overprinted by a later S2 schistosity, at 90° to S1, which again is probably 'pressure solution' controlled, and results in differentiation on a microfold scale. As such it can be properly termed a crenulation cleavage. The growth of new metamorphic minerals during and after this secondary deformation is well illustrated in albite schists at South Bay (NR867.714), of which a full description can be found in section 2.4.2.

2.4: Metamorphism

2.4.1: Introduction

The distribution of different primary mineral assemblages viewed over the whole of Knapdale reflects such factors as the distribution of various rock types, and their inferred depth of burial during metamorphism.

The tectonic model already described accounts for the general trend in metamorphic grade across the area, with the highest grade rocks found in the structurally deeper south, while particular mineral assemblages reflect in a more intimate manner the original nature of the metamorphosed rock.

These primary mineral assemblages show an estimated variation in temperature from north to south of roughly 400-550°C, pressures being more difficult to determine, but of the order of 8kb throughout (see Chapter 3).

To this rough conceptual framework, which describes the metamorphic conditions of formation of any one rock, must be added the effects of the presence or absence of metamorphic fluids, or the amount, composition, distribution and behaviour of fluid in the environment of formation of the rock. Throughout Knapdale, the fluid phase behaviour is perhaps the single most important control on the end result

in any rocks' evolution. Unfortunately, few generalisations can be made. Many factors determine the way in which a particular fluid affects a particular rock, and models of fluid behaviour must necessarily be specific rather than general.

The metamorphic rocks of interest in the area, with regard to the evolution and behaviour of fluids, are:

1. Non-calcareous metasediments: primary greenschist to epidote-amphibolite facies assemblages, secondary retrogression - the albite schists.
2. Metabasites: greenschist facies meta-lavas and sills, the garnet 'isograd'.
3. Metacarbonates: fluid domination of assemblages in carbonates.

'Non-calcareous' as used in this way is loosely defined, since many phyllites, psammites and quartzites are to some slight degree calcareous and may contain primary calcite and/or dolomite. Similarly, some lower grade metabasic rocks also contain calcite and/or dolomite. Consequently, many of the mineral assemblages under all these three headings can be found on a $T-X_{CO_2}$ diagram for metacarbonates, whose derivation is detailed in Chapter 3.

2.4.2: Non-calcareous metasediments

1. Primary assemblages

The psammitic and pelitic primary assemblages in Knapdale are as follows -

qz + ab + ms ±bt ±gt ±ksp ±cc ±dol ±sph ±rut,

and are similar to those found at similar grades throughout the Dalradian. Plagioclase is, however, without exception virtually pure albite (see Table 3.2). Secondary chlorite is ubiquitous, usually replacing muscovite and/or biotite where present, while rutile of both primary and secondary nature

can be found, in the latter case pseudomorphing sphene. A more complete description of assemblages and possible reactions involving these is contained in Graham *et al.* (1983).

It is a difficult problem to assess the nature and behaviour of the fluid phase which was present during the metamorphism of these rocks, because of their SiO_2 -rich, Ca-poor bulk composition. Unlike the carbonate lithologies, they did not produce, in metamorphism, minerals whose stabilities are tightly constrained to specific parts of a $T\text{-}X_{\text{CO}_2}$ diagram, in terms of ranges of temperature, X_{CO_2} or both. Thus little or no constraint can be placed on the composition of the fluid phase by its effect on the assemblages.

In general, the lack of fluid controlled assemblages can be explained by one of three different hypotheses -

- (i) fluid did not move through the rocks, as their porosity and permeability was too low.
- (ii) fluid moved through the rocks, but only by means of discrete fractures, which allowed only a minimum of interplay between fluid and rock.
- (iii) fluid moved through the rock pervasively, but the mineral assemblages were such that its effect (if any) cannot be recognised.

2. Secondary assemblages - the albite schists

Of major interest in Knapdale, however, is one locality where non-calcareous rocks can be seen to have been affected by metamorphic fluids, and whose assemblages can constrain fluid composition and behaviour. These are the 'albite porphyroblast schists', described by Gunn *et al.* (1897), Bailey (1922), Tilley (1925), Harker (1950) and Watkins (1983), which occur in South Bay, Barmore (NR867.714), but are traceable in a similar structural position to the NE as far as Balquhiddier, and SW into Northern Ireland.

These rocks outcrop in a 100m section, the albite porphyroblast zone or APZ of Watkins (1983), to the south of the Loch Tay limestone, and form part of the Green Beds

Formation (see Figure 2.12).

Unlike the APZ as described by Watkins, however, the APZ at South Bay falls wholly within the 'garnet zone'. The rocks are texturally very complex, and assemblages typically

qz + ab + ms + bt + gt + chl + rut + ksp + tourm ±cc,

represent several reactions rather than an equilibrium assemblage.

It is significant that these rocks only occur in an area which is affected by the secondary, or S2, structures, as their textures clearly evince two separate episodes of deformation.

Sedimentary rock type is also important; the South Bay rocks can be divided texturally into psammites (originally coarse sandstones) and pelites (originally finer grained silts or muds).

(i) Psammites: In these rocks primary biotite and muscovite define a crude S1 schistosity, and quartz is distributed evenly throughout the rock (see Plate 2.4). Garnet occurs as smallish, syn-S1 porphyroblasts, which are invariably retrograded to chlorite to a large degree. Albite porphyroblasts make up roughly 20% of the rock and are of a comparable grain size to quartz, but are dramatically embayed and contain large bleb-like quartz inclusions. This texture is suggestive of simultaneous albite and quartz growth and/or recrystallisation, which was probably syn- or post-S1. Faint hints of S2 foliation at a small (<45°) angle to S1 are seen, but the fabric is nowhere penetrative. Rare, thin Kfeldspar rims occur on albite porphyroblasts in muscovite-rich areas.

(ii) Pelites: These rocks consist of discrete quartz-rich and mica-rich zones (Q and M zones) aligned parallel to and defining an S1 schistosity (see Plates 2.5 and 2.6).

'Q Zones' - are generally lenticular, 1-10cm wide segregations of quartz and albite. The albite porphyroblasts have grown

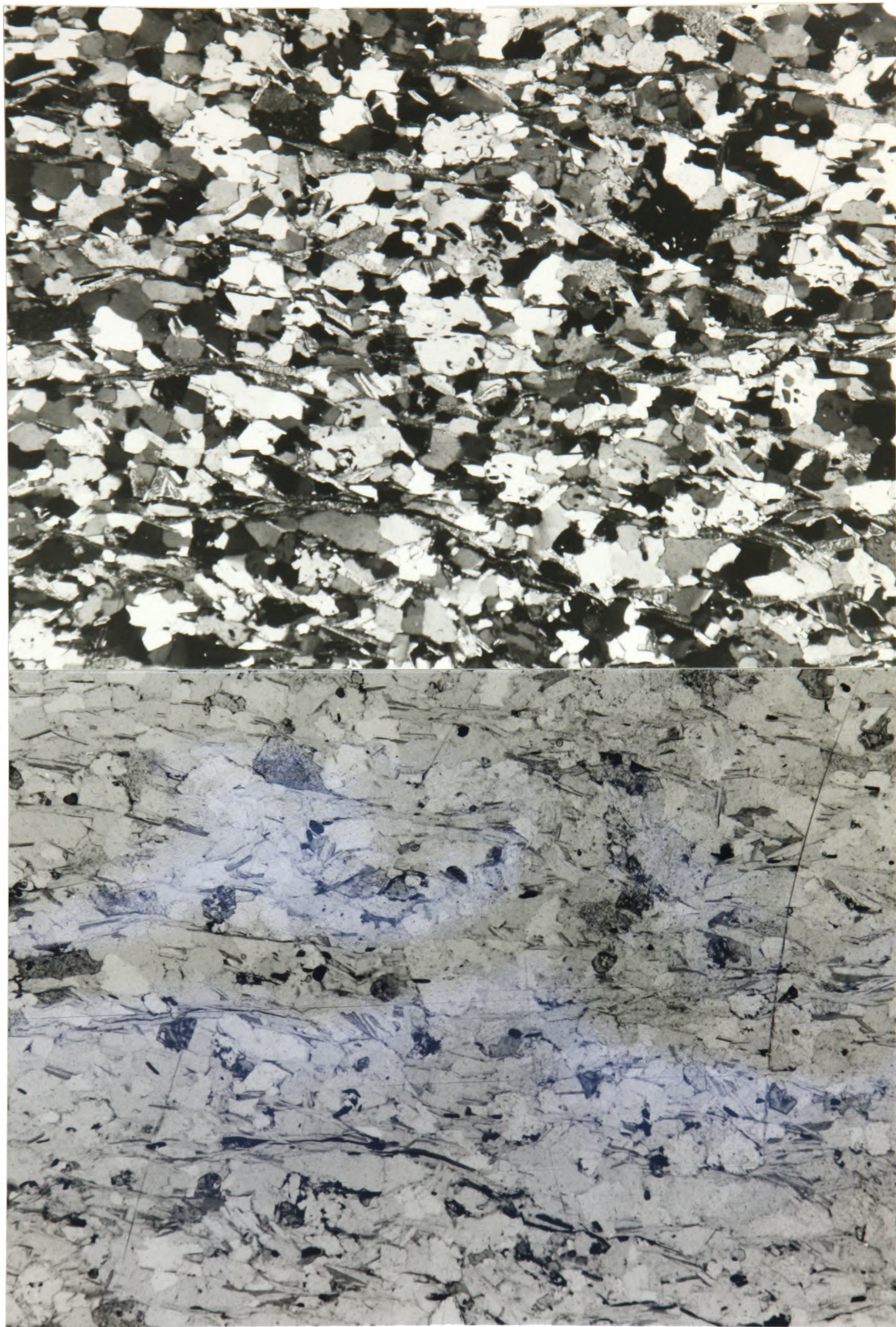


Plate 2.4: Psammitic albite schist Q-zone, with garnet and albite porphyroblast growth over quartz and micas. Rock CA19, South Bay. X16, xp and pp.

in competition with quartz, and while normally larger (<2mm), are embayed by and include quartz in a manner very similar to that seen in the psammitic rocks. Curved trails of finer grained inclusions in albite are often traceable from one grain to the next, and reflect S1 schistosity. Garnets occur both as larger grains, often partially altered to chlorite, and as smaller euhedral grains wholly within albites. Where small garnets are found only partially enclosed by albites, the half outside the albite is retrogressed, and the half inside remains unaltered. Little or no micas occur in these Q zones. At the margins of the zone, however, where albite is in contact with micas (the M zone) a continuous rim of Kfeldspar is found on the albite. In 'M Zones'- quartz occurs only as small patches, which rarely contain albite. The most obvious feature of these zones, other than the preponderance of micas, is the many large (often <5mm) porphyroblasts of albite. These are usually oval in shape and contain trails (often sinusoidal) of small inclusions of quartz and mica, and rods of rutile, which probably grew over S1. They are almost without exception encased in a thin (less than 1/10th diameter) rim of cloudy Kfeldspar.

Two mica-defined schistositities are discernable, an earlier S1 parallel to the long axis of quartz segregations, and a later S2 crenulation at an angle of roughly 60-90° to that. Rutile rods in the mica matrix are bent by S2, and some rotation of albite porphyroblasts, and growth of Kfeldspar, probably occurred at that time. Garnets in the M zones display the same range of textures seen in the Q zones, but are far more abundant.

Modal counts on pelitic rocks show that, taking Q and M zones together, albite makes up about 25% of the rock by volume (see Figure 2.6).

For the APZ viewed as a whole, several points are obvious -

- 1) Deformation was more intense in finer grained rocks during both S1 and S2 episodes, since:
 - a. during S1 only the pelites were segregated into Q and M

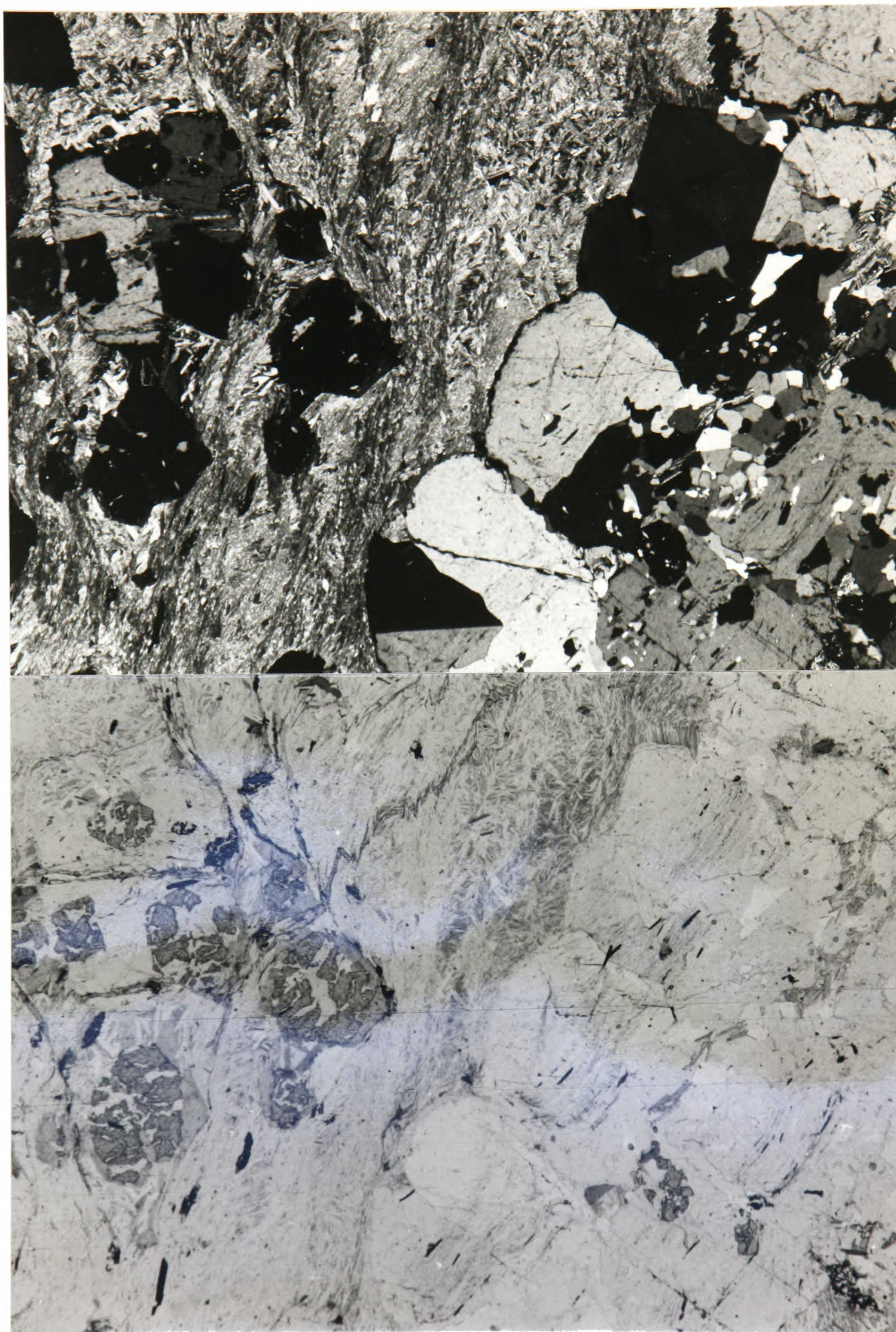


Plate 2.5: Pelitic albite schist Q- and M-zones (right and left halves of picture). Note proportions of quartz, micas and garnet, and shape of albites in each zone. Rock CA21, South Bay. X12.5, xp and pp.

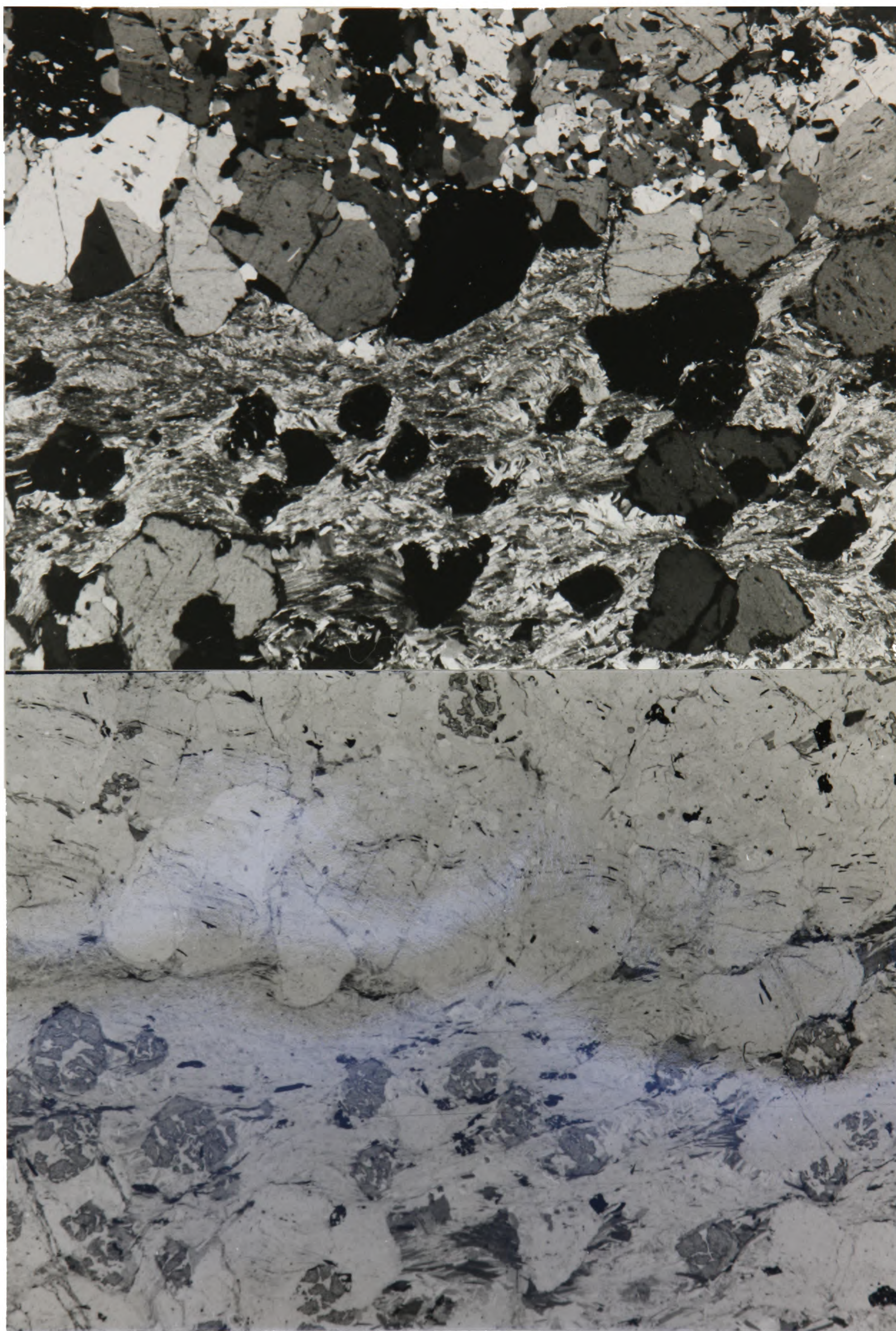


Plate 2.6: Pelitic albite schist Q- and M-zones. Note inclusion trails in Q-zone, and the S2 crenulation of micas in the M-zone. Rock CA21, South Bay. X8, xp and pp.

	<u>Q-ZONE</u>	<u>M-ZONE</u>
Quartz	44.38	6.45
Micas	29.42	58.58
Albite	20.06	24.36
Garnet	1.53	7.91
Kfeldspar	-	2.43
Others	4.59	0.23
Total	99.98	99.96
ROCKS:	CA19	CA21

Figure 2.6: Average modes of Q-zones and M-zones from counts of over 1000 points in albite schist samples CA19 and CA21. Values are expressed as volume percentages. Note the high (>20%), and roughly equal percentages of albite in the two zones.

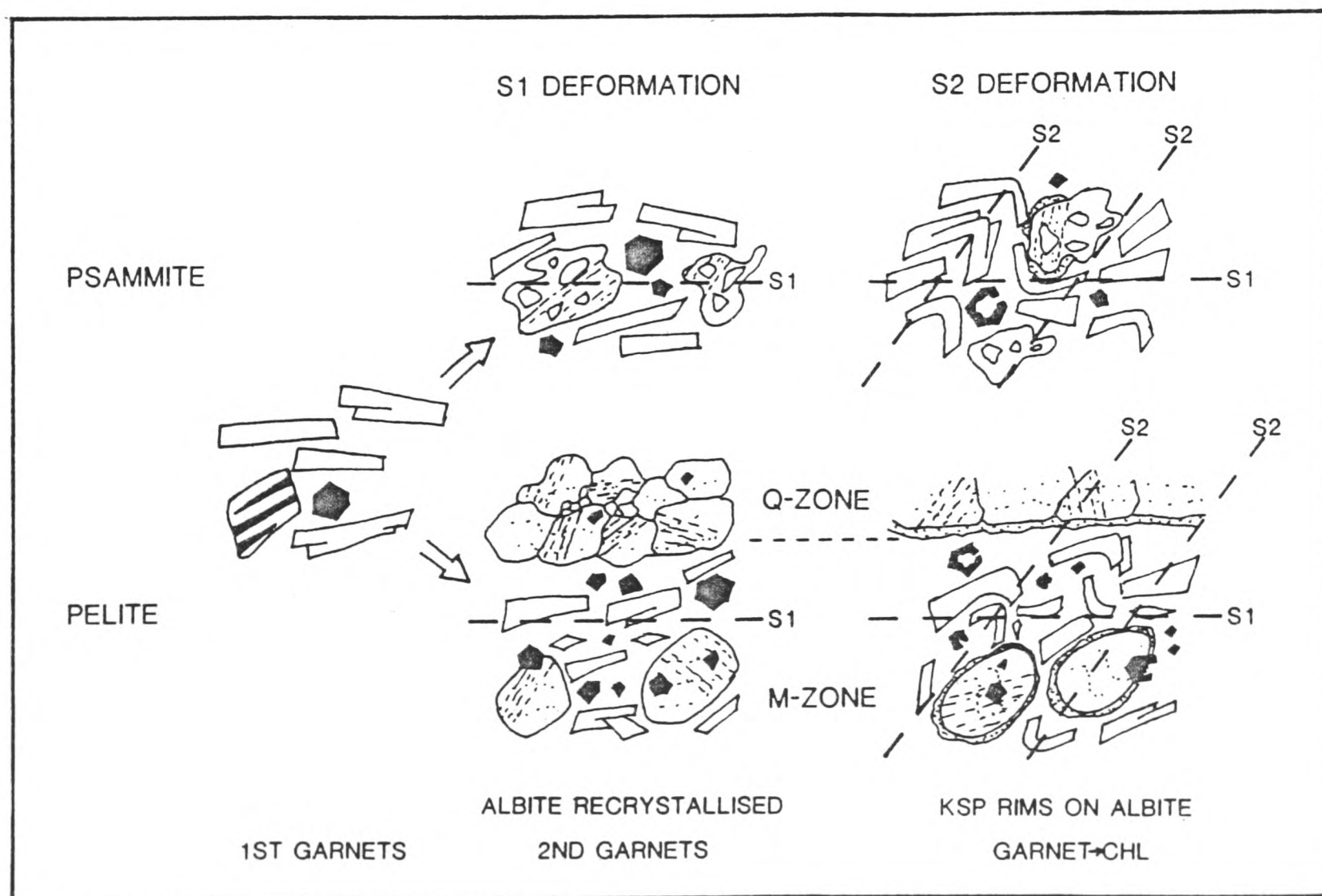


Figure 2.7: Synthesis of textural features in albite schist genesis. Early garnet growth is followed by recrystallisation of albite during S1 deformation. Albite porphyroblasts are rotated during S2 deformation, and Kfeldspar rims form. Note the separation during S1 of quartz-rich and mica-rich zones (Q and M zones) in pelitic rocks only, and the different albite grain shapes in psammites and pelites.

zones (perhaps by a stress-induced diffusive mass transfer process as described by Robin, 1979).

b. during S2 only the pelites developed a penetrative crenulation cleavage. (This is hardly a new observation, and most theoretical models of mass transfer have a grain size term on the denominator of strain rate equations.)

2) A large amount of albite (20-25% by volume) is found in both psammitic and pelitic rock types, and it grew syn- or post-S1, but pre-S2.

3) Where albite was in contact with micas during S2 deformation, Kfeldspar rims formed.

From all of this, a synthesis of the textural evolution of the albite porphyroblast schists can be made (see Figure 2.7).

The major problem arising from the study of these rocks is how to account for the large amounts of Na they contain. Either a) the sediments were particularly Na-rich to start with, or b) Na was introduced at some time. This problem may never be solved unequivocally, since no exactly equivalent, but unmetamorphosed, sediment exists. However, a fluid inclusion study could prove or disprove the quite plausible hypothesis that Na was introduced by a Na-rich metamorphic fluid (i.e. a brine).

2.4.3: Metabasites

1. Spilitisation

The metabasites of Knapdale can be divided into extrusive and intrusive types, as described before, but Graham(1973) has shown that these types are broadly comagmatic. A chemical distinction can be made, however, between those rocks which have been 'spilitised', i.e. have undergone Na enrichment, probably through low temperature interaction with sea water at a shallow level, and those which retain 'normal' basalt chemistry. Evidence for this distinction lies in the bimodal distribution of points on a

modal plagioclase versus normative plagioclase or weight% Na_2O diagram (see Figure 2.8).

The spilitisation process involves early constant volume replacement of Ca-rich by Na-rich plagioclase, and the release of Ca. Epidote segregations, which may be the repository for Ca liberated in this way, are commonly associated with spilites throughout Knapdale.

Subsequent isochemical metamorphism probably first involves a reaction of the form -



Consequently, metamorphosed unspilitised rocks are characterised at this stage by a lower modal amount of albite than metamorphosed spilites, whose plagioclase was albitic even before metamorphism proper began, and was produced by a constant volume process.

2. Greenschist facies

After Graham(1973) and Harte & Graham(1975), the mineral assemblages in greenschist metabasites of North Knapdale and Tayvallich can be divided into three types -

I: amphibole + epidote bearing

e.g. act + ep + chl + ab + qz + sph \pm ms \pm bt \pm stilp
and hbl + ep + chl + ab + qz + sph \pm bt \pm stilp

II: amphibole + epidote + calcite bearing

e.g. as above plus calcite

III: calcite \pm dolomite bearing, no amphibole

e.g. cc + ep + chl + ab + qz \pm ms \pm bt \pm sph \pm rut
and chl + ab + qz + ms + rut \pm cc \pm dol

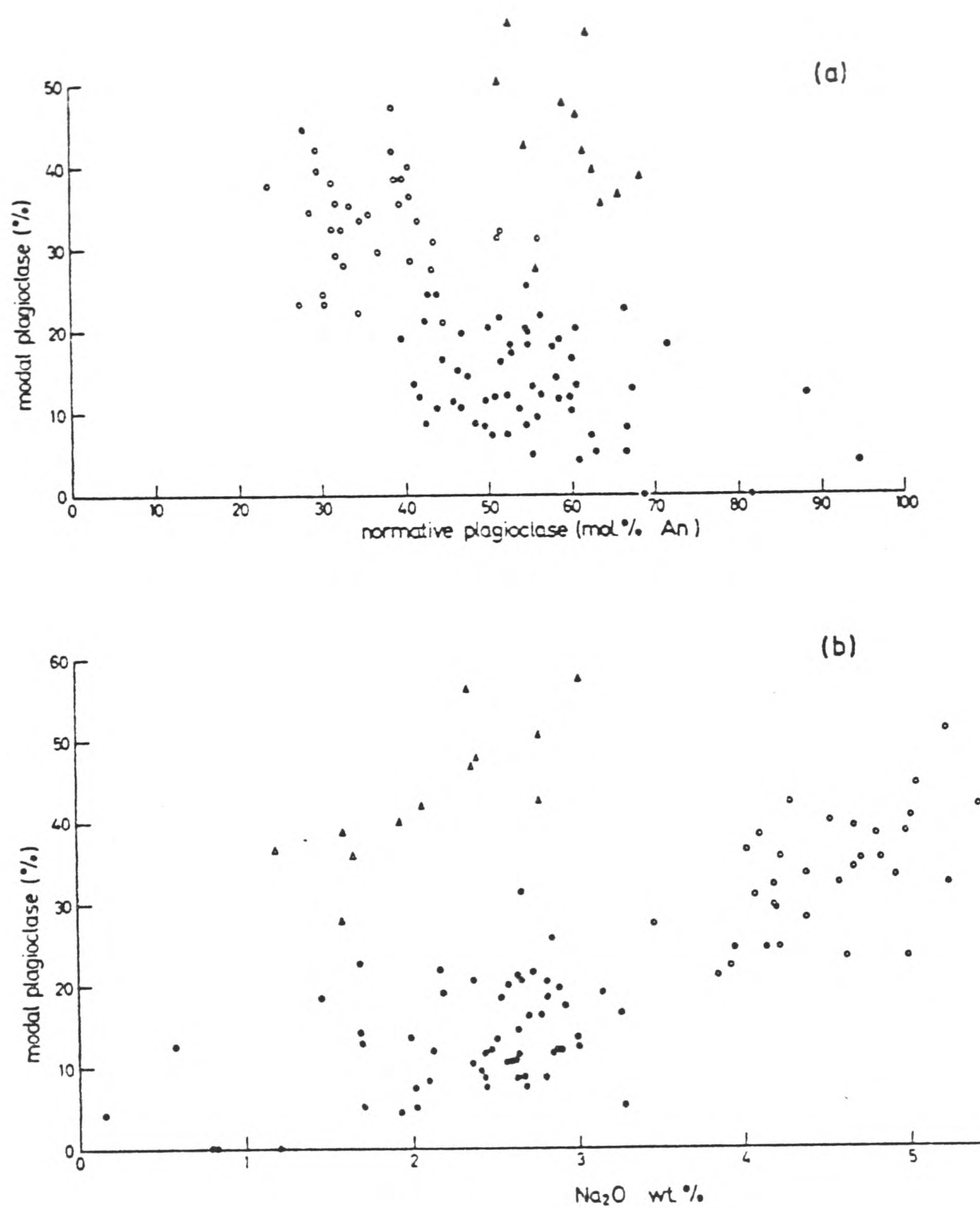
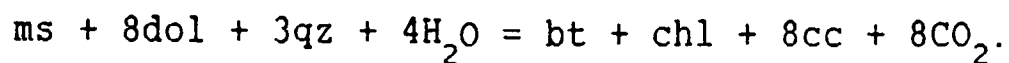
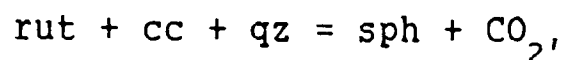
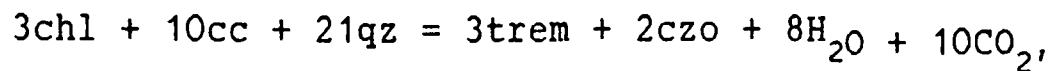


Figure 2.8: (a) Modal plagioclase vs. normative plagioclase. (b) modal plagioclase vs. wt.% Na₂O. Metabasites as follows - (●)= Low Na₂O group (unspilitised), (○)= high Na₂O group (spilitised). ((Δ))= dolerites etc. of Palisades Sill, New Jersey). Diagram taken from Graham(1973).

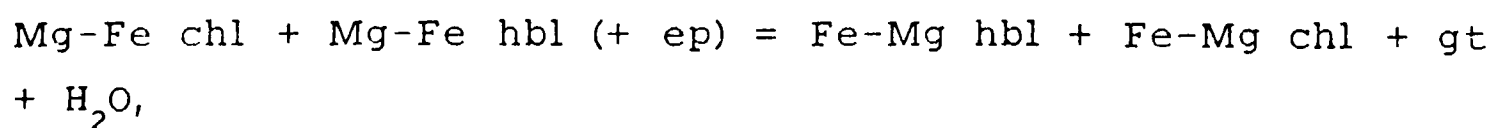
These three types of assemblage are related by the three reactions -



in a pure KCMASH system, which effectively delimit the fields of stability of each assemblage on a T-X_{CO₂} diagram (see Figure 2.9). Such theoretical relationships between assemblages are well supported by natural examples. For instance, some metabasite sills in Knapdale show spatial zoning of assemblages which suggest that sill margins were in equilibrium with fluid more CO₂-rich than their interiors were. This, plus field evidence of varying degrees of deformation at sill margins, has led to the conclusion (Harte & Graham, 1975; Graham *et al.*, 1983) that relatively more CO₂-rich fluids infiltrated sills during greenschist facies metamorphism. Stable isotope evidence for this is summarised in Chapter 5. Penetration of the fluid into the sills may have been deformation assisted, either by the production of discrete fractures along which fluid could move, or by the reduction of grain size at sill margins, thereby allowing diffusive mass transfer processes to operate.

3. Greenschist to epidote-amphibolite facies

The transition to epidote-amphibolite facies was a simple one, being marked by the appearance of garnet. Formulating the equation which describes this appearance is, however, not simple. A continuous reaction of the form -



cannot be written between phases of the compositions

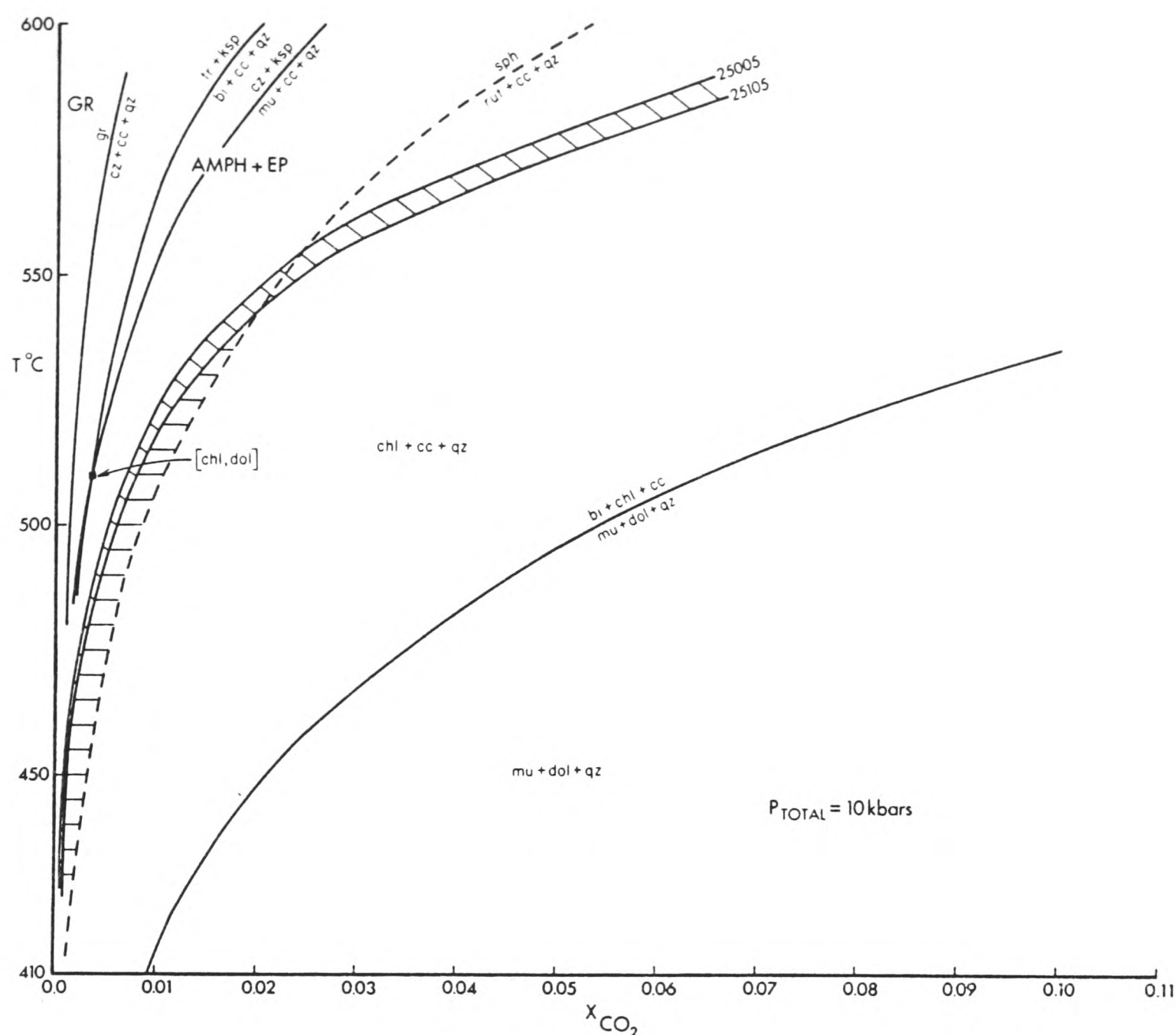
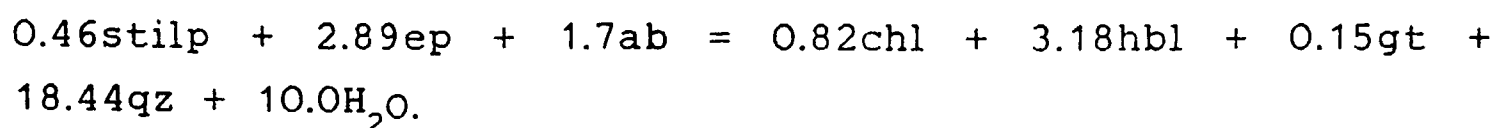


Figure 2.9: $T-X_{\text{CO}_2}$ section showing positions of reactions relevant to metabasite assemblages (from Graham *et al.*, 1983). Curves calculated at 10kb, using real mineral activities. Diagonal shading = locus of reaction 3 (see Table 3.1) for metabasite assemblages 25005 and 25105 (Graham, 1973). Horizontal shading = stability field of sphene + calcite + chlorite + quartz.

determined by Graham(1973). Instead the Fe-rich nature of most of the metabasites may have resulted in the widespread occurrence of stilpnomelane seen in Knapdale (Graham, 1973). Breakdown of this very H₂O-rich mineral, again calculated from real analyses, has the form -



One feature of this garnet producing reaction is that it implies prograde regional dehydration of metabasites, or the release of water, on a massive scale. This is of great importance to the metamorphic history of carbonate rocks in Knapdale.

Simple calculations from modal analyses in Graham(1973) suggest that something of the order of 330cm³ of water per 1000cm³ metabasite could be liberated by the reaction (see also Chapter 8).

2.4.4: Metacarbonates

2.4.4.1: Lower grade localities

Localities where good exposures of carbonate rock can be seen fall naturally into two groups based on metamorphic grade.

The first group is made up of localities at lower grades, mainly of Tayvallich limestone in the far NW of the area, plus a number of outcrops in South Knapdale which represent localised patches of limestone or calcareous sediment within the Erins Quartzite Formation.

The second group consists of outcrops of the laterally continuous Loch Tay limestone and the patchy Ashens limestone, which both lie at the highest grade, and within the zone defined by the presence of S2 'Tarbert Monoform' deformation.

Exposures of Tayvallich limestone are found at Keills (NR689.804), Danna Island (NR698.797) and Loch Leathan (NR868.991). These limestones have been described in Section 2.2.1, but have the mineralogy -

cc + qz + ms + rut \pm ab \pm bt \pm chl \pm dol.

Patchily calcareous sediments occur at Meall Mhor (NR864.736), see Section 2.2.1, and Loch Arail (NR807.799), the former locality containing primary calcite and secondary dolomite-bearing rocks with the assemblage -

qz + dol + ms + ksp.

The one remaining carbonate locality of interest outside the zone of S2 deformation is at Loch na Craige (NR768.744), where a fairly coherent, thin white limestone bed is found in close proximity to amphibolite sills. The assemblages -

qz + cc + gross + czo + di + ksp

qz + gross + di + ksp

qz + gross + czo + di + ksp

qz + cc + gross + czo + ksp

have been found here, which indicate that these rocks have more in common with the high grade rocks to the south than with the other low grade rocks. These assemblages, which require further investigation, may imply that an H₂O-rich fluid was present in this area during metamorphism (see subsequent chapters).

It is the higher grade localities which are better exposed, contain the more interesting assemblages and represent the main area of study.

2.4.4.2: Higher grade localities

1. Ronachan Point

Ronachan Point (NR742.555) lies 17km SW of Tarbert on the southern shore of West Loch Tarbert. The rocky promontary has a wide wave-cut platform on which clear contacts between several distinct lithological units can be seen (see Figure 2.10).

The limestone is variable in appearance and lies in a complicated zone 200m wide interfolded with quartzites, semi-pelitic schists and amphibolite. Within this zone, which runs roughly NNW-SSE across the point, there are two main limestone horizons.

Horizon A, which is the more NW lying of the two, is on the south side of the point roughly 15-20m thick and tightly folded around a core of semi-pelite, the fold nose being clearly visible. Here, the limestone is uniformly dark brownish in colour and contains a few sandy horizons in an otherwise structureless unit. The continuation of this limestone on the north side of the point is completely different, there being no discrete limestone layers. There is however a unit roughly comparable in size to that on the south which is coarsely psammitic, but which contains numerous 1-2m long, lensoid carbonate patches along with a brownish calcareous matrix.

The majority of Horizon B correlates well N-S across the point, and consists of a 15-20m thick limestone layer tightly folded around a sinuous, greenish-black amphibolite layer roughly 20m thick. In the south, however, there is also a small plunging fold closure of limestone surrounding amphibolite, just to the SE of the main exposure. The limestone of Horizon B does differ N-S though, in mineralogy and appearance. In the south the rock is dolomite-bearing, which gives it a sandy brown colour fresh, and a reddish weathering crust. In the north it is mainly calcitic and a deep blue-grey, but contains a complicated series of small crosscutting veinlets of quartz and calcite. Mineral

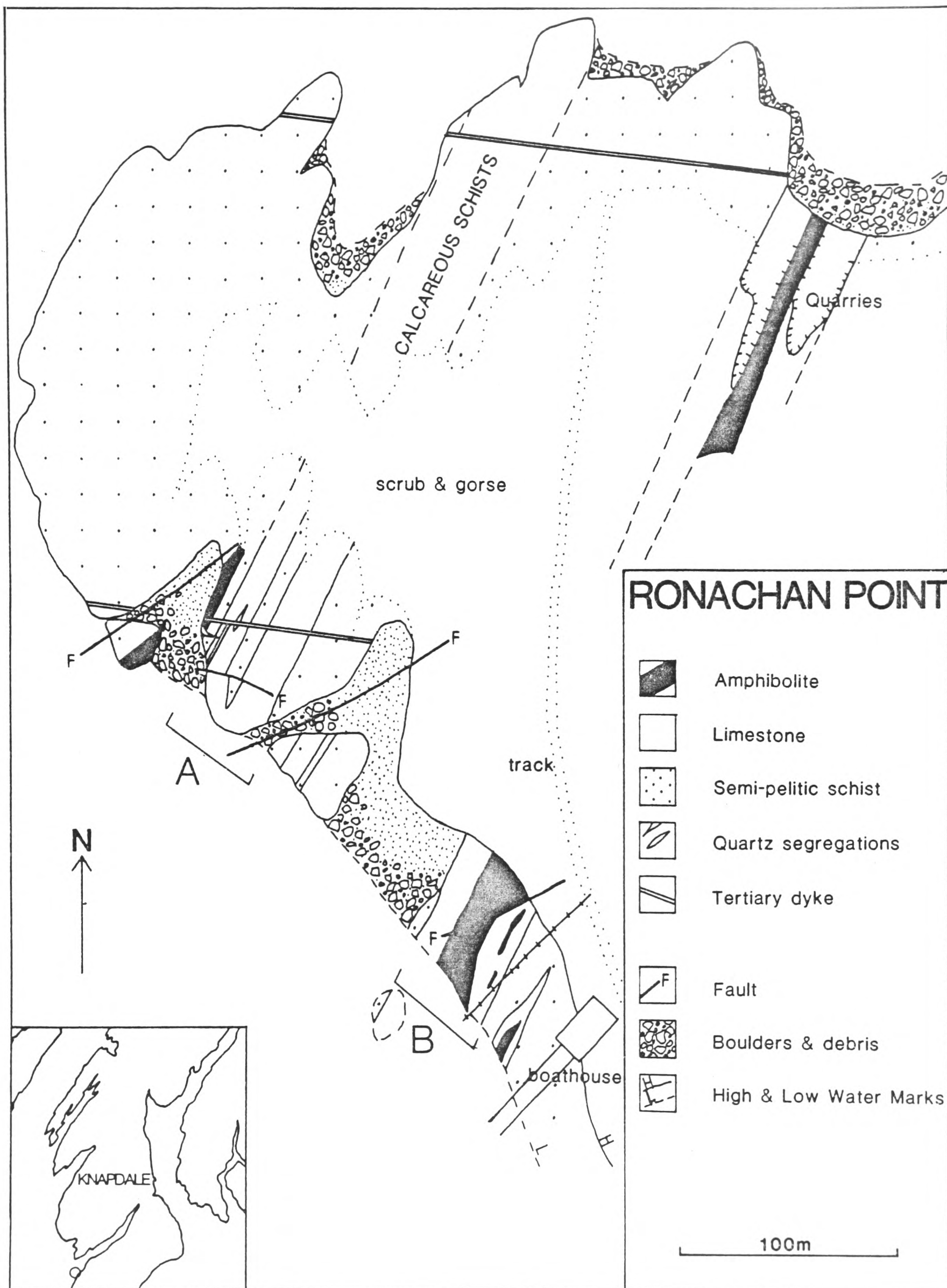


Figure 2.10: Geological sketch map of Ronachan Point, W. Loch Tarbert. Limestone horizons A and B are traceable SW-NE across the point, and outcrop patterns in both show evidence of folding.

assemblages found at this locality are -

qz + cc + dol + ksp + ms + bt

qz + dol + ksp + ms

qz + cc + ksp + ms + bt

qz + cc + gross + czo + amph + ksp

Surrounding the limestone 'zone' inland, and on the end of the point, are a series of variably quartzose schists, with many large (<1m) quartz segregations and complicated small folds. It is noticeable that quartz veining of demonstrably primary affinity is ubiquitous in the non-calcareous schists, but absent in the limestones.

2. Kennacraig

Two localities lie on the small island off Kennacraig 7.5km SW of Tarbert on the southern shore of West Loch Tarbert (NR819.626). The island is linked to the mainland by a causeway, and is the site of the mainland terminal of the Kennacraig-Port Askaig (Islay) ferry.

The first exposure is small, a 25 x 12m strip of rock on the SE shore of the island. Little structure can be seen. The outcrop consists of a 3m band of limestone, flanked on one side by quartzose schist, on the other by amphibolite. A 5m long lens of amphibolite lies within the limestone, which is impure, and consists of thinly interbedded limestone and quartzite layers. Much quartz veining is visible within the adjacent schist, which displays S1 and S2 fabrics.

The second exposure is a roadcut in the centre of the island. Here a 10-15m thick band of similar impure limestone with quartzose interlayers is found. Small S2 folds overprinting S1 schistosity are visible in both the limestone and surrounding quartz-rich schist. No amphibolite occurs here.

These two exposures probably represent Loch Tay

limestone in one or more tight isoclinal folds, and line up well with exposures of similar limestone along strike at Rhu Point and South Bay. Mineral assemblages found are -

qz + cc + ksp + ms + bt

qz + cc + czo + ksp + ms + bt

3. Rhu Point

Rhu Point (NR827.639) lies 6km SW of Tarbert on the southern shore of West Loch Tarbert. The relevant exposure lies in a small bay to the east of the point itself (see Figure 2.11), near high water mark. The section consists of 30m of alternating limestone and semi-pelitic schist, including a 7m thick amphibolite, but is unfortunately rather limited in landward extent along strike.

The repetition of limestone and quartzose schist with respect to the position of the amphibolite probably implies that the latter inhabits the core of an isoclinal fold which repeats beds on either side.

The limestones vary in colour from blue to grey, and contain less terrigenous material than those described previously. There are however many thin (1-10mm) stringers of silty material, some of which show a high degree of simple folding. Again quartz segregations are common and large (<30cm) in the non-calcareous rocks but virtually absent in the limestone and amphibolite. The bluish limestone at the edge of the exposure contains a network of very fine (1mm) quartz veins. This rock contains an H₂O-rich mineral assemblage -

qz + cc + czo + amph + ksp + bt,

and the remainder are -

qz + cc + dol + ksp + ms + bt

qz + cc + ksp + ms + bt.

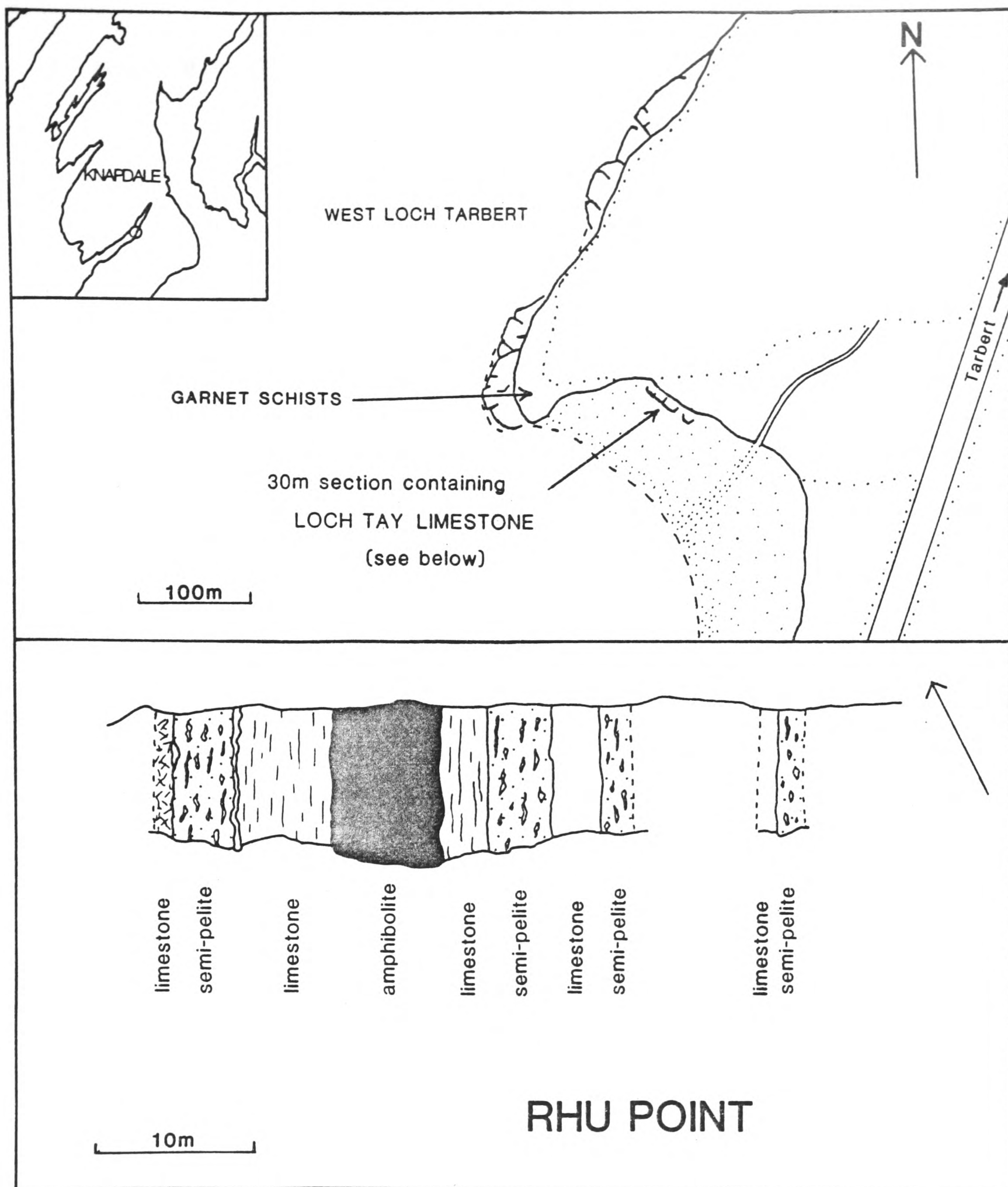


Figure 2.11: Upper half - location map of limestone exposures, Rhu Point, W. Loch Tarbert. Lower half - sketch section of limestone exposures, showing repetition of units about an amphibolite sill.

4. South Bay, Barmore

South Bay lies on the south side of Barmore Island on the western shore of Loch Fyne 2.5km north of Tarbert. The coastal exposure here (NR867.714), though steep and narrow, contains a near-complete section through the Loch Tay limestone and surrounding schists.

70m of typically thinly bedded, interlayered limestone and silt includes five separate amphibolite bodies (numbered 1-5, see Figure 2.12), none of which cross-cut sedimentary bedding. In places in the limestone units, carbonate-rich bands up to 10cm thick dominate, separated by thin (1cm), more resistant quartz-rich seams; elsewhere the rock is more pervasively quartz-rich. Throughout the section the bedded layering is sharp and prominent, often lensing, but sedimentary structures within the beds have been obliterated.

It is impossible to show unequivocally that this section comprises a series of tight isoclinal folds, but comparing overall limestone thickness with other localities, it does seem likely. If it is so, then folding was completed early on in the evolution of the section, as a fair amount of post-folding modification has taken place. In particular, zones of mineral assemblages are developed in each limestone unit (numbered A-F in Figure 2.12) which are distributed differently in each case. The section is also cut by several small faults.

To the NW of the limestones are poorly exposed quartz schists, in places red-stained, belonging to the Stonefield Schist Formation. To the SE a long section of Green Beds Formation schists contains many 'green beds' *sensu stricto*, and the albite schists described in Section 2.4.2.

In common with other localities, a marked distribution of quartz segregations is found, being very common in non-calcareous, and rare in calcareous (and amphibolite) rock types. A lot of small S2 folds can be seen in this area, especially in the semi-pelites, and the limestone B/ amphibolite II contact is folded in this way.



Figure 2.12a (upper photograph): South Bay exposure looking NW from junction of Loch Tay Limestone and Green Beds Schist.

Figure 2.12b (lower photograph): Detail of contact between Limestone B and Amphibolite 1.

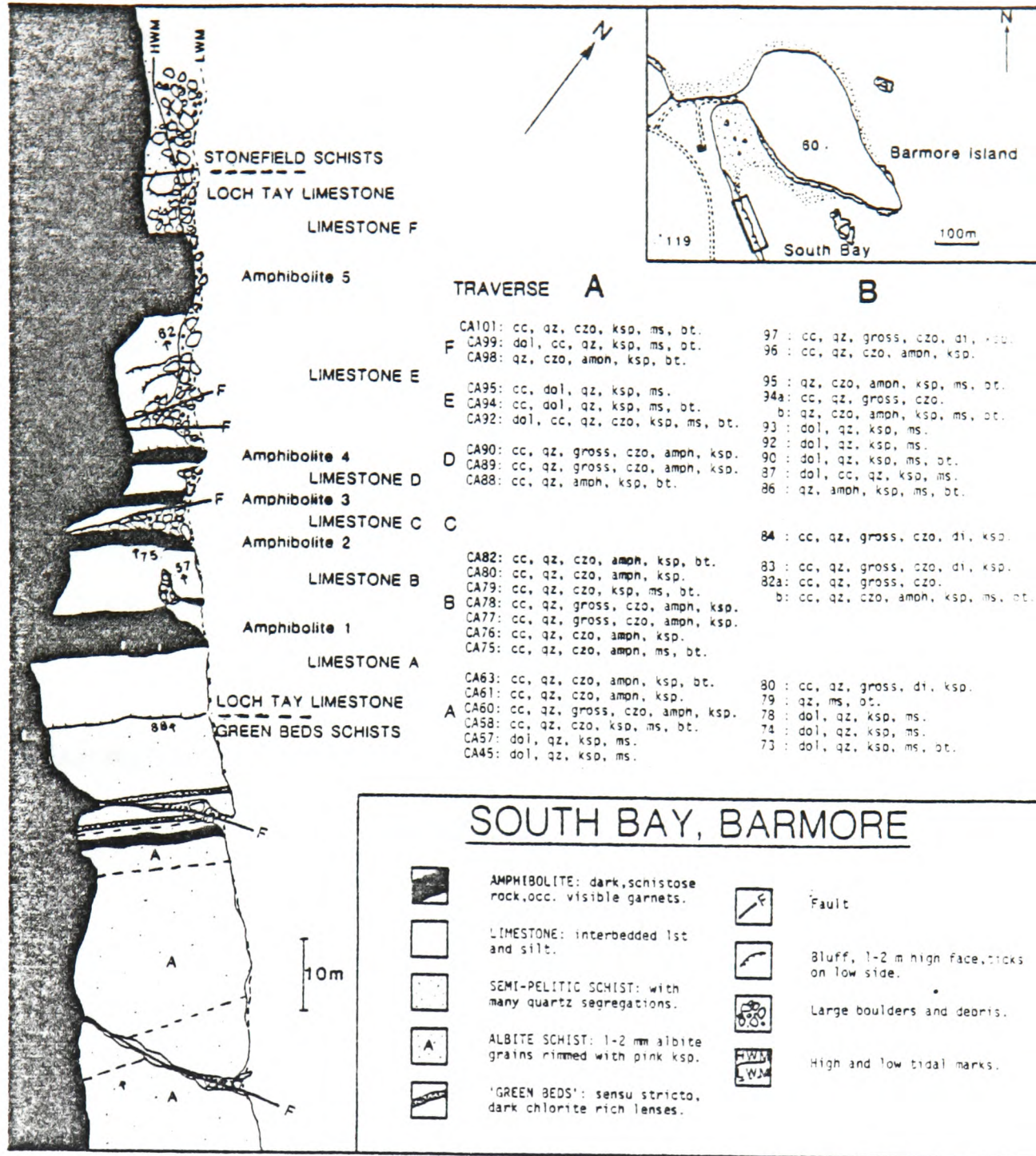


Figure 2.12c: Geological sketch map of South Bay, Barmore. Mineral assemblages in traverse A from this study, in traverse B from Graham *et al.* (1983). Note the repetition of amphibolite and limestone units, the variation in mineral assemblage in each limestone unit, and the distribution of secondary, dolomite-bearing assemblages.



The spatial distribution of mineral assemblages within each limestone unit is presented in Figure 2.12, which includes the previous samples described in Graham *et al.* (1983). These are by no means a complete description, since two or more assemblages may be found in a single thin section (see Section 4.2, Plates 4.9 and 4.10), and samples in these traverses were taken at 0.5m or more intervals. Assemblages vary greatly from band to band only, and not within a particular ^{10cm} bed, so in most places a single traverse was sufficient. Diopside has been found only in a few samples (compare Figures 2.12A and B). The probable reason for this is explained in Section 3.4. Obviously, more detailed sampling is necessary for exact definition of the spatial arrangement of assemblages. Consequently another traverse of samples, at smaller intervals, was made within Limestone B. The distribution of assemblages in this detailed subsection (see Figure 4.7) is described in Chapter 4.

2.4.4.3: Conclusions

The widespread, H₂O-rich nature of the mineral assemblages in the higher grade carbonates of Knapdale, make it obvious that metamorphic fluid, of an H₂O-rich nature, played a significant role in their metamorphic histories.

The great diversity and complex distribution of such assemblages in the South Bay section make it the obvious choice for more detailed study.

A necessary first step in such investigation, however, is the characterisation of the state variables of that carbonate system, and the construction of appropriate P-T-X_{fluid} diagrams using equilibrium thermodynamics. Hence this is the subject of the next chapter.

C H A P T E R 3: Equilibrium thermodynamics

3.1: Introduction

The objectives of this chapter are to outline the theory behind the use of equilibrium thermodynamics in metamorphic petrology, and to apply these methods to the example of the metacarbonate rocks of Knapdale. This involves, firstly, a brief discussion of the meaning of equilibrium in metamorphic systems, and of the assumptions involved in using equilibrium thermodynamic formulations. Secondly, the metacarbonate assemblages of Knapdale are broken up into phases and components and the Phase Rule used to construct a mineral reaction net, which is orientated in $T-X_{CO_2}$ space. This last stage involves further assumptions, about thermodynamic data, and these are described in full.

The result of this chapter, then, is a $T-X_{CO_2}$ section, which quantifies the conditions of formation of mineral assemblages in carbonates throughout Knapdale, and which is used in Chapter 4 to unravel the complicated history of the high grade rocks of South Bay, in order to define the behaviour of the fluid phase during that metamorphism.

3.2: Equilibrium

In some instances, for example the calcareous rocks of Beaver Brook, New Hampshire (Rumble *et al.*, 1982), the assumption that the mineral assemblages as they are found represent a state of equilibrium in a metamorphic process, is an easy one. In these rocks virtually all the criteria for the identification of chemical equilibrium between minerals

are satisfied, for example, lack of reaction textures between or within mineral grains, chemical homogeneity of minerals, constancy of cation ratio between mineral pairs, and little or no spatial or mineralogical variation in stable isotopic composition. So in that and other similar cases the logical next step of the assumption of applicability of equilibrium thermodynamics for the quantitative treatment of the chemical system is a correspondingly easy one.

This situation is probably the exception rather than the rule. Most metamorphic rocks when looked at in detail will reveal some evidence of disequilibrium, which underlines the general importance of kinetics in metamorphic processes. In mineral assemblages whose metamorphic histories are controlled by the presence of supercritical fluids of variable composition in greater or lesser amounts it is perhaps unreasonable to assume that simple equilibrium states were possible in a system which probably involved movement of mass, heat and electrical charge, not to mention chemical reaction.

The problem can be reduced to one of scale. If small enough elements are considered within a system (2-3mm in the Beaver Brook rocks described by Rumble *et al.*, 1982), each element can be seen as an isolated microenvironment in which equilibrium is attained, and the whole system is a mosaic of equilibria.

In fact, as discussed by Korzhinskii (1959), such a system, in Mosaic Equilibrium, really represents a stationary (or time-independent) state rather than an equilibrium one, since gradients of intensive parameters exist in it, which determine the course of the stationary processes (or flows of matter, heat etc.). The difference between stationary and non-equilibrium states is that in the former, intensive parameters are constant in time, although they do vary from point to point (or element to element).

So with the assumption of local equilibrium, which is often not demonstrable, being merely a reduction of element size to an imaginary necessary minimum, the use of equilibrium thermodynamics is thereby justified. In practice,

the choice of equilibrium domains is based on a mineral phase, or thin section scale, since this allows the use of the Phase Rule to generate mineral reactions, and study the relationships between different mineral assemblages

This means choosing to ignore smaller scale evidence of disequilibrium, such as variations of Fe/Mg ratio between or within phases. These variations may in any case be the result of retrograde processes.

3.3: Components and the Phase Rule

The choices and assumptions involved in the selection of components in any system is more difficult. The petrological world has never been completely happy with the distinction by Korzhinskii (trans. 1959), endorsed by J.B.Thompson(1957), of "inert" and "perfectly mobile" components. In part this probably stems from a lack of understanding of equilibrium and of variations in intensive and extensive parameters, and in part definitely from the ambiguities and genetic connotations in the terms themselves. For example, the $\delta^{13}\text{C}$ and $\delta^{18}\text{O}$ values of Tayvallich limestones (Graham et al., 1983) show that these rocks have experienced infiltration of a CO_2 -rich fluid (i.e. a 'physically' mobile component). Furthermore, CO_2 behaved as a 'perfectly mobile' component with respect to $\delta^{18}\text{O}$ values. However, it behaved as an 'inert' component with respect to $\delta^{13}\text{C}$ values, because the mass balance of carbon between the fluid and the rock was such that the $\delta^{13}\text{C}$ value of the rock was unaffected by that of the infiltrating fluid. This is an example of the ambiguity of the term 'mobile', and also illustrates how a component may behave differently with respect to different other components, at the same time.

The review by Rumble(1983) of the meaning and applicability of the terms goes to the logical extreme of treating them as precisely defined categories, into which all components in a rock system may be separated. The

problems in rigorously doing this are immense, because a strictly applied label "perfectly mobile" for one particular component involves elimination of all possibility of that component displaying any "inert" behaviour in any reaction with any other component in the system, so the complete chemistry and chemical history of the rocks must be known. Defined in this precise way the terms "inert" and "perfectly mobile" are of limited use.

In a less rigorous way, however, these terms are useful to distinguish the two broadly different types of behaviour of components in open systems. "Inert" components are those for which exchange between the system and the external medium is difficult (implying lack of physical mobility, or slow kinetics), so that in effect obeying closed system rules, extensive parameters of these components are factors of equilibrium of the system. In contrast, intensive parameters of "perfectly mobile" components are factors of equilibrium of the system, since their masses can change instantly in response to changes in chemical potential in the external medium. This separation of inert from perfectly mobile is of fundamental use in the application of the Phase Rule to mineralogical systems.

A set of components for a generalised system in equilibrium may thus be described (after Korzhinskii , 1959) in terms of -

- A. the perfectly mobile components
- B. the inert components, which include:
 - (i) trace components
 - (ii) isomorphous components
 - (iii) accessory (or indifferent) components
 - (iv) excess components
 - (v) determining inert components

The system representing metacarbonate rocks in Knapdale in general, and those of the South Bay section in particular, is made up of the following end-member mineral phases -

quartz, dolomite, calcite, grossular, diopside, clinozoisite, tremolite, albite, Kfeldspar, clinocllore, phlogopite, muscovite, sphene and rutile.

These phases can be described by the components -

CaO, MgO, SiO₂, Al₂O₃, FeO, K₂O, Na₂O, TiO₂, CO₂ and H₂O

which can be simplified thus -

A. perfectly mobile: CO₂, H₂O

B. inert:

(i) trace: -

(ii) isomorphous: FeO and MgO

(iii) accessory: Na₂O (appears only in albite)

(iv) excess: SiO₂ (quartz always present)

(v) determining inert: Al₂O₃, MFO, CaO, K₂O, TiO₂

TiO₂ may be neglected, since it occurs only in small amounts relative to the whole system, and when it does appear, as either rutile or sphene, may simply be added to the relevant parts of a paragenetic diagram. Also, only one reaction relating the two TiO₂-bearing phases is recognised, and this may similarly be added to T-X_{CO2} or P-T diagrams at a later stage.

Further, both grossular and diopside appear to be formed as a result of only one reaction in each case. Removing these phases from the computation of reactions simplifies matters considerably.

The system left after these simplifications contains 4 determining inert components -

K₂O, MFO, CaO and Al₂O₃,

and 8 phases -

tremolite, clinozoisite, clinocllore, phlogopite, muscovite,

Kfeldspar, calcite and dolomite.

i.e. $P = C + 4$. From the Phase Rule -

$$F = C + 2 - (C + 4) = -2,$$

it is therefore a multisystem with two negative degrees of freedom. The number of invariant points in it is equal to the number of $(C + 4)$ phases taken $(C + 2)$ at a time.

or,

$$C + 4/C + 2 = (C + 4)(C + 3)/2 = 28$$

(for $C = 4$).

Similarly , the number of univariant lines is -

$$C + 4/C + 1 = 56.$$

In the South Bay rocks, carbonate (either dolomite or calcite or both) is always present. In addition, dolomite is never found along with clinozoisite, tremolite or biotite without calcite also being present. This means that a number of invariant points and univariant lines must be discarded. The effect is to reduce the invariant points to 21, and the univariant lines to 35.

A full listing of these reactions was obtained using the program "Reaction" (Finger & Burt, 1972), and the 35 are reduced to 15 by degeneracy. These 15 reactions, plus the diopside and grossular forming reactions, are listed in Table 3.1.

Bundles of invariant lines associated with each invariant point can be combined to form a net which can be represented graphically in several ways. This can be done either (i) purely theoretically, or (ii) using thermodynamic data to calculate the position of each reaction in some

No.	Reaction
1	$8\text{qz} + 5\text{dol} + 1\text{H}_2\text{O} = 1\text{trem} + 3\text{cc} + 7\text{CO}_2$
2	$6\text{qz} + 4\text{cc} + 3\text{ms} = 2\text{czo} + 3\text{ksp} + 4\text{CO}_2 + 2\text{H}_2\text{O}$
3	$21\text{qz} + 10\text{cc} + 3\text{chl} = 3\text{trem} + 2\text{czo} + 10\text{CO}_2 + 8\text{H}_2\text{O}$
4	$24\text{qz} + 6\text{cc} + 5\text{bt} = 3\text{trem} + 5\text{ksp} + 6\text{CO}_2 + 2\text{H}_2\text{O}$
10	$3\text{qz} + 5\text{cc} + 2\text{czo} = 3\text{gross} + 5\text{CO}_2 + 1\text{H}_2\text{O}$
11	$2\text{qz} + 3\text{cc} + 1\text{trem} = 5\text{di} + 3\text{CO}_2 + 1\text{H}_2\text{O}$
100	$3\text{chl} + 8\text{ksp} = 9\text{qz} + 5\text{bt} + 3\text{ms} + 4\text{H}_2\text{O}$
101	$3\text{dol} + 1\text{ksp} + 1\text{H}_2\text{O} = 3\text{cc} + 1\text{bt} + 3\text{CO}_2$
200	$3\text{qz} + 15\text{dol} + 2\text{czo} + 11\text{H}_2\text{O} = 19\text{cc} + 3\text{chl} + 11\text{CO}_2$
300	$3\text{qz} + 5\text{dol} + 1\text{ms} + 3\text{H}_2\text{O} = 5\text{cc} + 1\text{chl} + 1\text{ksp} + 5\text{CO}_2$
301	$3\text{qz} + 8\text{dol} + 1\text{ms} + 4\text{H}_2\text{O} = 8\text{cc} + 1\text{chl} + 1\text{bt} + 8\text{CO}_2$
314	$6\text{qz} + 9\text{dol} + 3\text{ms} + 1\text{H}_2\text{O} = 5\text{cc} + 2\text{czo} + 3\text{bt} + 13\text{CO}_2$
319	$21\text{qz} + 32\text{cc} + 9\text{chl} + 15\text{ms} = 16\text{czo} + 15\text{bt} + 32\text{CO}_2 + 28\text{H}_2\text{O}$
322	$4\text{cc} + 3\text{chl} + 5\text{ksp} = 3\text{qz} + 2\text{czo} + 5\text{bt} + 4\text{CO}_2 + 6\text{H}_2\text{O}$
411	$5\text{qz} + 2\text{cc} + 1\text{chl} + 1\text{ksp} = 1\text{trem} + 1\text{ms} + 2\text{CO}_2 + 2\text{H}_2\text{O}$
414	$49\text{qz} + 16\text{cc} + 5\text{chl} + 5\text{bt} = 8\text{trem} + 5\text{ms} + 16\text{CO}_2 + 12\text{H}_2\text{O}$
446	$2\text{cc} + 9\text{trem} + 15\text{ms} = 42\text{qz} + 10\text{czo} + 15\text{bt} + 2\text{CO}_2 + 4\text{H}_2\text{O}$

Table 3.1: End-member mineral reactions in the Knapdale metacarbonate system.

co-ordinate system.

Thus: (i) For the theoretical approach, it is easier to draw the net in μ - μ space, (here for instance $\mu_{\text{H}_2\text{O}} - \mu_{\text{CO}_2}$), because with such co-ordinates the univariant lines are straight, and have slopes equal to -

$$-\Delta N_{\text{CO}_2} / \Delta N_{\text{H}_2\text{O}}$$

of the reaction. However, with a lack of knowledge of the absolute position of invariant points, for a system where $F = -2$, the relative position of a minimum of 3 invariant points must be estimated. Ultimately the vindication of such a choice lies in the observed relative stabilities of the mineral assemblages themselves. Furthermore, the assumption of the relative stability or metastability of the necessary number (again 3 here) of invariant points must be made, and this can only be verified with reference to the mineral assemblage actually seen.

The $\mu_{\text{H}_2\text{O}} - \mu_{\text{CO}_2}$ diagram constructed using these rules and assumptions is presented in Figure 3.1 .

(ii) The construction of the net in T - X_{CO_2} or P - T space can also be accomplished from first principles, but this is more difficult due to the curved form of the univariant lines. It is easier to calculate the position of each curve and plot them together to form the net. This method obviously depends on having a) a correct formulation of the equation of each curve, and b) correct thermodynamic data for each reaction (or at least an internally consistent data set).

Of course the ultimate test of these (and of the μ - μ diagram) is that the net so drawn is of the form demanded by the purely graphical rules of Schreinemakers, which constrain the relative positions of reactions emanating from each invariant point.

The construction of the T - X_{CO_2} reaction net presented in this thesis was first achieved theoretically, as an extension of the method used to construct the $\mu_{\text{H}_2\text{O}} - \mu_{\text{CO}_2}$ diagram. It was later refined, however, and positioned

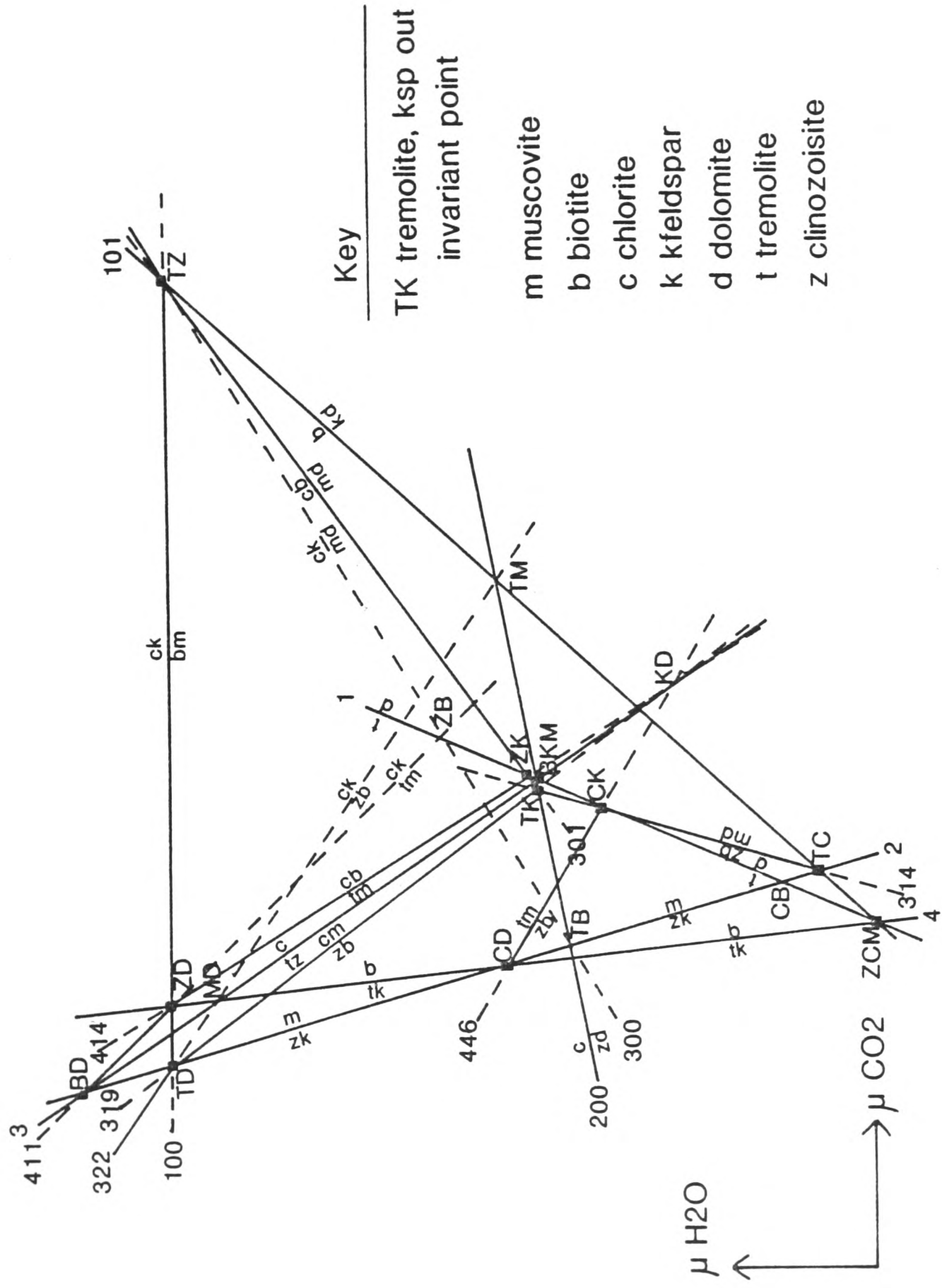


Figure 3.1: Reaction net for the Knapdale metacarbonate system, orientated in $\mu_{H_2O} - \mu_{CO_2}$ space. Topology of net constrained by Schreinermakers graphical rule.

correctly in $T-X_{CO_2}$ space using equilibrium thermodynamic formulations and data of which the next section is a detailed description.

3.4: Thermodynamic formulation and data

The equation used to calculate the position of a reaction in $T-X_{CO_2}$ space is defined thus: (see Appendix A for symbols)

At equilibrium,

$$\Delta\mu_{\text{reaction}} = 0,$$

and,

$$\Delta\mu_{\text{reaction}} = \Delta G^0 + RT \ln K$$

Now,

$$\Delta G_{P,T}^0 = \Delta H_{1,298} + \int_{298}^T \Delta C_p dt - T[\Delta S_{1,298} + \int_{298}^T \Delta C_p T^{-1} dt] + \int_1^P \Delta V_s dP + RT \ln (f_{CO_2}^0)^n (f_{H_2O}^0)^m, \dots \text{Equation (3.1)}$$

and,

$$RT \ln K = RT \ln K_s + RT \ln (a_{CO_2})^n (a_{H_2O})^m$$

Therefore,

$$\Delta\mu_{\text{reaction}} = 0$$

implies:

$$0 = \Delta H_{1,298} + \int_{298}^T \Delta C_p dt - T[\Delta S_{1,298} + \int_{298}^T \Delta C_p T^{-1} dt] + \int_1^P \Delta V_s dP + nRT \ln f_{CO_2}^0 a_{CO_2} + mRT \ln f_{H_2O}^0 a_{H_2O} + RT \ln K_s \dots \dots (3.2)$$

Inherent in this formulation is the assumption of a binary CO_2 - H_2O fluid phase. This seems reasonable in view of the absence of graphite from all assemblages, but less so when such species as NaCl are considered. For the moment, however, NaCl will be neglected, although it is acknowledged that if present, it may have a significant effect on T- X_{CO_2} topologies (Kerrick & Jacobs, 1981; Bowers & Helgeson, 1983).

Three distinct groups of data are required in Equation (3.2), namely

- i) entropies, heat capacities, volumes of solids, enthalpies
- (ii) fugacities of gases, activities of gases
- (iii) activities of solids

(i) The first three are relatively well known at 1 bar and 298 K, but the fourth is more problematical. Currently used enthalpy data is a combination of solution calorimetry results (e.g. Navrotsky *et al.*, 1980) and results interpolated from direct experiments on reaction positions in P-T- X_{fluid} space (e.g. Hewitt, 1975; Gordon & Greenwood, 1971). Any data set made up of results culled from many different sources should be organised and adjusted in such a way that it is internally consistent (i.e. linear combinations of reaction data should correctly predict that of other reactions). Very few such data sets have been published, but two that have are Powell(1978) and Helgeson *et al.* (1978). The latter has been used for most of the reactions presented here.

(ii) For the pressures and temperatures of interest, the mixing of CO_2 and H_2O is highly non-ideal. For this reason the Hard Sphere Modified Redlich-Kwong equation of state of Kerrick & Jacobs(1981) was used to calculate pure H_2O and CO_2 fugacities, and activities of CO_2 - H_2O mixtures. This equation, although essentially empirically derived, results in close agreement between the calculated and experimentally derived positions of reactions involving CO_2 - H_2O mixed

volatiles at pressures up to 6 kb (Jacobs & Kerrick, 1981).

(iii) Activities of solid phases were calculated using activity - composition relationships after Powell(1978) of ideal mixing on sites, and are the same formulations as detailed in Graham *et al.* (1983), (see Figure 3.2). Representative analyses of mineral phases from South Bay are presented in Table 3.2.

In the calculations using Equation (1), several simplifications can be made, and these approaches are quantitatively compared in the following section.

a) $\Delta V_s = \text{constant}$. Justification for this lies in the small and cancelling effects of the low coefficients of thermal expansion and compressibility for solid minerals (Holland, 1981; Helgeson *et al.*, 1978). With this assumption the term $\int_1^P \Delta V_s \cdot dP$ in Equation (1) can be replaced by $\Delta V_s (P-1)$.

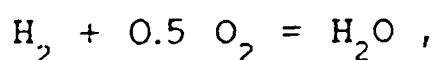
b) $\Delta C_p = 0$. This is a fairly reasonable assumption if solid-solid reactions are being considered, but not so for devolatilization reactions, as

$$C_{p_{H_2O, \text{fluid}}} > C_{p_{H_2O, \text{structural}}}$$

c) $\Delta C_p = \text{constant}$, r , so that the integral terms in Equation (1) reduce to -

$$F(C_p) = r(T-298) - rT \ln(T/298)$$

Fisher & Zen(1971) noted that a good approximation to the ΔC_p per mole of H_2O evolved in a dehydration reaction is given by ΔC_p of the reaction -



which they quoted as around 9 J. In fact they make the approximation that this value is acceptable in the range

End-member	Composition	Activity formulation	Range of activities
muscovite	$\text{KA1}_2\text{Si}_3\text{AlO}_{10}(\text{OH})_2$	$9.48 \cdot X_{\text{K,A}} \cdot (X_{\text{Al,M2}})^2 \cdot X_{\text{O,M1}} \cdot X_{\text{Al,T}} \cdot (X_{\text{Si,T}})^3 \cdot (X_{\text{OH,V}})^2$	0.467-0.493
celadonite	$\text{KMgAlSi}_4\text{O}_{10}(\text{OH})_2$	$4 \cdot X_{\text{K,A}} \cdot X_{\text{Mg,M2}} \cdot X_{\text{Al,M2}} \cdot X_{\text{O,M1}} \cdot (X_{\text{Si,T}})^4 \cdot (X_{\text{OH,V}})^2$	0.226-0.245
phlogopite	$\text{KMg}_3\text{Si}_3\text{AlO}_{10}(\text{OH})_2$	$9.48 \cdot X_{\text{K,A}} \cdot X_{\text{Mg,M1}} \cdot (X_{\text{Mg,M2}})^2 \cdot X_{\text{Al,T}} \cdot (X_{\text{Si,T}})^3 \cdot (X_{\text{OH,V}})^2$	0.090-0.177*
tremolite	$\text{Ca}_2\text{Mg}_5\text{Si}_8\text{O}_{22}(\text{OH})_2$	$X_{\text{O,A}} \cdot (X_{\text{Ca,M4}})^2 \cdot (X_{\text{Mg,M13}})^3 \cdot (X_{\text{Mg,M2}})^2 \cdot (X_{\text{Si,T1}})^4 \cdot (X_{\text{OH,V}})^2$	0.066-0.213
clinozoisite	$\text{Ca}_2\text{Al}_3\text{Si}_3\text{O}_{12}(\text{OH})$	$X_{\text{Al,M3}}$	0.82-0.96
grossular	$\text{Ca}_3\text{Al}_2\text{Si}_3\text{O}_{12}$	$(\text{Ca}/\text{Ca} + \text{Mg} + \text{Mn} + \text{Fe})^3$	0.98
Kfeldspar	KAlSi_3O_8	$\text{K}/\text{K} + \text{Na} + \text{Ca}$	0.95
albite	$\text{NaAlSi}_3\text{O}_8$	$\text{Na}/\text{K} + \text{Na} + \text{Ca}$	1.00
calcite	CaCO_3	$X_{\text{Ca,CC}}$	0.96-1.00
dolomite	$\text{CaMg}(\text{CO}_3)_2$	$X_{\text{Ca,M2}} \cdot X_{\text{Mg,M1}}$	1.00

Figure 3.2: Activity - composition formulations for end-member minerals in metacarbonates, after Graham *et al.* (1983), and activities calculated from probe analyses, representative values of which are given in Table 3.2. Note the small range of activities for all minerals, and the purity of grossular, Kfeldspar, albite, calcite and dolomite.

	1	2	3	4	5	6
SiO2	50.40	50.37	51.01	37.24	39.90	55.02
TiO2	0.19	0.08	0.07	1.03	0.48	0.06
Al2O3	27.79	28.00	26.91	16.77	14.84	1.94
FeO	1.83	1.83	1.91	16.18	11.53	8.49
MnO	nd	nd	nd	0.13	0.01	0.14
MgO	3.31	3.42	3.49	13.05	17.74	18.05
CaO	nd	0.01	0.17	nd	0.14	12.55
Na2O	0.17	0.16	0.11	0.07	0.05	0.35
K2O	10.58	10.60	10.70	8.86	9.11	0.08
total=	94.27	94.47	94.37	93.33	93.80	96.68
Si	6.78	6.76	6.86	5.67	5.90	7.83
Ti	0.02	-	-	0.12	0.05	-
Al	4.40	4.43	4.26	3.01	2.58	0.33
Fe2	0.21	0.21	0.21	2.06	1.43	1.01
Mn	-	-	-	0.02	-	0.02
Mg	0.66	0.68	0.70	2.96	3.91	3.83
Ca	-	-	0.02	-	0.02	1.91
Na	0.04	0.04	0.03	0.02	0.01	0.10
K	1.81	1.81	1.84	1.72	1.72	0.01
total=	13.93	13.95	13.93	15.58	15.62	15.05
oxygens=	[22]	[22]	[22]	[22]	[22]	[23]
1 MU1/X6NA		3 MU1/X19N		5 BI1/X19N		
2 MU3/X6NA		4 BI1/X1N		6 AM1/X6NA		
	7	8	9	10	11	12
SiO2	55.62	55.54	55.11	38.29	41.25	38.84
TiO2	0.01	nd	nd	0.21	0.63	0.23
Al2O3	2.92	2.64	3.55	27.09	26.42	27.67
FeO	8.55	9.73	9.01	7.19	5.32	6.12
MnO	0.15	0.09	0.16	0.06	0.09	0.13
MgO	17.45	16.76	17.19	0.05	0.08	0.06
CaO	12.36	12.27	12.23	23.47	22.79	23.93
Na2O	0.45	0.40	0.55	0.02	0.02	0.02
K2O	0.17	0.11	0.19	nd	nd	nd
total=	97.68	97.54	97.99	96.38	96.60	97.00
Si	7.82	7.86	7.75	3.19	3.37	3.20
Ti	-	-	-	0.01	0.04	0.01
Al	0.48	0.44	0.59	2.66	2.54	2.68
Fe2	1.01	1.15	1.06	0.50	0.36	0.42
Mn	0.02	0.01	0.02	-	-	-
Mg	3.66	3.53	3.60	-	-	-
Ca	1.86	1.86	1.84	2.09	1.99	2.11
Na	0.12	0.11	0.15	-	-	-
K	0.03	0.02	0.03	-	-	-
total=	15.01	14.99	15.05	8.47	8.32	8.45
oxygens=	[23]	[23]	[23]	[13]	[13]	[13]
7 AM330/CA88		9 AM361/CA88		11 EP4/X1N		
8 AM340/CA88		10 EP1/X1N		12 EP140/CA74		
	13	14	15	16	17	
SiO2	41.51	39.16	63.28	65.85	69.69	
TiO2	1.54	0.15	nd	nd	0.01	
Al2O3	20.20	20.89	18.33	18.31	19.34	
FeO	0.63	0.91	0.10	0.07	nd	
MnO	0.01	nd	nd	nd	nd	
MgO	0.01	nd	0.02	0.02	nd	
CaO	35.51	36.21	0.29	0.06	nd	
Na2O	0.05	0.05	0.13	0.54	11.86	
K2O	nd	nd	15.87	15.91	0.07	
total=	99.46	97.37	98.02	100.76	100.97	
Si	3.12	3.03	11.94	12.05	12.05	
Ti	0.09	-	-	-	-	
Al	1.79	1.91	4.08	3.95	3.94	
Fe2	0.04	0.06	0.02	0.01	-	
Ca	2.86	3.00	0.06	0.01	-	
Na	-	-	0.05	0.19	3.97	
K	-	-	3.82	3.71	0.02	
total=	7.90	8.01	19.96	19.93	19.98	
oxygens=	[12]	[12]	[32]	[32]	[32]	
13 GT1/X12W		15 AF1/X12W		17 PL1/X19N		
14 GT3/X12W		16 AF1/X19N				

Table 3.2: Representative probe analyses of minerals in the Knapdale high grade carbonates. Mineral numbers and rock samples given below each block of analyses. MU = muscovite, BI = biotite, AM = amphibole, EP = clinozoisite, GT = grossular, AF = Kfeldspar, PL = albite. For full probe data compilation see Appendix C.

600-1100 K, so the integral terms become a linear function of the form -

$$F(C_p) = p + qT$$

in fact quoted as:

$$F(C_p) = m(-4580 + 9.245T) \pm 150 \text{ J},$$

where m is the stoichiometric coefficient of H_2O . Holland(1981) has suggested a similar approach for decarbonation reactions, assuming linear $F(C_p)$ between 500-1200 K, resulting in the values -

$$F(C_p) = n(-9090 + 15.01T) \text{ J}.$$

Holland(1981) further suggests that the p and q values for dehydration reactions given by Fisher & Zen do not adequately represent the function $F(C_p)$ for most reactions, and that in fact each dehydration reaction has its own characteristic p and q constants. These can be back calculated from experimental work.

Powell(1978) considers the heat capacity difference between the free and structurally bound states of H_2O and CO_2 to be 13 J and 9 J respectively. Thus for the system considered here, assuming a linear $F(C_p)$ over the temperature range 723-823 K, these values give -

$$F(C_p) = (13m + 9n)(0.953T - 473.2) \text{ J},$$

where m and n represent the stoichiometric coefficients of H_2O and CO_2 respectively.

Combining the linear $F(C_p)$ function for dehydration (Fisher & Zen) with that of decarbonation (Holland, 1981) results in the equation -

$$F(C_p) = -(4580m + 9090n) + T(9.245m + 15.01n) \text{ J},$$

which over the temperature range 723-823 K gives the Cp difference between free and structurally bound states as 9.67-9.7 J for H₂O, and 15.7-19.2 J for CO₂, which are obviously quite different from those given by Powell.

The ultimate test is comparison of the position of curves calculated using each of these F(Cp) assumptions with calculated by evaluating the integrals iteratively over small temperature ranges at each value of X_{CO₂}. Obviously, errors in the linear formulation will be compounded by high stoichiometric coefficients of H₂O and CO₂ in a particular reaction.

For reactions 2 and 4 from this system, calculated at 10kb using various assumptions (see Figure 3.3), both linear F(Cp) methods appear to closely approximate the "real" position of the curves over the X_{CO₂} range shown. This is probably due to the steepness of these reactions in this region. It is likely that the approximations deviate to a larger degree from the real curves around the mid-range of X_{CO₂} from 0.3 to 0.7.

d) T-X_{CO₂} curves presented later in this chapter have been calculated by full evaluation of the Cp integral terms, using Cp data from Helgeson *et al.* (1978), and a computer program written by D.R.M. Pattison, which iterates Equation (3.1) on temperature to $\Delta G^{\circ}_{P,T} = 0$, for each X_{CO₂} value.

Also to be noted from Figure 3.3 is the large effect use of real solid activities can have on the position of an invariant point in T-X_{CO₂} space. In this instance, invariant point [CD] lies at X_{CO₂} = 0.15 for end-members, but at X_{CO₂} = 0.003 when Fe/Mg substitution in minerals is taken into account. This means that the X_{CO₂} value of fluid in equilibrium with invariant assemblage [CD] is actually much lower than consideration of end-member phases only would suggest. Furthermore, real activities allow the prograde sequence of Reaction 2, followed by Reaction 4, to proceed at lower X_{CO₂} values, a sequence which is visible texturally in South Bay rocks.

The use of real solid activities in the mineral reaction calculations also explains an apparent inconsistency between

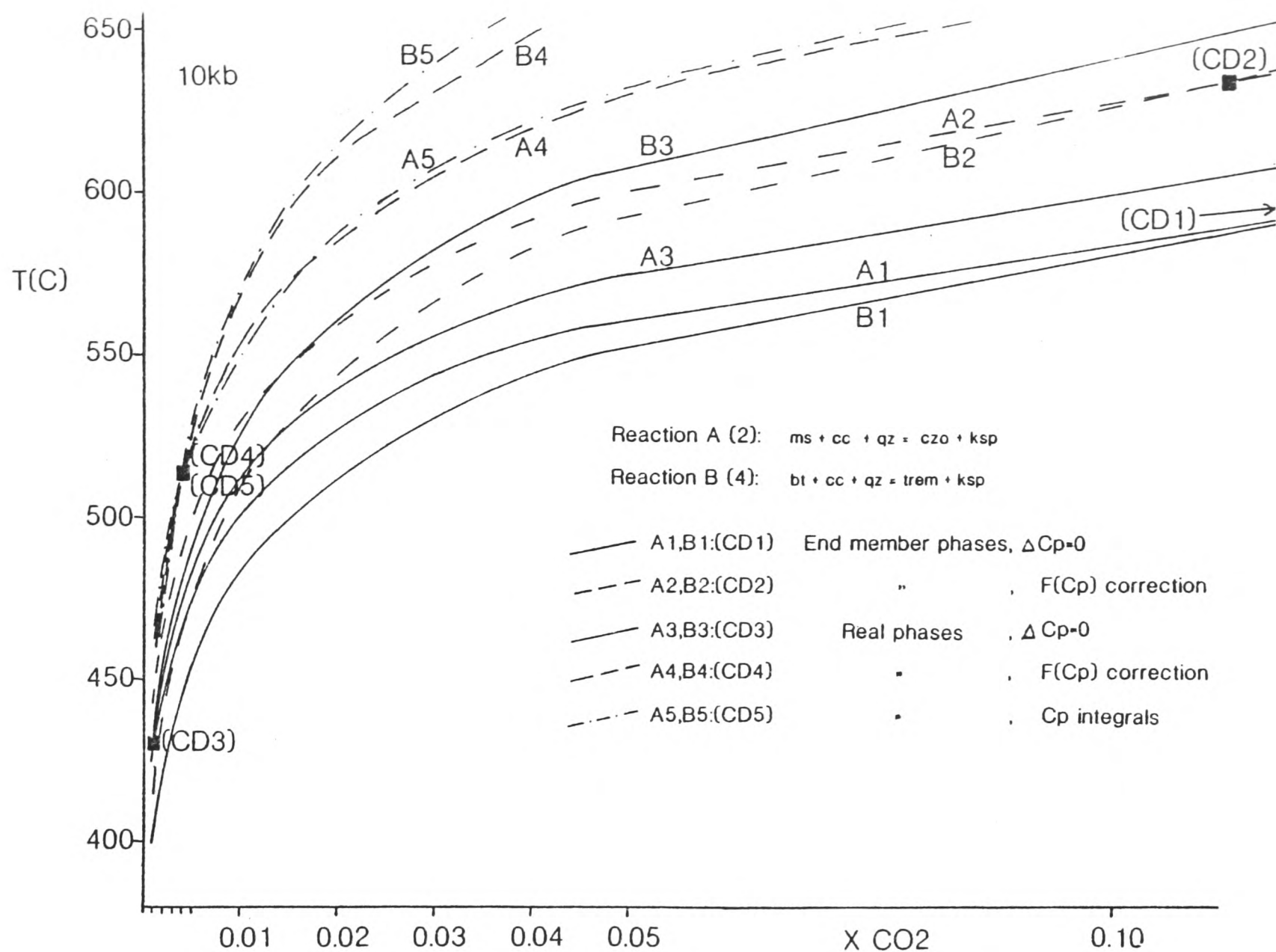
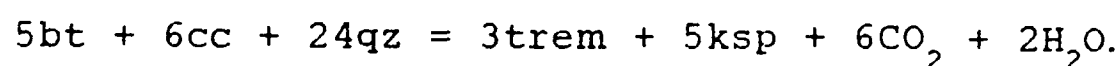


Figure 3.3: Comparison of Cp assumptions, showing the effect on the positions in $T-X_{CO_2}$ space of reactions 2 and 4, of various heat capacity formulations, combined with unit or measured solid activities. Note the large changes in the position of the invariant point [CD] brought about by the use of measured activities.

Figures 2.12A and B, namely the absence of diopside amongst the former assemblage list. This is because the position of the diopside producing reaction (11),



calculated with the measured average amphibole composition of Figure 3.2, lies on the lower temperature side of the main amphibole-producing reaction (4),



(see Figure 3.10). This explains the non-formation of diopside in the majority of the South Bay rocks. However, some rock layers must exist whose bulk composition is sufficiently Fe-rich (i.e. low tremolite activity) for reaction (11) to be placed at a higher temperature than reaction (4) in the X_{CO_2} range of interest.

Figure 3.4 shows how the relative positions of Reactions (11) and (4) are different when calculated with $a_{\text{trem,amph}} = 0.185$ (the average composition of Figure 3.2), and $a_{\text{trem,amph}} = 0.01$ (an Fe-rich bulk composition). Since the biotite activity in the Fe-rich case must also decrease, this was calculated by assuming that K_{solids} was the same in each case. The diagram shows how the diopside-bearing samples given in Figure 2.12B must represent Fe-rich layers in the limestone section which were unfortunately missed when the new collections, represented by Figures 2.12A, 4.6 and 4.7, were made.

3.5: Geobarometry and geothermometry

Few geobarometers are applicable to the rocks of Knapdale, largely because of the absence of any amount of

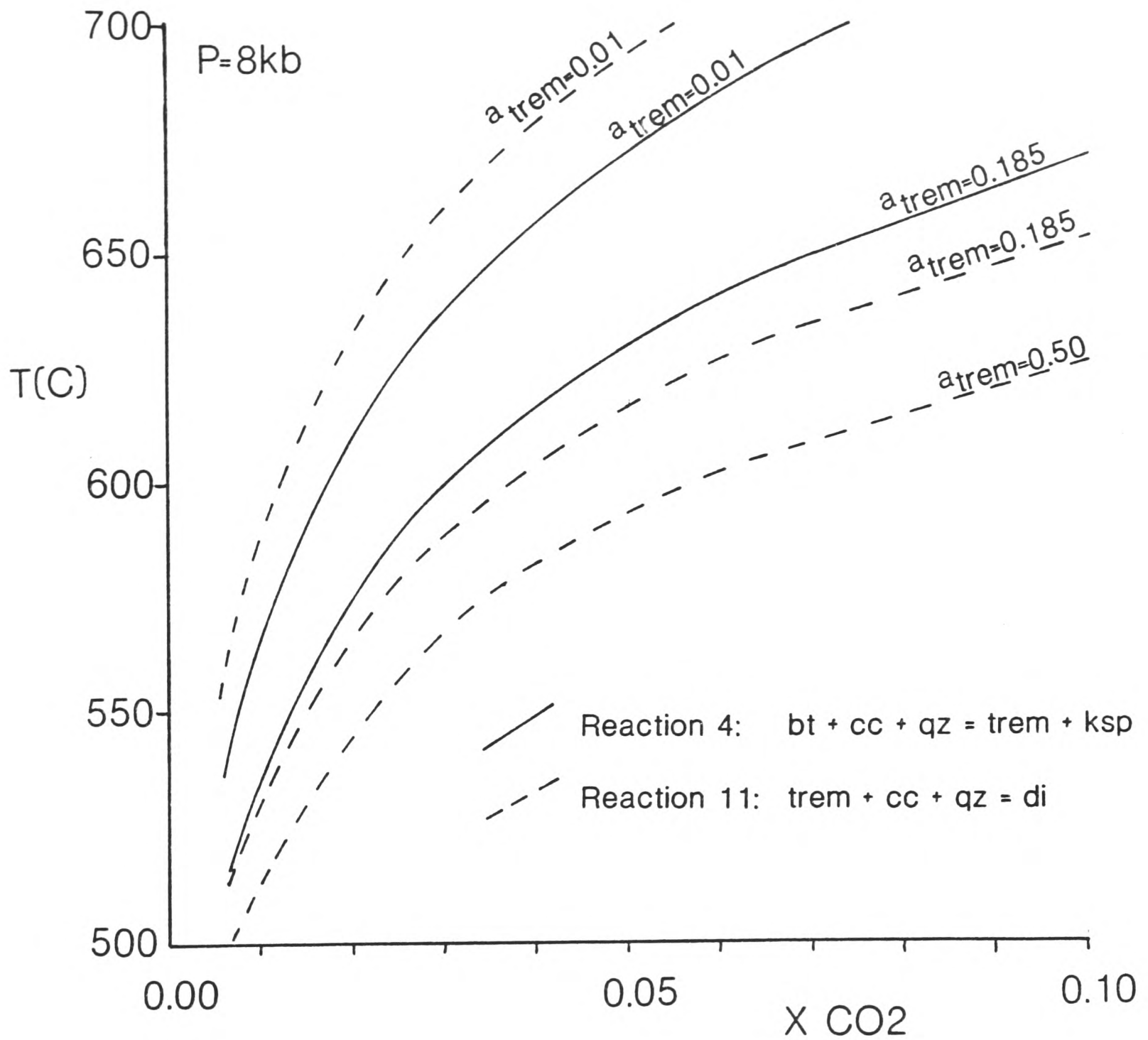
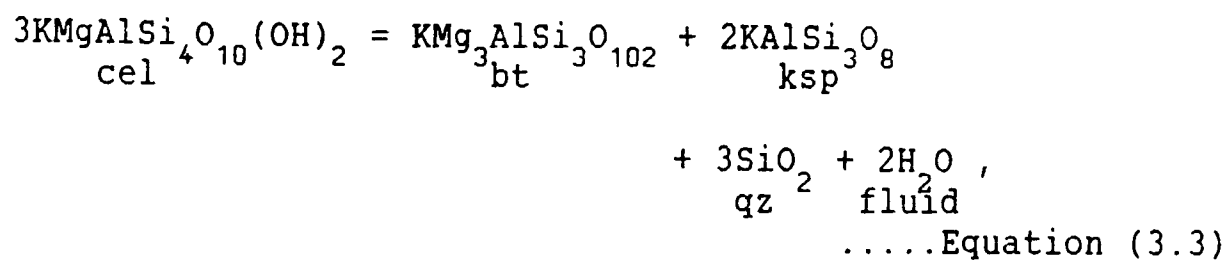
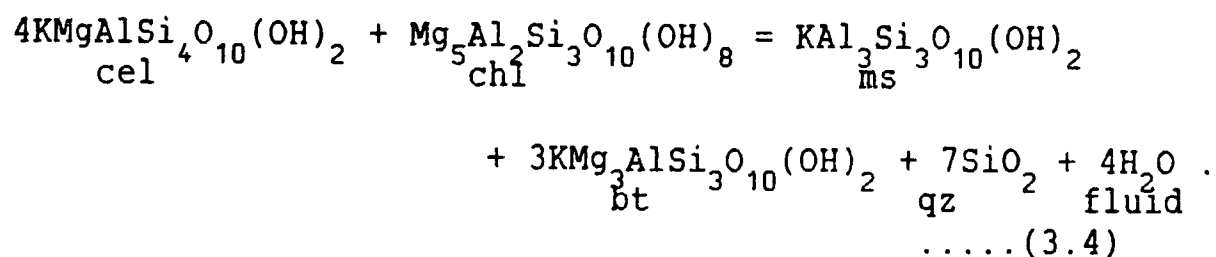


Figure 3.4: Comparison of the relative positions of reactions 4 and 11 in $T-X_{\text{CO}_2}$ space, using a range of solid activities. Measured $a_{\text{trem}} = 0.185$, $a_{\text{bt}} = 0.106$ (averages from Figure 3.2). Biotite activity for $a_{\text{trem}} = 0.01$ case calculated assuming constant K_D . a_{di} taken as 1.0 in each case. Note the switch in the relative positions of 4 and 11 for Fe-rich (low a_{trem}) compositions.

anorthite end-member in the plagioclase but two that can be used are the muscovite - biotite - Kfeldspar and phengite - biotite - chlorite barometers of Powell & Evans(1983), or the reactions -



and,



Pressures from these calculated over the whole of Knapdale, and from a range of rock types, give a consensus of around 8-10 kb (Graham, unpublished data, see Figure 3.5). Pressures calculated from carbonate assemblages at South Bay, however, using analyses from Table 3.2, are slightly lower, 6-8 kb. There are two main possible explanations for this apparent inconsistency in carbonate rock derived pressures - (i) these assemblages equilibrated at a later stage, at pressures lower than the metamorphic peak in surrounding rocks. (ii) the geobarometer is calculated for $a_{\text{H}_2\text{O}} = 1$, which is almost certainly not the case in carbonate rocks, and hence underestimates pressures.

However, recalculating the contour $\ln K = 5$ for the phengite - biotite - chlorite reaction using $X_{\text{CO}_2} = 0.05$ and 0.10, assuming the regular solution mixing model for $\text{H}_2\text{O}-\text{CO}_2$ of Powell(1978), shows only a slight repositioning of the line (see Figure 3.6). This adjustment results in variation in pressure estimates which is less than that demonstrated by the mineral assemblages themselves. Thus it seems likely that the higher $\ln K$ values calculated for some carbonate assemblages are real, and probably represent equilibration of

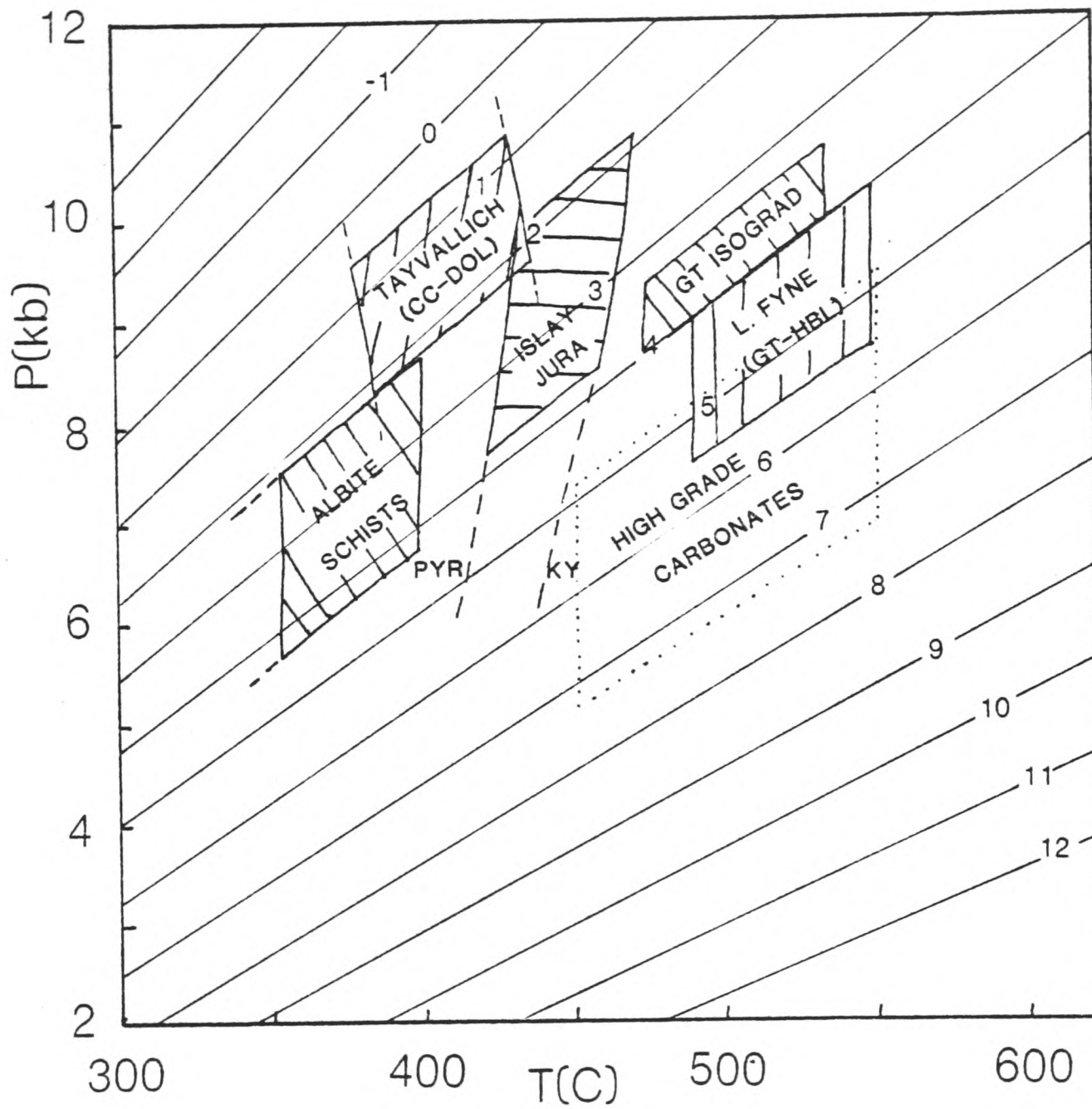


Figure 3.5: P-T data for SW Argyll rocks plotted on lnK contours of reaction 2 of Powell & Evans(1983). High grade carbonate data from this study, the rest (pelites) from Graham(unpubl. data). Carbonate values are significantly lower P than high grade pelite values.

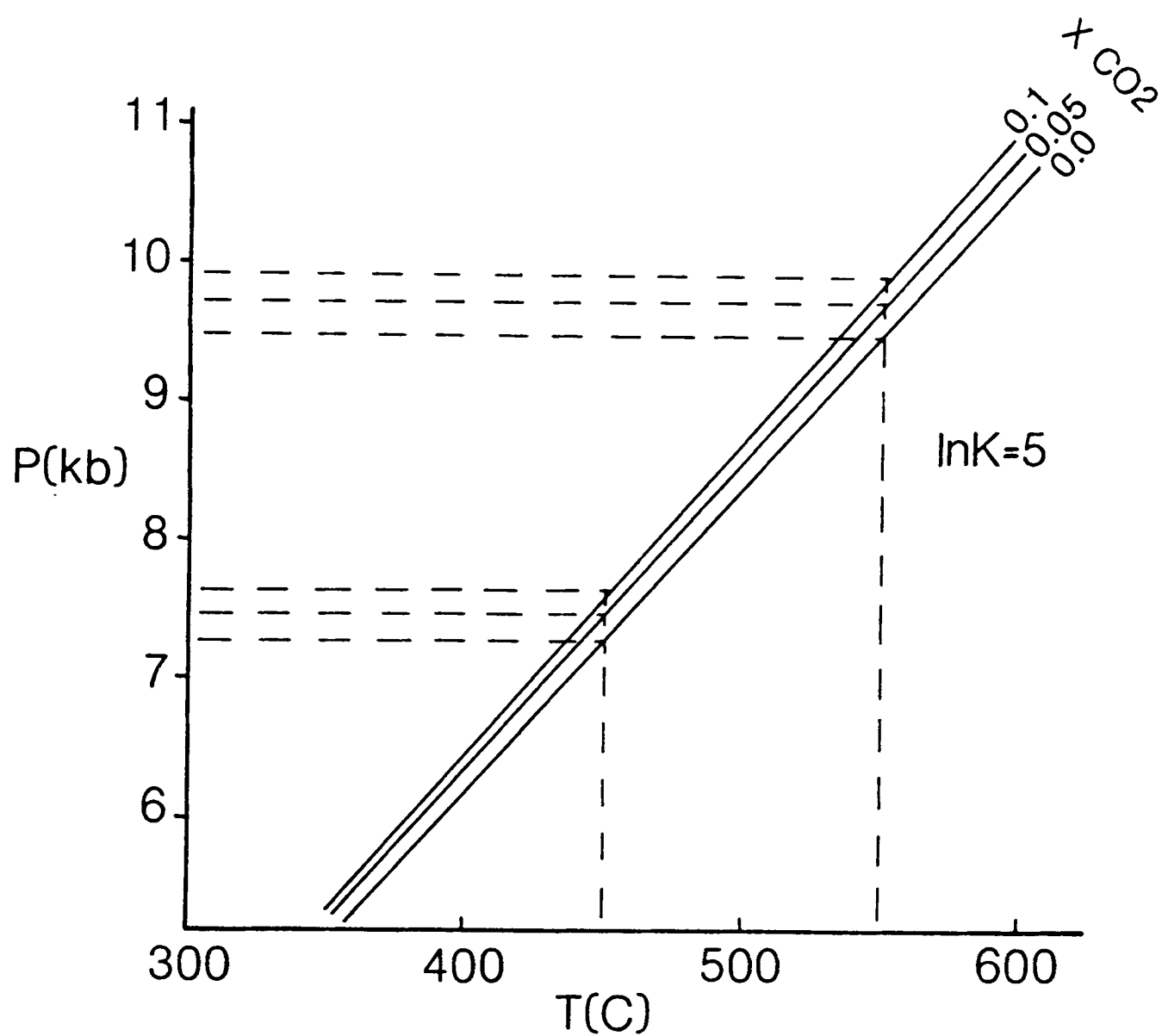


Figure 3.6: P-T position of $\ln K = 5$ contour of reaction 2 of Powell & Evans (1983), calculated for various X_{CO_2} values in an H_2O-CO_2 fluid. For peak metamorphic temperatures of $450-550^\circ C$, the various contours represent changes in P of less than 0.5 kb.

one or more phases at a later point on the P-T-time path.

Evidence that re-equilibration did take place in some other rocks is seen in $\ln K$ values for coexisting phengite + biotite + chlorite from albite schist assemblages. The range in $\ln K$ is mostly due to a measured variation in celadonite content of the white micas, which appears to decrease with increasing temperature, and vice versa (Figure 3.7, also Graham & Greig, in preparation). This is consistent with the continued regrowth of micas inferred from textural relationships in the albite schists, and with the overall model of metamorphic history of these rocks, as described in Chapter 2.

Temperature estimates for Knapdale rocks have been calculated using a variety of geothermometers: calcite-dolomite (Bickle & Powell, 1977) magnetite-ilmenite (Powell & Powell, 1977), garnet-hornblende (Graham & Powell, 1984), and garnet-biotite (Ferry & Spear, 1978; Hodges & Spear, 1983; Thompson, 1976; Holdaway & Lee, 1977; Pigage & Greenwood, 1982). The results (see Figure 3.8) show a range in temperature for peak metamorphism of roughly 400-550⁰C. These temperatures are primarily important in this study in that they determine the pressures calculated using the geobarometers, and the calculated fluid compositions. For the South Bay carbonate rocks, in view of the evidence stated above, it seems reasonable to choose a model pressure of 8 kb for the system, which is consistent with temperatures at the time of re-equilibration of around 500-550⁰C.

In conclusion, geobarometry and geothermometry in this study provides a check on the validity of modelling the carbonate system at 8 kb, and hence the construction of a T-X_{CO2} diagram at that pressure. In fact the use to which the calculated T-X_{CO2} diagrams are later put is not one demanding pin-point quantitative accuracy, but rather a semi-quantitative feel for the processes involved in the metamorphism of the carbonates. This is perhaps just as well, for the numerous inaccuracies and assumptions involved

GARNET ZONE

- psammites & pelites
- × albite schists
- ⊙ inclusion in albite schist
- + high grade carbonates

BIOTITE ZONE

- psammites & pelites
- ▲ basites

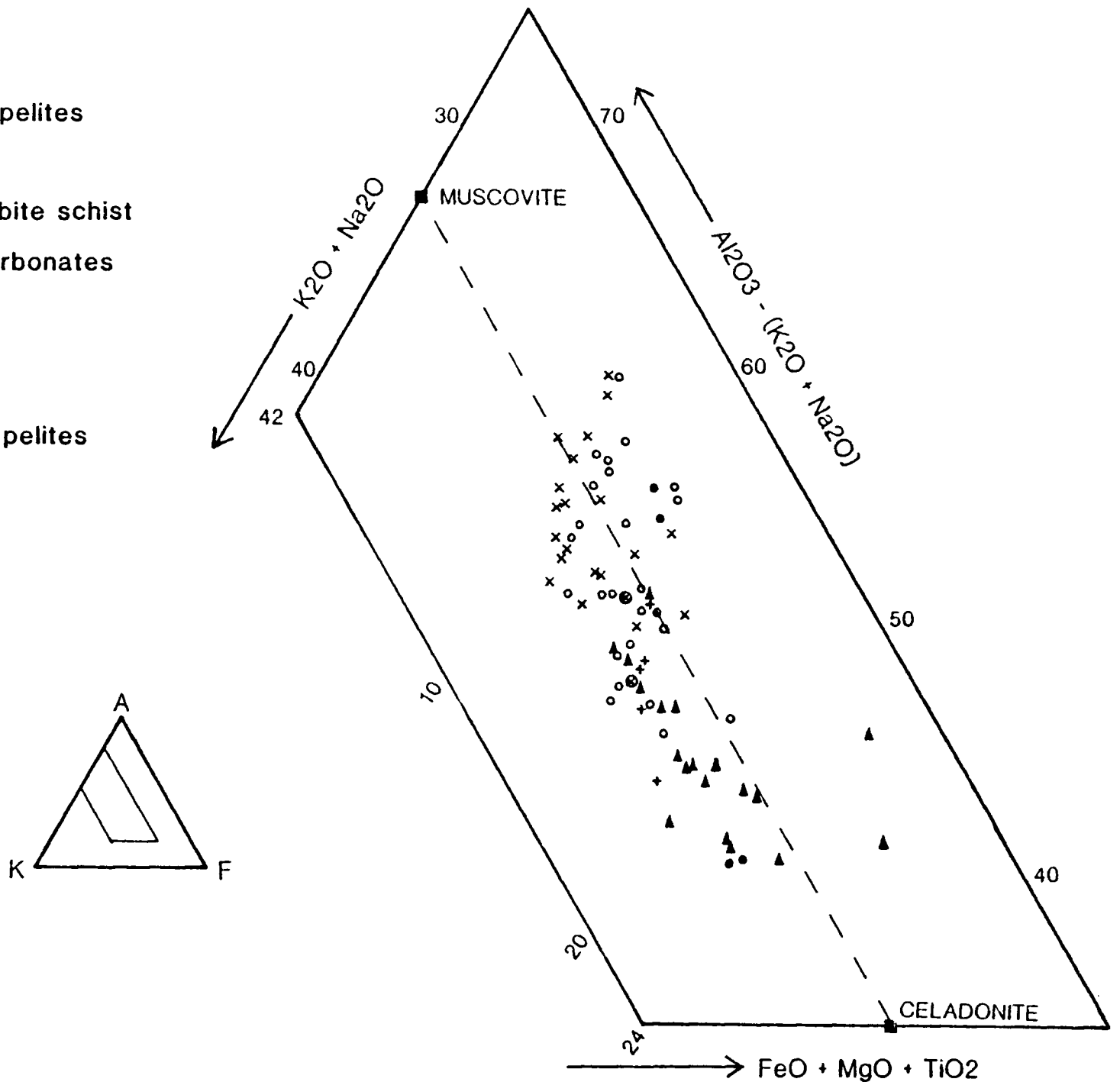


Figure 3.7: Phengite compositions plotted on a portion of an AKF diagram. High grade carbonate and some albite schist data from this study, the rest from Graham(unpubl. data). Celadonite content of phengites appears to decrease with increasing temperature.

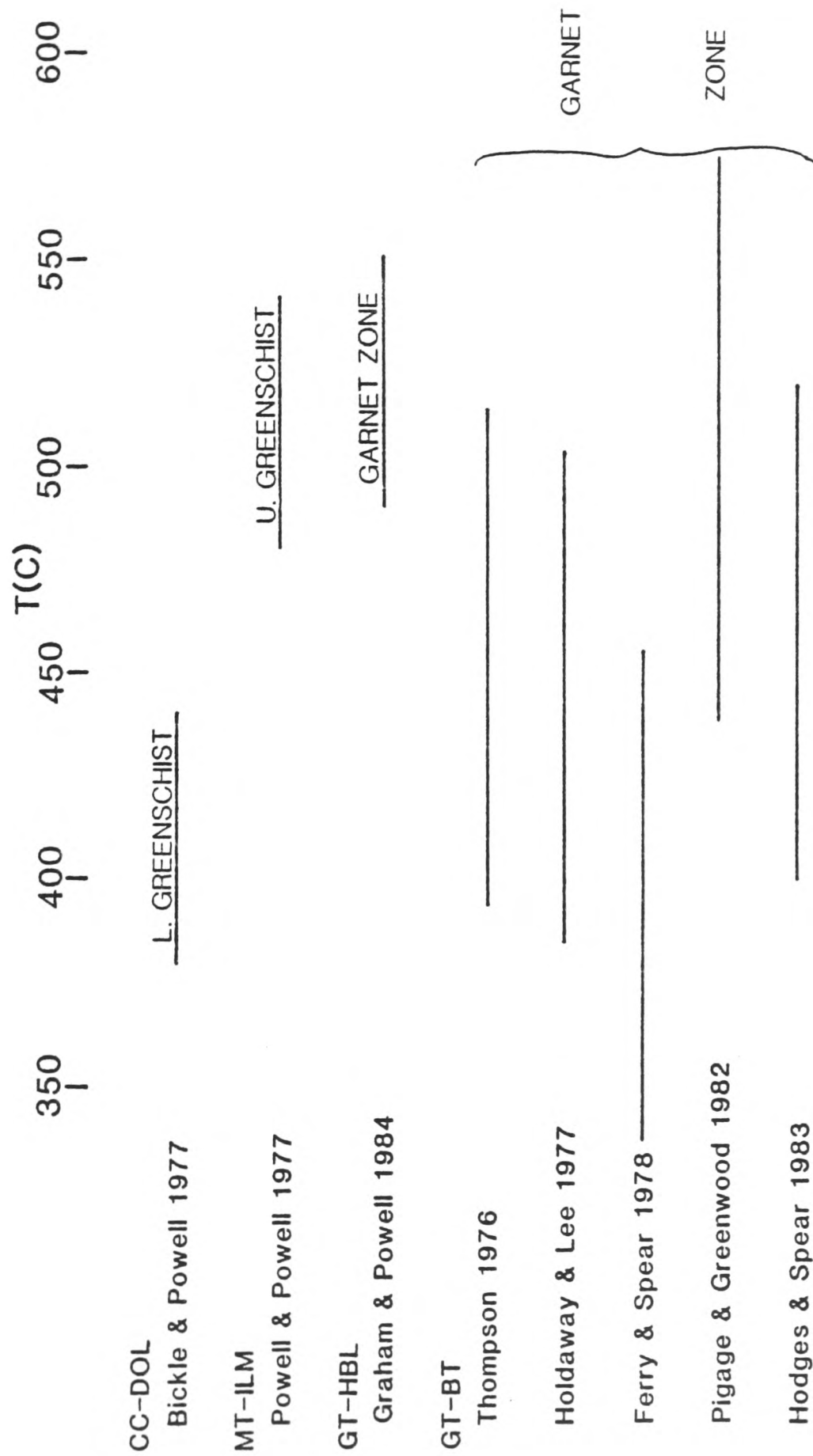


Figure 3.8: Ranges of metamorphic temperatures of Knapdale rocks calculated using various geothermometers. Gt-bt values from albite schists, this study, the rest from Graham *et al.* (1983). Note large range of garnet zone temperatures from gt-bt thermometers.

in the construction of the diagrams do not really justify the use of particular T or X_{CO_2} values in rigorous calculations. For example, an error of $\pm 50^\circ\text{C}$ in the geothermometry gives rise to an error of $\pm 1\text{kb}$ from Equation (3.4), and this error gives rise to a shift of $\pm 20\text{-}30^\circ\text{C}$ in the positions of reactions 2 and 4 at $X_{\text{CO}_2} = 0.05$.

3.6: Conclusions

T - X_{CO_2} diagrams presented here, calculated using the equilibrium thermodynamic equations given in section 3.3, and for real solid and fluid activities, are as follows -

(i) 8 kb, $X_{\text{CO}_2} = 0.0\text{-}1.0$ Figure 3.9

(ii) 8 kb, $X_{\text{CO}_2} = 0.0\text{-}0.1$ Figure 3.10

These provide the framework from which closer investigation of the mineral assemblages of the metacarbonates of South Bay can be made. This forms the subject of Chapter 4.

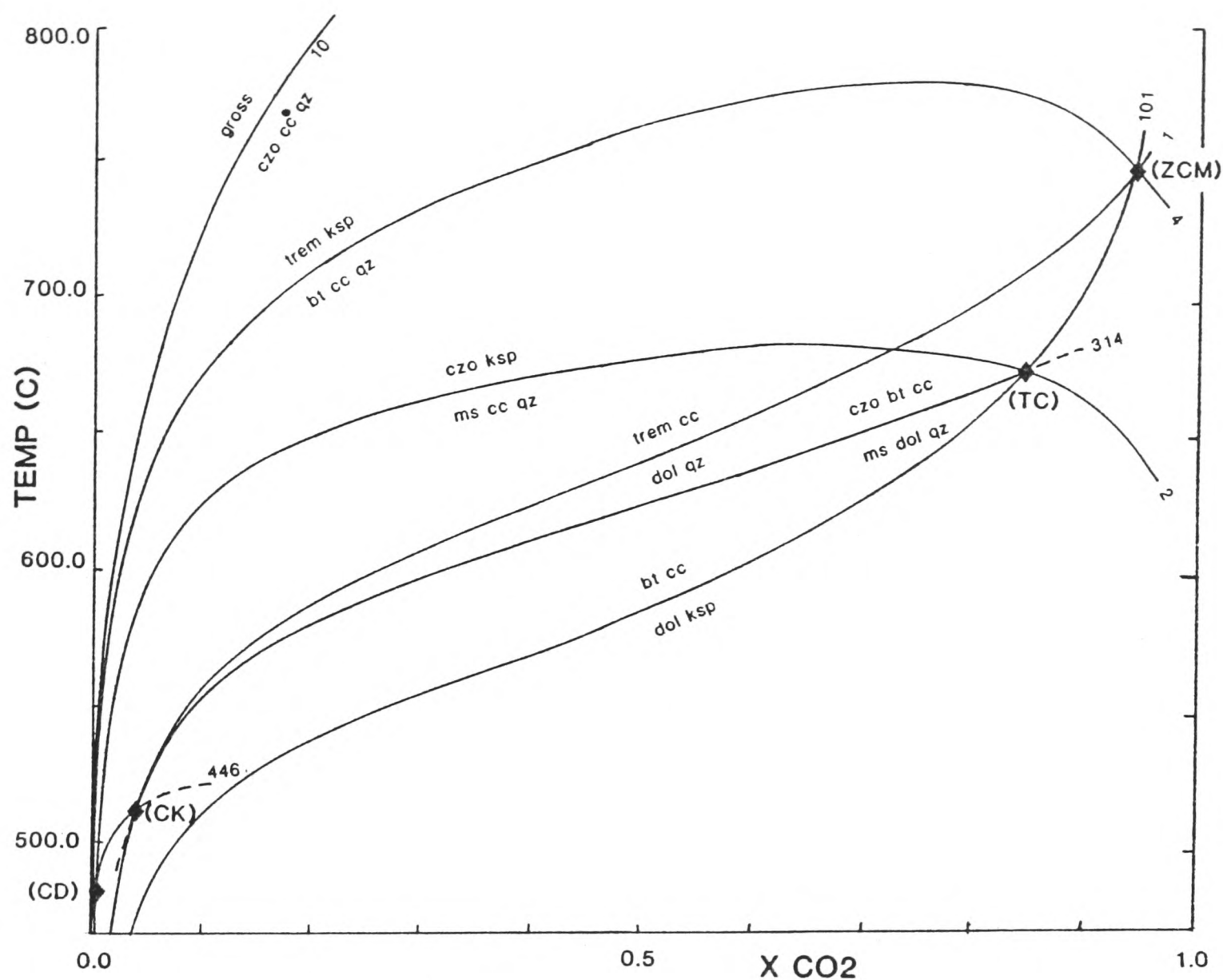


Figure 3.9: Positions of chlorite - absent reactions in $T-X_{CO_2}$ space at 8kb. Curves calculated by evaluation of C_p integrals, a non-ideal CO_2-H_2O mixing model, real activities, and thermodynamic data of Helgeson et al. (1978). Real activities are median values from Figure 3.2.

C H A P T E R 4: Evolution of the South Bay metacarbonates

4.1: Introduction

In this chapter, the evidence for the metamorphic process involved in the metamorphism of the carbonate rocks of South Bay, is examined. The description of mineral assemblages in the rocks, and their distribution, results in conclusions on the fluid $T-X_{CO_2}$ path during metamorphism. Further mineral assemblage evidence points conclusively to an infiltration model, which is described in detail.

The possible effects of bulk compositional control on this model are then weighed against control by variations in fluid:rock ratio. These ratios are calculated, using several critical assumptions, and the results presented in Table 4.2.

4.2: Mineral assemblages and mineral reactions

4.2.1: Shapes of $T-X_{CO_2}$ paths

The shape of a $T-X_{CO_2}$ path followed by a rock is clearly dependent on the nature of the metamorphic process involved. Figure 4.1 shows a series of model $T-X_{CO_2}$ paths for the evolution of a system which started with a grain boundary fluid of composition X_{gb} , and into which H_2O -rich fluid of composition X_{fluid} was introduced. If infiltration, with the bulk of the rock 'insulated' from the vein fluid, occurred, simple heating, in equilibrium with the fluid introduced, could result in a path with a vertical gradient, path D(vein). Note that in this case the rock grain boundary

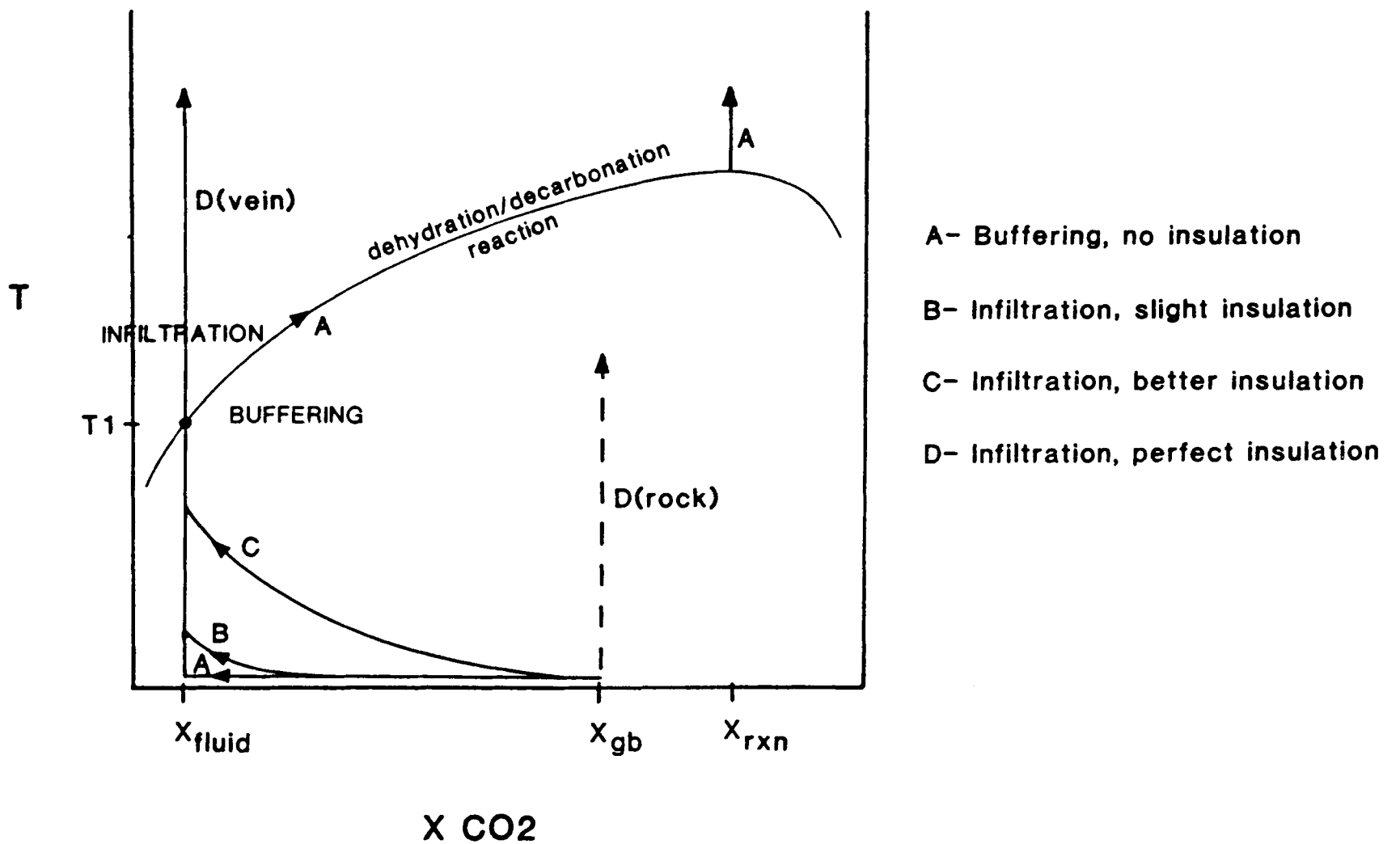


Figure 4.1: Contrasting T - X_{CO_2} paths for fluids during H_2O -rich fluid infiltration, and buffering by a mineral reaction. Infiltration paths B, C and D result in low X_{CO_2} grain boundary fluids, whereas the buffering path (A) results in high X_{CO_2} values.

fluid follows a different path, path D(rock). Alternatively, with total contact between fluid and rock, (and a low fluid:rock ratio), a buffering path, with a positive dT/dX_{CO_2} gradient, could occur (Path A).

In the case of infiltration, however, if the equilibrium X_{CO_2} value of the grain boundary fluid before infiltration (X_{gb}) was high, and that of the infiltrating fluid (X_{fluid}) was low, say pure H_2O , then the shape of the fluid path would more likely be a curve. This curve would have a negative gradient which became smaller (i.e. the steepness increased) as the value $X_{CO_2} = 0.0$ was approached with time. The precise shape of the curve would depend on the amount of infiltrating H_2O -rich fluid and the rate at which it infiltrated, relative to the overall rate of increase of temperature. Faster fluid infiltration relative to increasing temperature would result in shallower $T-X_{CO_2}$ paths. In addition, the shape of the curve would also depend on to what extent the country rock was 'insulated' from the incoming fluid (e.g. Paths B and C). This is obviously a complex problem to solve in any instance, not least because such factors as the temperature difference between the host rock and the infiltrating fluid, and the rate of thermal equilibration of the rock, must be known. This is tantamount to saying that the nature of the fluid pathways must be known, a topic which is explored in Chapter 6.

It is worth considering here the nature of assemblages formed during infiltration or buffering processes. Treating these as end member processes (e.g. Ferry & Rice, 1982), it is to be expected that pure infiltration will result in divariant assemblages only, since the process implies that mineral reactions, when encountered, are quickly crossed, and reactant(s) consumed. The possible exception to this would be when a reaction with extremely slow kinetics was 'frozen in'. In contrast, the buffering process will be characterised by univariant assemblages, in which reactants and products coexist, which represent the buffering of fluid composition along a mineral reaction. The products of buffered reactions may be volumetrically small, however, and

difficult to find (Greenwood, 1975).

In real systems, however, it is possible that curved, sub-horizontal $T-X_{\text{CO}_2}$ paths will occur, in which case a process which represents a half-way house between infiltration and buffering might operate. On a dehydration/decarbonation reaction such as Reaction (4), shown in Figure 4.2, infiltration of large volumes of fluid will tend to 'pull' the equilibrium X_{CO_2} value of the grain boundary fluid off the reaction and towards that of the infiltrating fluid. The CO_2 liberated by the reaction in doing this, however, will tend to 'pull' the X_{gb} to higher X_{CO_2} values (because of the proportions of CO_2 and H_2O liberated in the reaction). Thus the actual path taken by the overall fluid composition will depend on to what extent the infiltrating fluid can overcome the fluid liberated in the reaction. If fluid:rock ratios are not very high, this process may have a prolonged 'see-saw' nature (e.g. Ferry, 1983), and it is therefore more possible for such a univariant assemblage to be 'frozen in'.

Arriving at the nature of the process which operated during the metamorphism of the carbonate rocks at South Bay, Knapdale, requires that the mineral assemblage evidence for a $T-X_{\text{CO}_2}$ path be examined.

4.2.2

Textural evidence for fluid compositions and fluid $T-X_{\text{CO}_2}$ path

The mineral assemblages from carbonates at South Bay, (see Figures 2.12A and B), are divisible texturally into two groups. These are designated primary and secondary, as in the latter case relict grains of primary assemblages are frequently seen overgrown or consumed by new minerals (see Plates 4.1 and 4.2). These secondary minerals are often larger, and contain less evidence of inter- or intra-crystalline deformation. Characteristic of such assemblages is the occurrence of dolomite, which is most commonly found with Kfeldspar, muscovite (celadonite-rich)

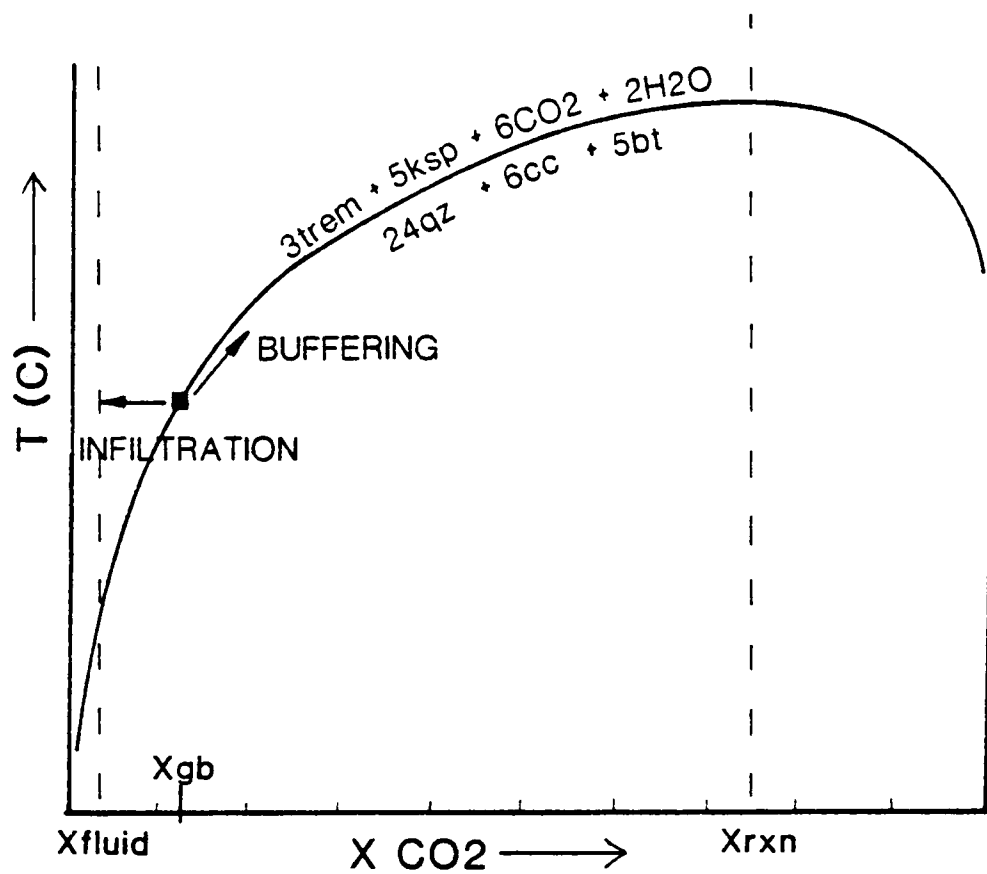


Figure 4.2: Diagram showing the effects of buffering versus infiltration at a point on a devolatilization reaction (reaction 4). Grain boundary fluid composition (X_{gb}) is held in balance by the amount of infiltration of H_2O -rich fluid (X_{fluid}) and the CO_2 -rich fluid liberated by the reaction (X_{rxn}).

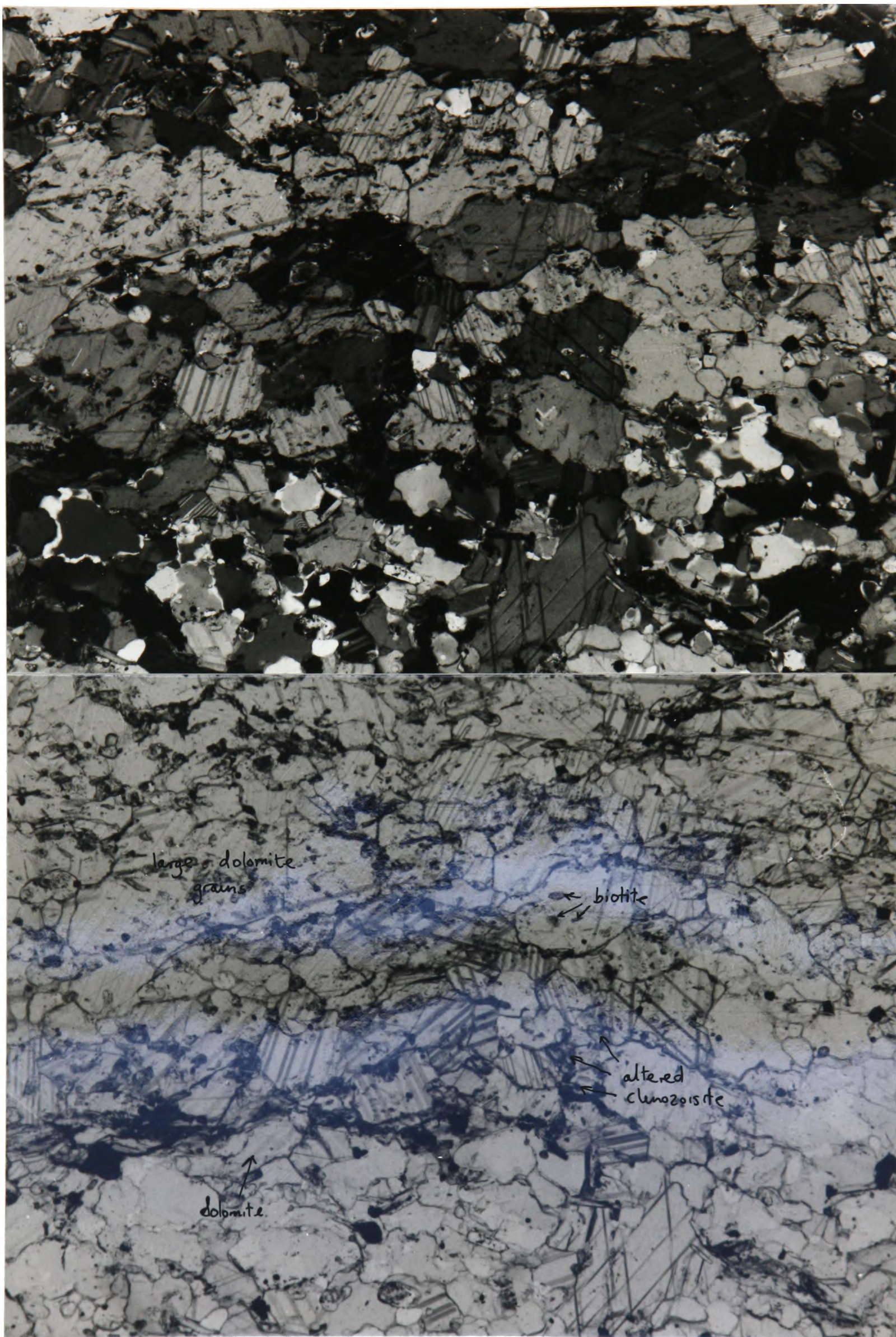


Plate 4.1: Secondary dolomite and Kfeldspar replacing a primary high grade assemblage. Messy remains of clinzoisite, amphibole, biotite occur as inclusions in large dolomite grains. Rock CE4, Meall Mhor. X18, xp and pp.

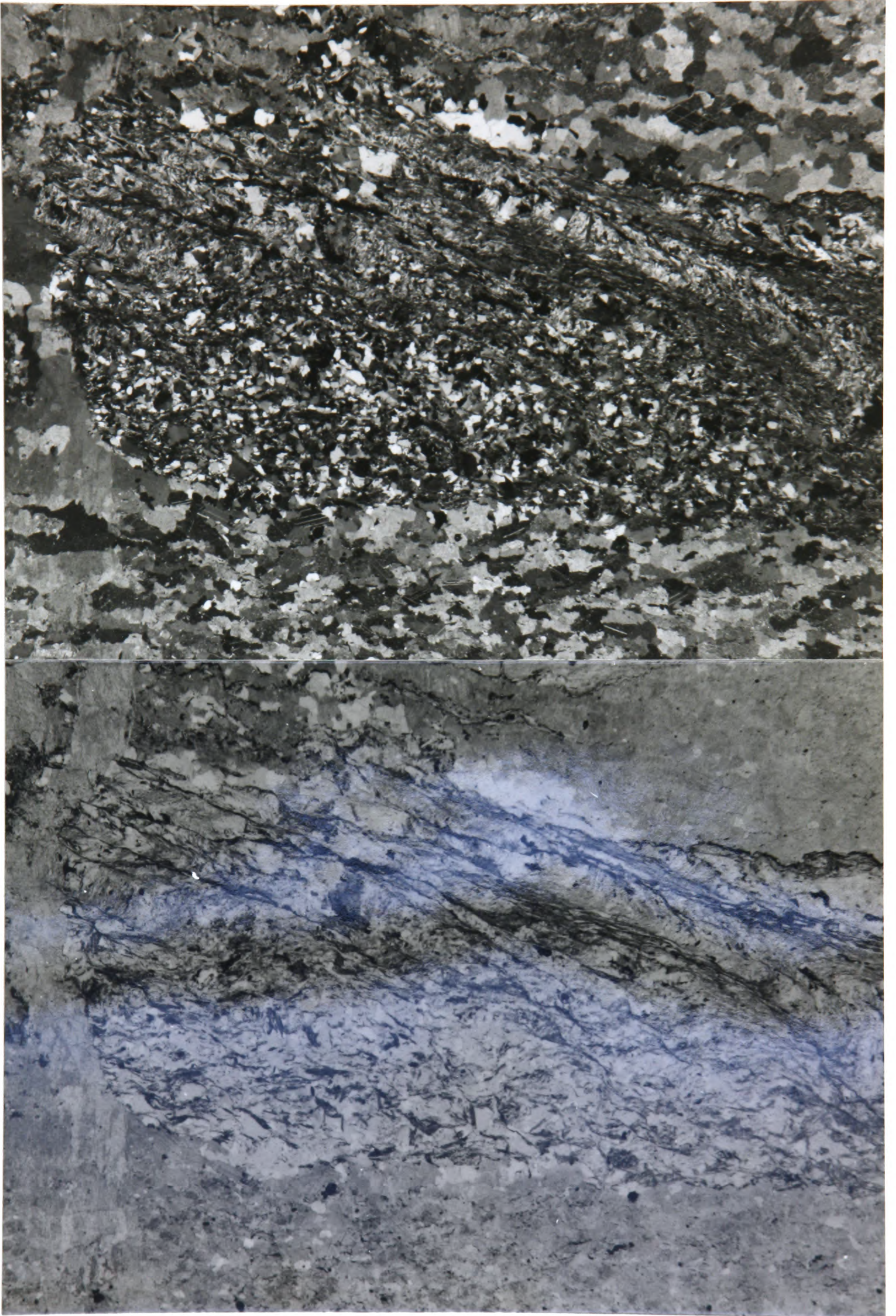


Plate 4.2: Secondary dolomite vein (left) invading primary, calcite-bearing schist. Note S2 crenulation of micas in central quartz-rich layer. Rock CA95, South Bay. X6.3, xp and pp.

and quartz.

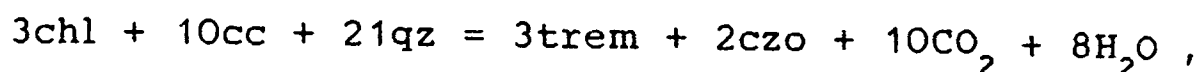
Those assemblages which can be definitely separated, using textural criteria, as being primary in nature, when plotted on an 8kb model T-X_{CO2} diagram, lie on the H₂O-rich side of that diagram (see Figure 4.3). In fact the majority of assemblages lie on or to the H₂O-rich side of the reaction -



which represents equilibrium with a fluid of composition X_{CO2} = 0.02 or less at 550°C.

The path along which the equilibrium fluid composition evolves across this T-X_{CO2} diagram through time, leading to the peak metamorphic conditions, is not easy to determine. Two points are of note, however, in terms of observation of these primary assemblages. (i) The absence of chlorite as a stable primary phase. (ii) The observation that clinozoisite nearly always formed before amphibole. This is well supported by textural evidence in all the South Bay rocks (e.g. Plate 4.3a), with the single exception of some large clinozoisites associated with amphibole in Rock X6NA.

The first point is an indication that the compositional evolution of the fluid, regardless of the orientation of its path on the T-X_{CO2} diagram, always proceeded to an extent beyond that of the last possible reaction involving prograde consumption of chlorite. Since that would be Reaction 3 -



the first implication is that the rocks always contained much more calcite and quartz relative to chlorite (more than 3.33 times (mole %) for calcite, and more than 7 times (mole %) for quartz) so chlorite was always used up first.

The implication of the second point, as a consequence of the first, is that in general the fluid evolution path did not cross Reaction 3, since amphibole and clinozoisite would form at the same time. This is not consistent with

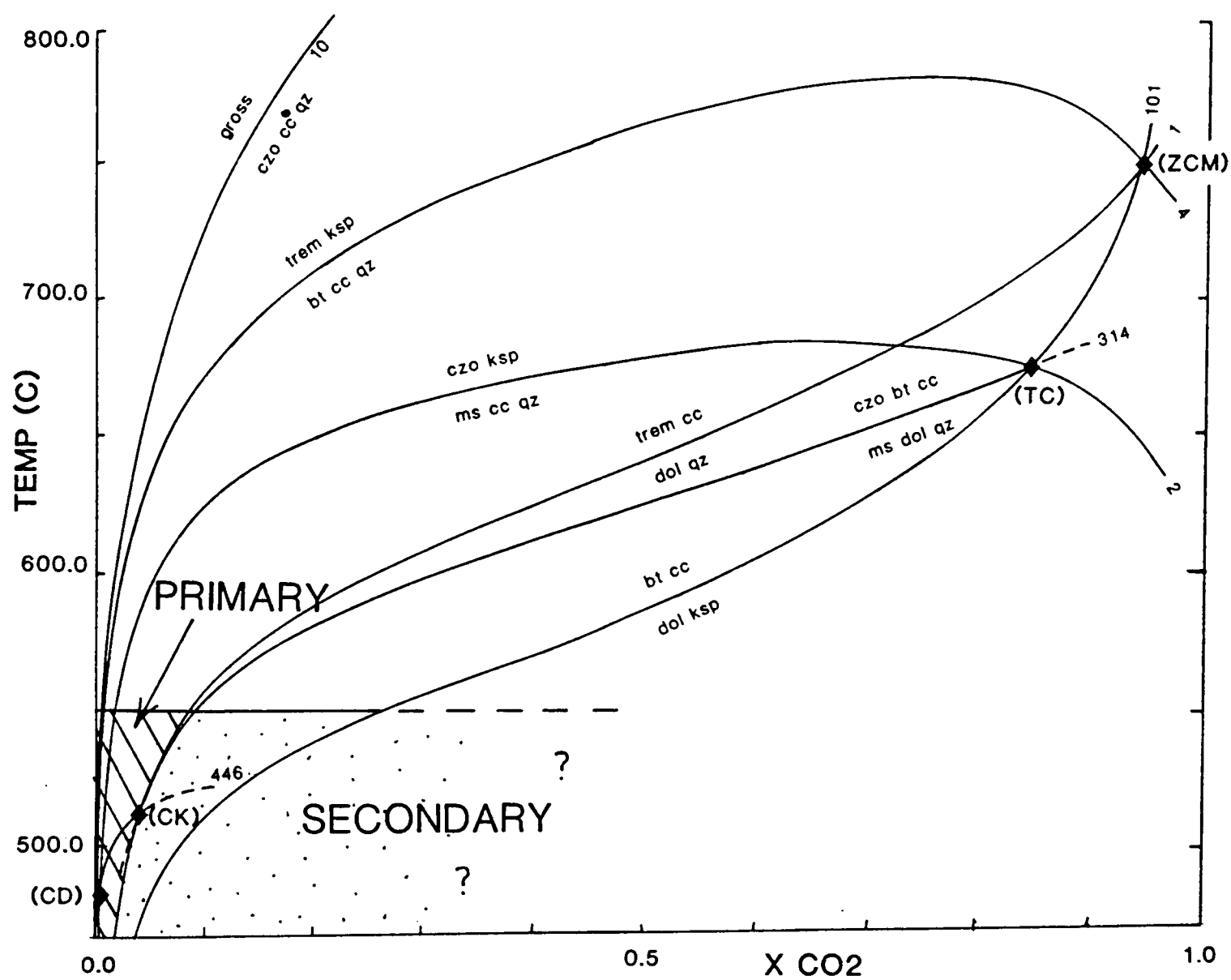


Figure 4.3: Positions in $T-X_{CO_2}$ space at 8kb of primary (calcite-bearing) and secondary (dolomite-bearing) assemblages from Knapdale. Primary assemblages are H_2O -rich, whereas secondary are less so, but poorly constrained.



Plate 4.3a: Primary high grade assemblage showing growth of clinozoisite before amphibole laths. Rock CA68, South Bay. X30, pp.

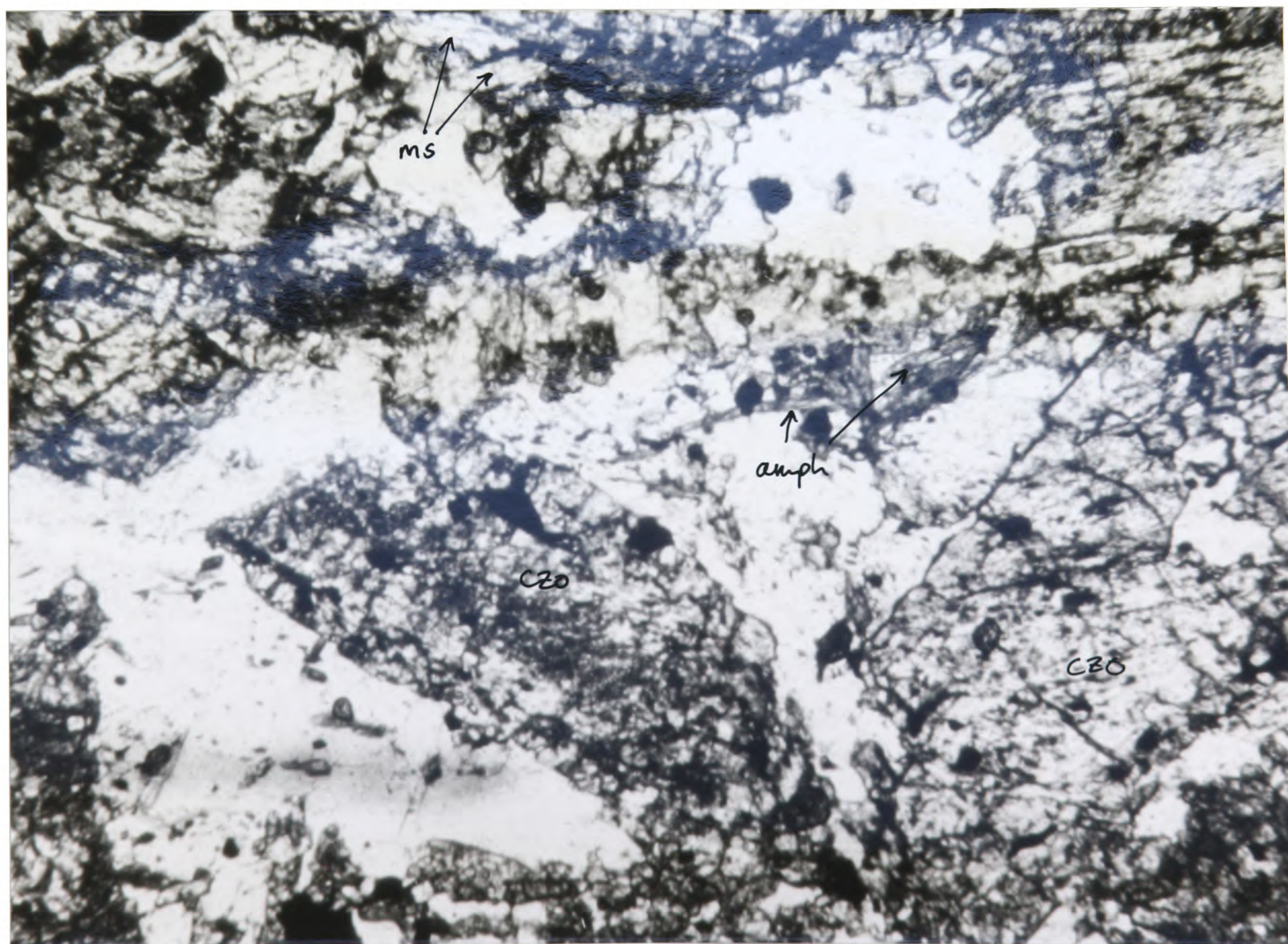


Plate 4.3b: Large clinozoisite blocks, amphibole and muscovite also present. Rock X6NA, South Bay. X20, pp.

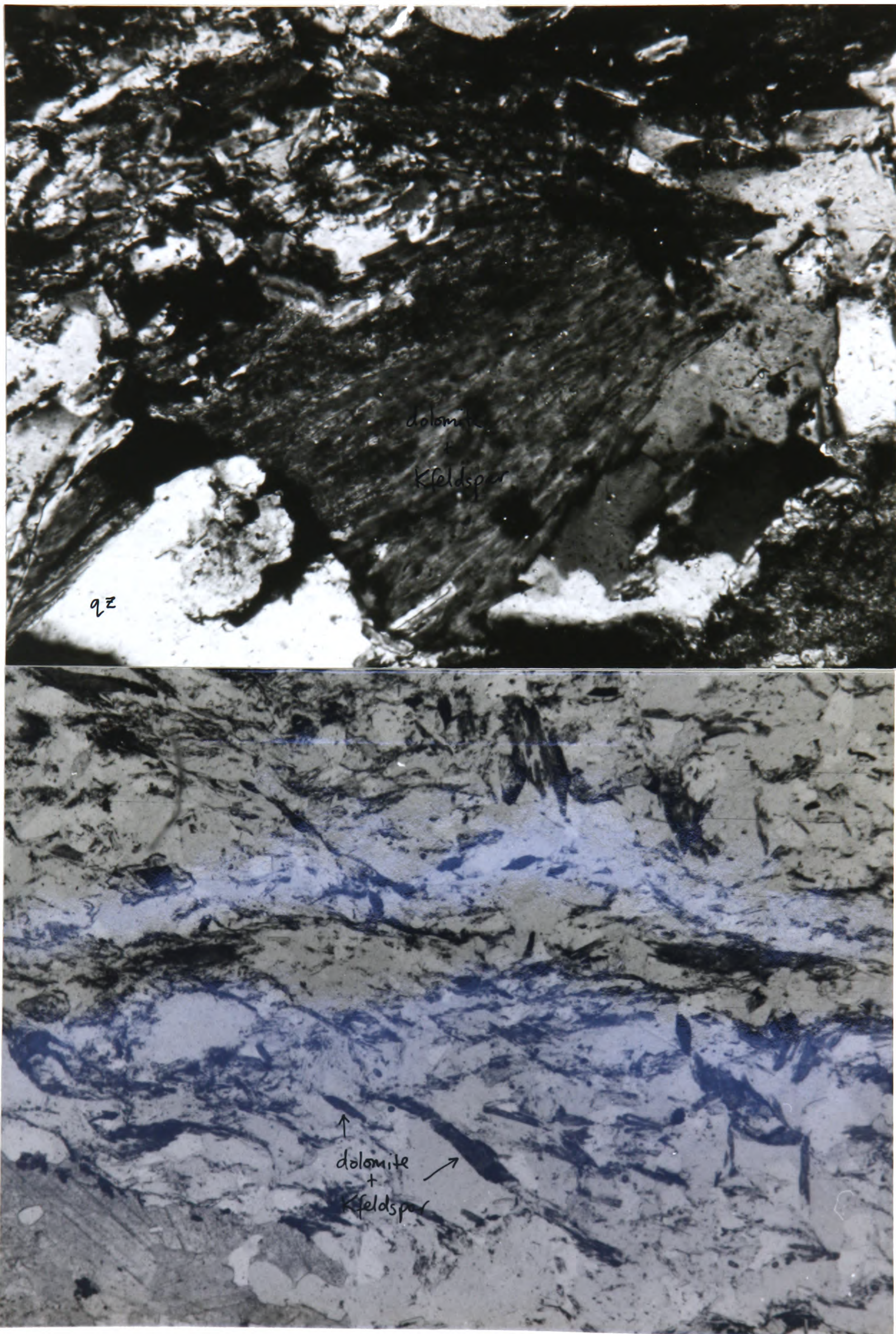
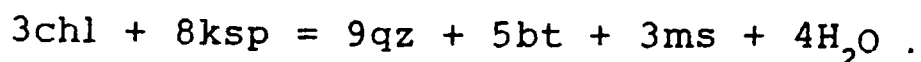


Plate 4.4: Detail of quartz-rich layer in Plate 4.2, showing secondary replacement of muscovite by dolomite and Kfeldspar. Rock CA95, South Bay. X70, xp and X25, pp.

observation, so either there was no chlorite in the rock at that stage, i.e. the breakdown of chlorite occurred at lower temperatures still, or alternatively, there may have been no chlorite in the rock at all, although this seems unlikely. The reaction which probably resulted in the early breakdown of chlorite is Reaction 100 -



The clinozoisites of Rock X6NA have a peculiar anomalous birefringence, which strongly resembles that of chlorite, and the grains as a whole are divided into foliated domains of differing birefringence which give them the textural appearance of chlorite (see Plate 4.3b). This phenomena may imply that amphibole and clinozoisite did form as a result of Reaction 3 in this rock. If this was so, it may simply reflect an original rock layer which was particularly rich in chlorite, so that enough was left after Reaction 100 for Reaction 3 to proceed to an appreciable degree.

The calculated temperature of peak metamorphism of these primary mineralogies is $525 \pm 25^\circ\text{C}$. Looking in detail at the H_2O -rich part of the $T-X_{CO_2}$ diagram for this system (Figure 3.10), it can be seen that a horizontal or sub-horizontal $T-X_{CO_2}$ trajectory probably passes on the high temperature side of invariant points [chl, dol] and [chl, ksp]. This is borne out by the observation again of the appearance of clinozoisite before amphibole, since above these points the tremolite producing reaction in chlorite-free assemblages (i.e. Reaction (4)) occurs after the clinozoisite producing reaction (Reaction (2)). There is some textural evidence for tremolite having been produced by reactions which involved the breakdown of dolomite (i.e. reactions 1 and 314, see Plate 4.4), but in the majority of cases reactions 2 and 4 dominated (see Plates 4.5 and 4.6). This may imply that the evolution of the fluid along a $T-X_{CO_2}$ path proceeded beyond the dolomite breakdown reactions in the majority of cases.

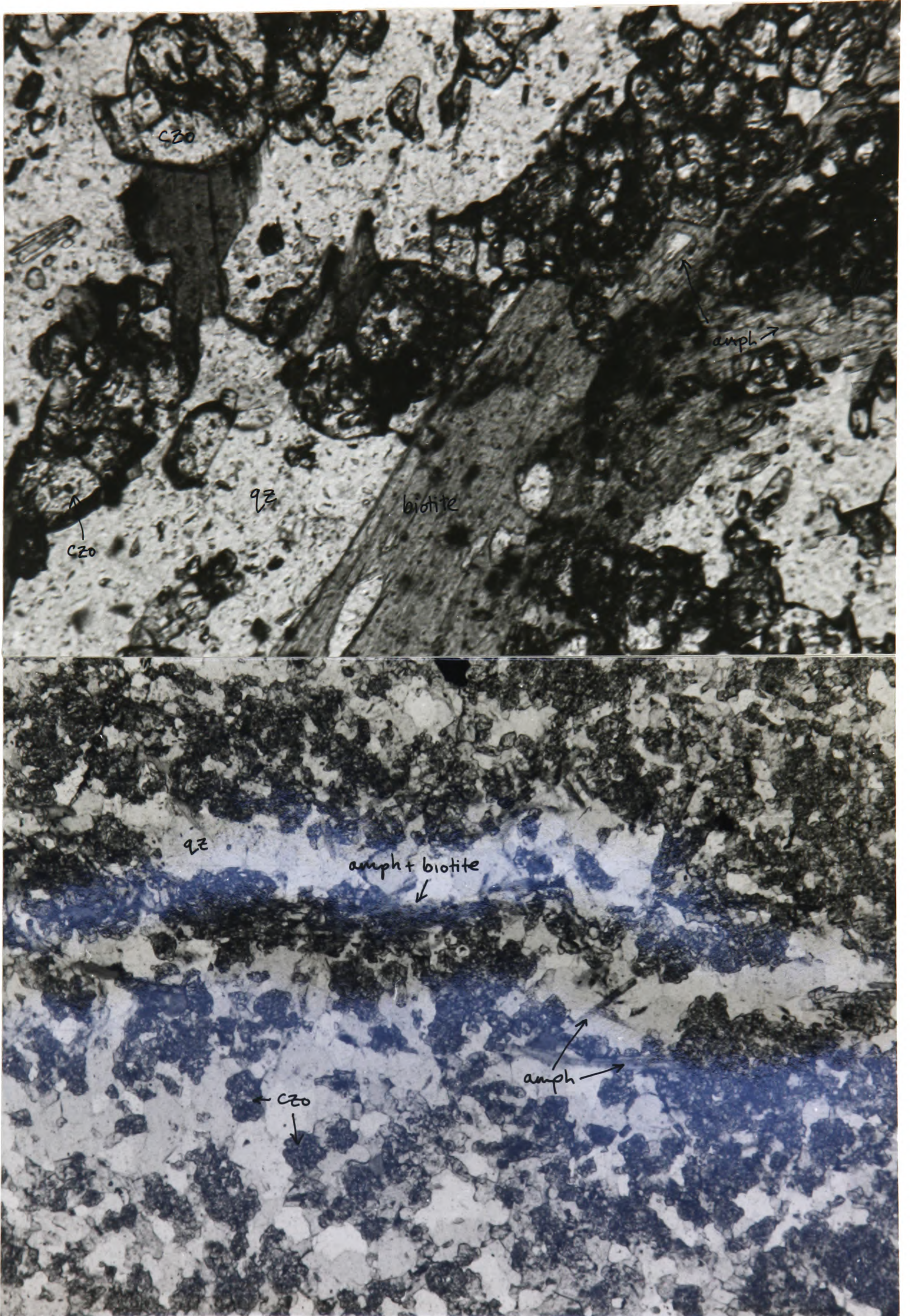


Plate 4.5: Primary high grade assemblage of clinozoisite, amphibole, Kfeldspar and biotite, in quartz-rich layer, showing growth of amphibole from biotite. Rock X1NA, South Bay. X50, pp and X20, pp.

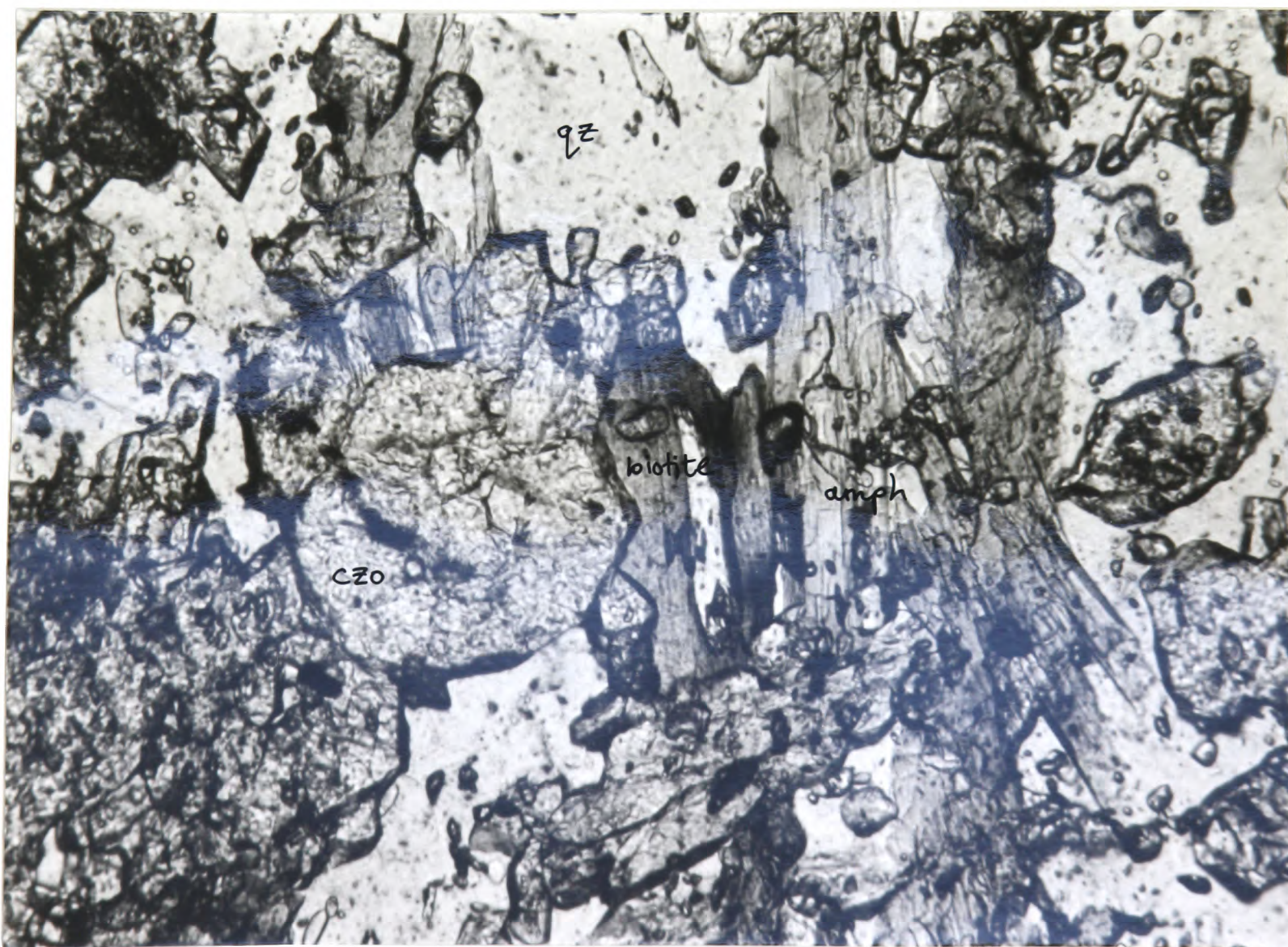
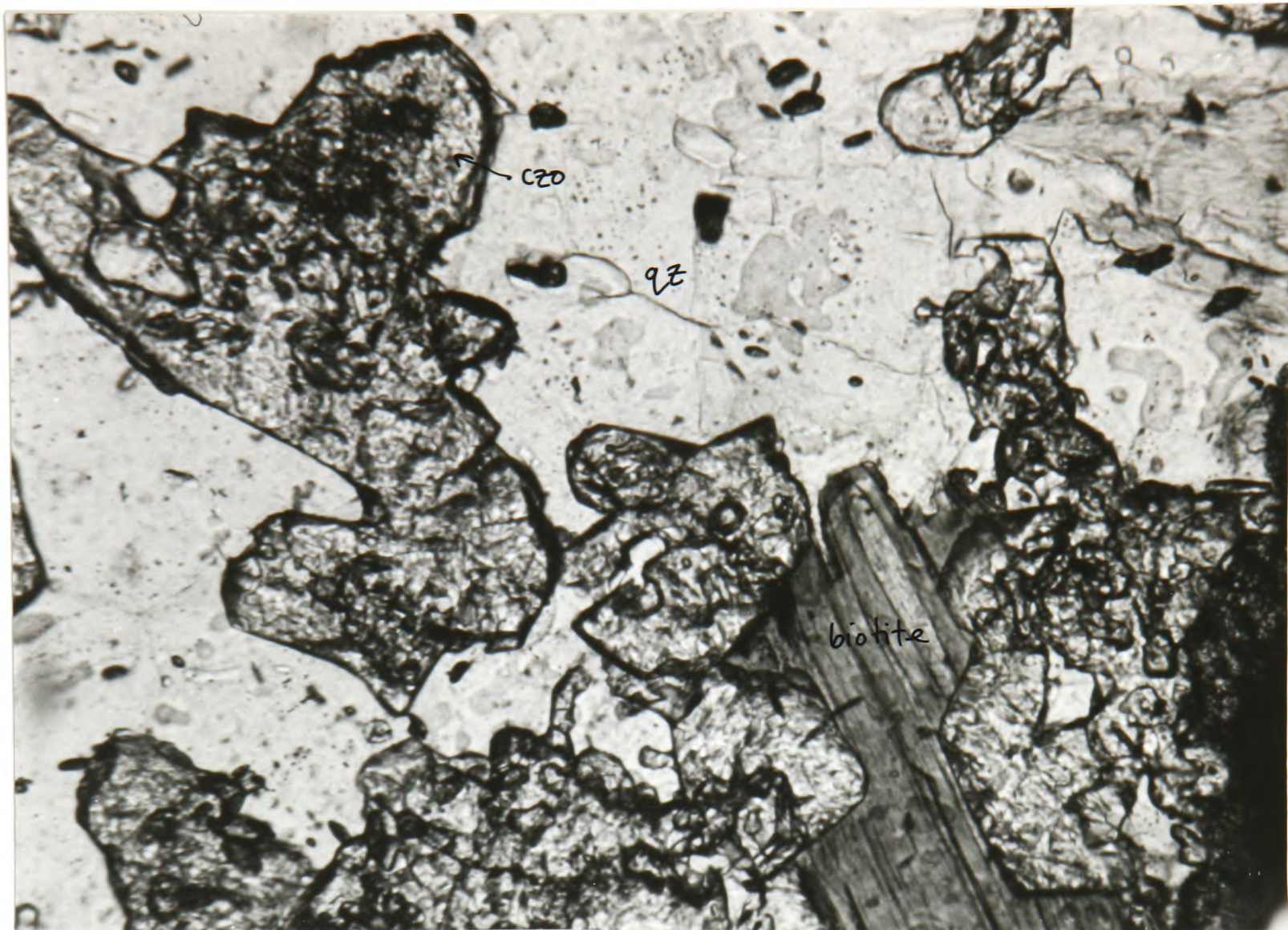


Plate 4.6: Primary high grade assemblage of clinozoisite, amphibole, Kfeldspar and biotite.

Rock CA68, South Bay. X60, pp.

The modal amounts of minerals produced by reactions 101, 314, 1, 2, 4 and 10 (see for example Table 4.1, Plates 4.7 and 4.8) are large enough that buffering, as a process, can probably be dismissed, since buffering invariably results in only small amounts of products (Greenwood, 1975).

The majority of assemblages, as they are displayed in Figures 2.12, 4.6 and 4.7 are univariant, which suggests that some degree of buffering, or else an infiltration-buffering 'see-saw' effect (see section 4.2) operated. A closer inspection of assemblages reveals that this is probably not the case. Figure 4.4 shows the location of thin sections taken in near-continuous sequence from Limestone B at the contact with Amphibolite 1, of which Plates 4.9 and 4.10 are photomicrographs. These Plates show the very small-scale distribution of prograde metamorphic assemblages, sometimes controlled by original rock layering, sometimes unrelated to layering (see for example Plate 4.9, of Rock X1NA). The detailed microscope delineation of mineral assemblages in these thin sections make it plain that univariant assemblages exist at a whole thin section scale, but not when smaller rock volumes are considered. Thus the letter codes assigned to samples in Figures 4.6 and 4.7 in the majority of cases represent an average, and do not necessarily imply some degree of buffering.

This complex distribution of divariant and univariant assemblages is indicative of an infiltration process which allows the completely pervasive contact of infiltrating fluid with the rock. The nature of such a process is discussed in Chapter 6.

The model presented here, on the basis of observed textural evidence for in particular reactions 2, 4 and 10, (although 1, 314 and 101 are clearly observed in reverse in secondary assemblages), and in conjunction with the argument presented above, is that of a curved $T-X_{CO_2}$ path for fluid compositions in equilibrium with primary mineralogies. This path was the result of infiltration of H_2O -rich fluid into the carbonate rocks from some external source, and reached a peak metamorphic position of roughly

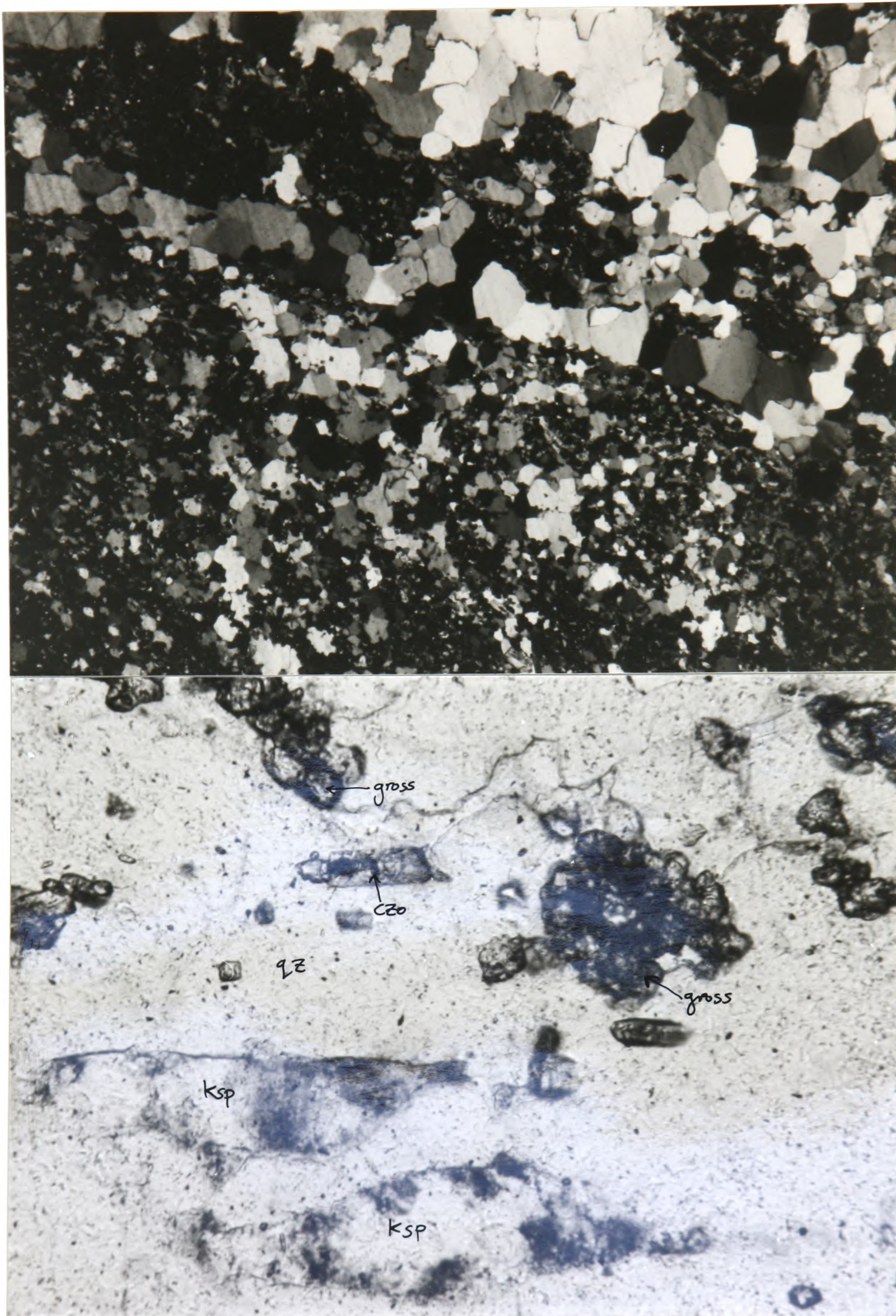


Plate 4.7: Primary high grade assemblage showing growth of grossular from clinozoisite in a quartz-rich layer. Note absence of micas. Rock X14N, South Bay. X20, xp and X50, pp.

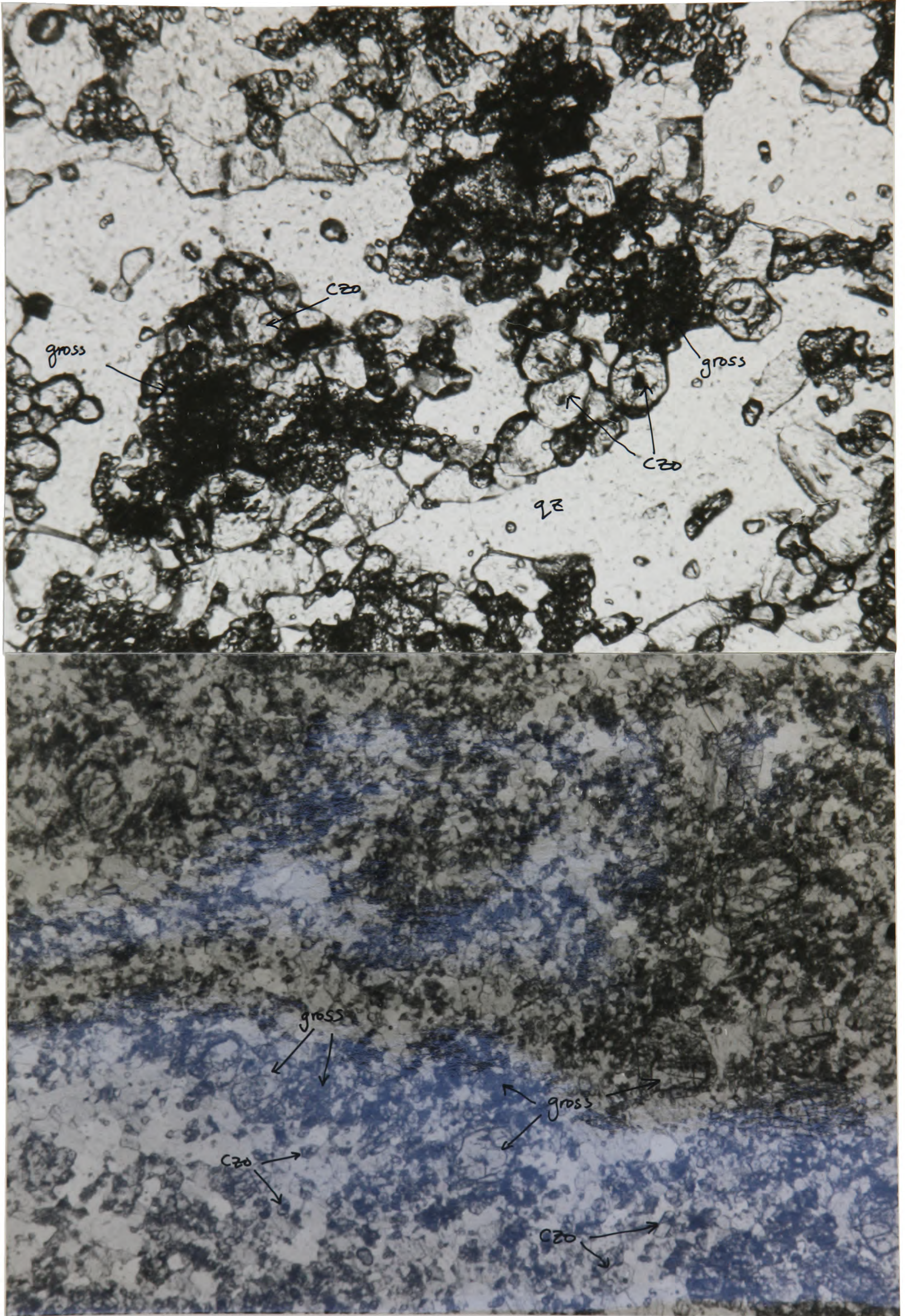


Plate 4.8: Growth of grossular from clinozoisite in a calcite-rich layer. Rock X14N, South Bay.

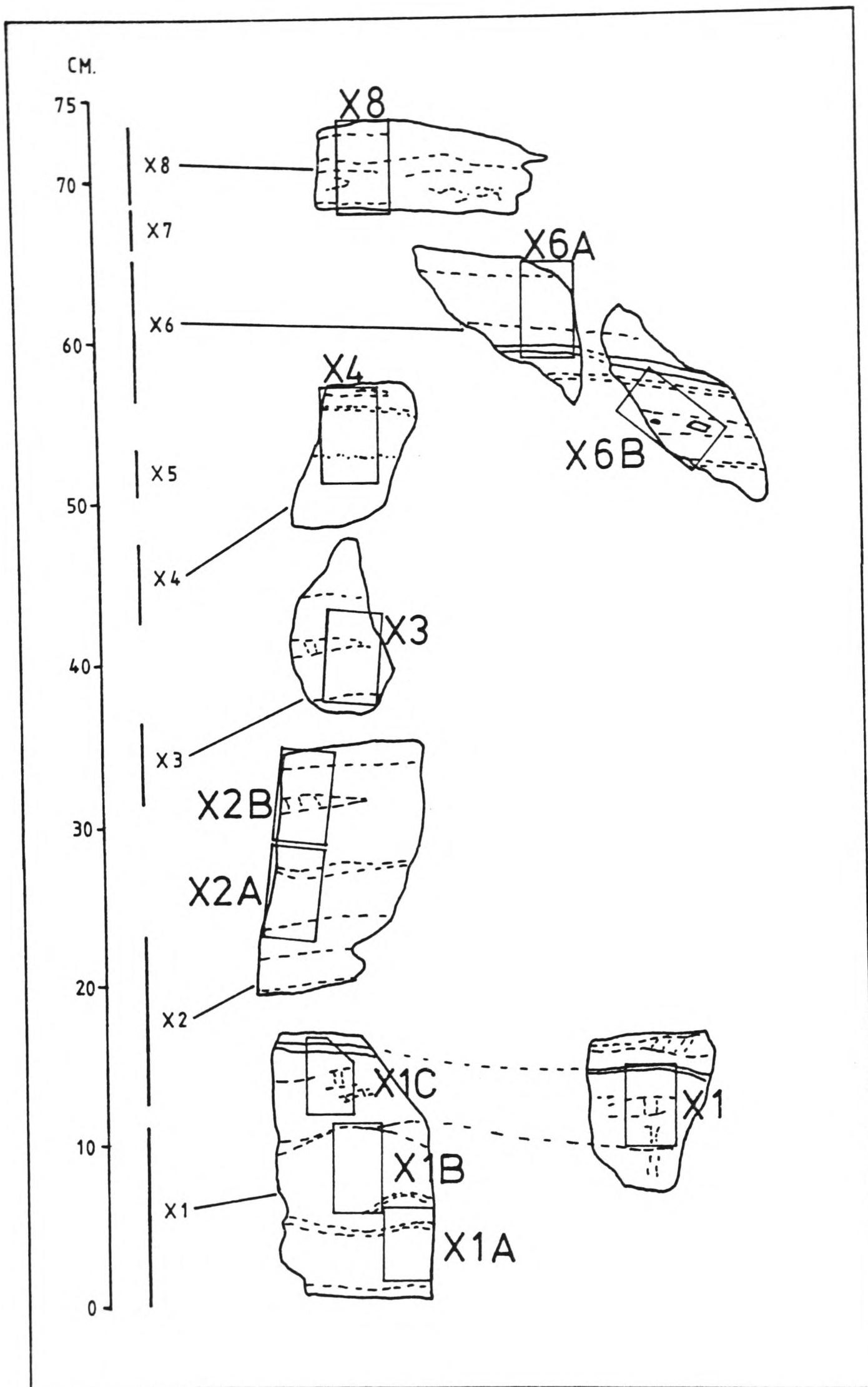


Figure 4.4: Location of rock samples and the thin sections taken from them in part of Limestone B, South Bay. Samples cover the 75cm of limestone adjacent to Amphibolite 1. Thin sections X1A and X1B are displayed in Plates 4.5 and 4.6 respectively.

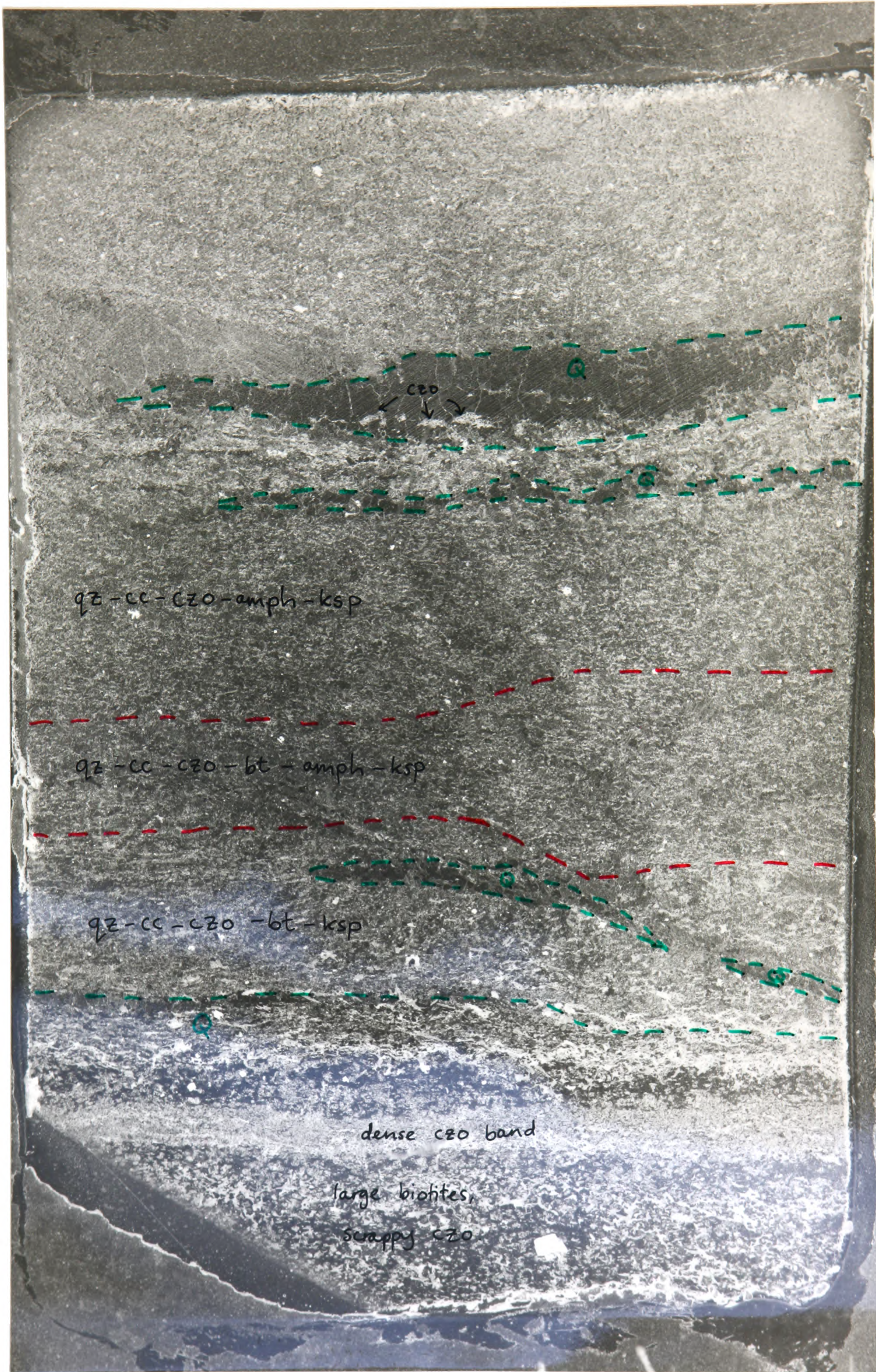


Plate 4.9: Distribution of mineral assemblages in a thin-section. Rock X1NA, Limestone B, South Bay (see Figure 4.4). Negative image taken of whole thin section.

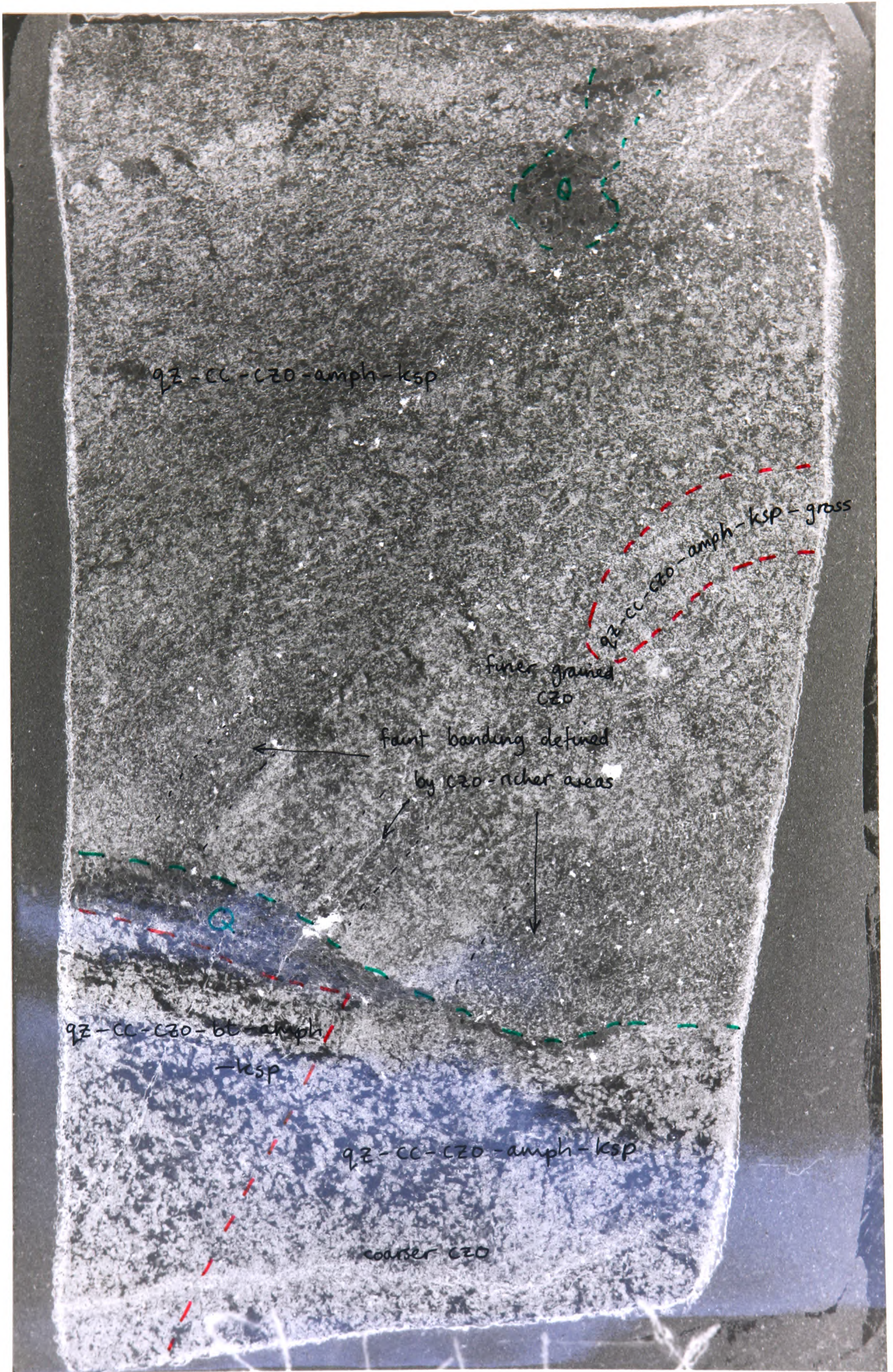


Plate 4.10: Distribution of mineral assemblages in a thin-section. Rock X1NB, Limestone B, South Bay. Negative image.

$T = 550^{\circ}\text{C}$, $X_{\text{CO}_2} < 0.01$.

4.2.3: Sequence of reactions, and possible assemblages

In the course of the infiltration model described above, starting from some unknown X_{CO_2} (but greater than 0.15 at 525°C , 8kb, see Figure 3.9), a sequence of six reactions is encountered and crossed, namely reactions 101, 314, 1, 2, 4, and 10. Since each of these reactions involves the evolution of CO_2 in some proportion, it follows that lower limits on the amount of infiltrating fluid needed to overcome the effect of dilution by CO_2 can be calculated at each reaction (following the method of Ferry, 1980, 1983).

In addition, for an assumed starting mineralogy consisting of dolomite, Kfeldspar, muscovite and quartz, the complete range of possible assemblages (univariant and divariant) which could exist as a consequence of these reactions, can be determined. These are presented as a flow diagram in Figure 4.5 .

The letter codes assigned to each assemblage reflect their greater or lesser equilibrium X_{CO_2} values at constant T , and codes for each assemblage have been included in the assemblage maps of Figures 4.6 and 4.7 .

On inspection of these figures, several points are of note: (i) Figure 4.7 clearly shows that although on a large scale (i.e. Figure 4.6 over the whole outcrop), the most H_2O -rich assemblages appear to be found closer to amphibolite bodies, on a small scale this is not the case. For example, assemblage F, the most H_2O -rich, is consistently found away from direct contact with the amphibolite margins.

(ii) No divariant or univariant assemblages associated with reactions 314 and 1 (i.e. B and C codes) are found at this locality. Because of the nature of the reaction net, it is not possible to determine whether this is due to the fact that either:

a) the dolomite was always consumed in preference to

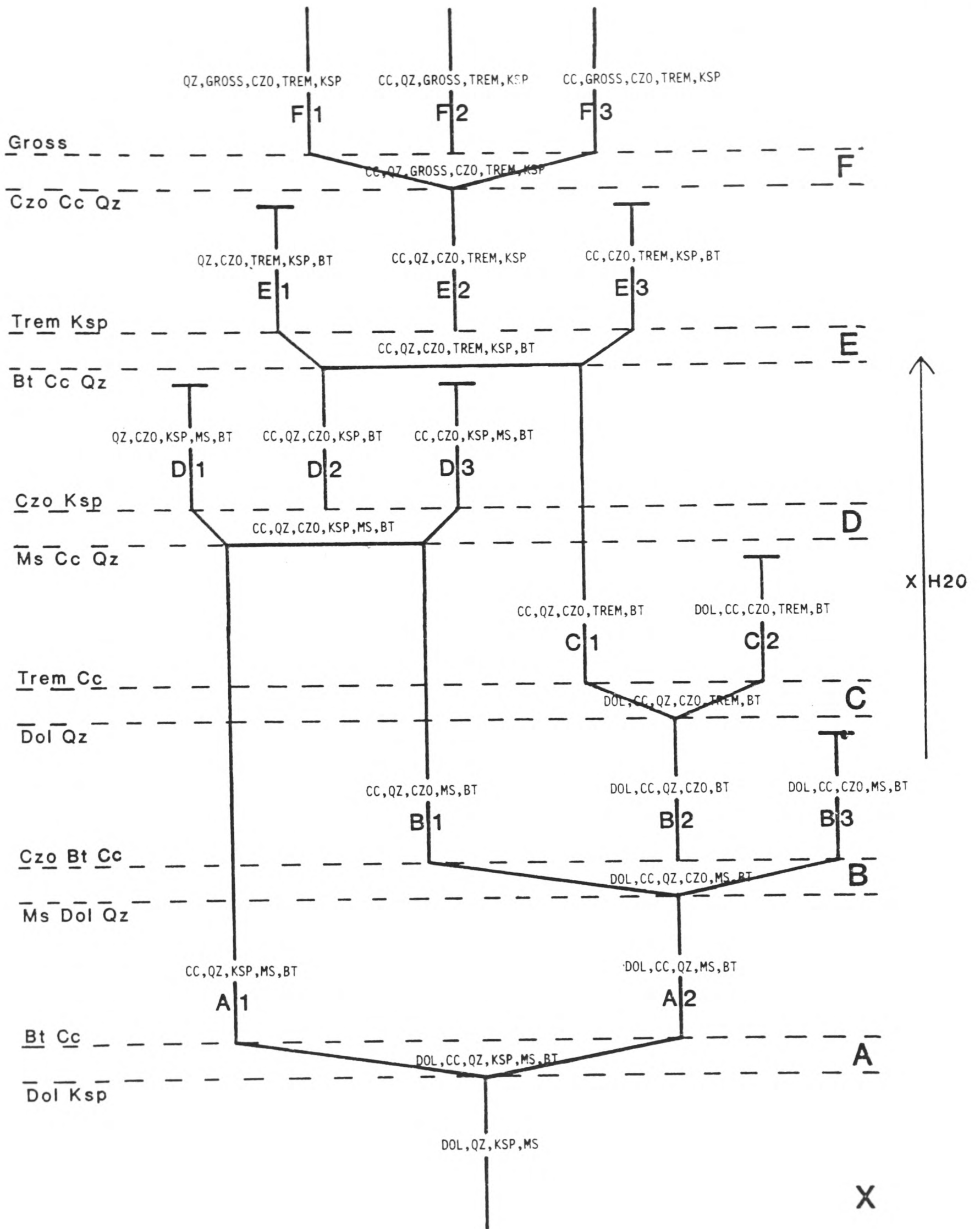


Figure 4.5: Assemblage flow diagram for reactions A, B, C, D, E and F (101, 314, 1, 2, 4 and 10 of Table 3.1). X_{H_2O} increases up the diagram as reactions are crossed. Letter codes denote assemblages, and these are used in Figures 4.6 to 4.11.

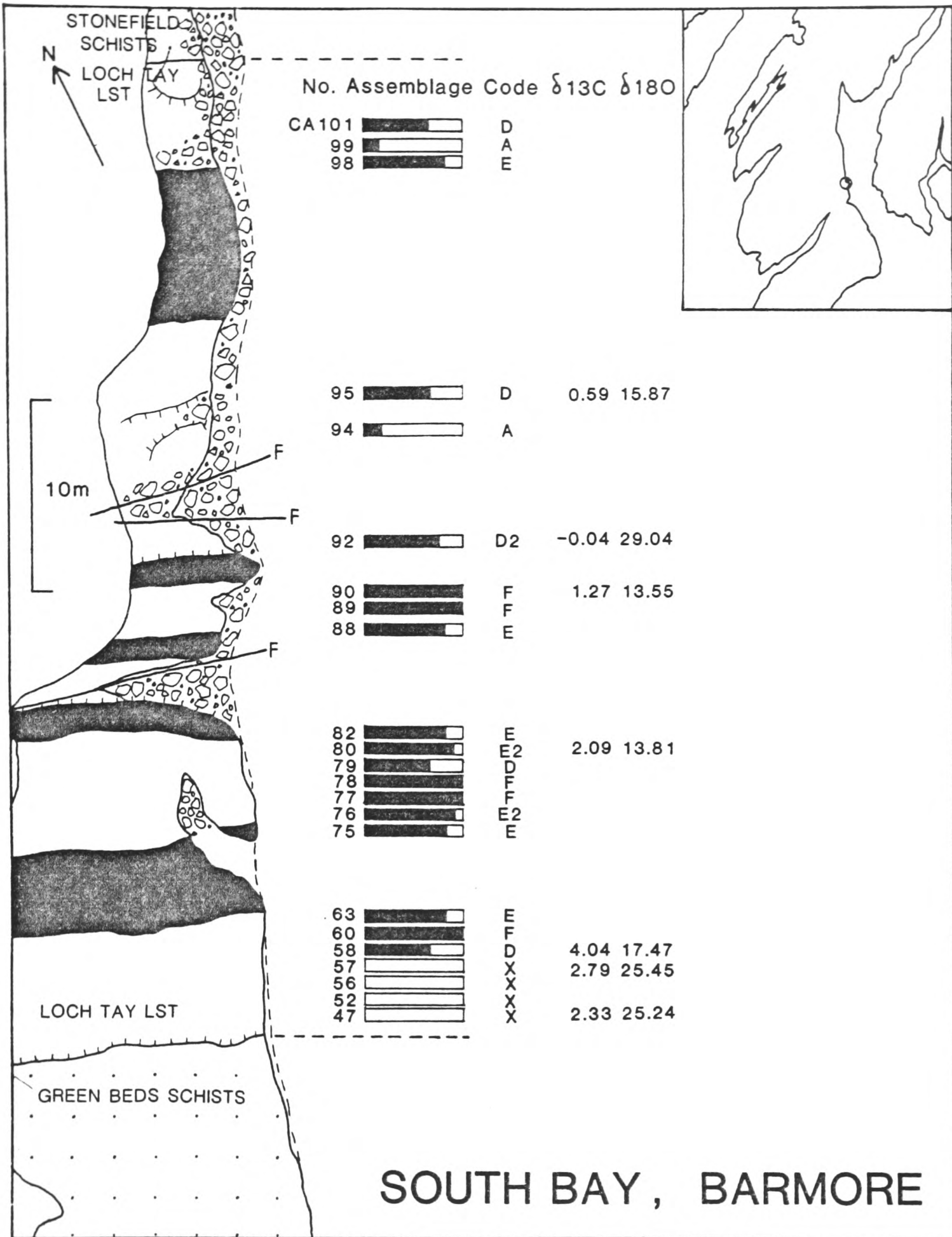


Figure 4.6: Mineral assemblages and stable isotope ratios in carbonates of South Bay, Barmore. Bar codes represent the extent of devolatilization reactions A to F (see Figure 4.5). The distribution of assemblages shows no regular zoning pattern.

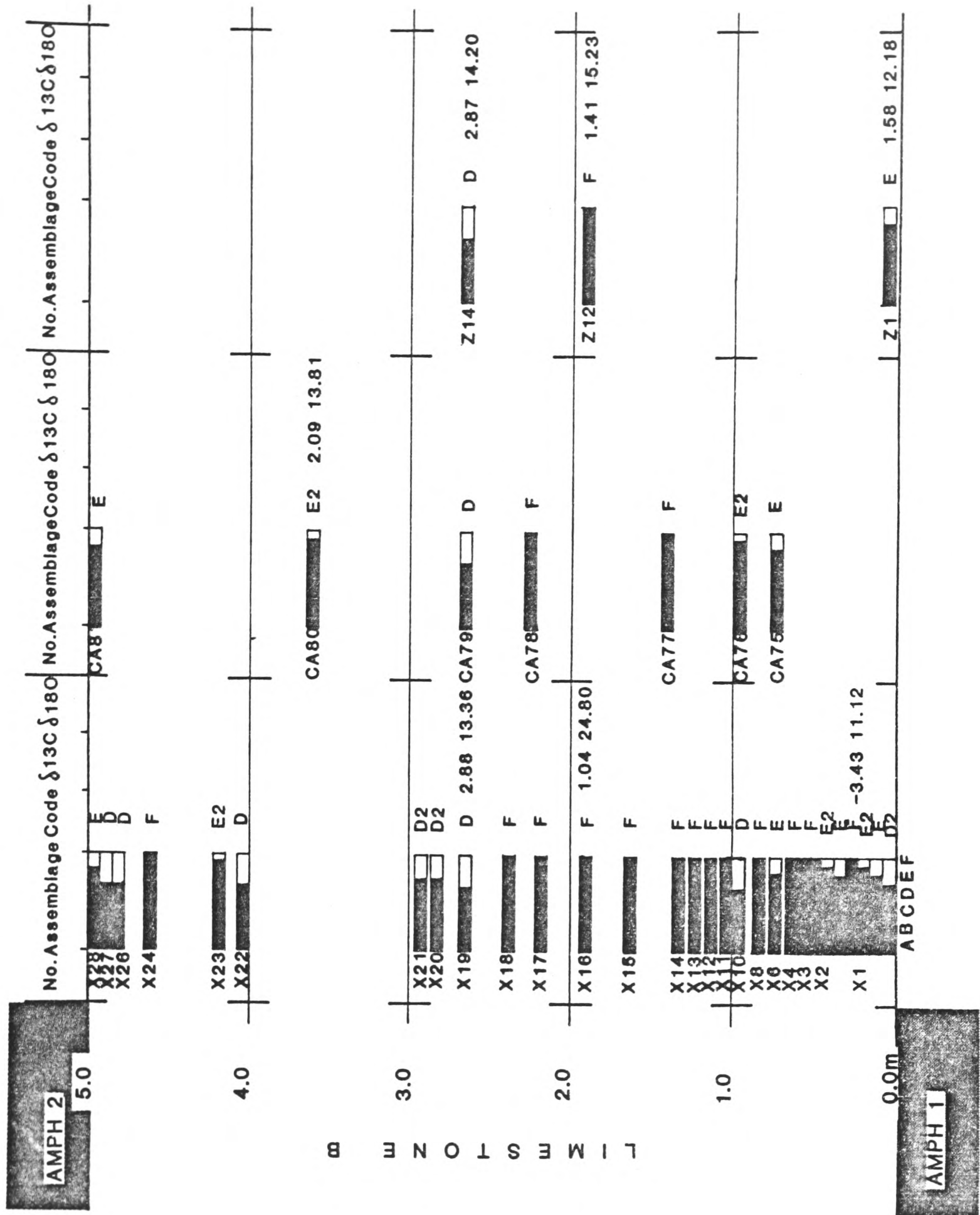


Figure 4.7: Mineral assemblages and stable isotope ratios in a detailed sample traverse across Limestone B, South Bay. Note that the most H_2O -rich assemblage (F) does not occur nearest to the amphibolites. A large number of F assemblages between 1.0 and 2.4m could reflect limestone layers of a similar bulk composition, or a high fluid flow pathway.

Kfeldspar at reaction 101.

or b) dolomite persisted beyond reaction 101, but was always consumed at either reaction 314 or reaction 1, and in addition products thus formed invariably proceeded to reactions 2 or 4, and these reactions proceeded to some extent.

This latter case is equivalent to saying again that the fluid evolution path proceeded beyond the breakdown of dolomite in all rocks.

The distribution of primary assemblages in the carbonates at South Bay can be accounted for by two different models of fluid infiltration.

1) H₂O-rich fluid flushed evenly through all the carbonates, with a fluid:rock ratio which was large, and constant from layer to layer. The different assemblages seen would then have to represent sedimentary layers of differing original bulk composition (manifested as variations in quartz content, and in feldspar plus mica content). These bulk compositional 'constraints' mean that as the rock proceeded along the T-X_{CO₂} path, some of the reactions encountered might be inapplicable, due to lack of a reactant. For example, in a quartz-rich, carbonate-poor layer, calcite might react completely out at say, reaction D (Figure 4.5), leaving further reaction by E and F impossible.

2) H₂O-rich fluid flushed unevenly through the carbonates, so that fluid:rock ratio ranged from high to quite low values, and varied considerably from layer to layer. The different assemblages seen could then represent different fluid:rock ratios at a particular point. This is because in the absence of any bulk compositional constraints, the major factor determining whether a reaction was possible would be whether the equilibrium X_{CO₂} of the pore fluid could be held at the necessary X_{CO₂} value in spite of the diluting effect of CO₂ liberated by the reaction, that is to say, whether the fluid:rock ratio of infiltrating fluid was high enough.

4.3: Bulk compositional control

4.3.1: Theoretical assemblages

In this section, an attempt is made to evaluate how vulnerable the metamorphic system of the six described reactions would be to changes in bulk composition. A simple computer program was written, which for input of a starting mineralogy (in mole % of each mineral), and a given balanced mineral reaction, calculated the percentage of each mineral in the assemblage after the reaction has proceeded to completion, with the consumption of one of the reactants. The program was then modified to deal with the six reactions of interest in turn, so that input of a starting mineralogy would result in the end-state assemblage after those six reactions had, in turn and where possible, been crossed. Of course all the assemblages generated in this way are divariant, since extent of reaction is always either one or zero.

Three parameters are of interest- (i) the ratio of quartz to dolomite in the starting assemblage (or initial qz:dol, IQD).

(ii) the total initial Kfeldspar plus muscovite in the starting assemblage (or IKM).

and (iii) the fraction of Kfeldspar to muscovite in that total, X_{KSP} (where $X_{KSP} = KSP / (KSP + MS)$).

These parameters can be combined to map out variations in final assemblages in an interesting way. Figures 4.8, 4.9, 4.10 and 4.11 represent graphs of IQD versus X_{KSP} for IKM values of 6, 10, 20 and 30 mole %, respectively. These show the restrictions on the different end assemblages (coded A to F as before), imposed by starting conditions with differing quartz:dolomite ratio, and differing proportions of Kfeldspar to muscovite, for each of the four total Kfeldspar plus muscovite values.

Several points of interest arise from these results:

(a) C assemblages are only generated at low IKM (6 mole %) and low IQD (1.0). The fact that no C assemblages are found in the South Bay limestones suggests that these rocks had

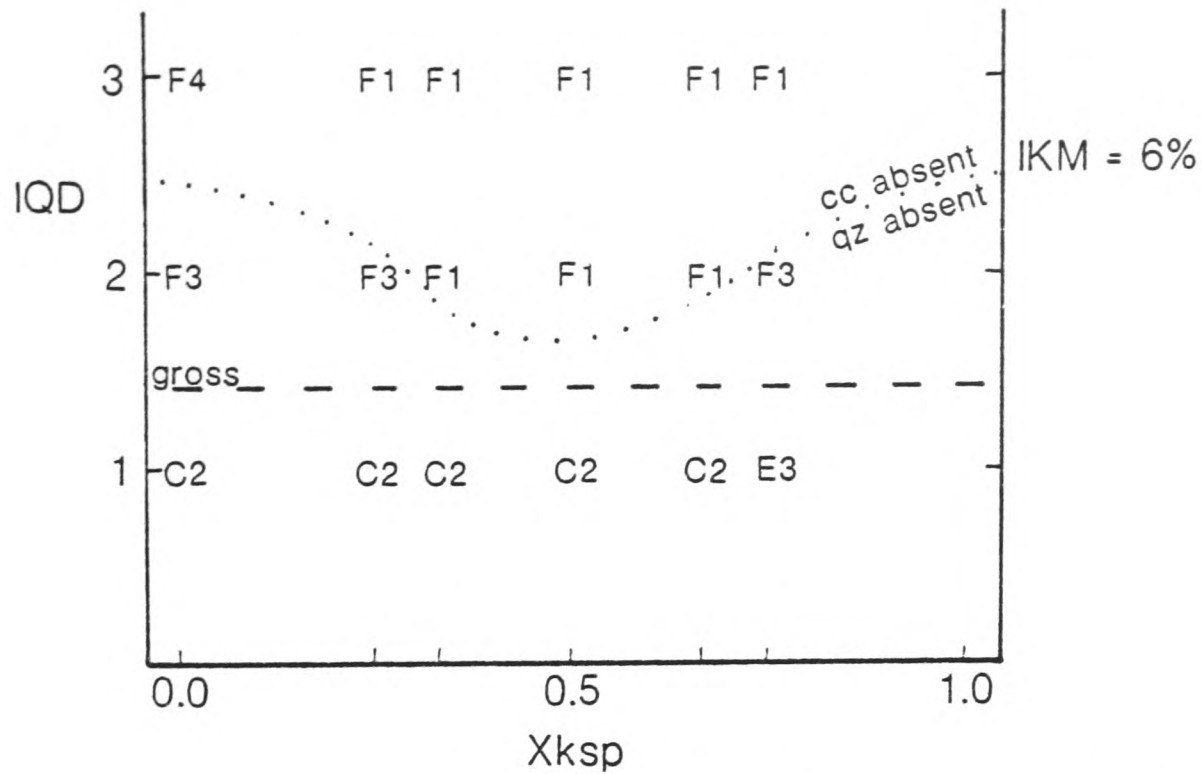


Figure 4.8: Bulk composition control diagram - IKM=6%.

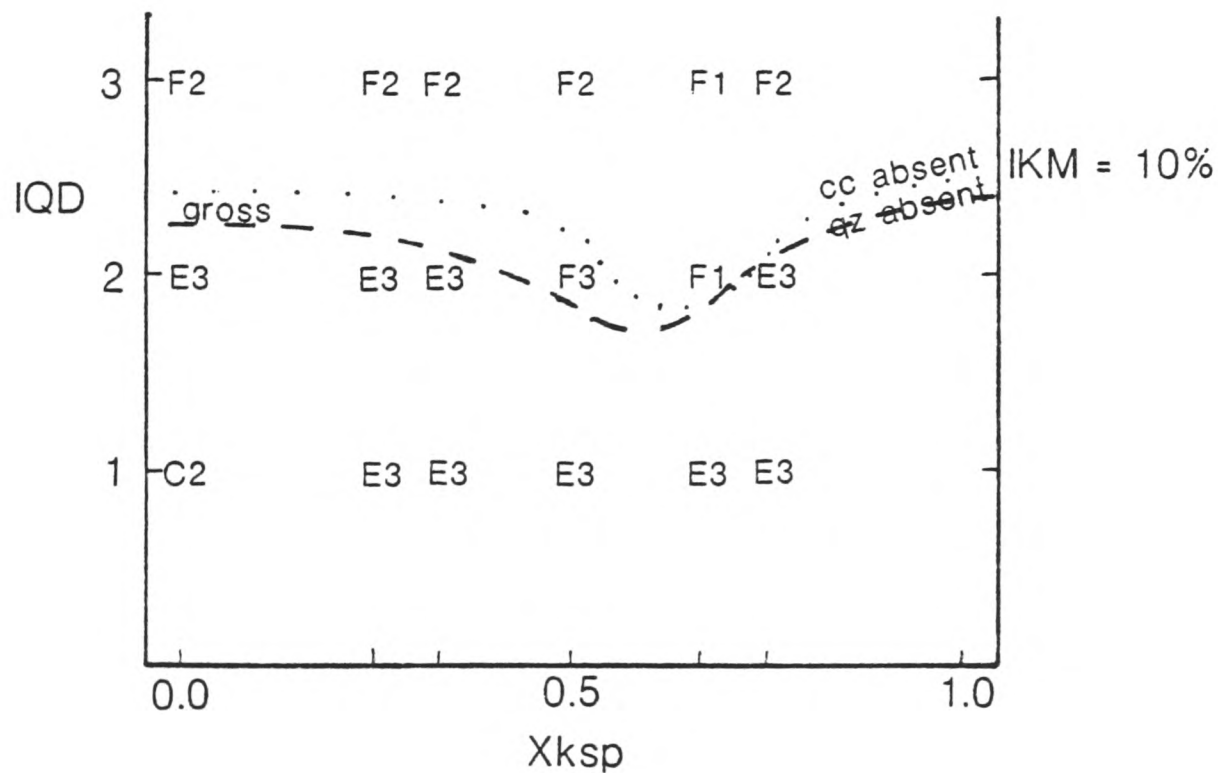


Figure 4.9: Bulk composition control diagram - IKM=10%.

Figures 4.8 to 4.11: Bulk composition control diagrams. Initial quartz/initial dolomite (IQD) versus ratio of Kfeldspar to muscovite (X_{ksp}), for a total Kfeldspar plus muscovite (IKM) in the starting assemblage of 6% (Figure 4.8), 10% (Figure 4.9), 20% (Figure 4.10) and 30% (Figure 4.11). These diagrams show the final assemblages achieved for various starting assemblages, using the sequence of reactions A to F. Above dotted line calcite is absent, below quartz absent. Above dashed line grossular is formed. See text for discussion of the inferences about bulk compositional control which can be made from information on all four diagrams.

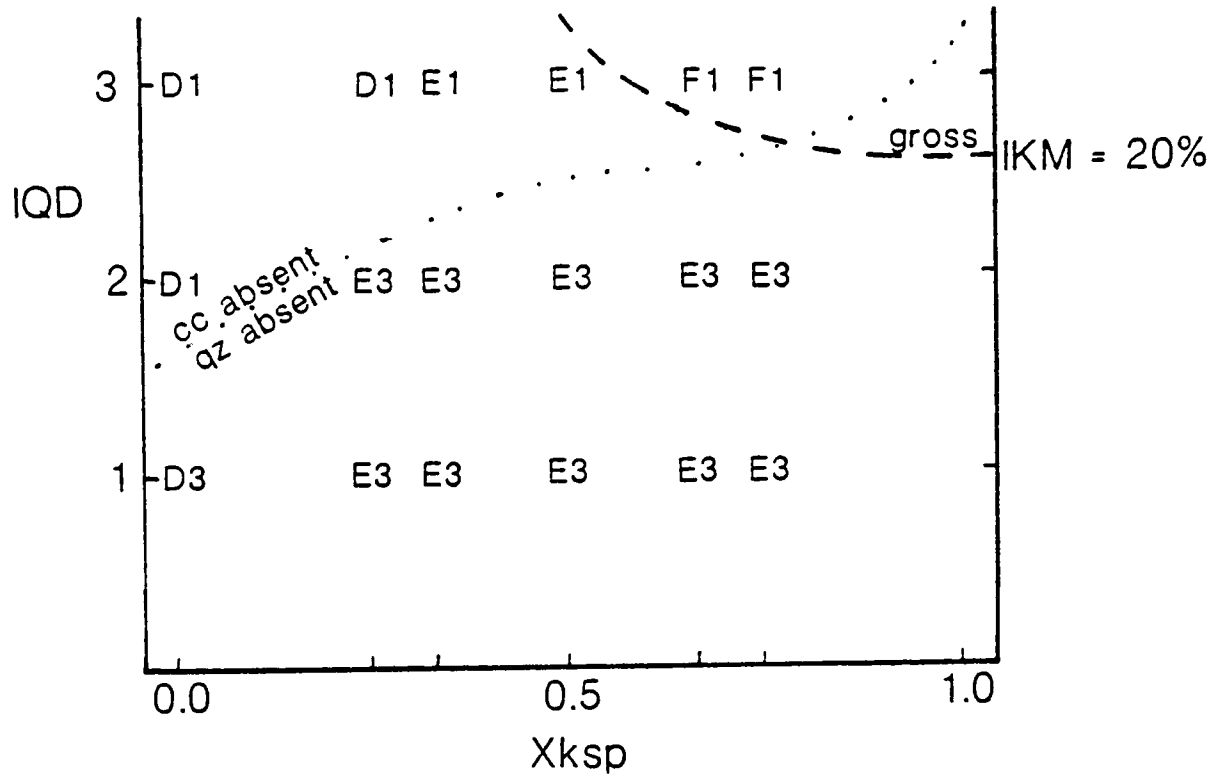


Figure 4.10: Bulk composition control diagram - $IKM=20\%$.

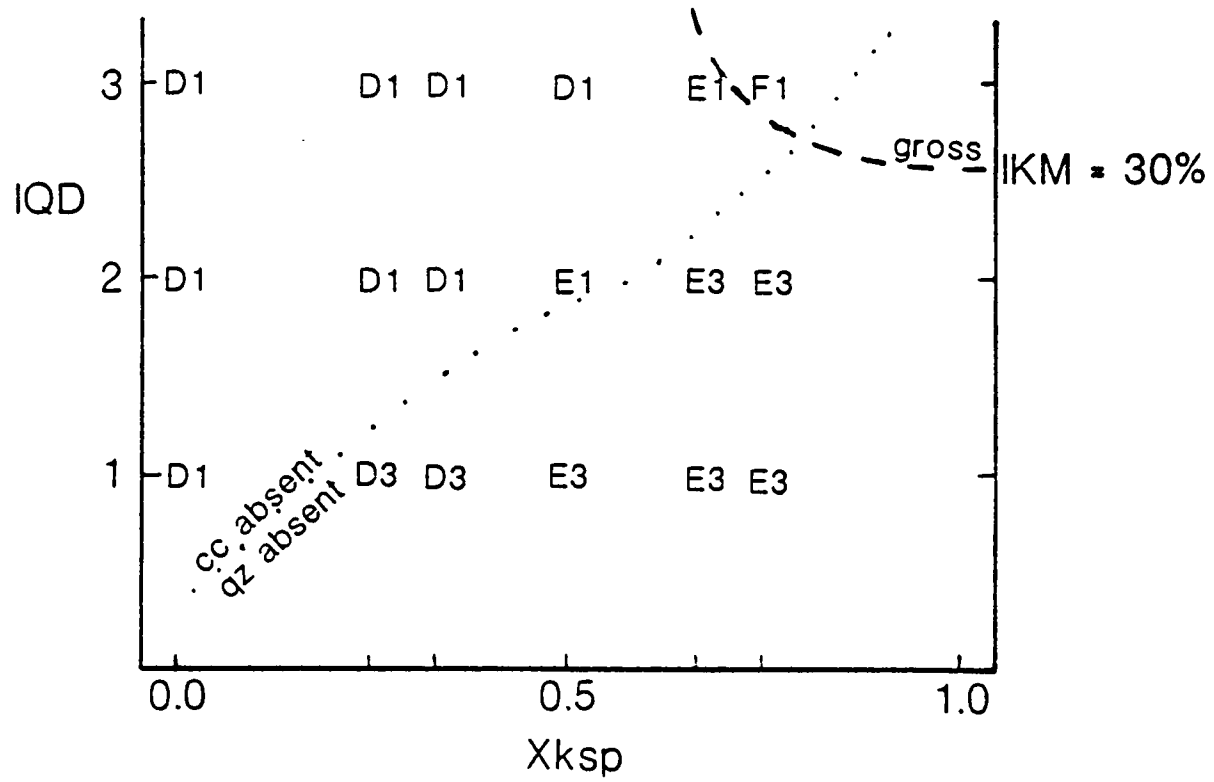


Figure 4.11: Bulk composition control diagram - $IKM=30\%$.

higher IKM and higher IQD.

(b) D assemblages are only generated at high IKM, but with no restrictions on IQD. However, D assemblages are generated at higher X_{KSP} , the higher the IKM. The fact that few D assemblages are found at South Bay places further constraints on the starting mineralogies of these rocks, i.e. they probably contained less than 20 mole % total Kfeldspar plus muscovite initially.

(c) Initial quartz:dolomite ratio (IQD) is obviously significant in determining 1) which reaction is achievable for a particular X_{KSP} (i.e. how low the upper limit of the equilibrium X_{CO2} value of the intergranular fluid can be). 2) whether the end assemblage is quartz or calcite free. Higher IQD appears to allow the completion of more reactions, and is more likely to result in a quartz-bearing end assemblage. The fact that most South Bay assemblages are quartz-bearing suggests that the IQD was fairly high, probably over 2.0 .

(d) The initial total Kfeldspar plus muscovite (IKM) obviously exerts an influence on the range of IQD and X_{KSP} values at which the formation of grossular is possible (assemblage F). The optimum value seems to lie below 10 mole %, above which IQD's of 3.0 are necessary.

Looking at the detailed map of assemblages in Limestone B at South Bay (Figure 4.7), it seems possible that the thick band of grossular bearing F assemblages represents a sedimentary layer which is quartz-rich. If, as is likely, because of the constraints on grossular production imposed at higher IKM, this value is around 10 mole % for these rocks, then this implies that the layer contained at least twice as much quartz as dolomite (in molar terms) before the infiltration event. That is to say, the layer was originally a quartz-rich or sandy limestone, rather than a pure one.

4.3.2: Real assemblages

The modes of some F assemblages found in the limestones at South Bay are presented in Table 4.1. Most of the real assemblages there are univariant, (see Figures 4.6 and 4.7) and all F assemblages are so. That is, they represent an extent of reaction of between zero and one, for their particular reaction. As a consequence of this, modes for real rocks in Table 4.1 are given as they would be if their extent of reaction was one. In each of these cases this would involve the consumption of clinozoisite rather than calcite or quartz. Such modes can thus be compared with some examples of predicted modes, calculated as described above. Observed modes represent volume percentages, however, and in order that correct comparison may be made, these volumes have been converted to molar percentages using the volume data of Helgeson *et al.* (1978).

This table shows some interesting features. The major discrepancy between the actual and the predicted lies in the relative proportions of grossular and tremolite, the amount of grossular in the predicted being consistently too low, and tremolite too high.

One possible way of solving this is to allow the starting mineralogy to contain mostly calcite, as well as some dolomite. Starting with calcite only is not feasible, as biotite and thus tremolite will then never appear. Starting with calcite and dolomite together implies the existence of some other calcite and dolomite-relating reaction, at lower temperature, perhaps, which in a sense negates the model method based on the six reactions described, but is otherwise perfectly reasonable. However, predicted modes calculated using these sort of starting assemblages consistently contain too little grossular, so they are no real solution.

The fact that a complete match for observed modes cannot be obtained by the computation as described can be seen as reflecting the difficulty of distinguishing tiny, low birefringence clinozoisite from grossular in thin section, or,

<u>STARTING ASSEMBLAGE</u>						<u>ROUTE</u>	<u>END ASSEMBLAGE (F2) $E_r = 1$</u>					
<u>PREDICTED</u>	qz	ksp	ms	dol	cc		qz	cc	gross	trem	ksp	czo
1*	75.00	1.92	1.92	21.15	-	ABCEF	67.65	13.24	3.68	8.09	7.35	-
	71.70	2.83	2.83	22.64	-	ABCEF	59.83	11.30	6.28	10.04	12.55	-
	72.73	4.55	4.55	18.18	-	ABDEF	65.41	-	6.02	7.52	18.80	2.26
	67.83	6.52	6.52	19.13	-	ADEF	50.82	-	3.77	8.64	29.46	7.31
2*	69.64	7.14	3.57	19.64	-	ADEF	58.78	2.29	7.63	8.40	22.90	-
3*	72.56	3.50	3.50	20.44	-	ABDEF	64.23	3.86	7.66	8.94	15.31	-
	67.57	2.70	2.70	4.50	22.52	ADEF	66.67	21.84	3.45	1.15	6.90	-
	67.58	2.70	2.70	9.50	17.52	ABDEF	63.80	21.79	3.89	2.74	7.78	-
<u>OBSERVED</u>						ROCK X17NA	61.63	23.23	8.26	2.04	4.84	-
						X12W	42.12	42.93	10.55	1.19	3.21	-
						CA60	50.56	8.99	35.09	2.21	3.20	-

Table 4.1: Real and predicted modes of grossular-bearing metacarbonates from South Bay. Predicted values calculated by methods described in text. All values given as molar percentages, and for $E_r = 1$. Predicted modes consistently contain less grossular than observed modes, and relative proportions of grossular and tremolite are incorrect.

perhaps more reasonably, as some measure of the inapplicability of such a simple set of model reactions (which neglect real solid activities) to a natural rock system.

4.3.3: Paths to grossular formation

The reaction path taken to form each grossular-bearing assemblage, in terms of the six reactions A to F, varies, and this variation is related to the value of the total initial Kfeldspar plus muscovite. This is simply because reactions A, B and C involve dolomite, and the different paths represent the different stages at which dolomite is consumed. For reaction A (101), if initial mole% Kfeldspar is greater than three times initial mole% dolomite then reaction stoichiometry implies that dolomite will be completely consumed in that reaction, and so on.

The three possible reaction paths to grossular formation are thus A-B-C-E-F, A-B-D-E-F and A-D-E-F, as can be seen from Figure 4.5. At South Bay it is not possible to determine which path dominated, because no B or C divariant assemblages occur. This may only mean that those reactions always proceeded to completion, rather than that the path always bypassed them. A consequence of this is that calculation of fluid:rock ratio for all the reactions in each of these sequences, based on modal counts, is not possible (see section 4.4.2).

4.4: Fluid:rock ratio

4.4.1: Calculation of fluid:rock ratio

The fluid:rock ratio for a reference volume of rock can

be derived from a knowledge of the equilibrium X_{CO_2} value of the fluid (i.e. the position of the reaction in T - X_{CO_2} space), and the extent of reaction (Ferry, 1980). One formulation of this, for infiltration of pure water, is given by Rumble et al. (1982) as:

$$V_{\text{H}_2\text{O}}^{\text{ext}} = V_{\text{H}_2\text{O}}^{\text{P,T}} [n_{\text{CO}_2}^{\text{rxn}} - X_{\text{CO}_2}^{\text{eq}} (n_{\text{CO}_2}^{\text{rxn}} + n_{\text{H}_2\text{O}}^{\text{rxn}})] / X_{\text{CO}_2}^{\text{eq}}$$

where $V_{\text{H}_2\text{O}}^{\text{ext}}$ = volume of externally derived water,
 $V_{\text{H}_2\text{O}}^{\text{P,T}}$ = molar volume of water at P,T of interest,
 $X_{\text{CO}_2}^{\text{eq}}$ = equilibrium X_{CO_2} value of the fluid,
 and n_i^{rxn} = number of moles of 'i' produced by a reaction in 1000cm^3 of rock.

The values n_i^{rxn} are calculated from observed modes (or volume%), converted to molar percentages using mineral volume data, using reaction stoichiometry and the extent of reaction, ξ_r . Obviously the form of the mineral reaction used is critical, as the reaction stoichiometry directly determines the relative amounts of volatiles evolved. Since end-member phase reactions are hardly likely to give the 'true reaction' stoichiometries, fluid:rock ratios are at best only an estimate of the true amounts of fluid involved.

The molar amounts of each mineral produced by the reaction are calculated relative to a reference volume, and the total amount of infiltrated fluid is always given relative to that same reference volume in the fluid:rock ratio. The absolute value of that reference volume is thus not critical to the numerical solution of the fluid:rock ratio, although it is usually quoted as 1000cm^3 , a 10cm cube. Using this value does assume that the fluid is moving through such a volume of rock evenly, and having a similar effect throughout. This may not be the case where fluid pathways are long, narrow veins.

A greater failing of fluid:rock ratio as a useful parameter is its time-averaged nature. Since the extent of reaction as observed represents an end-state to the infiltration process, and tells nothing of the time over

which the reaction was proceeding, the amount of infiltrating fluid needed to enable the reaction to proceed is thus calculated for that time as a whole. Fluid:rock ratio therefore tells nothing of the rate at which fluid infiltrated, or whether flow was uniform, or in spurts.

4.4.2: Fluid:rock ratios from South Bay metacarbonates

Calculation of fluid:rock ratios for reactions A to E in the South Bay carbonates involves several compromises.

a) Lack of observed A, B and C assemblages has made it necessary to use artificial modes, namely those predicted by the reaction sequence program.

b) The fluid:rock ratios for observed D and E assemblages cannot be given with any confidence, because extent of reaction cannot be calculated. This is because the reaction path before reactions D and E cannot be determined, and thus neither can the amount of some product minerals in the assemblage which may be in part the result of an earlier reaction. Therefore fluid:rock ratios for D and E assemblages have also been calculated using predicted modes. These modes, used in this way, are specific to the one of the three reaction paths in which they appear. The fact that predicted modes generally differ from the observed rock modes results in slight, but unavoidable, errors in the fluid:rock ratios calculated from them.

c) Since the reaction paths for real assemblages are not known, only a range of fluid:rock ratio for each reaction calculated from the predicted modes can be taken. These values, given also in Table 4.2, are as follows:

A : 0.18 - 0.56

B : 0.82 - 1.13

C : 1.50

D : 0.55 - 2.24

E : 3.67 - 5.70

REACTION:	A	B	C	D	E	F
<u>PREDICTED</u>						
1* :	0.18	0.82	1.49	-	3.66	5.53
2* :	0.55	-	-	2.23	5.57	8.84
3* :	0.32	1.12	-	0.55	5.69	9.66

CALCULATED

ROCK X17NA:	$E_r = 0.59$,	$n_{CO_2} = 1.86$,	$n_{H_2O} = 0.37$,	F:R= 9.26
X12W :	$E_r = 0.48$,	$n_{CO_2} = 1.85$,	$n_{H_2O} = 0.36$,	F:R= 9.71
CA60 :	$E_r = 0.39$,	$n_{CO_2} = 3.33$,	$n_{H_2O} = 0.66$,	F:R=16.59

Table 4.2: Predicted and calculated fluid:rock ratios from South Bay high grade carbonates. Predicted ratios are calculated from predicted modes 1, 2 and 3 of Table 4.1, for each reaction in the reaction sequences ABCEF, ADEF and ABDEF respectively, and are not cumulative. Calculated ratios are given for three grossular-bearing rocks, and can be compared with the predicted values for reaction F. E_r is extent of reaction, n_{CO_2} and n_{H_2O} are the number of moles of each volatile released by reaction F in 1000cm^3 of rock. All fluid:rock ratios are expressed relative to 1000cm^3 rock.

Fluid:rock ratios for reaction F, however, can be calculated with confidence. Since grossular only appears by this reaction, the amount of grossular is independent of path, and the extent of reaction can be determined. Values for real assemblages, also given in Table 4.2, are of the order of 9.0. These values are calculated assuming infiltration of pure water, and thus represent minimum estimates.

Looking at Table 4.2, several points are of note:

i) For each of the three reaction paths (ADEF, ABCEF, ABDEF), the necessary fluid:rock ratio increases along that path. This shows that a fluid:rock ratio great enough to allow grossular to form is great enough to allow all of reactions A to E to proceed to completion. This means that the amount of grossular in a rock will be dependent only on the extent of reaction in reaction F, (and thus the fluid:rock ratio for that rock), and not on a shortage of reactants due to incomplete reaction in previous reactions. It also shows that, putting aside any bulk compositional control, if the fluid:rock ratio dropped below 5.70 in any volume of rock, grossular would not form, and the assemblage that did form would be a measure of the fluid:rock ratio. This means that, in such conditions, the distribution of assemblages in Limestone B, for example (see Figure 4.7), could also be viewed as a distribution of fluid:rock ratios.

It has been noted, however, that many of the rocks in Limestone B contain several different assemblages within a thin section. This means that if the calculated variations of fluid:rock ratio are real, and thus occur on a thin section scale, then the fluid transport process must have been such that very small adjacent volumes of rock experienced different infiltration histories.

ii) The fluid:rock ratio for real F assemblages are very high, between 9 and 10 for rocks X12W and X17NA, and 16.5 for rock CA60.

The fact that the values for the same assemblage are not all the same necessarily implies real variation in fluid:rock ratio. However the values are all much higher than those necessary for reactions A to E to proceed to

completion. If such large volumes of fluid did infiltrate all the carbonates equally, this would explain why no A,B or C assemblages are found. The fact that D and E assemblages are found would then be evidence for bulk compositional control.

iii) The fluid:rock ratios for X12W and X17NA are very similar, and smaller than that of CA60. The former have broadly similar quartz:calcite proportions, and grossular contents, and indeed appear to form part of a thicker than average sedimentary unit, perhaps of uniform bulk composition (see Figure 4.7). In contrast, CA60 is less calcareous, and very clinozoisite and grossular-rich (see Table 4.1). Since the extent of reaction for CA60 is not significantly higher than for X12W and X17NA (in fact it is the lowest of the three), this implies quite striking variations in bulk composition.

4.5: Conclusions

The conclusions to be made from this chapter are as follows-

1. Infiltration of an H₂O-rich fluid occurred during prograde metamorphism of the South Bay carbonates. All of the rock was affected to some extent by this infiltration.
2. Two possibilities exist for the infiltration model: a) Equal, high fluid:rock ratio throughout, assemblages controlled in part by bulk compositional constraints. b) High to low variable fluid:rock ratio throughout, often variable over very small distances.
3. Neither of the two models above can be easily eliminated. The first seems likely, in view of the demonstrated effect slight variations in, for example, initial quartz:dolomite ratio could have. Such variations are perhaps to be expected in sandy limestone sequences.

The second possibility depends in part on whether it

can be demonstrated that such small-scale variations in fluid:rock ratio are feasible within metamorphosing carbonate rock. This demands knowledge of the nature of the fluid transport process, in particular the size and distribution of fluid pathways, and is the subject of Chapter 6.

4. The secondary, retrograde, assemblages have not been described in any detail in this chapter. This is because their metamorphic history is difficult to determine unequivocally without evidence of another sort, namely carbon and oxygen isotopic compositions. Therefore the treatment of these rocks is left until the end of the next chapter, Chapter 5, which describes the regional and local variations in those stable isotope compositions, in Knapdale.

C H A P T E R 5: Stable isotopes

5.1: Introduction

Variations in the stable isotope ratios of elements in natural systems are the result of two processes: a) radioactive decay of unstable parent to stable daughter isotopes. b) fractionation due to physico-chemical processes which are dependent on the mass of an isotope.

In systems of geological interest, the former phenomenon can be used to calculate the age of the rocks, and some features of its origin. This involves the use of the isotopes of uranium and lead, rubidium and strontium, samarium and neodymium, and potassium and argon.

The latter phenomenon is of interest mainly with respect to some lighter elements, namely carbon, oxygen, hydrogen and sulphur, and the isotope ratios of interest are $^{13}\text{C}/^{12}\text{C}$, $^{18}\text{O}/^{16}\text{O}$, D/H and $^{34}\text{S}/^{32}\text{S}$ respectively.

In metamorphic petrology these ratios can be used in three main ways: (i) as geothermometers. (ii) to study diffusion and the kinetics of reactions. (iii) as tracers, to allow isotopic comparison of rocks from different areas and/or at different metamorphic grades, to investigate the attainment and scale of equilibrium between rock or rock-fluid systems, and to determine the origin of metamorphic fluids.

The last of these three has been concentrated on in this study, which investigates carbon and oxygen isotope ratios in carbonates from Knapdale.

5.2: Isotopic notation

In stable isotope geochemistry, isotope ratios are presented as values relative to a standard, in the form of δ (per mil), where

$$\delta = \frac{R_{\text{sample}}}{R_{\text{standard}}} - 1 \times 1000 ,$$

and R = isotope ratio of interest (e.g. $^{18}\text{O}/^{16}\text{O}$).

The standards used internationally are, for oxygen, Standard Mean Ocean Water (SMOW), ($^{18}\text{O}/^{16}\text{O} = 1.99 \times 10^{-3}$), and for carbon, Peedee Formation belemnite (PDB), ($^{13}\text{C}/^{12}\text{C} = 1.122 \times 10^{-2}$).

The isotopic partition coefficient, or fractionation factor, for two phases or species is α , where -

$$\alpha_{AB} = \frac{R_A}{R_B}$$

From the definition of δ , and when $-10 < \delta < 10$, then to a good approximation,

$$1000 \ln \alpha_{AB} = \delta_A - \delta_B .$$

5.3: Analytical methods

Analyses of $^{13}\text{C}/^{12}\text{C}$ and $^{18}\text{O}/^{16}\text{O}$ ratios in carbonates from throughout Knapdale were performed in the Stable Isotope laboratories at the Scottish Universities Research and Reactor Centre, East Kilbride.

Whole rock metamorphic carbonate specimens were crushed and sieved, and the fraction under $78\mu\text{m}$ from each was collected. These fine-grained powders were reacted under vacuum at 25°C with 100% H_3PO_4 for a minimum of 14 hours, and the CO_2 gas thus liberated was extracted and purified in a vacuum line using liquid nitrogen and acetone-solid CO_2 cold traps. Samples along with laboratory standards were analysed in a double-collecting Phillips 903

spectrometer, precision of results being consistently of the order of 0.1 per mil for both carbon and oxygen, with good reproducibility.

5.4: Isotope fractionation effects

These can be divided into a) equilibrium isotope effects, and b) kinetic isotope effects.

The equilibrium fractionation between two species is related to the different partitioning of the various isotopes into the different available sites according to their vibration frequencies. These effects have been proven to be dependent on temperature, and possibly even pressure, where supercritical fluids are involved (Sheppard, 1979). For minerals, such equilibrium fractionation factors must be measured experimentally e.g. O'Neil & Taylor(1967), whereas for gases they can be calculated from spectroscopic data (Bottinga, 1969). Figures 5.1 and 5.2 show a number of fractionation factors for carbon and oxygen plotted as $1000\ln\alpha_{AB}$ versus temperature; these are taken from the compilation of theoretical and experimental data of Friedman & O'Neil(1977). The CO_2 -calcite fractionation curves indicate that the CO_2 in equilibrium with metamorphic calcite at 500°C is around 3 per mil richer in ^{13}C , and the H_2O -calcite fractionation curve that H_2O is around 1 per mil richer in ^{18}O .

Kinetic fractionation of isotopes arises because many chemical reactions are accompanied by non-equilibrium effects, in that isotopic mass can affect rates of reaction. In practice this may mean that the products of a reaction are enriched in the lighter isotope. For carbonate rocks undergoing metamorphism, this means that a series of decarbonation reactions could result in systematic changes in isotope ratios. Systematic lowering of $\delta^{18}\text{O}$ and $\delta^{13}\text{C}$ with increasing metamorphic grade has been described by Shieh & Taylor(1969), and by Rye et al. (1976).

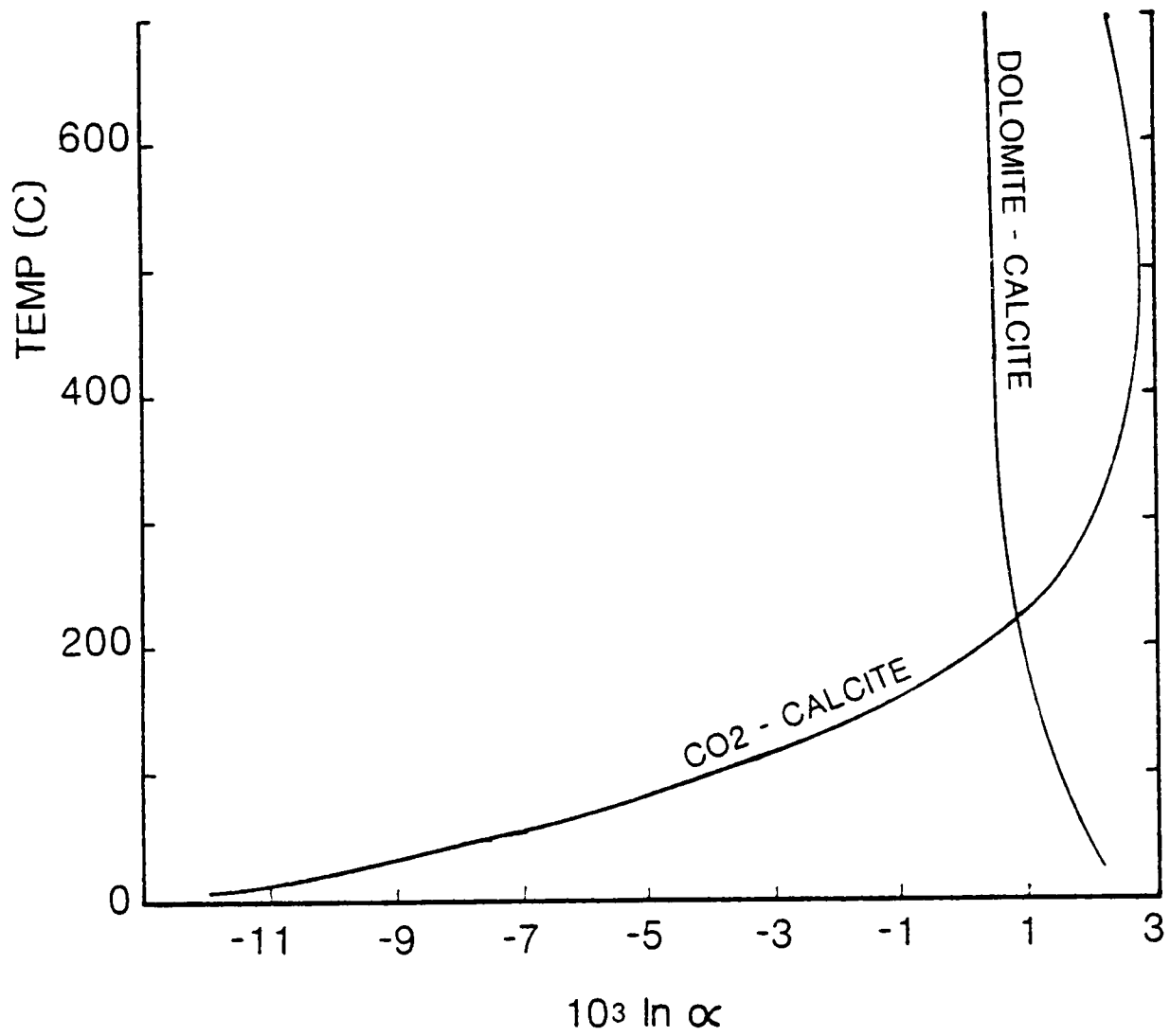


Figure 5.1: Fractionation curves for Carbon taken from Friedman & O'Neil(1977). Each curve shows the variation with temperature of the fractionation factor of $10^3 \ln \alpha$ (or per mil) between the phases named. At 500°C , $\delta^{13}\text{C}(\text{dolomite})$ is less than 1 per mil greater than $\delta^{13}\text{C}(\text{calcite})$.

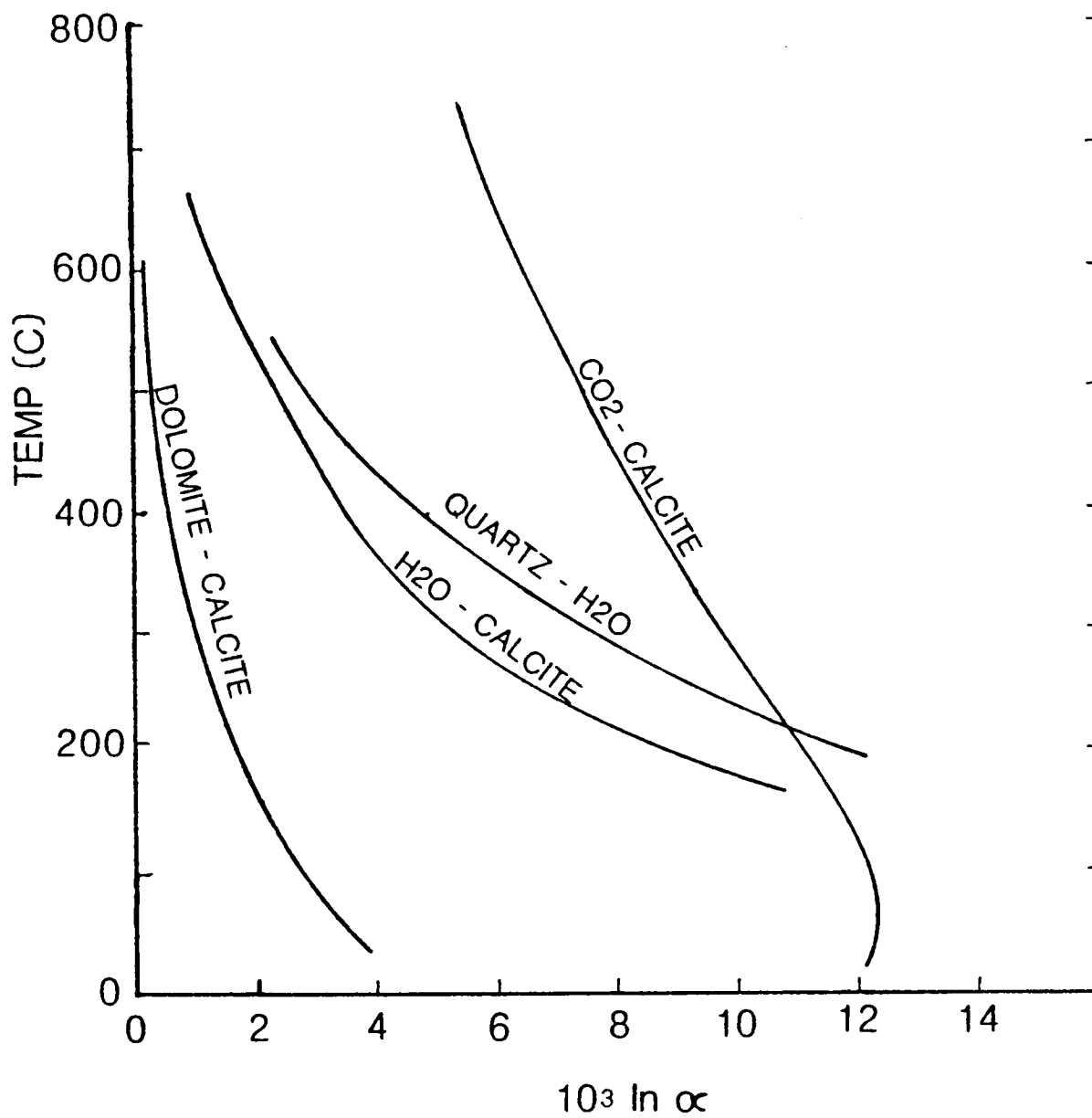


Figure 5.2: Fractionation curves for Oxygen taken from Friedman & O'Neil(1977). Each curve shows the variation with temperature of the fractionation factor of $10^3 \ln \alpha$ (or per mil) between the phases named. At 500°C , $\delta^{18}\text{O}(\text{dolomite})$ is less than 1 per mil greater than $\delta^{18}\text{O}(\text{calcite})$.

5.5: Results and interpretation

Measured carbon and oxygen isotope ratios of metacarbonate rocks from Knapdale are divided into three groups: (i) High Grade- South Bay, (ii) High Grade- Elsewhere in Knapdale, and (iii) Low Grade- Remainder of Knapdale; these are presented in Table 5.1 .

In addition, all results are plotted on a graph of $\delta^{13}\text{C}$ versus $\delta^{18}\text{O}$ (Figure 5.3). This graph also includes isotope data collected by B.Turi and S.M.F. Sheppard for Knapdale metabasites and their immediate country rock, which are summarised in Graham et al. (1983).

5.5.1: Isotopic variations: a three fluid model

Figure 5.3 shows that the data falls clearly into three separate groups, which are characterised as follows:

Group 1: $\delta^{13}\text{C} = -16$ to -4 per mil (PDB)
 $\delta^{18}\text{O} = +8$ to $+12$ per mil (SMOW)

Group 2: $\delta^{13}\text{C} = -4$ to $+8$ per mil (PDB)
 $\delta^{18}\text{O} = +9$ to $+19$ per mil (SMOW)

Group 3: $\delta^{13}\text{C} = -1$ to $+5$ per mil (PDB)
 $\delta^{18}\text{O} = +24$ to $+30$ per mil (SMOW)

Groups 2 and 3 contain all the carbonate rock values, and with the exception of Rock X16, which contains calcite and lies within Group 3, correspond exactly to a division into calcite and dolomite-bearing marbles, respectively. Group 1 is distinct from the two carbonate rock groups, and is composed entirely of values from the metabasite sills of Knapdale and from schists and phyllites adjacent or near-adjacent (<12m) to them. The single Tayvallich lava specimen, and its adjacent limestones, however, fall into the calcite marble group rather than into the sills group.

Figure 5.2 shows the dolomite-calcite fractionation factor for oxygen. At a presumed peak metamorphic

<u>SAMPLE NO.</u>	<u>LOCATION</u>	<u>^{13}C- PDB</u>	<u>^{18}O- SMOW</u>
CE5	L. Leathan	6.33	14.69
K1	Keills	6.08	15.81
K6	Keills	3.78	15.12
D5	Danna Is.	7.37	17.92
CA124	L. na Craige	3.30	14.01
* CE8	Meall Mhor	-0.20	25.34
CE3	Rhu Pt.	5.45	18.25
CE4	Rhu Pt.	7.54	13.24
CA2	Kennacraig	5.23	12.59
CA9	Kennacraig	-2.11	9.86
* CE10	Ronachan Pt.	4.73	28.30
CE12	Ronachan Pt.	7.39	13.23
CA95	South Bay	0.59	15.87
* CA92	"	-0.04	29.04
CA90	"	1.27	13.55
CA80	"	2.09	13.81
CA58	"	4.04	17.47
* CA57	"	2.79	25.45
* CA47	"	2.33	25.24
X19	"	2.88	13.36
X16	"	1.04	24.80
X1	"	-3.43	11.12
Z14	"	2.87	14.20
Z12	"	1.41	15.23
Z1	"	1.58	12.18

* dolomites

Table 5.1: Carbon and oxygen isotope values from Knapdale.

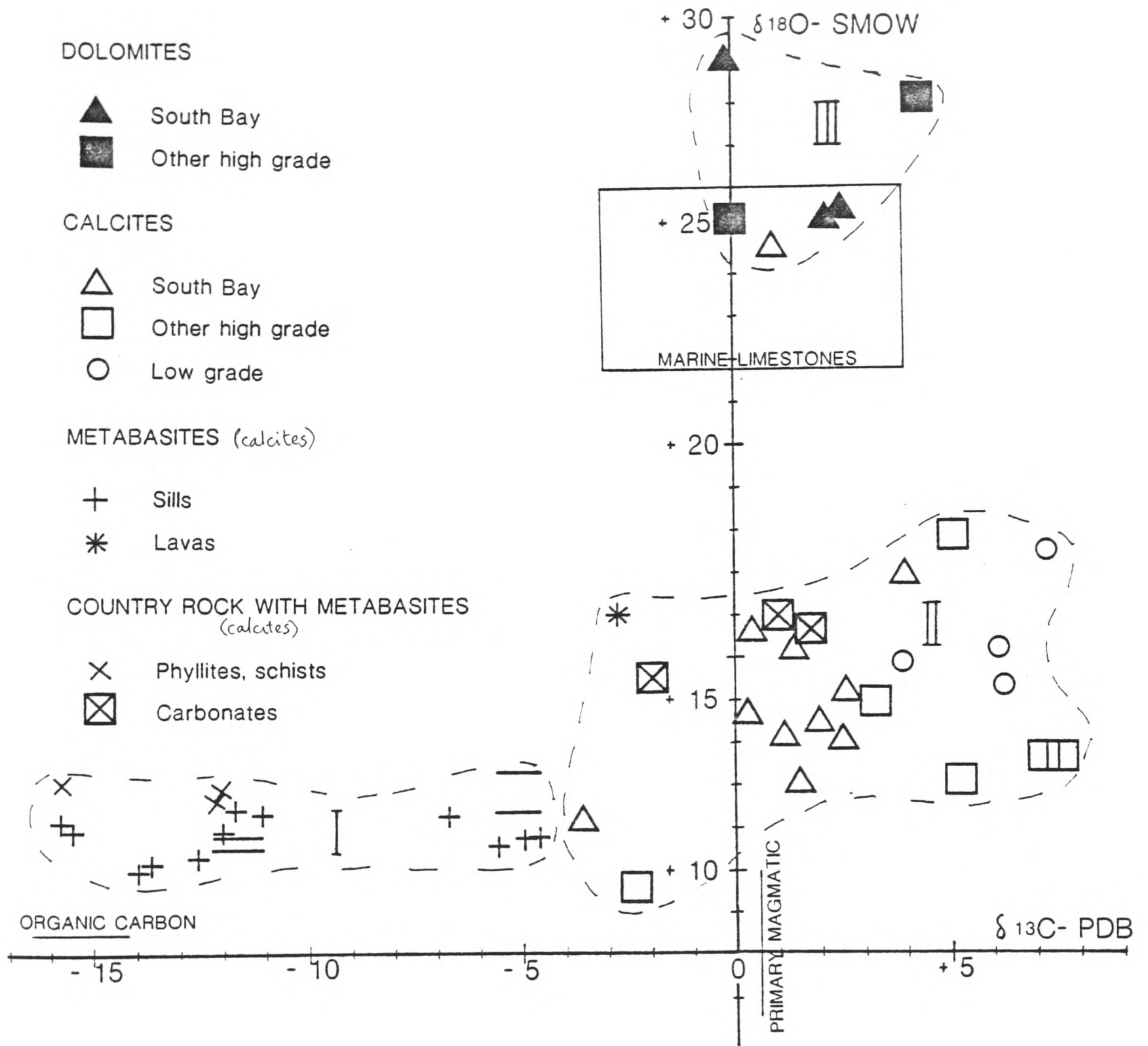


Figure 5.3: Isotope results - $\delta^{18}\text{O}$ versus $\delta^{13}\text{C}$ for Knapdale metacarbonates and metabasites. Dolomite and calcite analyses from this study, the remainder by B. Turi and S.M.F. Sheppard (unpubl.data). The data falls into three groups, labelled I, II and III. Group I is composed entirely of metabasite sills and their near-adjacent country rocks. Group II is composed of primary, calcite-bearing limestones, plus lava and limestone samples. Group III is composed of all secondary, dolomite-bearing limestones, plus one calcite sample.

temperature of $525 \pm 25^\circ\text{C}$, the maximum $1000 \ln \alpha$ value is less than 2. Therefore, barring the unknown effect of high pressure, it is safe to conclude that the observed distribution of isotope ratios in metacarbonates does not represent equilibrium fractionation, as the $\delta^{18}\text{O}$ difference between Groups 2 and 3 is a minimum of 5 per mil. Both these groups lie within the range of $\delta^{13}\text{C}$ and $\delta^{18}\text{O}$ values of metamorphic waters (Sheppard, 1979), and well outside those of magmatic or meteoric waters (plotted on Figure 5.3). Thus it must be inferred that the distribution represents equilibration of carbonates with two distinctly different metamorphic fluids.

It is not possible from the isotope values to demonstrate so clearly that Group 1 values represent equilibration of the rocks of that group with another, distinctly different, metamorphic fluid, because there is some degree of overlap between the groups. However, petrological evidence, or the X_{CO_2} values of the fluids in equilibrium with minerals in (i) metabasite sills at low grade (i.e. in the Tayvallich and North Knapdale areas), and (ii) high grade carbonate rocks (from South Knapdale, see Chapter 2), suggests that two distinct primary fluids did exist (see Graham *et al.*, 1983). The effects of the first, or primary low grade, less H_2O -rich fluid, have been demonstrated petrologically (Graham *et al.*, 1983), and the effects of the second, very H_2O -rich fluid, are in the same way the main subject of this thesis.

Overall, therefore, a three fluid model can be accepted, in which the first two fluids are designated 'primary' but are separate geographically or in structural position (and probably temporally as well), and the third fluid is designated 'secondary' or retrograde, and is also restricted in its area of effect (see Chapter 4).

5.5.2: The primary fluids

1. Primary low grade

The large range of $\delta^{13}\text{C}$ seen in Group 1 is probably a function of the low pre-metamorphic carbonate content of these rocks, which allowed a low $\delta^{13}\text{C}$ (but H_2O -rich) fluid to affect their carbon values.

The low $\delta^{13}\text{C}$ element in the fluid may have formed as a result of oxidation, during metamorphism, of organic material in phyllites, such as has been found in phyllites from Islay (C.M.Graham & R.S.Harmon, unpubl. data), and which has $\delta^{13}\text{C}$ values of around -18 per mil. The lower carbon values in Group 1 are those of the Ardrishaig Phyllites and their sills, and Crinan Grit values are noticeably higher. Thus phyllite within the area itself, although now graphite-free, may have been responsible for such a low $\delta^{13}\text{C}$ fluid, and this prevents 'external buffering' *sensu stricto* being invoked.

Schists and phyllites near to metabasites show $\delta^{18}\text{O}$ values very similar to those of the metabasites. This implies that the latter exerted some 'control' over the former. The extent to which this operated could be investigated further by sampling schists and phyllites at greater distances away from metabasite contacts.

Similar local control of isotope ratios is seen in the Tayvallich lava and limestone ratios, but in this case the lava ratio appears to have been 'controlled' by the limestones, which are locally very common in the lava pile.

2. Primary high grade

The small range of $\delta^{13}\text{C}$ values of Group 2 (and incidentally of Group 3 also), which is largely within that of normal marine limestones, confirms that fluid which affected these rocks was H_2O -rich, since carbonates were able to internally buffer the $\delta^{13}\text{C}$ to their own values.

Figure 5.4 shows the $\delta^{13}\text{C}$ data for calcites (Group 2) plotted against the mineral assemblage in the rock, using the assemblage codes described in Chapter 4. This is effectively $\delta^{13}\text{C}$ versus extent of decarbonation. Two points are of note in this diagram -

(i) the low grade rocks (assemblage B or lower) show significantly higher $\delta^{13}\text{C}$ values. Ohmoto(1970) and Rye & Ohmoto(1974) have shown that very high positive (>20 per mil) $\delta^{13}\text{C}$ values may be the result of a combination of low pH (<6), and very low $f\text{O}_2$ (< 10^{-41}) in graphite-bearing carbonate systems (see Figure 5.5). These high carbon values may only apply to fluid in a closed system in isotopic equilibrium, and as soon as solid phases appeared, some carbon would be removed from the fluid, and the isotopic ratio changed. It is possible that calcite which equilibrated with such a fluid would show $\delta^{13}\text{C}$ values which were some degree lower than that of the fluid, but still unusually high relative to 'normal' graphite-free fluid systems. Therefore, the low grade fluid in Knapdale, giving rise to high calcite isotope values of around +5 per mil, may have been originally CH_4 -rich.

Since the $\delta^{13}\text{C}$ value of such fluids may depend on both pH and $f\text{O}_2$, it is impossible to determine these factors directly. $\delta^{34}\text{S}$ values, however, also depend on pH and $f\text{O}_2$. Therefore with knowledge of both carbon and sulphur isotope ratios in minerals which equilibrated with the fluid, these factors might be evaluated.

(ii) with the exception of Rock CE12, the main group of high grade rocks show an excellent trend of decreasing $\delta^{13}\text{C}$ with increasing extent of decarbonation. Rock CE12 contains a later calcite vein which may bear witness to another, ^{13}C -enriched fluid, or possibly to another complicated fractionation event.

Rocks X1, CA9 and CA95 define a line which exactly parallels the main decarbonation trend. These rocks may have undergone the same process as the main group, but at some later stage have re-equilibrated to some degree with meteoric (very low $\delta^{13}\text{C}$) water.

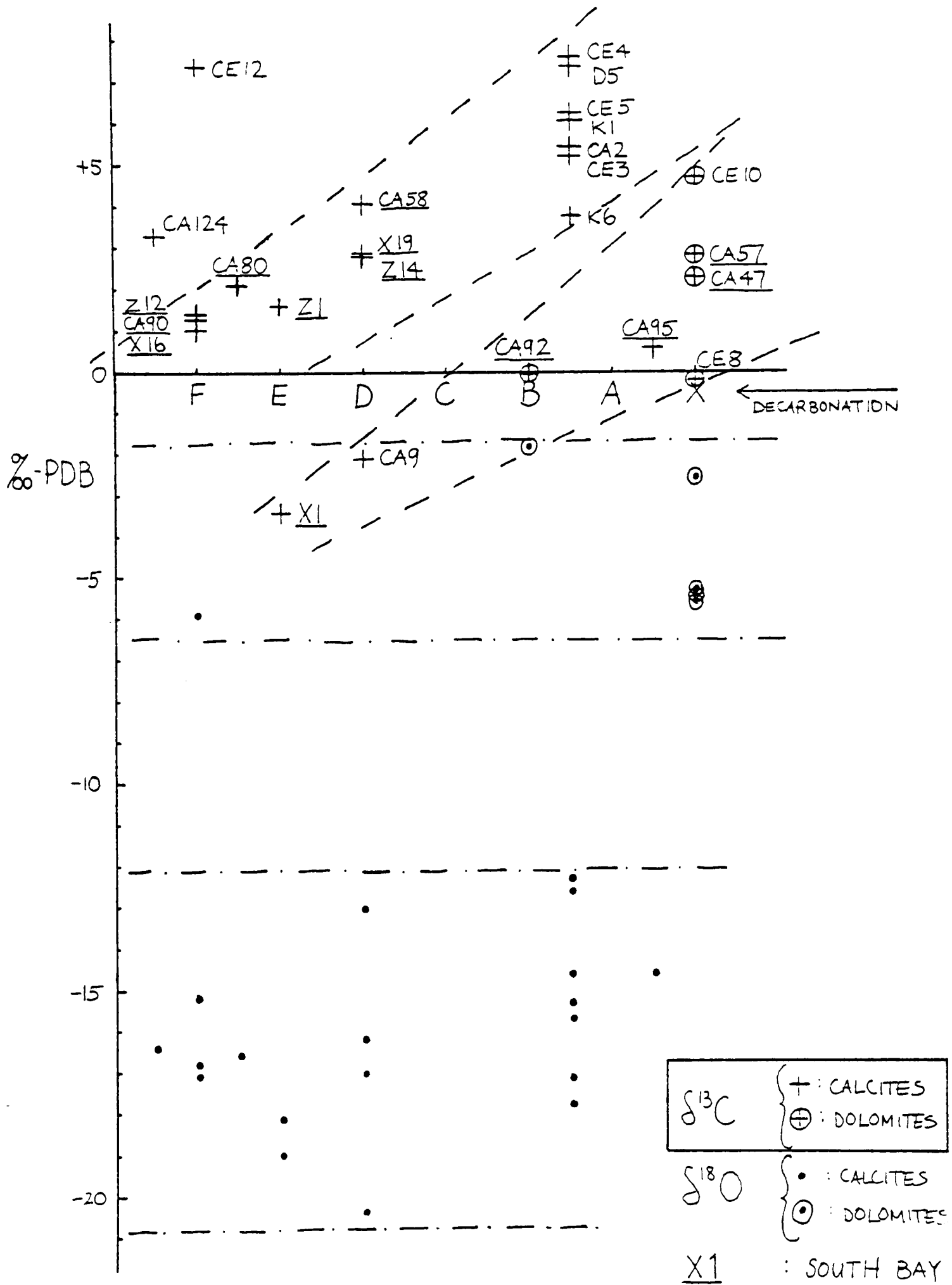


Figure 5.4: $\delta^{13}\text{C}$ versus mineral assemblage for Knapdale metacarbonates. Mineral assemblages are labelled as in Figure 4.5. Calcite samples show a trend of decreasing $\delta^{13}\text{C}$ with increasing extent of decarbonation. South Bay samples underlined.

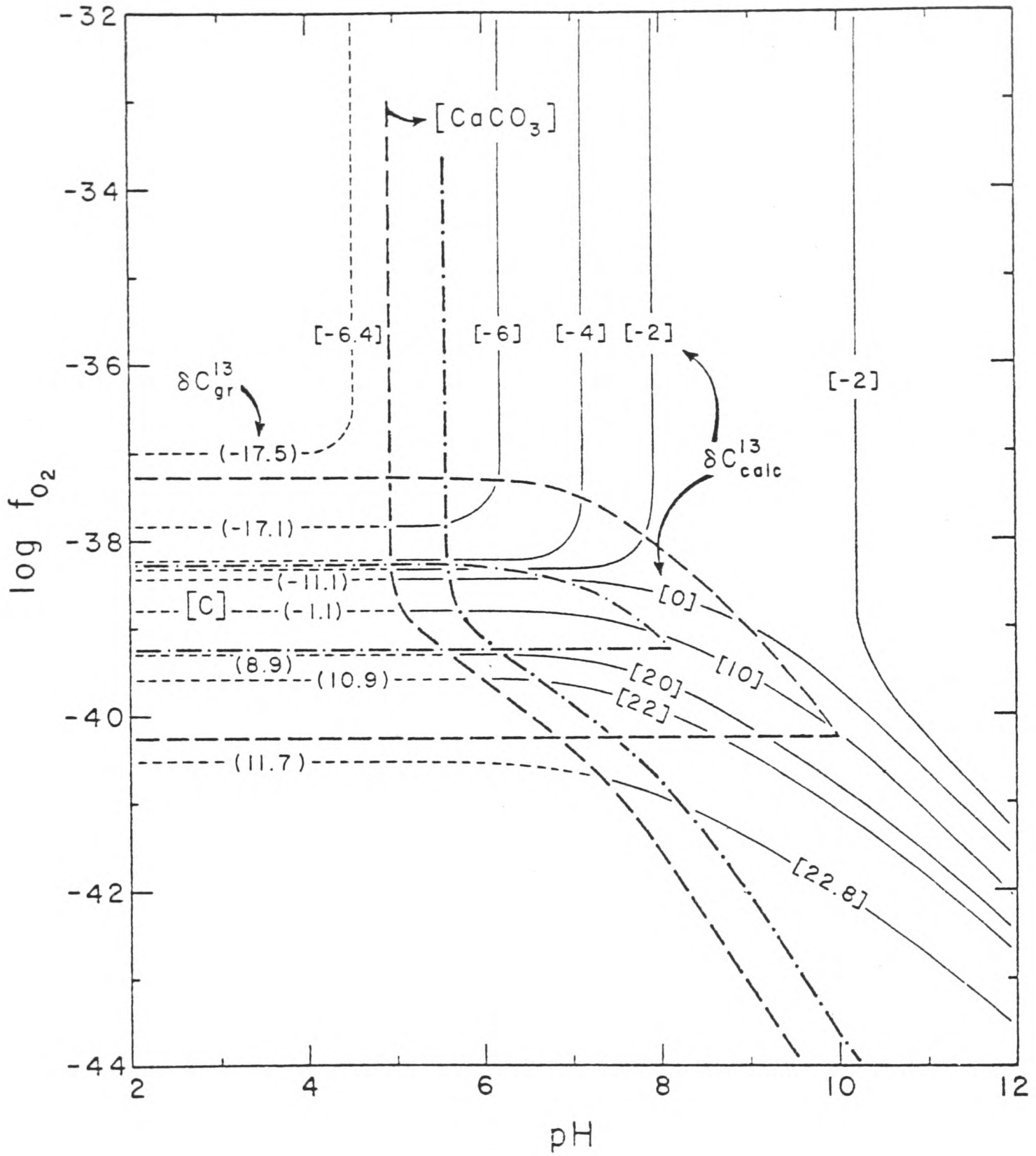


Figure 5.5: Possible variation of $\delta^{13}C$ values of calcite and graphite as functions of pH and oxygen fugacity. Above $f_{O_2} = 10^{-37}$ atm., $\delta^{13}C(\text{calcite})$ varies only as a function of pH. Below that value, however, it decreases with increasing pH, and f_{O_2} . $\delta^{13}C(\text{graphite})$ is strongly dependent on f_{O_2} .

from Ohmoto (1970)

Figure 5.6 shows the same diagram for oxygen ratios. Again removing X1, CA9 and CA95, it is here obvious, however, that no clear trend in $\delta^{18}\text{O}$ value with extent of decarbonation can be recognised. This system therefore stands in contrast to the Vermont and Grenville marbles described by Sheppard & Schwarz (1970), which showed clear decreasing trends in both $\delta^{13}\text{C}$ and $\delta^{18}\text{O}$ with increasing decarbonation.

It has been suggested that the primary fluid responsible for the high grade carbonate, water-rich assemblages was generated by dewatering of metabasite sills at the garnet 'isograd' (see Chapter 2). The normal $\delta^{18}\text{O}$ value for basic rocks is around +5 to +10 per mil (Graham & Harmon, 1983), so the difference between those values and the values of +9 to +19 per mil of the Group 2 rocks must be due to some fractionation process. It may simply reflect equilibrium fractionation of ^{18}O between metabasite minerals and calcite in the resultant fluid, or may be a function of a distillation process during the actual dewatering.

The petrological effects of this second (or primary high grade) fluid have been shown to be limited in extent to South Knapdale (see Section 2.5), so the low grade carbonates from Tayvallich and North Knapdale (open circles in Figure 5.3) cannot have equilibrated with this fluid. Instead they probably equilibrated with the primary low grade fluid, because they occupy the same structural position as the low grade metabasites. This means that the cluster of isotope values comprising Group 2 is in reality made up of two petrologically distinct sub-groups, the low grade carbonates and the high grade carbonates.

The fact that the two sub-groups coincide may mean that either -

(i) both equilibrated with separate fluids which by coincidence (or as part of a general rule?) resulted in their having similar degrees of lowering of $\delta^{18}\text{O}$ relative to unmetamorphosed limestones.

or, (ii) both equilibrated with the primary low grade fluid, and the primary high grade fluid had little or no effect on

the isotope ratios of the rocks through which it passed (aside from a slight shift due to fractionation during devolatilization reactions).

Figures 4.6 and 4.7 show how the South Bay data relate to the outcrop. It can be seen that variation of isotope ratios in primary assemblages from bed to bed is high, whereas ratios within a particular bed are nearly equivalent. This suggests that whereas adjacent beds equilibrated with the primary fluid to different extents, any individual bed equilibrated throughout to the same extent, implying that fluid was channelled along individual beds, as might be expected in the stress-field controlled microcrack propagation model. This is analogous to the case described by Ferry(1979), using a map of chemical potential differences within an outcrop. The persistence of isotopic differences between adjacent beds during and after the primary high grade fluid flow implies that, either -
 (i) there were no fluid pathways between beds,
 or, (ii) there were pathways, but the kinetics of isotopic equilibration along these was too slow.

The differences in ratio from bed to bed can be directly related to extent of decarbonation, which could be a function of fluid:rock ratio, or simply of control by bulk composition (see previous chapter).

This dilemma of variable fluid flow versus bulk composition control cannot be solved by the stable isotope results presented here.

5.5.3: The secondary fluid

Perhaps the most interesting result of this study is the separation of the data into such clearly separate groups, such that Groups 1 and 2 represent the primary metamorphic assemblages, and Group 3 the secondary retrograde assemblages.

With the exception of Rock X16, all the Group 3 values represent dolomite-bearing rocks, which furthermore occur

only in certain well-defined zones (see Figure 4.6). This seems to imply that retrograde fluids were channelled in a confined way, and could not reach the bulk of the carbonates in the section to re-equilibrate and change their primary fluid-imposed oxygen and carbon ratios.

However the major obstacle to overcome in this hypothesis of tightly channelled retrograde fluid flow, is Rock X16. This sample lies well within Limestone unit B, and contains not dolomite but the highest, most H_2O -rich assemblage seen. Yet its isotope ratios fall wholly within those of the retrograde group. Its $\delta^{18}O$ has obviously re-equilibrated with the later fluid, and since the $\delta^{13}C$ values of primary and secondary events are very similar, it seems reasonable to assume that its carbon isotopes have re-equilibrated too. Thus with no obvious physical evidence of later veining etc., one is forced to conclude that in some way fluid of the retrograde event came in contact with this rock, re-set the isotope ratios, but did not change the mineralogy. Furthermore, no adjacent rocks were affected. Although this points to the possibility of more widespread retrograde fluid flow, the evidence of the rest of the primary assemblages remains to show that that was not the case. It may have implications for the duration of fluid flow events and the kinetics of mineral reactions, though. It is possible that the retrograde fluid flushed through Rock X16 so quickly that, although isotope ratios were re-set in that time, mineral assemblages did not have time to change before the system again became 'sealed'.

As to the origin of the secondary fluid, it is clear that it was H_2O -rich, but that its $\delta^{18}O$ signature was substantially different from that of the primary fluids. The $\delta^{18}O$ values of +24 to +29 per mil are very high, higher even than marine limestone values, and as such represent a problem in interpretation. Some origin in processes outwith the Knapdale area must be invoked, for the secondary fluid cannot have been in equilibrium with any of the Knapdale rocks.

The only rocks in Knapdale which show petrographic

evidence of retrograde fluid infiltration are the high grade carbonates, and the albite schists (see Chapter 2), which both lie in the zone of secondary deformation (i.e. the Tarbert Monoform). Isotope data confirms the retrograde nature of the carbonates (now dolomite), but no albite schists have yet been analysed.

This lithological control may have been purely structural, with the aforementioned rocks acting as weaker zones along which the retrograde fluids easily passed. Alternatively, it may be that only in those rocks was the pre-existing mineralogy such that the retrograde fluid could react with the mineral assemblages. Or it may be a combination of both hypotheses. In any event, this example sheds light on the whole process of retrogression by fluids, and may be the first to demonstrate clearly the external-to-the-system (or 'exotic') nature of a retrograde fluid, by isotope means.

While it is possible to ascribe generation of the primary fluids to: (i) low grade dewatering of sediments, along with oxidation of organic matter, and (ii) dewatering of metabasite bodies, that is, processes which acted within the rock system, this stands in contrast to the secondary fluid, for which no obvious precursor or generative process exists.

C H A P T E R 6: Fluid transfer processes in metamorphism

6.1: Introduction

Fluids have been found to play a major role in many of the processes which transform the Earth's crust. In fact the role played by fluid in many cases may be termed so vital, that fluids can indeed be considered one of the major controlling factors on the course of such processes. The low grade metamorphism associated with spreading ridges is to a large extent controlled by the circulation of sea water (e.g. Spooner, 1977,1981). Granite batholiths, gabbroic plutons and basaltic lava piles have been found to be the site of widespread convective re-cycling of meteoric water (Taylor, 1974). Stratiform, hydrothermal vein and porphyry copper type mineral deposits, at all levels in the crust, have formed as a result of deposition of ore minerals from fluids moving through the crust. The instant of earthquake rupture in the crust may be controlled by the distribution of fluid, and the fluid flow process (Whitcomb *et al.*, 1973), and hydrological phenomena have been observed in the crust as a result of underground detonation of nuclear devices (Reed, 1970). It is not surprising, therefore, that the amount of research into fluid chemistry and the variations of this in many different environments, has so dramatically increased in the last 20 years. In particular, in metamorphic petrology, so many regional and contact metamorphic chemical systems have been studied theoretically, and through observation and measurement, that for any given system, most of the intensive and extensive variables of state can be determined. Furthermore, the composition of the metamorphic fluid, if present, can be determined to a high degree of accuracy.

What is surprising, though, is that for all the studies which have produced detailed information of this kind, very few have produced any information on the nature of the processes by which fluids affect metamorphism. That is to say, the laws which govern fluid behaviour are poorly understood. It is the intention in this chapter to outline the background to one of the more fundamental aspects of fluid behaviour in relation to metamorphic processes, namely the means by which fluid moves through rocks. Such a topic is obviously of wide interest and application (see above), but this chapter deals only with the fluid movement relevant to metamorphism, and is built on a foundation of the observations made on the Knapdale high grade metacarbonate system. However, that system exhibits behaviour which represents only one aspect of metamorphic fluid transport, and the full spectrum of behaviour is presented here. Furthermore, the models which are proposed are sufficiently general that they apply to all of the environments of fluid transport mentioned above, and more.

6.2: The framework of rock mechanics

Fluid transport processes in metamorphism can be viewed in a framework of rock mechanics. This divides fluid transport into end-member models based on the structural response of a rock to stress in a fluid-saturated environment. Thus for a particular environment, with a particular stress distribution, the possible responses of the rock, and the end-member models, are as follows:

- (a) Rock produces a set of discrete fractures on failure (obeys General Law of Effective Stress, or $\sigma = S - P(1-a)$, where a is a dimensionless factor which reduces the efficiency of P , the pore fluid pressure, and where S is the shear strength of the rock, and σ is the effective stress.)
- (b) Rock essentially disaggregates on failure, by the production, growth and migration of a set of microcracks (obeys Simple Law of Effective Stress, or $\sigma = S - P$).

(c) Rock does not fail.

Case (a): In general, quartz-rich rocks appear to behave in this way, where increase of stress beyond the tensile strength of the rocks results in the development of discrete fractures. Since these fractures effectively release the built up stresses in any area, often only a few, regularly spaced fractures form. These fractures are held open by pore fluid pressure for a certain time, during which fluid may move along them, driven by fluid pressure gradients. The term $(1 - a)$ in the Stress Law allows for some migration of fluid from the bulk of the rock into the vein, or spalling, when $P_{\text{pores}} > P_{\text{fracture}}$, while for the fracture process as a whole the latter value is greater, i.e. $P_{\text{fracture}} > P_{\text{pores}}(1 - a)$.

Case (b): The Griffiths model of crack propagation is well understood (e.g. Secor, 1969). Small flat elliptical microcracks are ubiquitous in most natural substances. In rock systems, carbonates are particularly liable to fracture through exploitation by elongation of such microcracks. Increase of pore fluid pressure causes the cracks to swell, and eventually rupture at the tips, thus releasing the fluid to an adjacent crack, with the original crack then being closed (e.g. Etheridge et al., 1984). Viewed overall, this mechanism has the effect of conferring an enhanced permeability on all of the volume of rock which behaves in this way. Fluid moves from crack to adjacent crack and thus pervasively through the rock, effectively coming into contact with all the mineral grains.

Case (c): If the rock does not fail, the only available pathways for incoming fluid is the interconnected network of pore spaces represented by the grain boundaries. In most rocks, but particularly in metamorphic rocks at high pressures and temperatures, such pore spaces are so small and permeability is effectively so near zero, that free flow of fluid is not possible, and fluid transport is achieved only by diffusion. Such diffusion is driven by chemical potential gradients, and is very much slower than free flow, either through open fractures or microcrack arrays. One

consequence of the presence of a fluid phase in grain boundaries may be the fluid-assisted transport of the grain material itself, or 'pressure solution' (Robin, 1979; Rutter, 1983).

In many respects cases (a) and (c) can be viewed as the two true end-member cases of fluid transport, with case (b) an in between model which combines features of both end-members. This will be discussed in more detail later, but for the present, movement of fluid in large, discrete fractures, and movement along grain boundaries, will be considered as the two end-member cases.

6.3: Metamorphic processes involving fluid transfer

The two end-member cases of fluid transfer in metamorphic terrains, controlled by rock mechanics, and thus to a large extent by lithology, can result in two different metamorphic processes, diffusion metasomatism and infiltration metasomatism. The word metasomatism is used here loosely, as the distinction between fluids carrying ionic species into a metamorphic system (which could be properly called metasomatic fluids) and fluids entering a metamorphic system, carrying little, but being themselves of a complex chemistry (which could thus still be called metamorphic fluids) is obviously a blurred one. Both processes were first studied theoretically by D.S. Korzhinskii (1970).

6.3.1: Diffusion metasomatism

A lot of research has been done on solving the well known diffusion equations for geochemical systems (e.g. Frantz & Mao, 1976,1979; Weare et al. 1976; Brady, 1975,1977). This work makes use of the formulations of Fick's law which relate mass transfer by diffusion to concentration gradients and diffusion coefficients for particular species. It is necessarily limited by the need to know these concentration

gradients and diffusion coefficients, which are by no means easy to calculate. This is because, ultimately, detailed knowledge of the chemical make-up of the grain boundary fluid must be achieved, which demands a greater knowledge of dissociation and speciation of components in such environments than is presently available, not least because the effects of such factors as non-hydrostatic stress states are not known. The structure of grain boundaries and the actual physical state of the grain boundary fluid phase is not yet fully understood.

An alternative approach to the study of diffusion metasomatism is to depart entirely from the atomistic or statistical approach and treat the problem phenomenologically. This involves the correlation of phenomena in a more formal manner, independent of specific chemical information, and is a method which has been successfully applied by Fisher & Elliott(1974), Joesten(1977) and Fisher(1977,1978). In this sort of treatment, mass transfer is related to chemical potential gradients and phenomenological coefficients, both of which are easier to quantify in geochemical systems. This and other aspects of the theoretical framework to this method, non-equilibrium or irreversible thermodynamics, form the basis of Chapter 7 of this thesis.

6.3.2: Infiltration metasomatism

Theoretical models which describe the effect of metasomatism which involves infiltration of fluid along discrete fractures have been presented by Hofmann(1972,1973), Fletcher & Hofmann(1974) and Frantz & Weisbrod(1974). These models use an extension of chromatographic theory to predict the effect of 'fronts' of infiltration which move through rocks. Perhaps the most obvious failing of these models is the lack of attention to the range of values of porosity and permeability which

obtain in differing rock types, and under differing metamorphic conditions. This problem is dealt with in sections 6.5 and 6.6 .

6.4: Fluid pathways

Based on the mechanical framework proposed earlier, three different fluid pathways can be identified within a metamorphic rock. These have features which determine, in the final analysis, how much and how quickly fluid can move through the rock. These features, also summarised in Figure 6.1, are as follows:

Open Fractures

Scale: cm-m
 Fluid driven by: fluid pressure gradients
 Porosity: high (effectively 100%)
 Permeability: high
 Percentage of reference volume of rock through which fluid travels: small
 Velocity of fluid: probably high (laminar flow?)
 Time in which fluid may equilibrate with rock: short, affects rock only in wall-rock alteration

Grain Boundaries

Scale: mm
 Fluid driven by: chemical potential gradients
 Porosity: low
 Permeability: very low (effectively zero)
 Percentage of reference volume of rock through which fluid travels: high (i.e. all available pore space)
 Velocity of fluid: very low
 Time in which rock may equilibrate with rock: long, possibly continuous re-equilibration

Microcracks

Scale: mm-cm
 Fluid driven by: fluid pressure gradients from crack to crack, chemical potential gradients from crack to rock
 Porosity: high
 Permeability: high
 Percentage of reference volume of rock through which

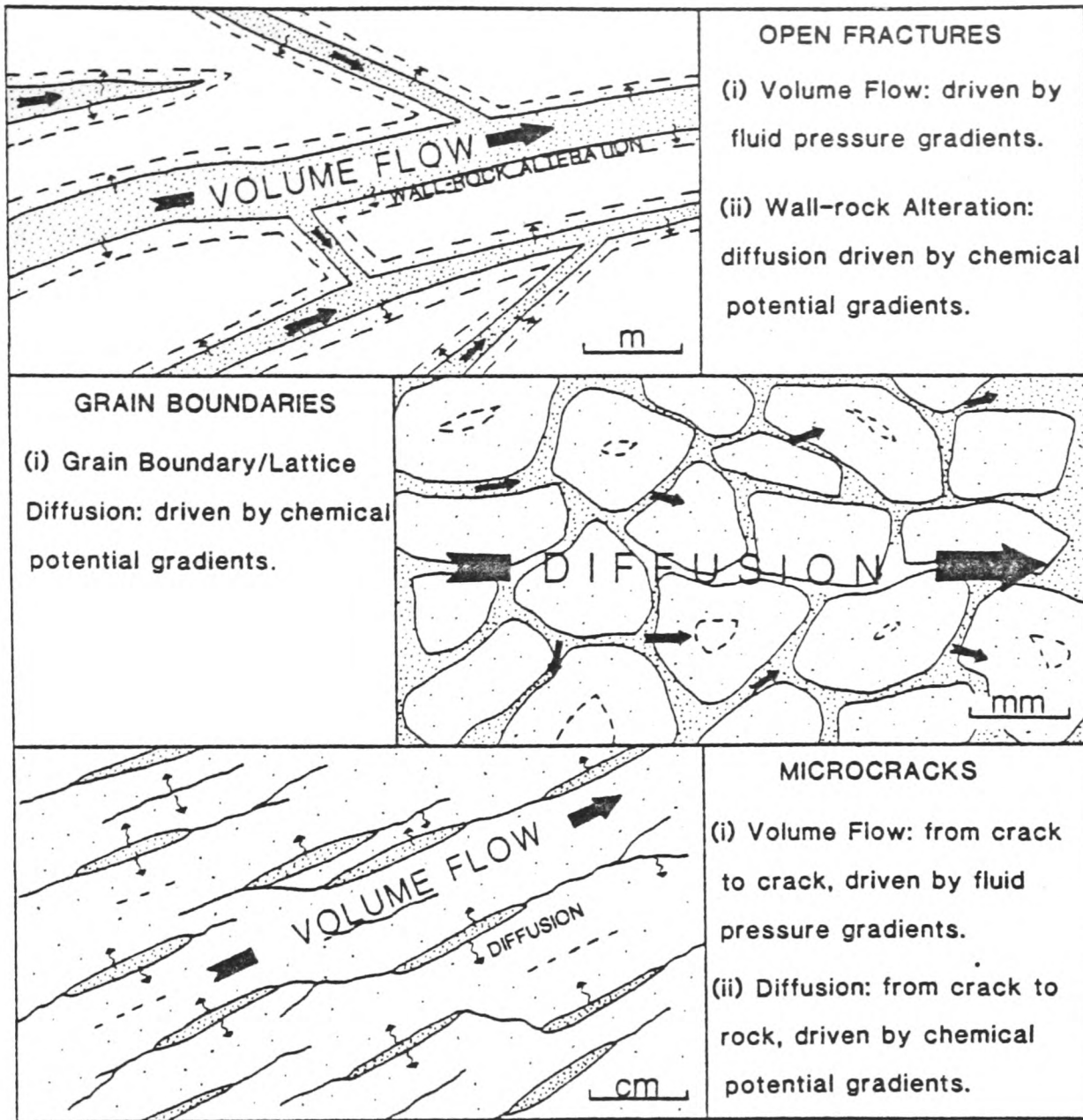


Figure 6.1: Fluid pathways. End member pathways in terms of scale are open fractures and grain boundaries. In these, volume flow (fast) and diffusion (slow), respectively, are the driving forces. Intermediate in scale are microcracks, in which volume flow also dominates. The stippled areas in each model show the parts of the rock which are affected by the fluid. Note that for microcracks, because the distance between cracks is small, all of the rock is affected by fluid.

fluid travels: very high, even more than pore space,
 since grains themselves are fractured
 Velocity of fluid: intermediate?
 Time in which fluid may equilibrate with
 rock: long?, vestiges of fluid left on sealed
 cracks may equilibrate totally with adjacent
 rock

In a sense the third pathway, that of microcracks, combines features of the first two models, and results in a 'best solution' to the problem of speedy equilibration of infiltrating fluid with the greatest possible volume of rock. High fluid:rock ratios over a wide area would characterise this sort of model pathway, and is therefore that which is proposed for the primary infiltration event in the carbonates at South Bay, Knapdale.

6.5: Porosity and permeability

Seismic data suggest that brittle rock failure and transient fractures occur at depths to at least 15-20km (Norton & Knapp, 1977). Thus most crustal rocks exhibit a significant porosity during metamorphism. In general, this value is taken to be of the order of 0.1 to 0.01%. However this total porosity comprises three separate types of fluid pathway. These are a) grain boundaries, b) open fractures or microcracks and c) residual unconnected pore spaces. Of these three, the last has been shown to constitute more than 90% of the total (Norton & Knapp, 1977). This means that in rocks which deform to produce discrete fractures, since in the bulk of the rock aside from these fractures the permeability is virtually zero, the effective porosity in the bulk of the rock is only that of the grain boundaries, along which fluid may diffuse, and is consequently much smaller. This example shows why the porosity, and therefore also the permeability, must be viewed in a context of the fluid pathway prevalent in the particular rock, under the particular P-T-X_{fluid} conditions. This is why

the porosity and permeability values derived by mechanically testing rock specimens in the laboratory (Brace et al., 1968) must be viewed with caution. A more useful approach is to model porosity and permeability using a method such as the network model (akin to finite element analysis) e.g. Seeburger & Nur(1984). In this model the effect of variations in a single parameter (such as bulk modulus, pore aspect ratio, confining pressure etc.) can be investigated separately. However, such models are not yet sufficiently sophisticated as to be able to predict permeabilities of real rocks. In the absence of conclusive data, the much-used value of 300nD ($3 \times 10^{-17} \text{m}^2$), Fletcher & Hofmann(1974), is used in this study. For comparison, unmetamorphosed sandstones and limestones with porosity of 5-15% typically have permeabilities of around 10-0.01mD (10^{-12} - 10^{-15}m^2).

6.6: Permeability and time

Within a metamorphosing rock, the continually changing physical and chemical conditions, with the growth and dissolution of minerals, and fluctuations in mass and heat transfer, mean that the permeability is continually changing. In a fluid infiltration event, these local changes may be viewed as a backdrop, which on a microenvironment scale, may largely control the course of the infiltrating fluid. On a larger scale, however, an infiltration event will have a characteristic signature of variation of permeability with time, over the whole duration of the event. Permeability-time diagrams may be drawn, analogous to those for the burial and compaction of sedimentary rocks. Such diagrams are shown in Figures 6.2 to 6.5. Figure 6.2 shows a generalised profile for complete evolution of a sediment from the time of its deposition on the sea-floor to its metamorphism. Figures 6.3 and 6.4 show more detailed curves, those proposed for metamorphic events which involved fluid generation in a rock volume, and movement of the fluid away through propagating microcracks

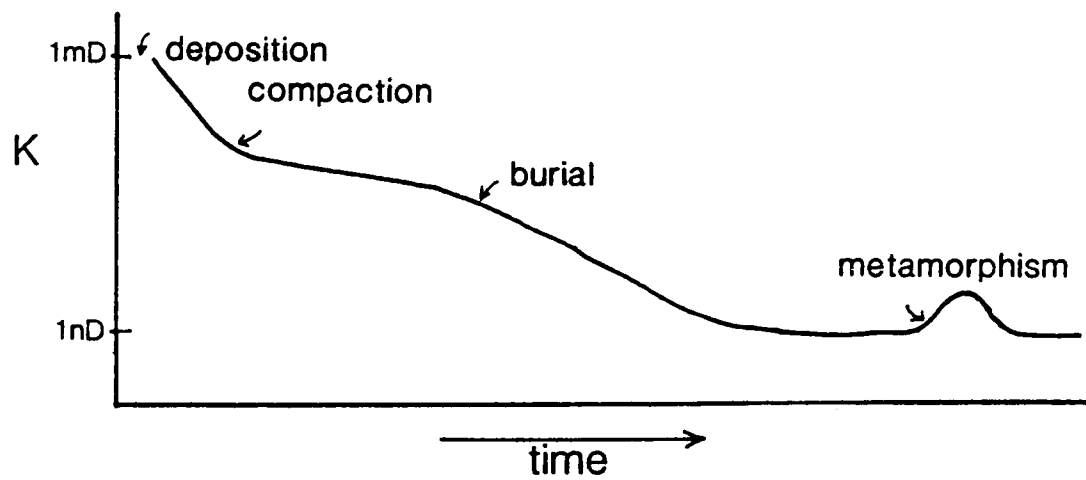


Figure 6.2: Permeability (K) profile through time of a rock, from deposition to deep burial and metamorphism. K values are order of magnitude estimates.

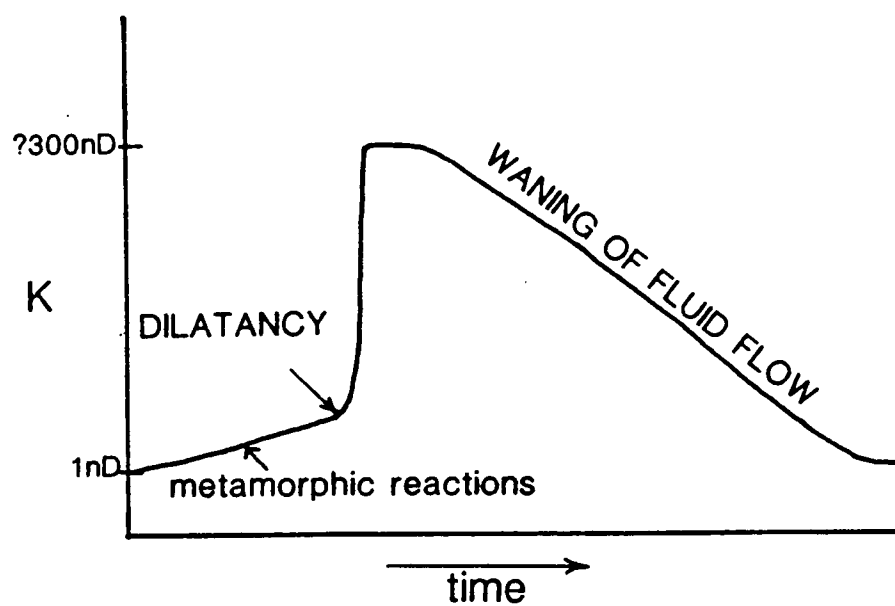


Figure 6.3: Permeability (K) - time profile for a rock volume in which fluid is generated by metamorphic reactions, and then transported away by fluid flow in microcracks. Waning fluid flow, as a result of cessation of metamorphic reactions, may isolate small pockets of fluid.

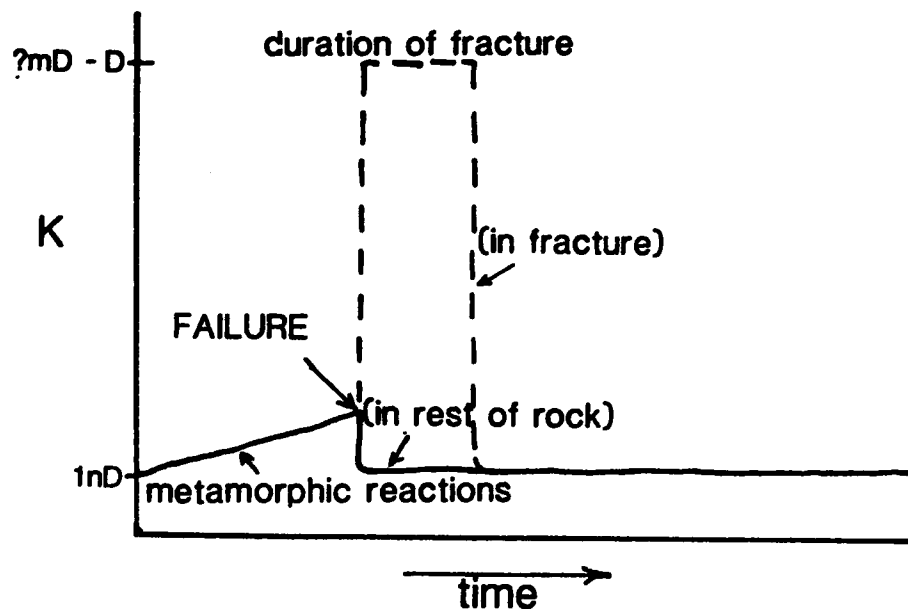


Figure 6.4: Permeability (K) - time profile for a rock volume in which fluid is generated by metamorphic reactions, then transported away by fluid flow in large open fractures. Note that the fracture volume has very high K during its lifetime, whereas in the rock between fractures K remains low.

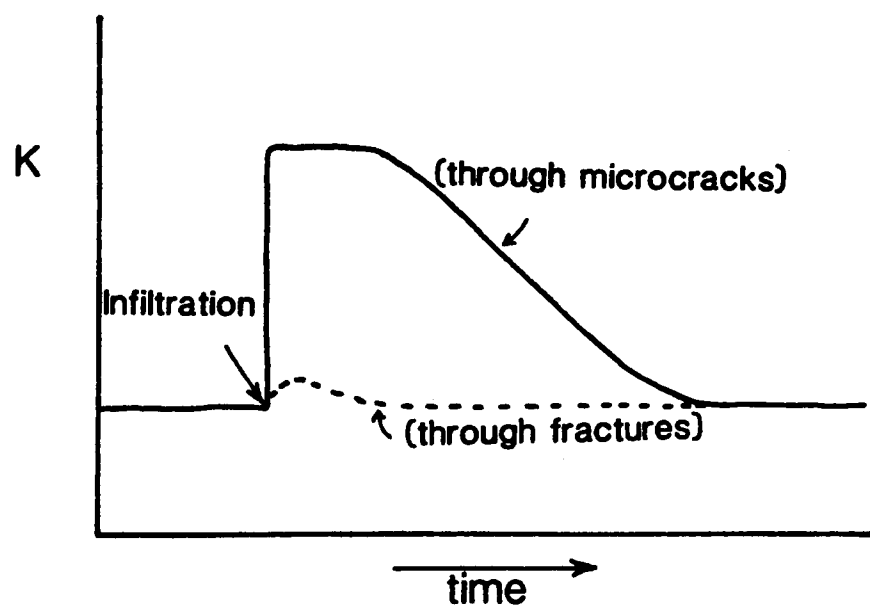


Figure 6.5: Permeability (K) - time profile for a rock volume which is infiltrated by an external fluid. Solid line = microcrack pathway, dashed line = fracture pathway. Rock between fractures will experience little change in K as it is quickly isolated by an impermeable fracture-wall alteration zone.

(6.3) and through open fractures (6.4). Features of these diagrams are -

- a) The slow gradual increase in pore fluid pressure due to dehydration and decarbonation reactions results in steadily increasing permeability in the bulk of the rock, as the pore spaces are held open by the fluid produced.
- b) At failure, the onset of deformation by crack propagation results in dilatancy and an increase in permeability of several orders of magnitude. The waning of fluid flow allows the gradual closing up of cracks, and a gradual decrease in permeability. This process may isolate small packets of fluid which may be buffered by mineral assemblages, creating many varied microenvironments, and may result in spatial differences in observed fluid composition. Ultimately the decline in fluid flow will grade into conditions of grain boundary diffusion only.
- c) At failure in the open fracture case, different parts of the rock volume will experience different permeability variations. The volume created by the fracture will experience an instantaneous dramatic increase in permeability which will be maintained for the life duration of the fracture. The rest of the rock will experience a rapid decrease in permeability as the pore fluid is essentially drawn off by the fracture, and the pore spaces contract.

Figure 6.5 is a permeability-time graph for rock volumes infiltrated by externally-derived fluids, with fluid moving through the rock by i) microcracks and ii) open fractures. This diagram shows the contrast between the first case, where the permeability of the whole volume is greatly enhanced, and the second case, where the permeability of the rock between the actual fractures maintains a fairly constant value. This is because in the latter case the bulk of the rock is isolated from the pressure effects of the infiltrating fluid by a low permeability wall-rock zone formed at an early stage by draining off of pore fluid from that zone, and to a certain extent also by the presence of massive vein deposits.

The complexities of variations of permeability with time in different fluid-dominated environments definitely point to their worth as a subject for further study.

6.7: Rates of transport processes

Few accepted models of metasomatism/metamorphism account for the rates of the processes acting, indeed most assume local equilibrium (Fletcher & Hofmann, 1974). This is because of the lack of dissociation and speciation data, mentioned before, for elements under geological conditions. This sort of data is an essential prerequisite to present kinetic formulations.

However, some general inferences on the relative rates of processes such as mass transport and chemical reaction can be made if steady-state equilibrium, in the form of a continuity equation, is assumed.

The continuity equation describes the local variations of concentration of component i as a balance between the consumption of component i by chemical reaction, and its introduction into the system. Thus -

$$\frac{\partial c_i}{\partial t} = -\text{div} J_i^m + v_i J_{ch} \quad \dots \text{Equation (6.1)}$$

where J_i^m = the rate of flow of i into the system,
 J_{ch} = the rate of chemical change by reaction,
 and v_i = the stoichiometric coefficient of component i in the reaction.

A general flow J_A can be written as the product of a driving force, X_B , and a phenomenological coefficient, L_{AB} , such that -

$$J_A = \sum_{B=1}^n L_{AB} X_B \quad \dots (6.2)$$

This equation forms part of the framework of non-equilibrium or irreversible thermodynamics, which is dealt with in greater detail in Chapter 7. It is enough to say here that phenomenological coefficients (L_{ij}) are akin to diffusion coefficients (D_{ij}) in their physical meaning, and that equations such as Fick's First Law, Fourier's Law and Darcy's Law are all equilibrium cases of the more general Equation (6.2).

Thus for mass transport -

$$J_i^m = \sum_{j=1}^n L_{ij}^m X_j^m \quad \dots(6.3)$$

where J_i^m = mass flow of component i towards reaction site,

L_{ij}^m = phenomenological coefficient for mass flow,
and X_j^m = a generalised driving force (real examples are chemical potential gradients, temperature gradients etc.

Similarly, for chemical reaction -

$$J_{ij}^R = \sum_{i=1}^n L_{ij}^R A_j^R \quad \dots(6.4)$$

where J_{ij}^R = rate of chemical reaction consuming i, or J_{ch} ,
 L_{ij}^R = phenomenological coefficient for chemical reaction,

and A_j^R = the reaction affinity.

Thus the equation of continuity (6.1) shows that the concentration of component i in a particular volume in local equilibrium, is a trade-off between reaction rate, J_{ch} , and mass transport rate, J_i^m .

Some interesting conclusions can be made concerning the relative values of these rate terms, when growth of metamorphic minerals by a steady-state process is assumed. For instance, if the dominant mass transfer process is one of diffusion, (either through bulk lattice, or along grain boundaries), then the driving force, X_j^m , will be a chemical potential gradient, $\text{grad } \mu_j$. Since diffusive transfer is very

slow (i.e. L_{ij}^0 is small), the mass transfer term in the continuity equation will be very much smaller than the chemical reaction term. In physical terms, this means that for a constant change in concentration of i , reactions will in effect be instantaneous, and the rate-controlling step will be the diffusive mass transfer. In other words the rate of the new mineral growth will depend on the rate of supply of component i to the reaction site. Differences of chemical potential of component i will be greatest at the boundaries between old and new minerals (or mineral assemblages). Thus diffusive transfer, and hence overall process rate will be greatest at these boundaries. This will result in the enhancement of these 'zone' boundaries, since new growth will be fastest there. In general terms, this means that systems which exhibit diffusive mass transfer-rate control will show strong spatial organisation, with mineral zones arranged in order of chemical potential (Fisher, 1977).

At the opposite extreme, where the dominant mass transfer process is that of infiltration, this fluid transfer, driven by fluid pressure gradients, $\text{grad } P_f$, may be so fast that reaction-rate is the rate-controlling step. This process would also have the effect of wiping out chemical potential gradients, so that zoned assemblages would not result. Layered mineral zones would then reflect variation in nucleation site favourability, bulk composition differences or fluid flow discontinuities.

In a real process, which may involve a combination of diffusive and infiltrative mass transfer, and many chemical reactions, the spatial distribution of minerals may be very complex, and it may be difficult to unequivocally ascribe effect to process. However, it may be possible in the South Bay metacarbonate system, which has been shown to be a good example of infiltration metamorphism. For that process implies reaction-rate control of the mineral growth, and earlier conclusions about the distribution of assemblages at South Bay (i.e. that these were a function of either bulk composition or fluid flow variations) are the conclusions

expected for such a process.

The assumption of 'steady-state' equilibrium is more difficult to justify. In view of the complex nature of the processes involved it seems more reasonable to define a natural system in terms of a more general, time-dependent framework. This forms the subject of the next chapter.

6.8: Conclusions

This chapter has described models of fluid transfer processes in metamorphosing rock. Consideration of factors such as rock mechanics, porosity and permeability variations, and type of metamorphic process allows the delimiting of three types of fluid transfer process, namely those associated with three types of fluid pathway: i) open fractures, ii) grain boundaries and iii) microcracks (see Figure 6.1).

The dominant fluid transfer process in the infiltration metamorphism of the high grade metacarbonates at South Bay, Knapdale, was that of movement through microcracks. This is evidenced by -

- a) The lack of ordered mineral zones (ordered by, for example, chemical potential gradient), which shows that diffusion-dominated processes can be ruled out.
- b) The high calculated fluid:rock ratios, showing that large volumes of fluid moved through the rocks.
- c) The fact that reaction-rate control of mineral growth may have dominated, since mineral distributions are the result of either bulk composition variations, or variations in fluid:rock ratio from bed to bed. This suggests that a fast fluid transport mechanism operated.
- d) The lack of quartz-filled veins in the carbonate rocks, in contrast to their common occurrence in adjacent semi-pelitic schists (see Section 2.5). This emphasises that fluid passes through both carbonates and semi-pelites, but by different

methods, which were probably dependent on the different mechanical properties of the rock types.

e) The pervasive effect of the fluid, in that all of the carbonates show H_2O -rich mineral assemblages, and the small scale distribution of these assemblages (see for example Plate 4.X). This shows that fluid flow in large spaced fractures can be ruled out.

The totally pervasive character of the microcracking process allows local, small scale variations of fluid:rock ratio, controlled by local permeability variations, to be possible. Thus the possibility of control of mineral assemblage distributions in the South Bay rocks by small scale variations of fluid:rock ratio cannot be ruled out.

C H A P T E R 7: Non-equilibrium thermodynamics

7.1: Introduction

In this chapter some of the methods of investigating metamorphic processes in terms of non-equilibrium thermodynamics are explored. These are based on the theoretical work of deGroot(1952), Prigogine(1955), deGroot & Mazur(1962) and Katchalsky & Curran(1965). Firstly the general equations used in this method are outlined. In section 7.4, the general case of fluid transfer is examined, and a relationship between buffering and infiltration processes obtained. Substitution of estimated values into this equation (7.24), with the aid of Darcy's Law (7.25), allows the calculation of a time duration for a typical infiltration event. Section 7.3 examines the specific case of fluid transfer through microcracks, where estimation of values allows calculation of the fluid pressure gradient in such a process, and the velocity of the fluid.

7.2: The framework of non-equilibrium thermodynamics

One possible formulation of the Second Law of Thermodynamics is -

$$\frac{d_i s}{dt} > 0, \quad \dots(7.1)$$

where $d_i s/dt$ is the change in internal entropy of a system.

This equation breaks down into two parts -

$$\frac{d_s s}{dt} = 0, \quad (7.2A)$$

and,

$$\frac{dS}{dt} > 0 . \quad (7.2B)$$

The first part (7.2A) represents the end-member case of equilibrium, or reversible processes. These are processes which, when reversed, result in no changes in the total surroundings of the system. As such they do not represent actual or natural processes, which occur in Nature, which are by definition irreversible. The second part (7.2B) thus represents natural processes. Equilibrium thermodynamics therefore, derives from an assumption of the validity of equation (7.2A), whereas non-equilibrium thermodynamics proceeds from the more general result of (7.2B).

The *modus operandi* of non-equilibrium thermodynamics is that of the formulation of equations which account for the increase of entropy in any particular process. These equations are called flow of entropy, or entropy production equations. It is convenient to define a local entropy production, σ , such that -

$$\frac{dS}{dt} = \int_V \sigma dV \quad ..(7.3)$$

where V is the volume of the whole system. The value σ characterises local processes and their contribution to the total entropy production, and may be written as a sum of the product of generalised 'flows' (J_i) and 'forces' (X_i), (see section 6.7), thus -

$$\sigma = \sum_{i=1}^n J_i X_i \quad ..(7.4)$$

These flows and forces are then assumed to be related to each other in a linear fashion, for example when $n=2$ -

$$\sigma = J_1 X_1 + J_2 X_2 \quad ..(7.5)$$

implies,

$$J_1 = L_{11} X_1 + L_{12} X_2 \quad ..(7.6A)$$

and

$$J_2 = L_{21}X_1 + L_{22}X_2 \quad \dots(7.6B)$$

where L_{ij} are phenomenological coefficients related to diffusion coefficients thus -

$$L_{ij} = \frac{D_i c_i}{RT} \quad \dots(7.7)$$

where D_i = diffusion coefficient,
 c_i = concentration of component i ,
 T = temperature
 R = gas constant.

Coefficients in phenomenological equations are related by Onsager's Law (Onsager, 1931a,b) -

$$L_{ij} = L_{ji} \quad \dots(7.8)$$

In describing a natural system, the choice of flows and forces is somewhat arbitrary, justification for a particular choice being simply the usefulness and validity of the resulting model.

For entropy production in a continuous system (where intensive quantities vary in space) a useful formulation is -

$$T\sigma = J_s \cdot \text{grad}(-T) + \sum_{i=1}^k J_i \cdot \text{grad}(-\mu) + J_{ch} A \quad \dots(7.9)$$

where J_s = entropy flow,
 J_i = flow of matter, 'flows'
 J_{ch} = chemical reaction.

and $\text{grad}(-T)$ = temperature gradient,
 $\text{grad}(-\mu)$ = chemical potential gradient 'forces'
 A = reaction affinity.

The term $T\sigma$ is often called ϕ , the dissipation function. The above equation is formulated for the most general case of flows and forces in three dimensions. Thus 'grad(-T)' represent a temperature gradient in x-, y- and z-coordinate space. This generality will be adhered to from now on, unless specifically stated otherwise.

7.3: Fluid transfer processes in metamorphism

7.3.1: Simplifications to a general model

To simplify the consideration of metamorphic processes which involve fluid transfer, or rather the fluid transfer processes themselves, it is easiest to consider a system which includes no chemical reaction amongst fluid species, and which involves no temperature gradient. The dissipation function then becomes, from (7.9) -

$$\phi = \sum_{i=1}^k J_i \cdot \text{grad}(-\mu_i) \quad \dots(7.10)$$

To investigate the part played by fluid pressure gradients in fluid transfer, it is necessary to separate the right hand side of equation (7.10) into parts using the relationship -

$$\text{grad}(-\mu_i) = \text{grad}(-\mu_i^c) + V_i \text{grad}(-P_f) \quad \dots(7.11)$$

where μ_i^c = the pressure independent part of μ_i .

V_i = the partial molar volume of component i.

and P_f = the fluid pressure.

Then, substituting (7.11) into (7.10) -

$$\phi = \sum_{i=1}^k j_i \cdot [\text{grad}(-\mu_i^c) + V_i \text{grad}(-P_f)] \quad \dots(7.12)$$

The next stage is to separate out the terms dealing with the forces acting on the solvent, w, from those acting on the solutes, $i = 1 \dots (k-1)$. This results in the equation -

$$\begin{aligned} \phi = \sum_{i=1}^{k-1} J_i^D \cdot \text{grad}(-\mu_i^c) \\ + \sum_{i=1}^k J_i \cdot V_i \text{grad}(-P_f) \quad \dots(7.13) \end{aligned}$$

where J_i^D = flow of solute relative to the solvent.

This equation illustrates the fact that for a system with $k=2$, two volume flows of matter, driven by fluid pressure,

arise, but only one flow of matter, driven by a chemical potential gradient. For a system with $\text{grad}(-P_f) = 0$, Equation (7.13) reduces to a completely general formulation of Fick's Law.

As a further simplification, it can be assumed that the fluid consists entirely of one species, H_2O , which can artificially be separated into a vanishingly small amount of solute, H_2O , and a large amount of solvent, H_2O^* . Equation (7.13) then becomes -

$$\phi = J_{\text{H}_2\text{O}}^{\text{D}} \cdot \text{grad}(-\mu_{\text{H}_2\text{O}}^{\text{c}}) + J_{\text{H}_2\text{O}}^{\text{V}} \cdot V_{\text{H}_2\text{O}} \text{grad}(-P_f) \\ + J_{\text{H}_2\text{O}^*}^{\text{V}} \cdot V_{\text{H}_2\text{O}^*} \text{grad}(-P_f) \quad \dots(7.14)$$

and by analogy with (7.5), (7.6A) and (7.6B), three linear equations for the flow of matter can be derived -

$$J_{\text{H}_2\text{O}}^{\text{D}} = -L_{\text{D}} \text{grad}(\mu_{\text{H}_2\text{O}}^{\text{c}}) - L_{\text{OH}} V_{\text{H}_2\text{O}} \text{grad } P_f \\ - L_{\text{OH}^*} V_{\text{H}_2\text{O}^*} \text{grad } P_f \quad \dots(7.15)$$

$$J_{\text{H}_2\text{O}}^{\text{V}} = -L_{\text{HD}} \text{grad}(\mu_{\text{H}_2\text{O}}^{\text{c}}) - L_{\text{H}} V_{\text{H}_2\text{O}} \text{grad } P_f \\ - L_{\text{HH}^*} V_{\text{H}_2\text{O}^*} \text{grad } P_f \quad \dots(7.16)$$

$$J_{\text{H}_2\text{O}^*}^{\text{V}} = -L_{\text{H}^*\text{D}} \text{grad}(\mu_{\text{H}_2\text{O}}^{\text{c}}) - L_{\text{H}^*\text{H}} V_{\text{H}_2\text{O}} \text{grad } P_f \\ - L_{\text{H}^*} V_{\text{H}_2\text{O}^*} \text{grad } P_f \quad \dots(7.17)$$

At the critical boundary where purely diffusive transfer gives way to infiltrative transfer -

$$J_{\text{H}_2\text{O}}^{\text{D}} = J_{\text{H}_2\text{O}}^{\text{V}} + J_{\text{H}_2\text{O}^*}^{\text{V}} \quad \dots(7.18)$$

Therefore, substituting (7.15), (7.16) and (7.17) into (7.18) and rearranging, this expression reduces to the important result

$$(L_{\text{D}} - L_{\text{H}^*\text{D}}) \text{grad}(\mu_{\text{H}_2\text{O}}^{\text{c}}) = (\omega_{\text{H}_2\text{O}} - L_{\text{H}^*\text{D}} V) \text{grad } P_f \quad \dots(7.19)$$

where $\omega_{\text{H}_2\text{O}} =$ the mobility of H_2O , $= L_{ij}/c_i$, and $V =$ the molar volume of the fluid.

This equation relates the ratio of chemical potential gradient over fluid pressure gradient to a combination of phenomenological coefficients plus physical properties of the fluid. These latter may be estimated with a fair degree of confidence, and thus the relative magnitudes of the driving 'forces' can be compared.

7.3.2: Estimation of parameters

The mobility of H_2O at the pressure and temperature of interest (8kb, $500^\circ C$) can be calculated using the relationships -

$$\omega_s = [N_A F]^{-1} \quad \dots(7.20)$$

where N_A = Avogadro's number, and F = the coefficient of friction acting on a particle.

and,

$$F = 6\pi r\eta \quad (\text{Stokes' Law}) \quad \dots\dots(7.20B)$$

where r = radius of the particle, and η = viscosity of the medium.

This gives rise to a calculated mobility of water ($r = 3 \times 10^{-10} m$) during this fluid transfer process of $\omega_{H_2O} = 5.87 \times 10^{-14} \text{ (mol.m.N}^{-1}\text{.sec}^{-1}\text{)}$.

The phenomenological coefficient for grain boundary diffusion under these conditions, for a rock with grain size of 1mm, can be estimated after Fisher(1977), as $L_0 = 8.72 \times 10^{-19} \text{ (mol}^2\text{.N}^{-1}\text{.m}^{-2}\text{.sec}^{-1}\text{)}$. This is of the same order of magnitude as the value calculated by Rutter(1983) for diffusion of solute ions in bulk water ($4 \times 10^{-19} \text{ mol}^2\text{.N}^{-1}\text{.m}^{-2}\text{.sec}^{-1}$).

The general local entropy equation (7.4) must always be

positive. This imposes two conditions on the arithmetic sign of the phenomenological coefficients, namely -

$$L_{ii} > 0 \quad \dots(7.21)$$

and

$$L_{ii}L_{jj} > L_{ij}^2 \quad \dots(7.22)$$

Since in this case, effectively $c_{H_2O^*} = 1$, thus -

$$L_{H^*} = \omega_{H^*} = \omega_H \quad \dots(7.23)$$

the maximum value of L_{DH^*} (and hence also L_{H^*D} can therefore be calculated, as -

$$L_{DH^*} = \sqrt{(5.87 \times 10^{-14} \cdot 8.72 \times 10^{-19})} = 2.26 \times 10^{-16}$$

Substituting the relevant values into (7.19), taking also $V = 2 \times 10^{-5} \text{ (m}^3\text{.mol}^{-1}\text{)}$, the result is -

$$\text{grad}(\mu_{H_2O}^c) = 260. \text{ grad } P_f \quad \dots(7.24)$$

7.3.3: General conclusions

Equation (7.24) accounts well for, and supports, common sense observations about the relative magnitudes of chemical potential and fluid pressure gradients in different metamorphic processes. For example,

a) In infiltration, fluid pressure gradients are likely to be of the order of 10^4 (see section 7.4). This would imply that massive chemical potential gradients would be required to overcome the dominance of volume flow as a transfer mechanism for fluid.

b) In diffusion, vanishingly small fluid pressure gradients would imply only marginally higher chemical potential gradients. These gradients may therefore be very small, explaining the relative slowness of the diffusive transfer

process.

c) The most interesting case is that where chemical potential gradients are high, since here fluid pressure gradients need not be great for a delicate balance between transport mechanism to exist. If both gradients could be measured, the probable dominant process could be identified.

Darcy's Law affords a method of calculating the fluid pressure gradients, as -

$$\text{grad } P_f = \frac{-Q \cdot \eta}{A \cdot k} = \frac{\beta \cdot v \cdot \eta}{k} \quad \dots (7.25)$$

where Q = volume flow of fluid per second,

A = cross sectional area of flow,

η = viscosity of the fluid,

k = permeability of the medium,

β = porosity of the medium,

and v = velocity of fluid flow.

But this equation also means that, knowing the fluid pressure gradient, and using working values of permeability and fluid viscosity, the volume flow rate through a given area can be calculated.

Equation (7.24) is therefore useful because an order of magnitude fluid pressure gradient can be calculated directly from a value for the chemical potential gradient where such occurs. Ferry(1979) has calculated μ_{H_2O} values of 25-314 J.mol⁻¹ in carbonate rocks from Maine, U.S.A., which have experienced an infiltration event with fluid:rock ratios of around 2:1 (per 1000cm³ rock). From (7.24) this implies minimum values of $\text{grad } P_f = 0.1-1.2 \text{ N.m}^{-2}$. Substituting these values into the Darcy equation, and using the values $\eta = 1.5 \times 10^{-2} \text{ N.sec}^{-1}.\text{m}^{-2}$ (Walther & Orville(1982),

$k = 1.0 \times 10^{-17} \text{ m}^2$, $A = 0.01 \text{ m}^2$ (the side of a cube of volume 1000cm³), there results -

$$Q = 2.12 \times 10^{-11} \text{ to } 2.5 \times 10^{-10} \text{ m}^3/\text{year}.$$

For a fluid:rock ratio of 2:1 per 1000cm³, this implies a maximum time duration for the event of -

$$\frac{2 \times 10^{-3} \text{ m}^3}{Q} = 94.3 \text{ to } 7.8 \text{ million years.}$$

In this case, since the process acting is demonstrably infiltration (because of the high fluid:rock ratios), then Equation (7.18) probably does not hold, the volume flow terms being much greater than the diffusive flow terms. This means that the value of 7.8 million years for the duration of the event is probably an overestimate, which sheds great light on the infiltration process.

7.4: Fluid transfer through microcracks

7.4.1: In theory

Whilst equations such as (7.13) can be manipulated, and order of magnitude values inserted to obtain numerical solutions, it is also worthwhile to use such equations to assess the physical meaning of some metamorphic processes. In this way, equations can be derived which reveal much about the relationships between the various flows and driving forces in the process. For example, fluid transfer through microcracks is the process which has been proposed to account for various features of the infiltration metamorphism of the carbonate rocks of South Bay, Knapdale (see Chapter 4).

From equation (7.13), letting $k=2$, and examining only the diffusion and solvent volume flow terms, there results -

$$\phi = J_i^D \cdot \text{grad}(-\mu_i^c) + J_i^V \cdot V_i \text{grad}(-P_f) \quad \dots(7.26)$$

From this, the linear flow to force relations are -

$$J_i^D = -L_D \text{grad} \mu_i^c - L_{DV} V_i \text{grad} P_f \quad \dots(7.27)$$

$$J_i^V = -L_{VD} \text{grad} \mu_i^c - L_V V_i \text{grad} P_f \quad \dots(7.28)$$

These two equations represent the theoretical formulation of a two-stage process where:

- i) Fluid moves from crack to crack, driven by a fluid pressure gradient,
- ii) Fluid moves from crack to the rock, driven by a chemical potential gradient.

(see Figure 6.1).

Now,

$$\Delta\mu_i^c = \frac{\Delta\pi}{c_i}, \quad \dots(7.29)$$

(Katchalsky & Curran, 1965, p.118),

where π = the osmotic pressure across a membrane,

and c_i = the concentration difference across a membrane.

The wall-rock boundary layer between a fluid-filled cavity and the bulk of the rock may be treated as if it were a semi-permeable membrane (Thompson, 1957). Substituting (7.29) into (7.27) and (7.28) results in -

$$J_i^D = \frac{-L_{DV}}{c_i} \text{grad}\pi - L_{DV} V_i \text{grad} P_f \quad \dots(7.30)$$

$$J_i^V = \frac{-L_{VD}}{c_i} \text{grad}\pi - L_V V_i \text{grad} P_f \quad \dots(7.31)$$

Thus for a two-stage transfer process,

Stage 1: $\text{grad} \pi = 0$, since in the cracks, the constant infiltration of new fluid ensures that chemical potential gradients are everywhere equalised. Therefore,

$$J_i^D = -L_{DV} V_i \text{grad} P_f \quad \dots(7.32)$$

$$J_i^V = -L_V V_i \text{grad} P_f \quad \dots(7.33)$$

which illustrates that in Stage 1, the fluid transfer is driven by the fluid pressure gradient. Note, however, that a small (since L_{DV} will probably be small) amount of diffusive flow is driven by the pressure gradients also. This is a

'cross effect' and is analogous to the Soret effect in systems with temperature gradients.

Stage 2: $\text{grad } P_f = 0$, because no pressure differences are supported by the semi-permeable crack wall. Thus -

$$J_i^D = \frac{-L_{D_i}}{C_i} \text{grad } \pi \quad \dots(7.34)$$

$$J_i^V = \frac{-L_{V_i}}{C_i} \text{grad } \pi \quad \dots(7.35)$$

which shows that the diffusion of fluid away from the crack is essentially driven by the osmotic pressure gradient. Here again there will be a small but noticeable 'cross effect' (7.35), the volume flow of fluid driven by an osmotic pressure gradient.

7.4.2: Application - the South Bay infiltration

The fluid infiltration of the carbonates of South Bay, giving rise to mineralogy-derived fluid:rock ratio estimates of around 9:1 (see Table 4.2), can be described simplistically by equation (7.33). To recap, this equation assumes a one component fluid, with no temperature, electric potential or chemical potential gradients. Within these constraints, it can be use to calculate order of magnitude solutions for the fluid pressure gradient, and hence by Darcy's Law (7.25), the velocity of the infiltrating fluid.

Thus, a fluid:rock ratio of 9:1 represents flux of 9000cm^3 of fluid through the 100cm^2 face of a cubic rock volume of 1000cm^3 . Using $V_{\text{H}_2\text{O}}$ at 8kb, $500^\circ\text{C} = 20 \text{ cm}^3.\text{mol}^{-1}$ (calculated from the tables of Burnham et al.(19XX), this represents 450 mol per 100cm^2 over the whole event. Letting the duration of the event be T sec, the flow of fluid at South Bay becomes -

$$\frac{450}{T} \text{ mol per } 100\text{cm}^2 \text{ per sec}$$

Converting to the S.I. units for J_{iV} of $\text{mol.m}^{-2}.\text{sec}^{-1}$, this becomes -

$$\frac{45000}{T} \text{ mol.m}^{-2}.\text{sec}^{-1}$$

Therefore, from (7.33) -

$$J_{\text{H}_2\text{O}}^V = \frac{45000}{T} = L_{\text{H}_2\text{O}} V_{\text{H}_2\text{O}} \text{grad } P_f$$

Using $L_{\text{H}_2\text{O}} = w_{\text{H}_2\text{O}} = \text{approx. } 10^{-14}$ (see section 7.3.2), and $V_{\text{H}_2\text{O}} = 2 \times 10^{-5} \text{ m}^3.\text{mol}^{-1}$ (see above), then -

$$\text{grad } P_f.T = 4.5 \times 10^{23} \quad \dots(7.26)$$

Section 7.3.3 showed that the fluid infiltration event in Maine (Ferry(1979)) had a maximum duration of the order of 10 to 1 million years. Using these two values, (7.36) becomes -

$$\text{grad } P_f = 1.4 \times 10^9 \text{ to } 1.4 \times 10^{10} \text{ N.m}^{-3}$$

Then from Darcy's Law, Equation (7.25) -

$$\text{grad } P_f = \frac{\beta.v.\eta}{k}$$

and using $\beta = 10^{-4}$ (0.01%), $\eta = 1.5 \times 10^{-2}$ (N.sec.m⁻²), $k = 1.0 \times 10^{-17}$ (m²), -

$$v = 0.009 \text{ to } 0.09 \text{ m.sec}^{-1} \quad \dots(7.37)$$

This result is also of great value in the understanding of the fluid infiltration process. It means that for a particular 1m section of rock, a particular element of fluid will pass through that rock in only 1.85 mins. to 11 sec. Since the kinetics of mineral reactions can hardly be expected to keep pace with such very limited residence times, it is likely that the equilibration of fluid with the minerals comprising the rock volume will depend on the continued passage of identical fluid through the rock for a longer time. It might therefore explain how one high grade

rock (X16) had equilibrated with respect to stable isotope values of the secondary infiltration, but not with respect to mineral assemblage (see Chapter 5).

Another interesting point is that the calculated velocities are an average for the whole event. The calculations do not therefore preclude faster moving fluids which infiltrated in spurts, separated by periods of quiescence.

7.5: Conclusions

Non-equilibrium thermodynamics offers a phenomenological, or non-statistical approach to the study of metamorphic processes. It further provides a conceptual framework in which processes such as fluid transfer can be seen as the interplay between various 'flows', driven by 'forces'. With the estimation of various parameters, order of magnitude solutions to specific problems can reveal much about the kinetics of metamorphic processes, or their time durations.

C H A P T E R 8: Conclusions - The fluid history of Knapdale

1. The conclusions arising from this thesis, concerning mineral assemblages in metacarbonate rocks in Knapdale, SW Argyll, can be summarised thus:

a. Primary mineral assemblages may be split into low grade and high grade groups. Typical low grade assemblages are -

cc + qz + ms + rut \pm ab \pm bt \pm chl \pm dol,

whereas typical high grade assemblages consist of some combination of the minerals -

cc, qz, gross, czo, di, amph, ksp, bt, ms, sph, ab.

Primary high grade assemblages formed at conditions of roughly 8kb and 450-550°C, and represent the effect of infiltration by a binary H₂O-CO₂ fluid of composition X_{CO₂} < 0.1, which infiltrated by the pervasive movement of fluid through microcracks, driven by a fluid pressure gradient, with a time-averaged fluid:rock ratio of the order of 9:1 (relative to 1000cm³ rock). Primary high grade carbonates have stable isotopic compositions of $\delta^{18}\text{O} = +9$ to +19 per mil (SMOW) and $\delta^{13}\text{C} = -4$ to +8 per mil (PDB). Preliminary fluid inclusion work confirms the H₂O-rich nature of the fluid, but suggests the additional presence of 3-5 wt.% NaCl. A non-equilibrium thermodynamic model of the fluid transfer process suggests that the velocity of fluid moving through the carbonates may be of the order of 0.009 to 0.09 msec⁻¹, if a maximum event duration of 10 to 1 million years is assumed.

b. Secondary mineral assemblages are typically -

dol + qz + ksp + ms + ab ±rut ±chl.

The P-T- X_{CO_2} conditions of formation of secondary assemblages are as yet unrefined, and require further work. However, rough estimates can be made, of pressures around 6kb, temperatures <450°C and a fluid composition which is H₂O-rich, but probably greater than $X_{CO_2} = 0.15$. Stable isotope compositions of $\delta^{18}O = +24$ to +30 per mil (SMOW) and $\delta^{13}C = -1$ to +5 per mil (PDB) are interesting, in that the $\delta^{18}O$ values are unusually high. The fact that no obvious source for fluid with such an isotopic composition exists in Knapdale is good evidence for the secondary fluid being derived from outside the system. This poses many questions about the apparent channelling of the secondary fluid, and its lack of mineralogical and isotopic equilibrium with rocks elsewhere in the terrain, and points to further work which must be done on retrograde fluids in general.

2. Thus it has been shown that mineral assemblages in metacarbonate rocks in Knapdale can be divided into primary low grade, primary high grade and secondary groups, by both the nature of the minerals present in each, and their reaction textures, and by their oxygen and carbon isotopic signatures. The latter two assemblage groups are the result of two separate episodes of fluid infiltration, during which the chemistry of the fluids dominated the rock system, allowing the growth of new minerals, whose P-T- X_{CO_2} stabilities reflect the composition of the external fluid reservoir.

In Section 2.4.3 it was mentioned that the prograde release of water at a 'garnet isograd' reaction which involved the breakdown of chlorite and stilpnomelane (common at lower grade in Knapdale metabasic rocks) could result in roughly 330cm³ of H₂O per 1000cm³ of metabasite. Assuming a fluid:rock ratio of 9:1 in the high grade carbonates of South Knapdale, and estimating their areal

extent as $4 \times 10^5 \text{ m}^2$, then the volume of metabasite needed to supply that fluid (assuming it to be pure H_2O) would be $(1.08 \times 10^7)d \text{ m}^3$, where d is the depth to which carbonates occur. Comparing the area of Knapdale (roughly $2 \times 10^8 \text{ m}^2$) with the necessary areal extent of metabasites shows that metabasite sills of average length 1km, and of average thickness 100m, would need to represent only 5.45% of the total surface area, and this is easily the case (see Graham(1973), Geological Survey Sheets 28 and 29). Therefore, it can be concluded that prograde dewatering of metabasite sills by the breakdown of chlorite and stilpnomelane to form garnet could provide enough fluid to account for fluid:rock ratios of 9:1 in the high grade carbonates.

Harte & Graham(1975) and Graham et al. (1983) have shown that some metabasic rocks in Knapdale were infiltrated by a primary, low grade fluid whose stable isotopic signature (see Figure 5.3) is significantly different from those found in the carbonate rocks. This fluid may have formed by the low grade dewatering of the sediment pile and the thermal expansion of water, along with the regional oxidation of graphite in pelites, by mixing of fluid reservoirs of differing X_{CO_2} and $f\text{O}_2$.

Overall then, during the metamorphic history of Knapdale, three (or more?) fluids moved through the sediment pile, and affected the mineral assemblages in it. Evidence of the presence of primary, low grade fluid, however, is limited to metabasic rocks in the North Knapdale and Tayvallich areas, and the presence of primary, high grade fluid to carbonate rocks in South Knapdale. It is not possible from the present work to determine whether the primary high grade fluid was channelled through the carbonate lithologies only, or whether it flushed through all the rock units, because of the lack of mineralogical information in the quartzites, semi-pelites and pelites. However, an oxygen isotope study of quartz and other silicates from a variety of lithologies would answer this question.

The secondary fluid is limited in effect to South

Knapdale also, in the zone of secondary 'Tarbert Monoform' deformation, but its presence is further limited to discrete zones within carbonate units. This points strongly to some form of channelling, probably with structural or rock mechanical control.

Finally, therefore, the overall picture of metamorphism in Knapdale can be seen to be one of several sources and sinks of fluid, and of spatial and temporal variations in fluid history. This demonstrates that studies of regional metamorphic terrains must be approached with great care, because their fluid histories may be such that the mineral assemblages seen now are the end result of a long and complicated series of events.

Acknowledgements

Firstly, I would like to thank Jo, and to say that beside her, this thesis means nothing to me.

Secondly, I would like to heartily thank my father, mother, and sister, Elspeth, because they provided continual moral and financial support, for which I am very grateful.

Thirdly, I am grateful to Colin Graham, my supervisor, for his enthusiasm throughout, and for his conscientious reviews of earlier drafts.

Fourthly, I would like to thank the following, as they also changed the course of this project: Diana Baty, Phil Bentley, John Boyle, David Braunholtz, Alice Carter, Colin Chaplin, Cameron Clark, Eddie Clark, Ben Crail, John Craven, Dave Cooper, John Dixon, Terry Donnelly, Simon Eaton, Tony Fallick, Steve Farrell, Leo Harrison, Ben Harte, Andy Hockey, Julian Holbrook, Bob Hunter, Dave Ince, Peter Isaacson, Ian James, Phil Lightfoot, Andy .Martin, Dave Pattison, Roger Powell, John Ridley, Terry Scoffin, Graham Shimmield, Sandy Tudhope, Tabitha, Douglas Turner, and finally Ulysses, who may one day return.

Fifthly, I acknowledge the receipt of a N.E.R.C Studentship.

References

Anderton, R. (1979) Slopes, submarine fans and syndepositional faults: sedimentology of parts of the Middle and Upper Dalradian in the SW Highlands of Scotland. In: A.L. Harris et al., Eds., *The Caledonides of the British Isles - Reviewed*. Spec. Publ. Geol. Soc. London **8**, 483-488.

Bailey, E.B. (1922) The structure of the SW Highlands of Scotland. *J. Geol. Soc. London* **78**, 82-131.

Bickle, M.J. & Powell, R. (1977) Calcite-dolomite geothermometers for iron-bearing carbonates: the Glockner area of the Tauern Window, Austria. *Contrib. Mineral. Petrol.* **59**, 281-292.

Bird, D.K. & Norton, D.L. (1981) Theoretical prediction of phase relations among aqueous solutions and minerals: Salton Sea geothermal system. *Geochim. Cosmochim. Acta* **45**, 1479-1493.

Borradaile, G.J. (1973) Dalradian structure and stratigraphy of the Northern Loch Awe district, Argyllshire. *Trans. Roy. Soc. Edinburgh* **69**, 1-21.

Bottinga, Y. (1969) Calculated fractionation factors for carbon and hydrogen isotope exchange in the system calcite-CO₂-graphite-CH₄-H₂-H₂O-vapor. *Geochim. Cosmochim. Acta* **33**, 49-64.

Bowers, T.S. & Helgeson, H.C. (1983) Calculation of the thermodynamic and geochemical consequences of non-ideal mixing in the system H₂O-CO₂-NaCl on phase relations in geologic systems: Equation of state for H₂O-CO₂-NaCl fluids at high pressures and temperatures. *Geochim. Cosmochim. Acta*

47, 1247-1275.

Bowman, J.R. & Essene, E.J. (1982) P-T-XCO₂ conditions of contact metamorphism in the Black Butte aureole, Elkhorn, Montana. *Am. J. Sci.* **282**, 311-314.

Brace, W.F., Walsh, J.B. & Frangos, W.T. (1968) Permeability of granite under high pressure. *J. Geophys. Res.* **73**, 2225-2236.

Bradbury, H.J., Harris, A.L. & Smith, R.A. (1979) Geometry and emplacement of nappes in the Central Scottish Highlands. In: A.L. Harris et al., Eds., *The Caledonides of the British Isles - reviewed*. Spec. Publ. Geol. Soc. London **8**, 213-221.

Brady, J.B. (1975) Reference frames and diffusion coefficients. *Am. J. Sci.* **275**, 954-983.

_____ (1977) Metasomatic zones in metamorphic rocks. *Geochim. Cosmochim. Acta* **41**, 113-126.

Bucher-Nurminen, K. (1981) The formation of metasomatic reaction veins in dolomitic marble roof pendants in the Bergell intrusion (Province Sondrio, Northern Italy). *Am. J. Sci.* **281**, 1197-1222.

Burnham, C.W., Holloway, J.R. & Davis, N.F. (1969) Thermodynamic properties of water to 1000°C and 10000bars. *Geol. Soc. Am. Spec. Paper.* **132**, 96pp.

Cermignani, C. & Anderson, G.M. (1973) Origin of a diopside-tremolite assemblage near Tweed, Ontario. *Can. J. Earth Sci.* **10**, 84-90.

Chatterjee, N.D. (1971) Phase equilibria in the Alpine metamorphic rocks of the environs of the Dora-Maira Massif, Western Italian Alps. *N. Jahrb. Mineral. Monat.* **114**, 181-245.

Crawford, M.L. (1972) Plagioclase and other mineral equilibria

- in a contact metamorphic aureole. *Contrib. Mineral. Petrol.* 36, 293-314.
- _____, Kraus, D.W. & Hollister, L.S. (1979) Petrologic and fluid inclusion study of calc-silicate rocks, Prince Rupert, British Columbia. *Am. J. Sci.* 279, 1135-1159.
- deGroot, S.R. (1952) *Thermodynamics of Irreversible Processes*. North-Holland, Amsterdam.
- _____ & Mazur, P. (1962) *Nonequilibrium Thermodynamics*. North-Holland, Amsterdam.
- Erdmer, P. (1981) Metamorphism at the northwest contact of the Stanhope pluton, Quebec Appalachians: mineral equilibria in interbedded pelite and calc-schist. *Contrib. Mineral. Petrol.* 76, 109-115.
- Ernst, W.G. (1972) CO₂-poor composition of the fluid attending Franciscan and Sanbagawa low-grade metamorphism. *Geochim. Cosmochim. Acta* 36, 497-504.
- Etheridge, M.A., Wall, V.J. & Cox, S.F. (1984) High fluid pressures during regional metamorphism and deformation: implications for mass transport and deformation mechanisms. *J. Geophys. Res.* 89, 4344-4358.
- Evans, B.W. & Trommsdorf, V. (1974) Regional metamorphism of ultramafic rocks in the central Alps: paragenesis in the system CaO-MgO-SiO₂-H₂O. *Schweiz. Mineral. Petrog. Mitt.* 50, 481-507.
- Ferry, J.M. (1979) A map of chemical potential differences within an outcrop. *Am. Mineral.* 64, 966-985.
- _____ (1980) A case study of the amount and distribution of heat and fluid during metamorphism. *Contrib. Mineral. Petrol.* 71, 373-385.

_____ (1981) Petrology of graphitic sulfide-rich schists from south-central Maine: an example of desulfidation during prograde regional metamorphism. *Am. Mineral.* 66, 908-930.

_____ (1983) Regional metamorphism of the Vassalboro Formation, south-central Maine, USA: a case study of the role of fluid in metamorphic petrogenesis. *J. Geol. Soc. London* 140, 551-576.

_____ & Burt, D.M. (1982) Characterization of metamorphic fluid composition through mineral equilibria. In: J.M. Ferry, Ed., *Characterization of Metamorphism through Mineral Equilibria*. Min. Soc. Am., Washington, D.C. 223-263.

_____ & Spear, F.S. (1978) Experimental calibration of the partitioning of Fe and Mg between biotite and garnet. *Contrib. Mineral. Petrol.* 66, 113-117.

Finger, L.W. & Burt, D.M. (1972) REACTION, a FORTRAN IV computer program to balance chemical reactions. *Yb. Carnegie Inst. Wash.* 71, 616-620.

Fisher, G.W. (1977) Nonequilibrium thermodynamics in metamorphism. In: D.G. Fraser, Ed., *Thermodynamics in Petrology*. Riedel, Holland. pp.381-403.

_____ (1978) Rate laws in metamorphism. *Geochim. Cosmochim. Acta* 42, 1035-1050.

_____ & Elliott, D. (1974) Criteria for quasi-steady diffusion and local equilibrium in metamorphism. In: A.W. Hofmann et al., Eds., *Geochemical Transport and Kinetics*. Carnegie Inst. Wash. Publ. 634, 231-241.

_____ & Lasaga, A.C. (1981) Irreversible thermodynamics in petrology. In: A.C. Lasaga & R.J. Kirkpatrick, Eds., *Kinetics of Geochemical Processes*. Min. Soc. Am., Washington, D.C. pp.171-211.

Fisher, J.R. & Zen, E-A. (1971) Thermochemical calculations from hydrothermal phase equilibrium data and the free energy of H₂O. *Am. J. Sci.* 270, 297-314.

Fletcher, R.C. & Hofmann, A.W. (1974) Simple models of diffusion and combined diffusion-infiltration metasomatism. In: A.W. Hofmann et al., Eds., *Geochemical Transport and Kinetics*. Carnegie Inst. Wash. Publ. 634, 243-259.

Frantz, J.D. & Mao, H.K. (1976) Bimetasomatism resulting from intergranular diffusion: I. A theoretical model for monomineralic reaction zone sequences. *Am. J. Sci.* 276, 817-840.

_____ & _____ (1979) Bimetasomatism resulting from intergranular diffusion: II. Prediction of multimineralic zone sequences. *Am. J. Sci.* 279, 302-323.

_____ & Weisbrod, A. (1974) Infiltration metasomatism in the system K₂O-SiO₂-Al₂O₃-H₂O-HCl. In: A.W. Hofmann et al., Eds., *Geochemical Transport and Kinetics*. Carnegie Inst. Wash. Publ. 634, 261-271.

Friedman, I. & O'Neil, J.R. (1977) Compilation of stable isotope fractionation factors of geochemical interest. In: M. Fleischer, Ed., *Data of Geochemistry, Chapter KK*. U.S. Geol. Surv. Prof. Paper 440-KK.

Ghent, E.D. & deVries, C.D.S. (1972) Plagioclase-garnet-epidote equilibria in hornblende-plagioclase bearing rocks from the Esplanade Range, British Columbia. *Can. J. Earth Sci.* 9, 618-635.

_____, Robbins, D.B. & Stout, M.Z. (1979) Geothermometry, geobarometry and fluid compositions of metamorphosed calc-silicates and pelites, Mica Creek, British Columbia. *Am. Mineral.* 64, 874-885.

Gordon, T.M. & Greenwood, H.G. (1971) The stability of grossularite in H₂O-CO₂ mixtures. *Am. Mineral.* **56**, 1674-1688.

Graham, C.M. (1973) Chemical petrology of metamorphosed basic rocks of the Dalradian Series, with particular reference to the Knapdale area of Argyll. *Unpubl. Ph.D. Thesis, University of Edinburgh.*

_____ (1976) Petrochemistry and tectonic significance of Dalradian metabasic rocks of the SW Scottish Highlands. *J. Geol. Soc. London* **132**, 61-84.

_____ & Borradaile, G.J. (1984) The petrology and structure of Dalradian metabasaltic dykes of Jura: implications for early Dalradian evolution. *Scott. J. Geol.* **20**, 257-270.

_____, Greig, K.M., Sheppard, S.M.F. & Turi, B. (1983) Genesis and mobility of the H₂O-CO₂ fluid phase during regional greenschist and epidote amphibolite facies metamorphism: a petrological and stable isotope study in the Scottish Dalradian. *J. Geol. Soc. London* **140**, 577-599.

_____ & Harmon, R.S. (1983) Stable isotope evidence on the nature of crust-mantle interactions. In: C.J. Hawkesworth & M.J. Norry, Eds., *Continental Basalts and Mantle Xenoliths*. Shiva, Nantwich, Cheshire. pp.20-46.

_____ & Powell, R. (1984) A garnet-hornblende geothermometer: calibration, testing and application to the Pelona Schist, Southern California. *J. Metamorphic Geol.* **2**, 13-31.

Grambling, J.A. (1981) Kyanite, andalusite, sillimanite and related mineral assemblages in the Truchas Peak region, New Mexico. *Am. Mineral.* **66**, 702-722.

Greenwood, H.G. (1967) Mineral equilibria in the system

MgO-SiO₂-H₂O-CO₂. In P.H. Abelson, Ed., *Researches in Geochemistry II*. John Wiley & Sons, New York, pp. 542-549.

_____ (1975) Buffering of pore fluids by metamorphic reactions. *Am. J. Sci.* **275**, 573-593.

Guidotti, C.V. (1970) The mineralogy and petrology of the transition from the lower to upper sillimanite zone in the Oquossoc area, Maine. *J. Petrol.* **11**, 277-336.

Gunn, W., Clough, C.T. & Hill, J.B. (1897) The geology of Cowal. *Mem. Geol. Surv. Scotland*.

Harker, A. (1950) *Metamorphism*. Methuen, London.

Harte, B. & Graham, C.M. (1975) The graphical analysis of greenschist to amphibolite facies mineral assemblages in metabasites. *J. Petrol.* **16**, 347-370.

Helgeson, H.C., Delany, J.M., Nesbitt, H.W. & Bird, D.K. (1978) Summary and critique of the thermodynamic properties of rock-forming minerals. *Am. J. Sci.* **278A**, 1-229.

Hewitt, D.A. (1973) The metamorphism of micaceous limestones from south-central Connecticut. *Am. J. Sci.* **273A**, 444-469.

_____ (1975) Stability of the assemblage phlogopite - calcite - quartz. *Am. Min.* **60**, 391-397.

Hodges, K.V. & Spear, F.S. (1983) Geothermometry, geobarometry and the Al₂SiO₅ triple point at Mt. Moosilauke, New Hampshire. *Am. Min.* **67**, 1118-1134.

Hofmann, A.W. (1972) Chromatographic theory of infiltration metasomatism and its application to feldspars. *Am. J. Sci.* **272**, 69-90.

_____ (1973) Theory of metasomatic zoning. A reply to Dr.

D.S. Korzhinskii. *Am. J. Sci.* 273, 960-964.

Holdaway, M.J. & Lee, S.M. (1977) Fe-Mg cordierite stability in high grade pelitic rocks based on experimental, theoretical and natural observations. *Contrib. Mineral. Petrol.* 63, 175-193.

Holland, T.J.B. (1981) Thermodynamic analysis of simple mineral systems. In: R.C. Newton et al., Eds., *Thermodynamics of minerals and melts*. Springer-Verlag, New York. pp.19-23.

Holloway, J.R. (1977) Compositions and volumes of supercritical fluids in the Earth's crust. In: L.S. Hollister & M.L. Crawford, Eds., *Fluid Inclusions: Applications to Petrology* Min. Ass. Can., Calgary. pp.13-39.

Hoschek, G.(1980) Phase relations of a simplified marly rock system with application to the Western Hohe Tauern (Austria). *Contrib. Mineral. Petrol.* 73, 53-68.

_____ (1981) The effect of Fe-Mg substitution on phase relations in marly rocks of the Western Hohe Tauern (Austria). *Contrib. Mineral. Petrol.* 75, 123-128.

_____ (1984) Alpine metamorphism of calcareous metasediments in the Western Hohe Tauern, Tyrol: mineral equilibria in COHS fluids. *Contrib. Mineral. Petrol.* 87, 129-137.

Hoy, T. (1976) Calc-silicate isograds in the Riondel area, southeastern British Columbia. *Can. J. Earth Sci.* 13, 1093-1104.

Jacobs, G.K. & Kerrick, D.M. (1981) Devolatilization equilibria in H₂O-CO₂ and H₂O-CO₂-NaCl fluids: an experimental and thermodynamic evaluation at elevated temperatures and pressures. *Am. Mineral.* 66, 1135-1153.

Jansen, J.B.H., van de Kraats, A.H., van der Rijst, H. &

Schuiling, R.D. (1978) Metamorphism of siliceous dolomites at Naxos, Greece. *Contrib. Mineral. Petrol.* **67**, 279-288.

Joesten, R. (1977) Evolution of mineral assemblage zoning in diffusion metasomatism. *Geochim. Cosmochim. Acta* **41**, 649-670.

Jones, J.W. (1972) An almandine garnet isograd in the Rogers Pass area, British Columbia: the nature of the reaction and an estimation of the physical conditions during its formation. *Contrib. Mineral. Petrol.* **37**, 291-306.

Katchalsky, A. & Curran, P.F. (1965) *Nonequilibrium Thermodynamics in Biophysics* 248pp. Harvard University Press.

Kerrick, D.M., Crawford, K.E. & Randazzo, A.F. (1973) Metamorphism of calcareous rocks in three roof pendants in the Sierra Nevada, California. *J. Petrol.* **14**, 303-325.

_____ & Jacobs, G.K. (1981) A modified Redlich-Kwong equation for H₂O, CO₂ and H₂O-CO₂ mixtures at elevated pressures and temperatures. *Am. J. Sci.* **281**, 735-767.

Knill, J.L. (1959) Palaeocurrents and sedimentary facies of the Dalradian metasediments of the Craginich - Kilmelfort district. *Proc. Geol. Ass.* **70**, 273-282.

_____ (1963) A sedimentary history of the Dalradian Series. In: M.R.W. Johnson & F.H. Stewart, Eds., *The British Caledonides*. Oliver & Boyd, Edinburgh & London. pp.99-120.

Korzhinskii, D.S. (1959) *Physicochemical Basis of the Analysis of the Paragenesis of Minerals*. (trans.) Consultants Bureau, New York.

_____ (1970) *Theory of metasomatic zoning*. 162pp. Clarendon Press.

Kreulen, R. (1980) CO₂-rich fluids during regional metamorphism on Naxos (Greece): carbon isotopes and fluid

inclusions. *Am. J. Sci.* 280, 745-771.

_____ & Schuiling, R.D. (1982) N₂-CH₄-CO₂ fluids during formation of the Dome de l'Agout, France. *Geochim. Cosmochim. Acta* 46, 193-203.

Melson, W.G. (1966) Phase equilibria in calc-silicate hornfels, Lewis and Clark County, Montana. *Am. Mineral.* 51, 402-421.

Moore, J.M. & Kerrick, D.M. (1976) Equilibria in siliceous dolomites of the Alta aureole, Utah. *Am. J. Sci.* 276, 502-524.

Navrotsky, A., Hon, R., Weill, D.F. & Henry, D.J. (1980) Thermochemistry of glasses in the systems CaMgSi₂O₆ - CaAl₂O₈ - NaAlSi₃O₈, SiO₂ - CaAl₂Si₂O₈ - NaAlSi₃O₈ and SiO₂ - Al₂O₃ - CaO - Na₂O. *Geochim. Cosmochim. Acta* 44, 1409-1423.

Nesbitt, B.E. & Essene, E.J. (1983) Metamorphic volatile equilibria in a portion of the southern Blue Ridge province. *Am. J. Sci.* 283, 135-165.

Norton, D. & Knapp, R. (1977) Transport phenomena in hydrothermal systems: the nature of porosity. *Am. J. Sci.* 277, 913-936.

Ohmoto, H. (1970) Systematics of sulfur and carbon isotopes in hydrothermal ore deposits. *Econ. Geol.* 67, 551-578.

O'Neil, J.R. & Taylor, H.P. Jr. (1967) The oxygen isotope and cation exchange chemistry of feldspars. *Am. Mineral.* 52, 1414-1437.

Onsager, L. (1931a) Reciprocal relations in irreversible processes. *Phys. Rev.* 37, 405-426.

_____ (1931b) Reciprocal relations in irreversible processes. *Phys. Rev.* 38, 2265-2279.

- Phillips, F.C. (1930) Some mineralogical and chemical changes induced by progressive metamorphism in the Green Bed Group of the Scottish Dalradian. *Mineral. Mag.* 22, 239-256.
- Pigage, L.C. & Greenwood, H.J. (1982) Internally consistent estimates of pressure and temperature: the staurolite problem. *Am. J. Sci.* 282, 943-969.
- Powell, R. (1978) *Equilibrium thermodynamics in petrology: an introduction*. Harper & Row, London.
- _____ & Evans, J. (1983) A new geobarometer for the assemblage biotite - muscovite - chlorite - quartz. *J. Metamorphic Geol.* 1, 331-336.
- _____ & Powell, M. (1977) Geothermometry and oxygen barometry using co-existing iron-titanium oxides: a reappraisal. *Mineralog. Mag.* 41, 257-263.
- Prigogine, I. (1955) *Introduction to the Thermodynamics of Irreversible Processes*. Thomas, Springfield, Illinois.
- Reed, W.E. (1970) Transport of water away from a buried heat source with special reference to hydrologic phenomena observed at Aardvark Nuclear Detonation. *J. Geophys. Res.* 75, 415-430.
- Rice, J.M. (1977a) Contact metamorphism of impure dolomitic limestone in the Boulder aureole, Montana. *Contrib. Mineral. Petrol.* 59, 237-259.
- _____ (1977b) Progressive metamorphism of impure dolomitic limestone in the Marysville aureole, Montana. *Am. J. Sci.* 277, 1-24.
- _____ & Ferry, J.M. (1982) Buffering, infiltration and the control of intensive variables during metamorphism. In: J.M. Ferry, Ed., *Characterization of Metamorphism through Mineral Equilibria*.

Min. Soc. Am., Washington, D.C. 263-326.

Roberts, J.L. (1966) Sedimentary affiliations and stratigraphic correlation of the Dalradian rocks in the SW Highlands of Scotland. *Scott. J. Geol.* 2, 200-223.

_____ (1974) The structure of the Dalradian rocks in the SW Highlands of Scotland. *J. Geol. Soc. London* 130, 93-124.

_____ (1977) The Dalradian rocks of Knapdale and North Kintyre. *Scott. J. Geol.* 13, 113-124.

_____ & Treagus, J.E. (1977) Polyphase generation of nappe structures in the Dalradian rocks of the SW Highlands of Scotland. *Scott. J. Geol.* 13, 237-254.

_____ & _____ (1979) Stratigraphical and structural correlation between the Dalradian rocks of the SW and Central Highlands of Scotland. In: A.W. Harris et al., Eds., *The Caledonides of the British Isles - reviewed*. Spec. Publ. Geol. Soc. London 8, 199-205.

Robin, P-Y. F. (1979) Theory of metamorphic segregation and related processes. *Geochim. Cosmochim. Acta* 43, 1587-1600.

Roedder, E. (1972) The composition of fluid inclusions. In M. Fleischer, Ed., *Data of Geochemistry*, U.S. Geol. Surv. Prof. Paper 440-JJ

Rosasco, G.J. & Roedder, E. (1979) Application of a new Raman spectrometer to nondestructive analysis of sulfate and other ions in individual phases in fluid inclusions in minerals. *Geochim. Cosmochim. Acta* 43, 1907-1915.

Rumble, D. (1978) Mineralogy, petrology and oxygen isotopic geochemistry of the Clough Formation, Black Mountain, New Hampshire, U.S.A. *J. Petrol.* 19, 317-340.

_____ (1983) The role of perfectly mobile components in metamorphism. *Ann. Rev. Earth Planet. Sci.* 10, 221-233.

_____, Ferry, J.M., Hoering, T.C. & Boucot, A.C. (1982) Fluid flow during metamorphism at the Beaver Brook fossil locality, New Hampshire. *Am. J. Sci.* 282, 886-919.

Rutter, E.H. (1983) Pressure solution in nature, theory and experiment. *J. Geol. Soc. London* 140, 725-740.

Rye, R.O., Schuiling, R.D., Rye, D.M. & Jansen, J.B.H. (1976) Carbon, hydrogen and oxygen isotope studies of the regional metamorphic complex at Naxos, Greece. *Geochim. Cosmochim. Acta* 40, 1031-1049.

_____ & Ohmoto, H. (1974) Sulfur and carbon isotopes and ore genesis: a review. *Econ. Geol.* 69, 826-842.

Secor, D.T. (1969) Mechanics of natural extension faulting at depth in the Earth's crust. *Geol. Surv. Can. Paper* 68, 52-75.

Seeburger, D.A. & Nur, A. (1984) A pore space model for rock permeability and bulk modulus. *J. Geophys. Res.* 89, 527-536.

Sheppard, S.M.F. (1979) Stable isotope geochemistry of fluids. In: D.T. Rickard & F.E. Wickman, Eds., *Chemistry and geochemistry of solutions at high temperatures and pressures*. *Phys. Chem. of the Earth* 13,14, 419-443.

_____ & Schwartz, H.P. (1970) Fractionation of carbon and oxygen isotopes and magnesium between coexisting metamorphic calcite and dolomite. *Contrib. Mineral. Petrol.* 26, 161-198.

Shieh, Y.N. & Taylor, H.P. Jr. (1969) Oxygen and carbon isotope studies of contact metamorphism of carbonate rocks. *J. Petrol.* 10, 307-331.

- Sisson, V.B., Crawford, M.L. & Thompson, P.H. (1981) CO₂-brine immiscibility at high temperatures, evidence from calcareous metasedimentary rocks. *Contrib. Mineral. Petrol.* 78, 371-378.
- Sivaprakesh, C. (1981) Chemographic analysis of metabasite assemblages from central Scottish Highlands. *Lithos* 14, 29-33.
- Spear, F.S. & Selverstone, J. (1983) Water exsolution from quartz: implications for the generation of retrograde metamorphic fluids. *Geology* 11, 82-85.
- Spooner, E.T.C. (1977) Hydrothermal model for the origin of the ophiolitic cupriferous pyrite ore deposits of Cyprus. In: *Volcanic Processes and Ore Genesis*. Inst. Mining & Metallurgy, Geol. Soc. London pp58-71.
- _____ (1981) Fluid inclusion studies of hydrothermal ore deposits. In: L.S. Hollister & M.L. Crawford, Eds., *Fluid inclusions: applications to petrology*. Min. Ass. Can., Calgary. pp.209-241.
- Suzuki, K. (1977) Local equilibrium during the contact metamorphism of siliceous dolomites in Kasuga-Mura, Japan. *Contrib. Mineral. Petrol.* 61, 79-89.
- Sveinbjornsdottir, A.E. (1983) Water-rock interaction in Krafla and Reykjanes geothermal systems, Iceland. (extended abstract) *J. Geol. Soc. London* 140, 549-550.
- Taylor, H.P. Jr. (1974) The application of oxygen and hydrogen isotope studies to problems of hydrothermal alteration and ore deposition. *Econ. Geol.* 69, 843-883.
- Thomas, P.R. (1979) New evidence for a Central Highland Root zone. In: A.L. Harris et al., Eds., *The Caledonides of the British Isles - reviewed*. Spec. Publ. Geol. Soc. London 8, 205-213.
- Thompson, A.B. (1976) Mineral reactions in pelitic rocks: II.

Calculation of some P-T-X(Fe-Mg) phase relations. *Am. J. Sci.* 276, 425-454.

Thompson, J.B. Jr. (1955) The thermodynamic basis for the mineral facies concept. *Am. J. Sci.* 253, 65-103.

Tilley, C.E. (1925) A preliminary survey of metamorphic zones in the southern Highlands of Scotland. *J. Geol. Soc. London* 81, 100-112.

Trommsdorf, V. (1972) Change in T-X during metamorphism of siliceous dolomite rocks of the central Alps. *Schweiz. Mineral. Petrog. Mitt.* 52, 567-571.

Valley, J.W. & Essene, E.J. (1980) Calc-silicate reactions in Adirondack marbles: the role of fluids and solid solution: summary. *Bull. Geol. Soc. Am.* 91, 114-117.

Van de Kamp, P.C. (1970) The Green Beds of the Scottish Dalradian Series: geochemistry, origin and metamorphism of mafic sediments. *J. Geol.* 78, 281-303.

Walther, J.V. & Orville, P.M. (1982) Volatile production and transport in regional metamorphism. *Contrib. Mineral. Petrol.* 79, 252-257.

Watkins, K.P. (1983) Petrogenesis of Dalradian albite porphyroblast schists. *J. Geol. Soc. London* 140, 601-618.

Weare, J.H., Stephens, J.R. & Eugster, H.P. (1976) Diffusion metasomatism and mineral reaction zones: general principles and application to feldspar alteration. *Am. J. Sci.* 276, 767-816.

Whitcomb, J.H., Garmany, J.D. & Anderson, D.L. (1973) Earthquake prediction: variation of seismic velocities before the San Francisco earthquake. *Science* 180, 632-635.

Williams-Jones, A.E. (1981) Thermal metamorphism of siliceous limestones in the aureole of Mount Royal, Quebec. *Am. J. Sci.* 281, 673-696.

Yardley, B.W.D. (1983) Quartz veins and devolatilization during metamorphism. *J. Geol. Soc. London* 140, 657-663.

A P P E N D I X A: List of symbols

- a_i = activity of component i
 A = cross-sectional area of fluid flow [m^2]
 A_j = affinity of a chemical reaction
 c_i = molar concentration of component i [$mol.m^{-3}$]
 C_p = heat capacity of a mineral reaction [J]
 D_{ij} = generalised diffusion coefficient [$m^2.sec^{-1}$]
 f_i^0 = fugacity of pure component i
 F = coefficient of friction on a particle [$N.sec.m^{-1}.mol^{-1}$]
 $F(C_p)$ = linear function of C_p with temperature
 G^0 = standard Gibbs free energy of a reaction [J]
 H_2O = water as a solute
 H_2O_* = water as a solvent
 $H_{1,298}$ = enthalpy of reaction at 1bar, 298K [J]
 J = absolute flow of component i [$mol.m^{-2}.sec^{-1}$]
 J_i^d = diffusive flow of i relative to solvent
 J_i^v = volume flow of i relative to solvent
 J_{ch} = chemical reaction
 J_s = flow of entropy
 k = permeability [m^2]
 K_s = equilibrium constant for solids in a mineral reaction
 L_{ij} = phenomenological coefficient [$mol^2.m^{-2}.N^{-1}.sec^{-1}$]
 n_i = number of moles of component i
 N_A = Avogadro's number
 P = total pressure [kbar]
 P_f = fluid pressure [$N.m^{-2}$]
 Q = volume of fluid flow per sec [$m^3.sec^{-1}$]
 r = radius of a particle [m]
 R = universal gas constant [$J.mol^{-1}.K^{-1}$]
 $S_{1,298}$ = entropy of reaction at 1bar, 298K [$J.K^{-1}$]
 $d_i S$ = entropy produced within a system
 T = temperature [K]
 v = velocity of fluid [$m.sec^{-1}$]
 v = molar volume [$m^3.mol^{-1}$]
 v_i = partial molar volume

V_s = molar volume of solids

X_i = thermodynamic force acting on component i

X_{CO_2} = mole fraction of CO_2 in a CO_2 - H_2O mixture

β = porosity

μ_i = chemical potential of component i [$N.m.mol^{-1}$]

μ_i^c = concentration dependent part of the chemical potential

v_i = stoichiometric coefficient of component i in a reaction

ξ_r = extent of reaction

η = viscosity of a medium [$N.sec.m^{-2}$]

π = osmotic pressure [$N.m^{-2}$]

σ = local entropy production

ϕ = dissipation function

ω_i = mobility of component i [$m.N^{-1}.sec^{-1}.mol$]

A P P E N D I X B: Graham et al. (1983)

Graham, C.M., Greig, K.M., Sheppard, S.M.F. & Turi, B. (1983) Genesis and mobility of the H₂O-CO₂ fluid phase during regional greenschist and epidote amphibolite facies metamorphism: a petrological and stable isotope study in the Scottish Dalradian. *J. Geol. Soc. London* **140**, 577-599.

This paper, which combines some of Colin Graham's thesis work on the metabasites of Knapdale with some unpublished stable isotope data collected by Colin, Simon Sheppard and Bruno Turi, and the early results from my work on the metacarbonates, was written at the end of the first year of my project, and therefore presents little more than a reconnaissance view of the metacarbonate system, the present level of understanding of which, I hope, a reading of this thesis will make clear.

Genesis and mobility of the H₂O-CO₂ fluid phase during regional greenschist and epidote amphibolite facies metamorphism: a petrological and stable isotope study in the Scottish Dalradian

C. M. Graham, K. M. Greig, S. M. F. Sheppard & B. Turi

SUMMARY: During high-pressure, low-temperature greenschist and epidote-amphibolite facies metamorphism in Dalradian rocks of the SW Scottish Highlands, mineral assemblages in metabasites and calcareous metasediments were dominantly controlled by infiltration of hydrous fluids; consequently, mineral assemblages capable of buffering the fluid phase composition were rare. Equilibrium prograde H₂O-CO₂ fluids usually contained less or much less than about 1–2 mol% CO₂.

Three fluid infiltration events are recognized. During prograde greenschist facies metamorphism, metabasic sills were infiltrated by large volumes of CO₂-bearing hydrous fluid; carbon isotope studies indicate that the CO₂ was locally derived by widespread oxidation of graphite or other organic carbon in adjacent metasediments. This may have occurred under approximately lower greenschist facies conditions as a result of mixing of fluids of varying f_{O_2} initiated by thermal expansion of water during heating, decompression and consequent hydraulic fracturing. In the epidote-amphibole facies (garnet zone), dehydration reactions in metabasites generated large quantities of water, which removed carbonate from metabasites on a regional scale and infiltrated calcareous metasediments to produce assemblages containing grossular, diopside, K-feldspar, amphibole, clinozoisite and sphene. A late retrograde infiltration of CO₂-bearing hydrous fluid under lower greenschist facies conditions generated assemblages containing K-feldspar + chlorite + rutile ± dolomite in calcareous rocks and albite prophyroblast schists in zones of intense secondary deformation.

Large-scale infiltration of fluid into greenschist-facies metadolerite sills was intimately related to, and possibly controlled by, penetrative deformation and, in the absence of a penetrative deformation, grain-boundary diffusion by itself was an ineffectual mechanism of fluid transport.

Recent advances in our understanding of the origins, compositions, and behaviour of the metamorphic fluid phase have resulted in large part from the application of experimental, theoretical and thermodynamic methods to the study of mineral-fluid phase equilibria (e.g. Kerrick 1974; Ferry 1976*a,b*, 1980, 1983). Fluid inclusion studies (e.g. Touret 1977) and the application of stable isotope techniques (e.g. Rye *et al.* 1976) have provided important alternative and additional constraints on metamorphic fluid phase composition and behaviour.

In this study, we have used both phase equilibria and stable isotope techniques to deduce the origins, compositions and behaviour of the metamorphic fluid phase in a high-pressure – low-temperature greenschist to epidote-amphibolite facies regional metamorphic terrain devoid of syn- or post-metamorphic intrusive rocks (*cf.* Ferry 1967*b*, 1983). In particular, we have concentrated on the changes in fluid composition and behaviour across a major regional dehydration isograd, on the identification of sources and sinks for metamorphic fluid, on the nature and influence of retrograde fluid/rock interactions, and on the structural controls on fluid transport processes. This paper presents results and conclusions to date from a current project (Greig, unpubl. data) and

from earlier work by the other authors (Graham 1973; Turi *et al.* 1973).

Geological background

The area of study includes the Tayvallich and Knapdale areas of the SW Scottish Highlands (Figs 1 & 2) where rocks of the Argyll and Southern Highland Groups of the Dalradian Supergroup (Harris & Pitcher 1975), of probable late Precambrian and Lower Cambrian age, have been metamorphosed in the greenschist and epidote-amphibolite facies in a prograde Caledonian regional metamorphic event of probable Lower Ordovician age. It is relevant here to outline both the nature of the lithologies, which influences the composition of the metamorphic fluid phase, and the nature of the deformation, which influences the transport and behaviour of the fluid phase.

Lithologies

The Dalradian rocks of Knapdale may be subdivided into a metasedimentary and a metabasaltic component. Metasediments include grits, conglomerates and psammites, semi-pelitic schists, phyllites,

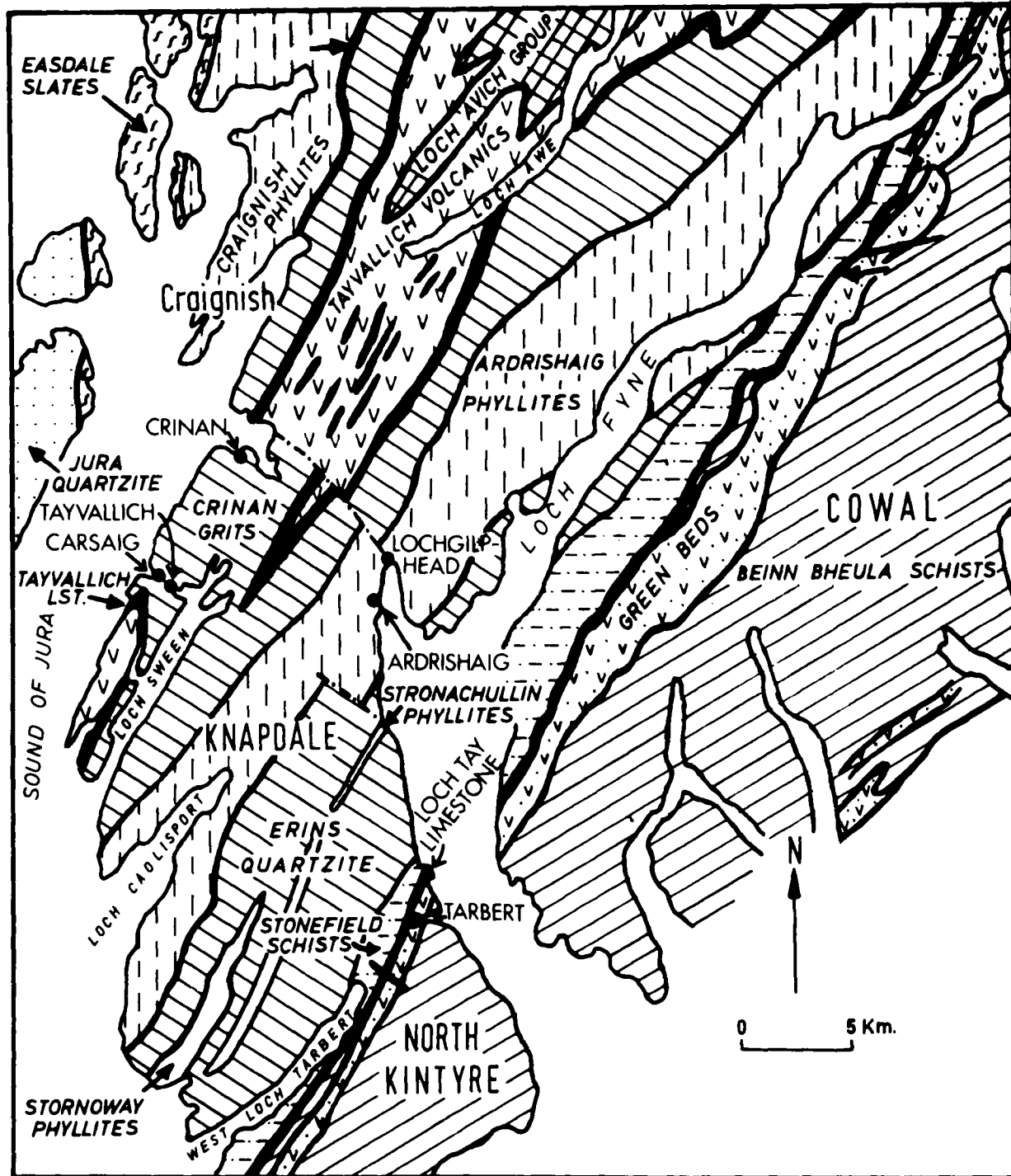


FIG. 1. Geological map of Dalradian rocks of the SW Scottish Highlands, modified after Roberts (1966). Intrusive metabasic rocks are omitted for clarity; their distribution in Knapdale is illustrated by Graham (1976, fig. 1).

variably siliceous and aluminous carbonates, dolomites and calc-mica-schists (Fig. 1; Roberts 1966; Harris & Pitcher 1975; Anderton 1979). Aluminous pelites are not common. The metabasaltic rocks comprise abundant conformable doleritic and gabbroic sills up to 140 m in thickness, and contemporaneous overlying basaltic volcanics (Tayvallich Volcanics; Fig. 1), many of which have undergone spilitic alteration (Graham 1976). Metabasaltic rocks are most thickly developed within the Loch Awe Syncline (Fig. 2) and comprise about 30% of the total lithostratigraphic succession. For clarity these are omitted from Fig. 1, but their

distribution in the area of study is illustrated by Graham (1976, fig. 1).

Structure

The deformation of Dalradian rocks in Knapdale (Roberts 1974, 1977) may be divided into primary and secondary. The upward-facing primary Loch Awe Syncline, comprising the Tayvallich and Kilmory Bay Synclines (Fig. 2), represents a zone of divergence between two primary recumbent anticlinal structures. Of these, the Ardrishaig Anticline (Fig. 2) is considered

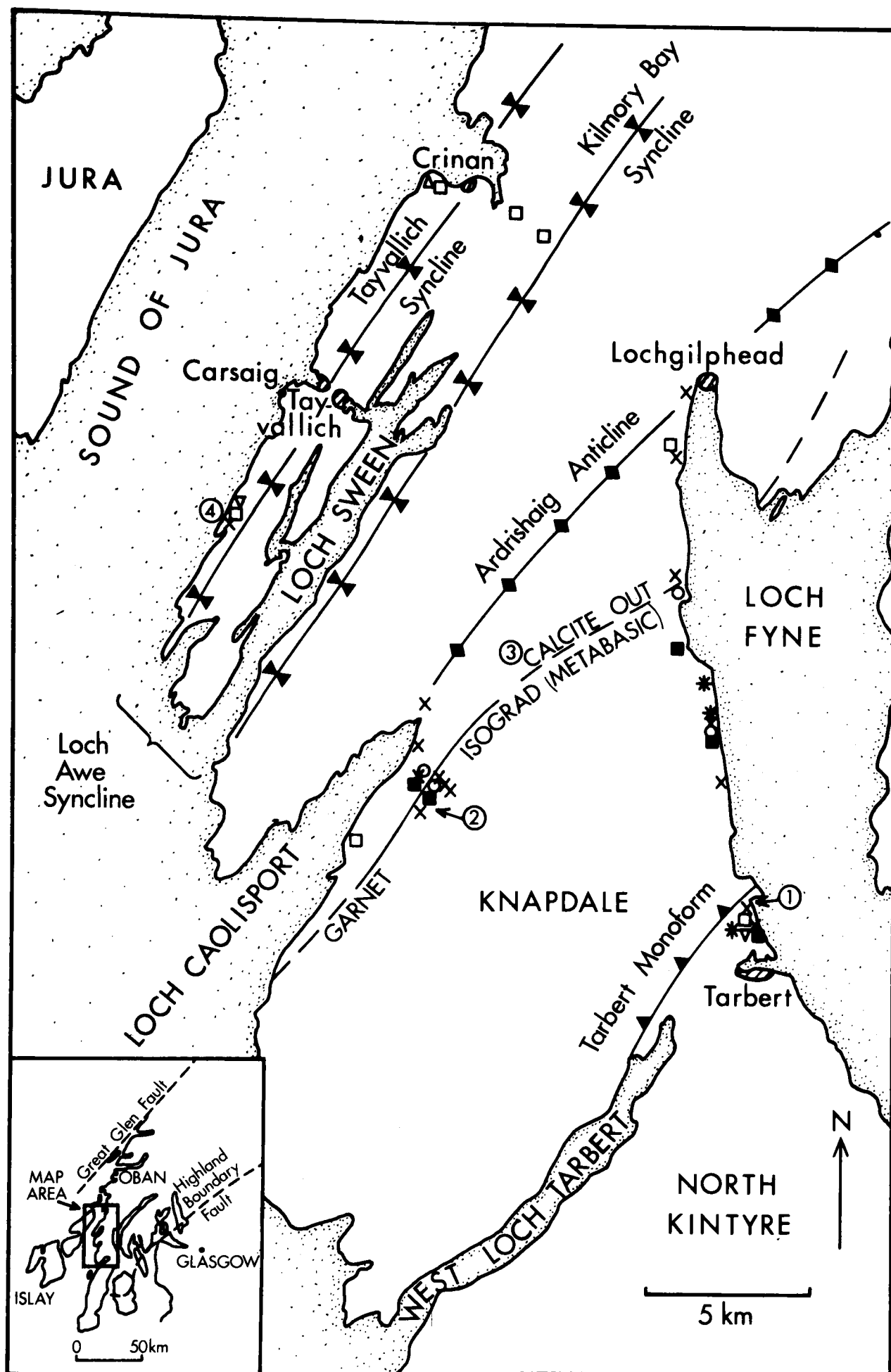


FIG. 2. Outline map of Knapdale area of the SW Scottish Highlands, indicating major primary and secondary structures (see text), trace of garnet isograd for metabasic rocks, and principal localities (1-4) for study of metasedimentary assemblages. Symbols indicate occurrences of various key minerals and/or assemblages in metasediments as follows: triangle, stilpnomelane; inverted triangle, dol + mu + qz; cross, bi(±chl ± cc); open square, sph + rut + cc + qz; filled square, sph ± cc (rut absent); circle, gt ± bi ± chl; asterisk, rut + cc/dol + qz in garnet zone.

to constitute the SE-facing core of the Tay Nappe. Its axis within the Ardrishaig Phyllites (Fig. 1) separates a right-way-up succession within the Loch Awe Syncline from the equivalent inverted succession to the SE. Primary axial planar schistosity is approximately parallel to bedding in the overturned limb (Knapdale Steep Belt), but at a high angle to bedding within the Loch Awe Syncline.

Primary structures and fabrics are re-folded by the secondary Tarbert Monoform in SE Knapdale (Fig. 2). The intensity of this later deformation is greatest in the vicinity of the Tarbert Monoform axis and decreases north-westward. Fabrics are usually non-penetrative, affecting only pelitic horizons, except near the axis of the monoform, and are generally manifested as crenulations of primary fabrics.

Deformation of low-grade metabasic sills and volcanics is very variable in intensity, according to the thickness and primary igneous grain-size of metabasic sheets and the angular discordance between bedding and schistosity in adjacent metasediments. Most thick sills show only marginal deformation, affecting zones of variable width but typically several metres thick, which takes the form of a zone of crude schistosity parallel to sill margins. Many sills are entirely unaffected by penetrative deformation, retaining throughout relict igneous textures overprinted during static crystallization of metamorphic assemblages. In higher grade metabasites, within the Knapdale Steep Belt, most amphibolites are largely or wholly schistose. In general, metabasic sheets are very much less flattened and elongated than intervening metasediments.

Metamorphism

On the basis of previous detailed studies of metabasic assemblages (Wiseman 1934; Graham 1973, 1974; Harte & Graham 1975), the area of study can be divided into a greenschist facies zone and an epidote-amphibolite facies zone separated by a garnet isograd whose location is dependent on bulk-rock Fe/Mg (Fig. 2). Metamorphism of metasediments in Knapdale (e.g. Elles & Tilley 1930) has not been described in detail, but a reconnaissance survey of metasedimentary parageneses described below has been carried out in order to elucidate fluid phase composition and behaviour.

Metamorphic textures and fabrics indicate that prograde metamorphism accompanied, and may have outlasted, primary recumbent folding and development of primary fabrics. Quartz inclusion trails in garnets in amphibolites and mica-schists affected by secondary deformation indicate that prograde metamorphic crystallization ceased prior to secondary deformation (see also Knill 1960). Albite in albite-porphyroblast schists in the Tarbert area (Fig. 2)

crystallized during the later stages of secondary deformation (see below).

P-T conditions of metamorphism

The P-T conditions and P-T-time paths of Dalradian metamorphism in the SW Scottish Highlands are the subject of a separate study (Graham & Greig, work in progress), but preliminary results of that study are briefly outlined here in order to constrain the calculated mineral-fluid phase equilibria (Fig. 9).

Temperatures of metamorphism, deduced by several methods, yield the following estimates: $410 \pm 30^\circ\text{C}$ for the lowest grade greenschist facies rocks near Tayvallich (calcite-dolomite thermometry; Bickle & Powell 1977); $510 \pm 30^\circ\text{C}$ for the upper greenschist facies rocks near the garnet isograd (magnetite-ilmenite thermometry; Powell & Powell 1977); $510\text{--}535^\circ\text{C}$ ($\pm 30^\circ\text{C}$) for the garnet zone of Knapdale, with temperatures increasing consistently SE across Knapdale from the garnet isograd towards Tarbert (garnet-hornblende Fe-Mg exchange thermometry; Graham & Powell, unpubl. data). Pressures of metamorphism deduced for both the greenschist facies and epidote amphibolite facies from the celadonite contents of white micas in equilibrium with biotite and chlorite (Powell & Evans 1983) is 10 ± 2 kbar.

The late retrograde crystallization event recognized in SE Knapdale along the Tarbert Monoform from the growth of chlorite + K-feldspar + dolomite in carbonates and calc-mica-schists (see discussion below) is assigned an approximate temperature of $300\text{--}400^\circ\text{C}$ and a maximum pressure (deduced as above) of 6 ± 2 kbar.

Representation and calculation of mineral-fluid equilibria

The following primary metamorphic minerals have been identified in Knapdale metamorphic assemblages: (accessory minerals and abbreviations in square brackets):

Metabasites: amphibole (actinolite-hornblende), chlorite, albite, epidote (ep), quartz, biotite, white mica (mu), garnet (gt), stilpnomelane (st), calcite, dolomite-ankerite, [sphene (sph), rutile (rut), ilmenite, magnetite, pyrite].

Metasediments: quartz, albite, K-feldspar, white mica, chlorite, biotite, calcite, dolomite-ankerite, stilpnomelane, almandine-grossular garnet, grossular (gr), hydrogrossular (hy'gr), clinozoisite-epidote, diopside, amphibole (amph), [sphene, rutile, pyrite, pyrrhotite] tourmaline.

Plagioclase is always albite, margarite is absent, and stilpnomelane and almandine-rich garnet are stable only in Fe-rich rock compositions. Graphite has not been positively identified in metasedimentary assemblages studied to date. Representative mineral analyses are given in Table 1.

The phase relations amongst major phases in Knapdale metamorphic rocks may be represented in the system $\text{K}_2\text{O}\text{--}\text{CaO}\text{--}\text{MgO}\text{--}\text{Al}_2\text{O}_3\text{--}\text{SiO}_2\text{--}\text{H}_2\text{O}\text{--}\text{CO}_2$ (KCMASH- CO_2) (e.g. Hoschek 1980). Possible reactions with excess quartz amongst the (pure) phases quartz (qz), tremolite (tr),

TABLE 1. Representative mineral analyses from SW Highland (Knapdale) metamorphic rocks

	77-39			77-40			77-42			77-47			71-1			CA-83		25005		25105	
	gr	hy'gr	di	ksp	ksp	bi	mu	ksp	dol	ksp	mu	chl	mu	chl	bi	ksp	dol	gt	amph	chl	chl
SiO ₂	39.69	36.79	53.10	65.01	64.57	38.53	49.44	64.47	—	64.46	47.60	25.77	48.09	25.02	36.18	65.44	—	38.03	56.10	25.83	24.35
TiO ₂	—	1.80	—	—	—	1.03	0.34	—	—	—	0.54	—	0.47	—	1.56	—	—	—	—	—	0.07
Al ₂ O ₃	21.57	16.94	0.73	18.15	18.66	16.31	27.56	17.96	—	18.08	31.83	21.56	31.35	20.89	17.71	18.29	—	21.27	1.83	21.36	19.83
FeO ₂₊	2.88	3.03	7.71	—	—	14.82	2.27	—	4.87	—	1.26	18.18	2.79	31.26	24.33	—	5.39	32.39	8.68	19.03	27.80
MnO	—	0.15	0.25	—	—	—	—	—	0.21	—	—	—	—	0.17	0.17	—	1.23	0.36	0.11	0.29	0.37
MgO	—	1.95	12.87	—	—	14.38	3.05	—	17.56	—	1.79	20.56	1.58	11.28	7.34	—	17.41	0.83	18.05	19.29	13.17
CaO	36.59	35.61	24.84	0.32	0.24	—	—	0.09	32.03	0.12	—	—	—	—	0.12	—	29.52	8.56	12.33	—	—
Na ₂ O	—	—	—	0.26	0.47	—	0.28	—	—	—	—	—	—	—	—	—	—	—	0.32	—	—
K ₂ O	—	—	—	15.55	15.19	9.06	10.37	15.68	—	16.70	9.35	—	9.62	—	8.96	16.85	—	—	0.10	—	—
Total	100.74	96.27	99.49	99.29	99.13	94.11	93.30	98.65	54.66	99.36	91.93	86.07	93.89	88.63	96.38	100.59	53.55	101.43	97.52	85.80	85.59
(O=)	(12)	(12)	(6)	(8)	(8)	(22)	(22)	(8)	(3)	(8)	(22)	(14)	(22)	(14)	(22)	(8)	(3)	(12)	(23)	(14)	(14)
Si	2.99	2.95	1.99	3.01	2.99	5.77	6.74	3.01	—	3.00	6.50	2.66	6.49	2.69	5.56	3.01	—	3.01	7.90	2.69	2.68
Al ^{IV}	—	—	0.01	0.99	1.01	2.24	1.26	0.99	—	0.99	1.50	1.34	1.52	1.31	2.44	0.99	—	—	0.10	1.31	1.32
Al ^{VI}	1.92	1.60	0.02	—	—	0.64	3.16	—	—	—	3.55	1.29	3.47	1.34	0.76	—	—	1.99	0.20	1.32	1.25
Ti	—	0.11	—	—	—	0.12	0.04	—	—	—	0.06	—	0.05	—	0.19	—	—	—	—	—	0.01
Fe	0.18	0.20	0.24	—	—	1.86	0.26	—	0.19	—	0.15	1.57	0.32	2.81	3.12	—	0.22	2.15	1.02	1.66	2.56
Mn	—	0.01	0.01	—	—	—	—	—	0.01	—	—	—	—	0.02	0.02	—	0.05	0.02	0.01	0.03	0.04
Mg	—	0.23	0.72	—	—	3.21	0.62	—	1.21	—	0.37	3.17	0.32	1.81	1.68	—	1.23	0.10	3.79	3.00	2.16
Ca	2.96	3.05	1.00	0.02	0.01	—	—	0.01	1.59	0.01	—	—	—	—	0.02	—	1.50	0.73	1.86	—	—
Na	—	—	—	0.02	0.04	—	0.08	—	—	—	—	—	—	—	—	—	—	—	0.09	—	—
K	—	—	—	0.92	0.90	1.73	1.80	0.94	—	0.99	1.63	—	1.66	—	1.76	0.99	—	—	0.02	—	—

Mineral analyses by Cambridge Instruments Microscan 5 Electron Microprobe with EDS attachment (Edinburgh University); 77-39, High-T carbonate assemblage, locality 1 (cf. assemblage 80, Fig. 7); 77-40, 77-42, CA-83, High-T calc-mica schist assemblage, locality 1; (cf. 82(b), Fig. 7). Epidote in 77-42 has composition Ps12 (where Ps = Fe/Fe + Al); 77-47, low temperature retrograde calc-mica schist, locality 1 (cf. 93, Fig. 7); 71-1, Albite porphyroblast schist (locality 1, Fig. 7); 25005, 25105, amphibolites, locality 2 (see also Graham 1974, fig. 1); Amphibole analyses in Graham (1974). Epidotes are Ps12.9 (25005) and Ps17 (25105). + Fe total as FeO. See discussion in text. Mineral abbreviations as in text.

K-feldspar (ksp), clinozoisite (cz), clinocllore (chl), phlogopite (bi), muscovite (mu), grossular (gr), calcite (cc), dolomite (dol) and diopside (di), applicable to metabasites and calcareous metasediments, were identified and listed using the computer program 'REACTION' (Finger & Burt 1972). The large number of possible reactions may be reduced to manageable proportions by assuming that diopside and grossular, which are stable in calcareous rocks only in the presence of very H₂O-rich fluid, are each produced in the assemblages under consideration by one possible reaction involving the other phases in the system. A T-X_{CO₂} reaction grid for constant pressure was then constructed by Schreinemaker's analysis, assuming that the fluid may be approximated by a binary H₂O-CO₂ fluid phase (consistent with the absence of graphite in studied assemblages). Reactions of inferred petrological importance from this grid were then calculated using the relationship:

$$\begin{aligned} \Delta G_{(P,T)} = & \Delta H_{(1,298)} - T \Delta S_{(1,298)} \\ & + \int_1^P \Delta V_s dP + nRT \ln f_{CO_2}^0 \cdot a_{CO_2} \\ & + mRT \ln f_{H_2O}^0 \cdot a_{H_2O} + RT \ln K_s \\ & + \int_{298}^T \Delta Cp \cdot dT - T \int_{298}^T \frac{\Delta Cp}{T} dT \end{aligned}$$

where $f_{CO_2}^0$ and $f_{H_2O}^0$ are the fugacities of pure CO₂ and H₂O, a_{CO_2} and a_{H_2O} are the activities of CO₂ and H₂O in the binary H₂O-CO₂ fluid at the pressure and temperature of interest, n and m are the stoichiometric coefficients of CO₂ and H₂O respectively, and K_s is the equilibrium constant for solid phases in the reaction of interest. Standard state is 1 bar and the temperature of interest. ΔV_s was taken to be constant.

Equilibrium T-X_{CO₂} curves for reactions of interest were calculated twice using the following simplifying assumptions:

- $\Delta Cp = 0$
- the Cp integral terms approximate to a linear function $F(Cp)$, where $F(Cp) = (3.11m + 2.15n)(0.953 - 473.2)$ cal (Powell 1978).

The latter assumption (Figs. 3, 4 & 7) gave rise to temperatures typically 30°C higher than the former (not plotted) for a particular X_{CO₂}, but with trivial changes in X_{CO₂} at a given temperature. This is a measure of the steepness of curves in the H₂O-rich region of T-X_{CO₂} diagrams.

Entropies, enthalpies and volume changes of reaction for all reactions of interest excluding those involving clinocllore were calculated directly from the data of Helgeson *et al.* (1978). Use of clinocllore data of Helgeson *et al.* results in a very limited stability field of chlorite + calcite + quartz, and absence of a stability field for chlorite + K-feldspar, both of which are inconsistent with field based petrological observation (Hoschek 1973, 1980; this study). Following Hoschek (1980) we have used experimental data for the reaction $3chl + 10cc + 21qz = 3tr + 2cz + 8H_2O + 10CO_2$ derived from Best (1978) ($\Delta H^0 = 395873$ cal; $\Delta S^0 = 756.34$ cal K⁻¹; $\Delta V_s^0 = -8.6996$ cal bar⁻¹; Hoschek 1980, table 3, adjusted for clinozoisite rather than zoisite). Other reactions involving chlorite were then calculated by summation of reactions, as described by Hoschek (1980).

To take account of the very non-ideal mixing of H₂O and CO₂ at the P and T of interest (10 kbar, 400–540°C), we have derived activity data for H₂O and CO₂, together with

fugacities of pure H₂O and CO₂, from the Hard-Sphere Modified Redlich-Kwong equation of Kerrick & Jacobs (1981). Fluid data were tabulated using a computer program written by Jacobs & Kerrick (1981a). Use of this mixing model gives good agreement between calculated and experimentally determined mixed-volatile equilibria in T-X_{CO₂} sections at pressures up to 6 kbar (Jacobs & Kerrick 1981b). Estimated values of X_{CO₂} (fluid) deduced below for mineral assemblages are strongly dependent on the validity of the mixing model chosen for the non-ideal fluid phase, but the relative order of reaction is unaffected.

T-X_{CO₂} sections for Knapdale metamorphic rocks have been calculated at model pressures of 10 kbar (prograde event) and 6 kbar (retrograde event) (Figs. 3, 4 & 7). Data for the reaction $sph + CO_2 = cc + rut + qz$ were derived from Jacobs & Kerrick (1981b) by Ferry (1983). In the 10 kbar phase diagram the restriction of all relevant equilibria to very H₂O-rich fluid compositions of less than about 4 mol% CO₂ at the temperature range of interest is a consequence of the high activities of CO₂ in water-rich H₂O-CO₂ fluids at high pressures and low temperatures (Kerrick & Jacobs 1981, figs. 11 & 12). High pressure is important in stabilizing carbonates in very H₂O-rich fluids. Thus, for example, the equilibrium $5dol + 8qz + H_2O = tr + 3cc + 7CO_2$ is located at X_{CO₂} ≈ 0.015 at 500°C, 10 kbar (Fig. 3), but at X_{CO₂} ≈ 0.08 at 500°C, 6 kbar.

Some equilibria of potential petrological importance in real assemblages are metastable at high pressure in the pure KCMASH-CO₂ system (Fig. 3). For example, the equilibrium $19mu + 9chl + 32cc + 21qz = 15bi + 16cz + 28H_2O + 32CO_2$, is of likely importance in limiting chlorite stability in calc-mica-schists in presence of H₂O-rich fluids at epidote-amphibolite facies conditions. Absence of primary chlorite in high-temperature hydrous assemblages makes it difficult to assess the effect of additional components in real mineral compositions on this equilibrium. Additional components (e.g. FeO, Na₂O) have a large effect in shifting the location of most mineral equilibria in T-X_{CO₂} space relative to the pure KCMASH-CO₂ system (compare Figs. 3 and 4). The equilibrium $2cz + CO_2 = 3an + cc + H_2O$ is restricted to very CO₂-rich fluids and high temperature (e.g. ~700°C at X_{CO₂} = 0.70) at 10 kbar consistent with the presence of albite in epidote-amphibolite facies calcareous rocks in Knapdale.

We conclude that use of the above thermodynamic data and procedures gives phase relations consistent in most instances with petrological observation, especially when corrections are made for activities of solids in real mineral assemblages (Table 2). Deficiencies and uncertainties in the data set, particularly as they relate to the relative and absolute locations of chlorite-bearing equilibria, are being explored further using alternative data sets derived directly from experimentally determined mineral equilibria studied where possible in the presence of H₂O-CO₂ fluids. In some cases, this will involve experimental determination or re-determination of key equilibria involving chlorite.

Mineral assemblages

Mineral assemblages are separated in this discussion into metabasic and metasedimentary. Although there

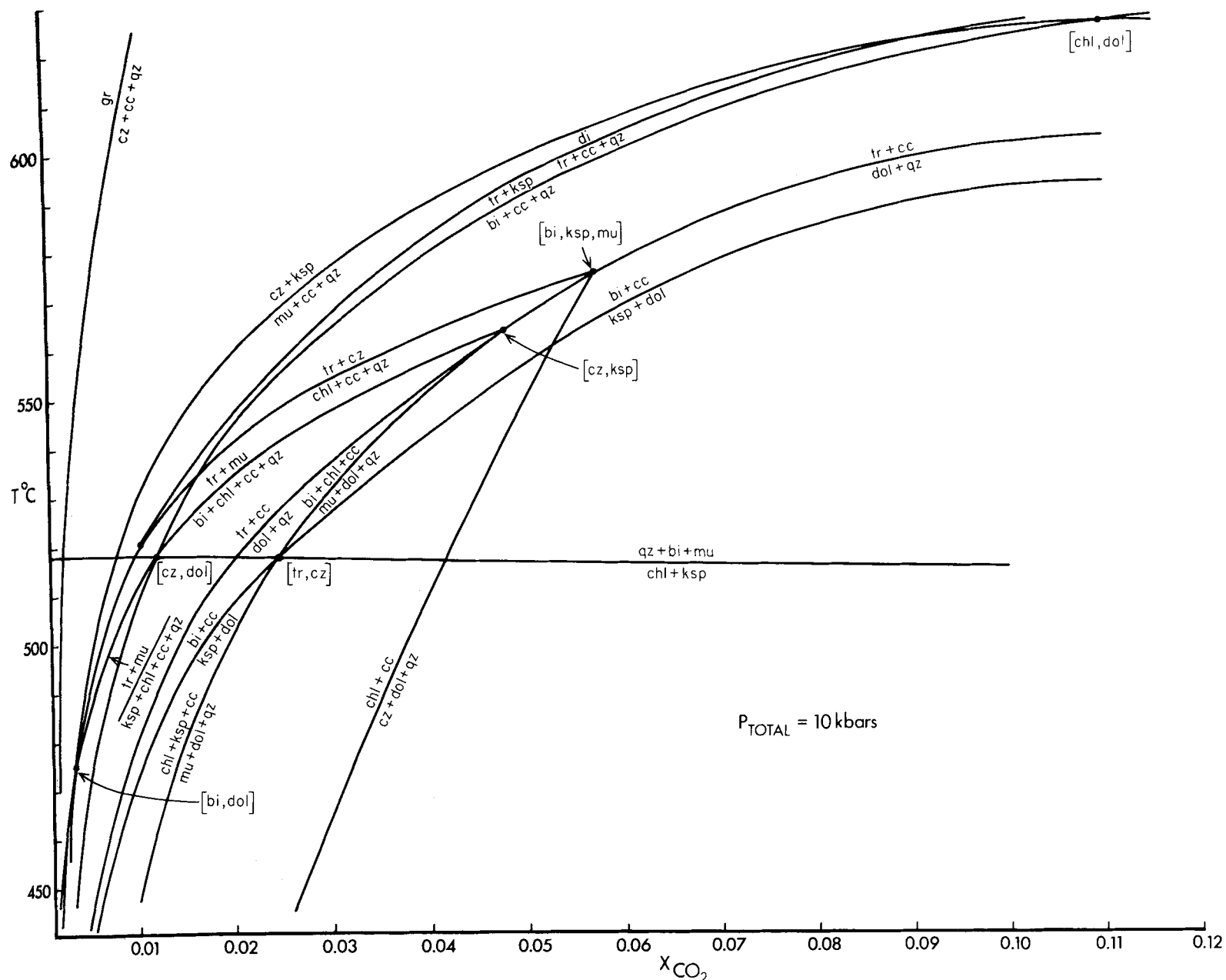


FIG. 3. T - X_{CO_2} section showing reactions with excess quartz amongst pure phases in the system KCMASH-CO₂ at $P(\text{fluid}) = 10$ kbar, calculated using mineral thermodynamic data of Helgeson *et al.* (1978), Powell (1978) and Hoschek (1980), and H₂O-CO₂ fluid data of Kerrick & Jacobs (1981) and Jacobs & Kerrick (1981a). For clarity, only a small number of reactions relevant to petrogenesis of SW Highlands metamorphic assemblages is shown. Invariant points are labelled according to phases absent in the usual notation. See text for discussion of phases (with abbreviations), reactions, and calculation procedures.

is considerable overlap between the two groups of assemblages, they evolved independently to a considerable degree and had different histories of fluid-rock interaction.

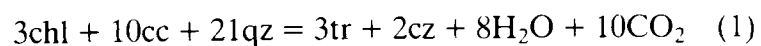
The garnet isograd in metabasic rocks is taken as a reference dividing line between the greenschist and epidote-amphibolite facies assemblages.

Metabasic assemblages

Greenschist facies

Typical metabasic greenschist-facies assemblages may be divided, after Harte & Graham (1975), into type I assemblages, with amphibole and epidote but

no calcite; type II assemblages, with amphibole + epidote + calcite; and type III assemblages, with calcite (\pm dolomite-ankerite) and no amphibole. These assemblages are related by the (pure KCMASH) reaction:



Typical type I assemblages contain act + chl + ep + ab + qz + sph \pm mu \pm bi \pm st and hbl + chl + ep + ab + qz + sph \pm bi \pm st. Hornblendes vary from edenitic in the lower greenschist facies to pargasitic in the upper greenschist facies, and actinolites become increasingly aluminous with increasing grade (Graham 1974; Grapes & Graham 1978; Graham, unpubl. data). Type II assemblages have calcite as an additional

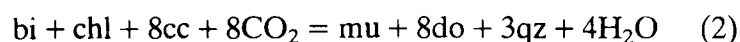
TABLE 2. Formulation of activity-composition relationships for mineral solid-solution series

Mineral	End members	Composition	Activity formulation
white mica	muscovite	$\text{KAl}_2\text{Si}_3\text{AlO}_{10}(\text{OH})_2$	$a_{\text{mu}}^{\text{mica}} = (9.48)X_{\text{K}}^{\text{A}}(X_{\text{Al}}^{\text{M2}})^2(X_{\square}^{\text{M2}})(X_{\text{Al}}^{\text{iv}})(X_{\text{Si}}^{\text{iv}})^3$
biotite	phlogopite	$\text{KMg}_3\text{Si}_3\text{AlO}_{10}(\text{OH})_2$	$a_{\text{phlog}}^{\text{bi}} = (9.48)X_{\text{K}}^{\text{A}}(X_{\text{Mg}}^{\text{M2}})^2(X_{\text{Mg}}^{\text{M1}})(X_{\text{Al}}^{\text{iv}})(X_{\text{Si}}^{\text{iv}})^3$
chlorite	clinochlore	$\text{Mg}_5\text{Al} \cdot \text{Si}_3\text{AlO}_{10}(\text{OH})_8$	$a_{\text{chl}}^{\text{chl}} = (64)(X_{\text{Mg}}^{\text{Br}})^2(X_{\text{Al}}^{\text{Br}})(X_{\text{Mg}}^{\text{Tc}})^3(X_{\text{Al}}^{\text{iv}})(X_{\text{Si}}^{\text{iv}})^3$ where $X_{\text{Al}}^{\text{Br}} = \text{Al}^{\text{vi}}$
amphibole	tremolite	$\square \text{Ca}_2\text{Mg}_5\text{Si}_8\text{O}_{22}(\text{OH})_2$	$a_{\text{tr}}^{\text{amph}} = X_{\square}^{\text{A}}(X_{\text{Ca}}^{\text{M4}})^2(X_{\text{Mg}}^{\text{M1-M3}})^5(X_{\text{Si}}^{\text{T1}})^4$
epidote	clinozoisite	$\text{Ca}_2\text{Al}_3\text{Si}_3\text{O}_{12}(\text{OH})$	$a_{\text{cz}}^{\text{ep}} = X_{\text{Al}}^{\text{M3}}$ $= (1 - X_{\text{Fe}}^{\text{M3}})$
K-feldspar	K-feldspar	KAlSi_3O_8	$a_{\text{kfsp}}^{\text{ksp}} = \frac{\text{K}}{\text{K} + \text{Na} + \text{Ca}}$
garnet	grossular	$\text{Ca}_3\text{Al}_2\text{Si}_3\text{O}_{12}$	$a_{\text{gross}}^{\text{gt}} = (X_{\text{Ca}}^{\text{D.C.S.}})^3$ where D.C.S. = divalent cation sites $= \frac{\text{Ca}}{\text{Ca} + \text{Mg} + \text{Mn} + \text{Fe}}$
calcite	calcite	CaCO_3	$a_{\text{cc}}^{\text{cc}} = X_{\text{Ca}}^{\text{cc}}$
dolomite-ankerite	dolomite	$\text{CaMg}(\text{CO}_3)_2$	$a_{\text{dol}}^{\text{dol-ank}} = X_{\text{Ca}}^{\text{M2}}X_{\text{Mg}}^{\text{M1}}$

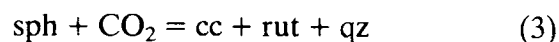
Formulations of activity-composition relationships after Powell (1978) and Bickle & Powell (1977) except for chlorite. Chlorite is assumed to be composed of talc(Tc)-like layers ($\text{Mg}_6\text{Si}_4\text{O}_{10}(\text{OH})_2$) and brucite (Br)-like layers ($\text{Mg}(\text{OH})_2$), and Al substitution is considered to occur only in the brucite layers in the chlorite lattice. Numerical coefficients for activity expressions for sheet silicates are normalization factors. Amphibole is assumed to have 2 sorts of tetrahedral sites (T_1 and T_2) with Al substitution occurring only on T_1 sites.

phase to type 1 assemblages. Typical dolomite-free type III assemblages contain chl + cc + ab + qz + ep ± mu ± bi ± sph ± rut, while dolomite-ankerite bearing type III assemblages contain chl ± dol + ab + qz + mu + rut ± cc.

Dolomite-ankerite bearing metabasites always contain rutile and white mica, but lack sphene and biotite, and are confined in occurrence to the lowest grade rocks in the vicinity of Tayvallich and Carsaig (Fig. 2), especially within the lowermost Tayvallich Volcanics (Fig. 1). These assemblages are related to dolomite-ankerite-absent type III assemblages by the reaction:



The phases sphene and rutile are related by the reaction:



and have an ordered distribution in excellent agreement with calculated T- X_{CO_2} phase relations (Fig. 4), such that sphene is present in types I, II, and (dolomite-free) III metabasites, while rutile is confined to both dolomite-bearing and dolomite-free type III assemblages.

Typical greenschist facies metabasic sills have a characteristic zonation of mineral parageneses from margins to interiors, schematically illustrated in idealized cross-section in Fig. 5. Calcite-free type I parageneses occur in the interiors of most massive sills, while type III assemblages occur in deformed, schistose margins, and type II assemblages occupy

intermediate zones. In thin and/or thoroughly schistose sills, type I and even type II assemblages may be lacking, while in massive undeformed metadolerites, type I assemblages may predominate and type II assemblages may be lacking or occur in very thin (~5–10 cm) zones at sill margins. These relationships indicate that gradients of fluid composition from relatively CO_2 -rich at sill margins to H_2O -rich in sill interiors are commonly preserved by metabasite assemblages, and that the distribution of carbonate-rich type III metabasites is directly related to the extent and degree of penetrative deformation and development of schistose fabrics.

A range of textural evidence consistently demonstrates that initially hydrous, lower greenschist facies, type I metabasic assemblages in sills have been infiltrated by a CO_2 -bearing fluid from the country rock metasediments, converting them into type II and type III assemblages. These include replacement of amphibole prisms and porphyroblasts by chlorite and calcite, carbonate reaction rims around epidote grains, and replacement of sphene rhombs by rutile ± calcite.

The mineral assemblages, textures, and field relations of the greenschist-facies metabasites, together with their calculated phase relations (Figs. 3 & 4) indicate the following conclusions:

(1) The presence or absence of biotite in metabasic assemblages in the greenschist-facies in the SW Highlands is not dependent on metamorphic grade, but is determined by the prevailing X_{CO_2} of the fluid phase according to reaction (2) above.

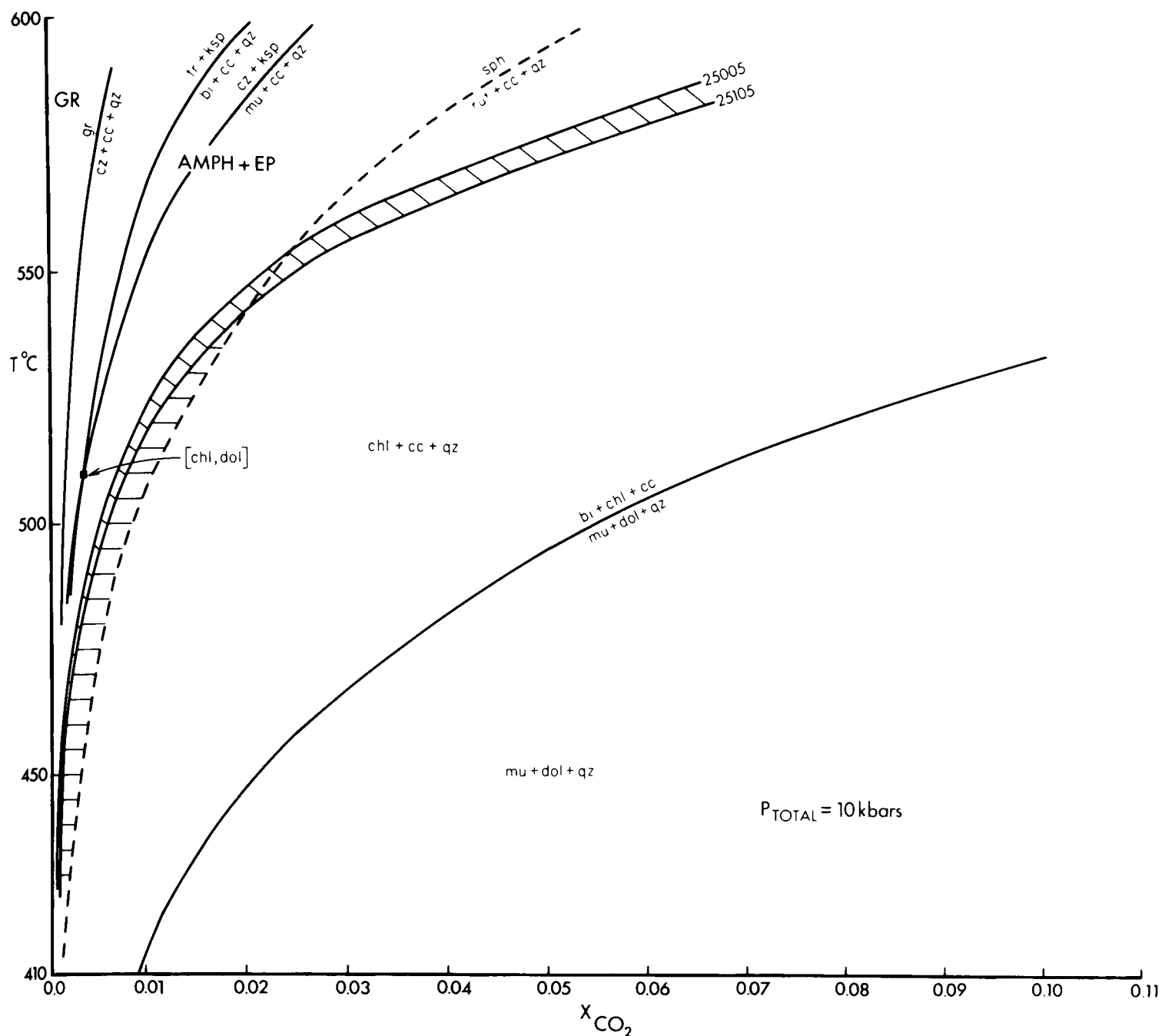


FIG. 4. T - X_{CO_2} section showing approximate locations of some key reactions from Fig. 3 recalculated at $P_{total} = 10$ kbar to take account of real mineral compositions using activities for solids formulated in Table 2, and mineral compositions given in Table 1. Because of the paucity of assemblages containing reactants plus products, positions of curves are approximate. Stability limit of chl + cc + qz (reaction 1) is calculated for 2 metabasic assemblages (25005, 25105, Table 1) of varying Fe/Mg (diagonal shaded area). Stability limits of mu + cc + qz and bi + cc + qz (reactions 5 and 6) are calculated using mineral compositions of 77-42 and CA-83 (Table 1) of comparable Fe/Mg, and assuming $a_{Ksp} = 0.95$. Stability limit of mu + dol + qz (reaction 2) is calculated using data (not in Table 1) from 2 greenschist facies metabasic assemblages of comparable rock composition. Field of stability of sphene + calcite + chlorite + quartz (rutile and amphibole absent) is shown by horizontal shading.

(2) Calculated and observed phase relationships are in excellent agreement, and assemblages allow us to estimate (Fig. 4) that X_{CO_2} (at 10 kbar, 440°C) varied from <0.001 in calcite-free (type I) sill interiors through 0.001–0.002 in sphene-bearing type III, 0.002 to 0.018 in rutile-bearing type III, to >0.018 in dolomite-ankerite + white mica bearing type III assemblages. As a consequence of high activities of CO_2 in H_2O - CO_2 fluids at high pressures and low temperatures (Kerrick & Jacobs 1981) both calcite and

dolomite-ankerite carbonates may be stabilized in greenschist facies metabasic assemblages in equilibrium with very water-rich fluids with as little as 1 mol % CO_2 or less.

(3) Mineral assemblages containing both reactants and products of reactions (1) to (3) are capable of buffering the fluid composition. Only buffer assemblages corresponding to reactions (1) and (3) are found in greenschist-facies metabasic sills (type II and type III metabasite assemblages) and these assemblages

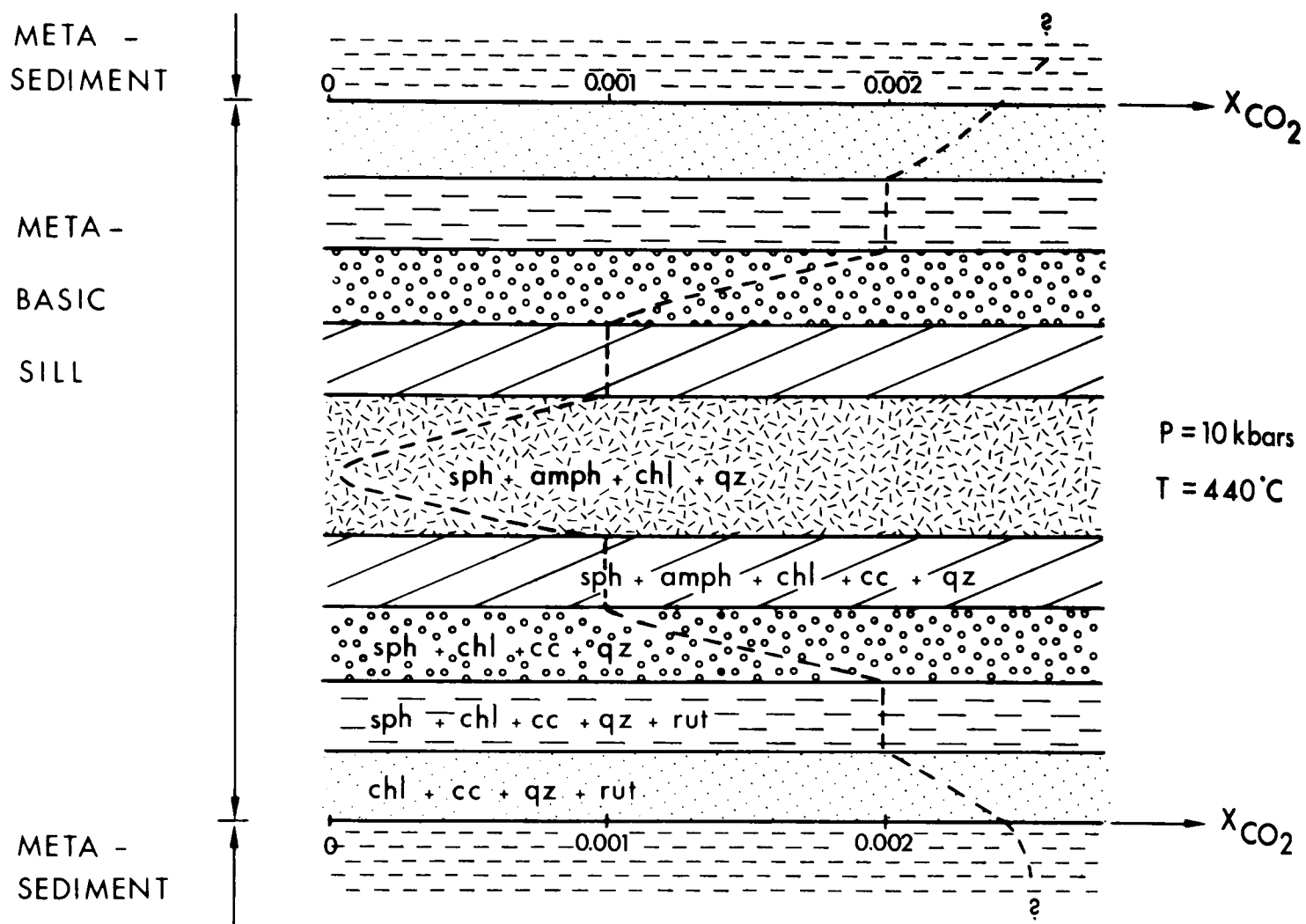


FIG. 5. Idealized schematic cross-section of metabasic sill in greenschist-facies showing distribution of type I, type II and type III metabasic assemblages as defined in text. Approximate variation of fluid composition (X_{CO_2}) across sill is shown by dashed line, based on Fig. 4 and model temperature of 440°C.

invariably represent zones of incomplete reaction of unbuffered type I assemblages to unbuffered type III assemblages (e.g. Fig. 5). Buffering of fluid phase composition in these assemblages does *not* imply absence of mass transport of the fluid phase.

(4) A CO_2 -bearing hydrous fluid of approximate composition $X_{CO_2} \geq 0.010$ (at 440°C), generated externally to metabasic sills in the greenschist-facies, actively infiltrated sills where penetrative deformation processes permitted (Fig. 7A). In the absence of penetrative deformation, however, intergranular diffusion by itself was ineffective except over very short distances of the order of centimetres at the most, as indicated by the dominance of type I relative to type II assemblages in massive, undeformed meta-dolerites. Infiltration accompanied by pervasive reaction occurred on the scale of at least tens of metres where enhanced by penetrative deformation. Infiltrating hydrous fluid may have moved into sills along hydraulic fractures opened perpendicular to the direction of minimum compressive stress, or alternatively diminution of grain size by deformation may have made grain-boundary diffusion an effective process.

(5) The f_{O_2} of the infiltrating fluid, as inferred from the compositions of coexisting magnetite and ilmenite in a type III metabasic assemblage, was near 10^{-21} bars (Powell & Powell 1977).

(6) Type III metabasites (e.g. Fig. 5) commonly contain up to 5–6 wt. % CO_2 , whose precipitation as calcite from an infiltrating aqueous fluid with $X_{CO_2} \approx 0.003$ to 0.01 (e.g. Fig. 4) requires very large cumulative or time-averaged fluid/rock ratios. Preliminary calculations suggest that these were in the range 6:1 to 20:1 or higher (cf. Rumble *et al.* 1982; Ferry 1983).

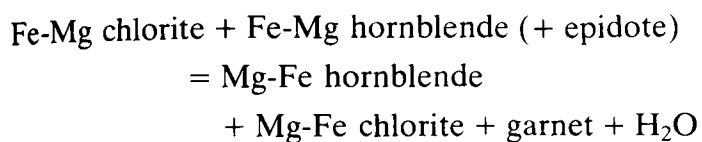
(7) Incomplete reaction of type I assemblages to type III, permitting preservation of type II buffering assemblages and freezing-in of X_{CO_2} gradients, may be a consequence of the cessation of the deformation-enhanced infiltration mechanism before completion of reaction.

Epidote-amphibolite facies

Typical metabasic assemblages in the epidote-amphibolite facies (garnet zone) in Knapdale, which

have been described by Graham (1974) and Harte & Graham (1975), are act + chl + ab + ep + qz + sph ± bi ± mu in more Mg-rich rock compositions, and hbl + ab + ep + qz + sph + bi ± gt ± chl in more Fe-rich rock compositions. Hornblendes are blue-green subcalcic pargasitic hornblendes with up to 16 wt% Al₂O₃ (Graham 1974 and unpubl. data) and actinolites are more aluminous than in the greenschist facies. Sphene is ubiquitous, and an important characteristic of all garnet zone metabasic assemblages in Knapdale is the absence of primary carbonate. The garnet isograd in metabasic rocks (Fig. 2) is equally an isograd delineating the disappearance of carbonate in metabasic rocks.

The garnet isograd reaction is strongly dependent on bulk-rock Fe/Mg, and the incoming of garnet in amphibolites (Fig. 2) corresponds to a transition from a zone of *relatively* low Fe/Mg metabasites to one of Fe-rich metabasites. The reaction may be represented in AFM-projection by the movement of the three phase triangle gt-hbl-chl towards more Mg-rich compositions (Harte & Graham 1975), and may be written as:



The significant increase in alumina-content of amphiboles in the epidote-amphibolite facies (Graham 1974), combined with the garnet-isograd reaction, results in a large decrease in modal chlorite in metabasic assemblages, and its disappearance in some Fe-rich garnet amphibolites. Type I metabasic assemblages in the greenschist facies typically have 3–4 wt% H₂O compared to 1–2 wt% H₂O for garnet-zone amphibolites.

The epidote-amphibolite facies (garnet-zone) in Knapdale is, therefore, a zone of major, regional dehydration of metabasic rocks. The elimination of carbonate from all metabasites is a consequence of the flushing of essentially pure water outwards from sill interiors, infiltrating zones of type II and type III assemblages and converting chl + cc ± rut + qz back to amph + ep + sph (reactions (1) and (3)). Generation of large quantities of water should lead to the enhanced permeability of sills and adjacent metasediments, with hydraulic fracturing and extensive infiltration of adjacent metasediments by hydrous fluid.

The increasing aluminium contents of amphiboles from upper greenschist facies metabasites can only be achieved by a decrease in modal chlorite with consequent dehydration, and so it is likely that dehydration of metabasites and infiltration of adjacent metasediments by hydrous fluid may also have occurred, at least locally, in the upper greenschist facies. Evidence for this is discussed below.

Metasedimentary assemblages

Mineral parageneses in Dalradian phyllitic, psammitic, semi-pelitic and calcareous metasediments in the SW Highlands have to date been studied in detail at several localities, including the Tarbert area (locality 1, Fig. 2), the vicinity of the garnet (localities 2 and 3, and the Tayvallich-Crinan area (locality 4, but large tracts of intervening terrain are as yet sparsely sampled.

Greenschist facies

Carbonate-bearing metasediments of various types in the lower greenschist facies are comparable to those in schistose, rutile-bearing type III metabasites, and the typical assemblage is: qz + mu + cc + rut ± chl ± dol-ank ± ab ± tourm. Many slates and phyllites are devoid of carbonate, containing qz + mu + chl + rut + ab ± tourm. In some of these, rutile appears to have replaced rhombs of sphene, although if reaction (3) has occurred, this would require loss of CaCO₃ from the system.

In sedimentary bands intercalated amongst the lower flows of the Tayvallich Volcanics (locality 4, Fig. 2), the assemblage qz + mu + chl + bi + cc + ab + rut + tourm has been found. An adjacent assemblage, and a sample of coarse grit from Crinan, lack biotite but contain sphene.

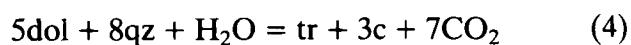
The buffering assemblage qz + mu + dol-ank + bi + chl + cc (reaction (2)) has not been observed in metasediments in the lower greenschist facies. This observation, and the comparability of most metasedimentary assemblages with those of many rutile-bearing type III metabasic assemblages, are consistent with the equilibrium of all these assemblages with a mobile CO₂-bearing hydrous fluid such as the fluid which infiltrated greenschist-facies metabasic sills. The local preservation of biotite- and sphene-bearing metasedimentary assemblages is a consequence of their intercalation amongst less permeable metabasic flows or grits and conglomerates.

Phyllites and semi-pelites containing sphene and biotite become more common in the Ardrishaig Phyllites in the upper greenschist facies (Fig. 2), in assemblages such as: qz + mu + chl + cc + rut ± ep ± ab ± sph ± tourm and qz + mu + bi + chl + cc + rut ± tourm. Carbonate-free phyllites with qz + mu + chl + rut persist upgrade throughout the greenschist facies but dolomite-ankerite bearing assemblages have not to date been positively identified in prograde micaceous metasediments outside the Tayvallich area.

An unbuffered assemblage containing mu + dol-ank + qz + chl + cc will, on heating, remain in equilibrium with a fluid of constant X_{CO₂} (Fig. 4) until it encounters reaction (2), at which point biotite will form. Further heating generates more biotite, together with a fluid of CO₂:H₂O = 2:1 with increase of X_{CO₂}.

until dolomite or white mica are lost. Further heating takes place at constant X_{CO_2} in the stability field of biotite + chlorite + calcite. If such buffering has occurred in greenschist facies metasediments in Knapdale, the appropriate assemblages remain to be identified. The disappearance of dolomite-ankerite and common occurrence of biotite + chlorite + calcite in the upper greenschist facies require either that buffering of fluid composition occurred over a small temperature range if at all, or that widespread removal of dolomite-ankerite and generation of biotite was a result of infiltration by a mobile, water-rich fluid phase, probably from dehydration reactions in adjacent lithologies.

Evidence for the infiltration model includes the identification of large amphibole prisms (now retrogressively altered to dolomite + quartz + chlorite) in thin mica-free carbonate bands at locality 4 (Fig. 2), indicating that the reaction (Fig. 3):



has been exceeded. Further evidence is found at an outcrop of pelitic schist adjacent to a hornblende-bearing metabasic sill at locality 2 (Fig. 2). The schist contains qz + ab + ep + bi + chl + sph ± gt (no rutile or carbonate) and the adjacent metabasic sill contains crudely schistose type I and type II assemblages. Therefore infiltration of water-rich fluid in upper greenschist facies metasediments has occurred, at least locally, probably as a result of dehydration in metabasic sills associated with reduction in modal chlorite and production of increasingly aluminous amphiboles, as discussed above.

A corollary to this section is that the assignment of most of the greenschist facies of the SW Highlands (Elles & Tilley 1930) to the chlorite zone is probably incorrect. Temperatures were sufficient for biotite stability throughout Knapdale, but the high activity of CO_2 in the fluid phase in lower greenschist facies metasediments was usually sufficient to prevent the formation of biotite according to reaction (2).

Epidote-amphibolite facies

Garnet zone parageneses have been investigated in detail at localities 1 and 2 (Figs. 2, 6) in Knapdale where a wide range of metasedimentary lithologies including abundant carbonates and calc-mica-schists is in contact with garnetiferous amphibolites. Typical non-calcareous metasediments (phyllites, psammities, mica-schists) have been sampled from various localities throughout the garnet zone, particularly along the coast of Loch Fyne (Fig. 2), and these are described first.

Typical non-calcareous metasedimentary assemblages in the garnet zone contain qz + ab + mu + chl +

rut ± bi ± gt ± cc ± tourm ± ep. Although rutile is ubiquitous, primary calcite is rare, and the assemblage rut + cc + qz is recorded only at two localities on the coast of Loch Fyne (Fig. 2). Although it is likely that rutile has replaced primary sphene in some non-calcareous metasediments, the absence of sphene may simply be the result of very Ca-poor rock compositions, and in these assemblages the composition of the equilibrium fluid phase is not well constrained.

The instability of the assemblage mu + dol-ank + qz (except as a retrograde assemblage at locality 1) relative to bi + cc + chl at some garnet zone localities sets very approximate upper limits to X_{CO_2} in the fluid phase of about 0.07 to 0.10 at garnet-zone temperatures (Fig. 6). Assemblages capable of buffering fluid composition are absent in non-calcareous metasediments.

Mineral assemblages in calcareous metasediments in the garnet zone have been studied in a representative section at locality 1 (Figs. 2, 6) at South Bay, Barmore, where the Loch Tay Limestone crops out on the coast of Loch Fyne near the axis of the secondary Tarbert monoform (Figs. 1, 2). Lithologies comprise carbonates, calc-mica-schists, metabasic garnet amphibolites, albite-porphyroblast schists, garnet mica schists and psammities. Mineral assemblages in calcareous metasediments at South Bay fall into two distinct groups.

(i) *High-temperature hydrous assemblages.* These are characterized by the absence of chlorite (except as secondary alternation after amphibole and biotite) and of dolomite-ankerite, and by the occurrence of grossular, clinozoisite, diopside, K-feldspar, amphibole, biotite, white mica and sphene. (Comparable assemblages occur in carbonates adjacent to garnet amphibolite at locality 2 (Fig. 2)). These assemblages occur in close proximity to garnet amphibolites, and may be further subdivided according to their T- X_{CO_2} phase relations (Figs. 3, 4, 7).

Extremely H₂O-rich unbuffered assemblages (e.g. 80, Fig. 6) contain gr + cc + qz + sph ± di ± ksp ± hy'gr, and occur in K-poor carbonate bands. White-mica and biotite are absent, and diopside and K-feldspar are very minor in amount and may be so fine-grained as to be detectable only by microprobe EDS scanning. Garnets are close to pure grossular in composition, K-feldspar contains up to 2.5 mol% albite, and clinopyroxenes lie close to the diopside-hedenbergite join (Table 1). The assemblages have equilibrated with a fluid of virtually pure water composition (<0.4 mol% CO_2 at 530°C; Fig. 4), as determined by the stability of grossular. Hydrogrossular (hy'gr) occurs as tiny elongate prisms (a most unusual habit for garnet) in the groundmass of some grossular-bearing, clinozoisite-free carbonates. Hsu (1980) showed experimentally that the maximum temperature stability of hydrogrossular is about 420°C

SHORE SECTION, SOUTH BAY, BARMORE

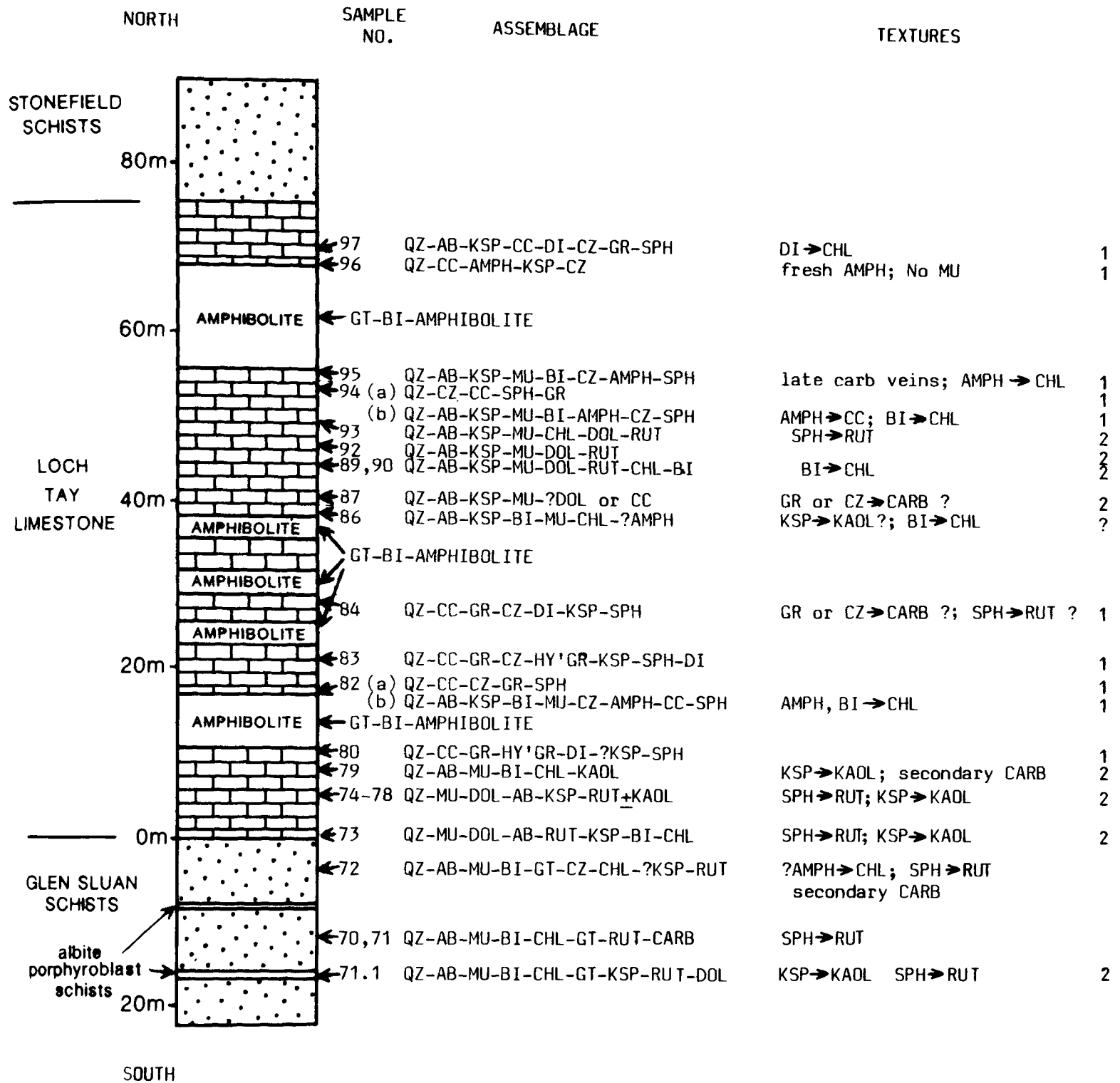


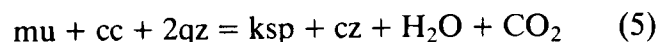
FIG. 6. Sketch section through Loch Tay Limestone and adjacent lithologies at South Bay, Barmore (near Tarbert) (locality 1, Fig. 2), indicating distribution of mineral assemblages identified in a detailed petrographic study. Mineral abbreviations as listed in text. Assemblages are the inferred primary assemblages based on observed mineralogy and textural evidence (for example, amph is often altered to chl but its former presence is readily identified on textural grounds). 1 = high-temperature (epidote-amphibolite facies) hydrous assemblages. 2 = low temperature (greenschist-facies) retrograde dolomite-bearing assemblages.

at 2 kbar, while Schiffman & Liou (1980) grew hydrogrossular metastably at 400°C and 8 kbar. It is likely therefore that hydrogrossular in the South Bay assemblages grew metastably under garnet zone conditions, the usual habit perhaps indicating replacement of earlier prisms of clinozoisite.

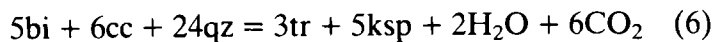
Extremely H₂O-rich buffered assemblages are quite common in carbonates close to garnet amphibolites (e.g. 82, 87, 84, 94, 97, Fig. 6) and are characterized by the coexistence of qz + cc + gr + cz (together with di, ksp and sph). This assemblage buffers the fluid composition to very H₂O-rich values, for example $X_{\text{CO}_2} \approx 0.004$ at 530°C.

H₂O-rich unbuffered assemblages include mica-free assemblages containing qz + ksp ± ab + cc + amph + cz + sph (e.g. 96, Fig. 6), and calcite-free assemblages containing qz + ksp ± ab + mu + cz + amph ± bi + sph (e.g. 94, 95, Fig. 6). In these assemblages grossular and diopside are absent but the stability limits of mu + bi + cc + qz have been exceeded (Figs 3, 4, 7). X_{CO_2} of the fluid in equilibrium with these assemblages (at 530°C) is greater than 0.004 but probably less than approximately 0.005 to 0.007, although the upper limit for real mineral assemblages is strongly dependent on rock Fe/Mg (Figs 4, 7).

H₂O-rich buffered assemblages (e.g. 82, Fig. 6) contain qz + ksp + ab + mu + bi + cz/ep + cc + amph + sph, implying that the fluid phase composition is simultaneously buffered by the reactions:



and



at the model invariant point [chl, dol] (Fig. 3). Amphibole and biotite are frequently extensively altered to chlorite. The effect of additional components in real mineral assemblages is to shift reactions (5) and (6) to more H₂O-rich compositions and to move the invariant point [chl, dol] to lower T and X_{CO_2} (Fig. 4). Although there is some uncertainty regarding the equilibrium amphibole and K-feldspar compositions in assemblage 77-40 (Table 1), whose mineral analyses have been used to calculate equilibria (5) and (6) in Fig. 4, the invariant point [chl, dol] for real mineral compositions in Fig. 4 lies (perhaps fortuitously!) at about 510°C, close to the model temperature of about 530°C for the South Bay rocks. The fluid composition for these assemblages is $X_{\text{CO}_2} \approx 0.005$ (Fig. 4).

It is clear from Fig. 6 that a range of high-temperature hydrous mineral assemblages, in equilibrium with very water-rich fluids of nonetheless variable CO₂ content, coexisted in close proximity to each other on a scale of centimetres or metres, or even on the scale of a thin section, in calcareous rocks at the South Bay locality. Only some of these assemblages

buffered the fluid composition. All these assemblages lie within centimetres or metres of sheets of garnet amphibolite. As in the case of type II greenschist-facies metabasite assemblages, the buffered assemblages do not imply absence of mass transport of the fluid phase. All these assemblages have been infiltrated by the same water-rich fluid, probably nearly pure water, generated by the dehydration reactions which led to growth of garnet and pargasitic hornblende in the adjacent garnet amphibolites and to the elimination of carbonate from all epidote-amphibolite facies metabasites.

Identification of comparable high-temperature hydrous calcareous assemblages at locality 2 (Fig. 2), together with the regional disappearance of carbonate in metabasic rocks, suggests that dehydration reactions in metabasic rocks in Knapdale in the vicinity of the garnet isograd provided the source of water for a regional water-infiltration event affecting metabasics and metasediments. However, mineralogical evidence for this event may very likely be confined to calcareous metasediments, as the potential for mineralogical reaction was absent in non-calcareous psammites and mica-schists.

(ii) *Low-temperature dolomitic assemblages.* The second group of calcareous assemblages (carbonates and calc-mica-schists) in the Loch Tay Limestones and related lithologies at locality 1 is quite distinct from the high-temperature hydrous assemblages, and occurs in zones or bands separated from garnet amphibolite sheets by zones of high-temperature hydrous assemblages (Fig. 6). Typical assemblages contain qz + mu + dol-ank + ksp + rut ± chl ± bi ± ab. Kaolinite is widespread and may in some instances be primary, although it clearly replaced K-feldspar or white mica in some rocks. The characteristic mode of occurrence of chlorite is as large porphyroblasts. K-feldspar is nearly always pure and lacking in Na, and frequently occurs as rims and overgrowths on albite grains. White micas usually have significantly lower celadonite contents than those in prograde, hydrous assemblages (Table 1).

The evidence for the low temperature of crystallization of these assemblages is the stable coexistence of ksp + chl + mu ± bi, which is characteristic of low-temperature greenschist-facies conditions as determined by the reaction:



(e.g. Figs 3, 7; see also Mather 1970; Hoschek 1973, 1980). Observed assemblages suggest that crystallization occurred at or below the temperature of this equilibrium. The absence of calcite and coexistence of mu + dol-ank + qz + ksp allows us to set lower limiting values of X_{CO_2} in the equilibrium fluid, as indicated in Fig. 7.

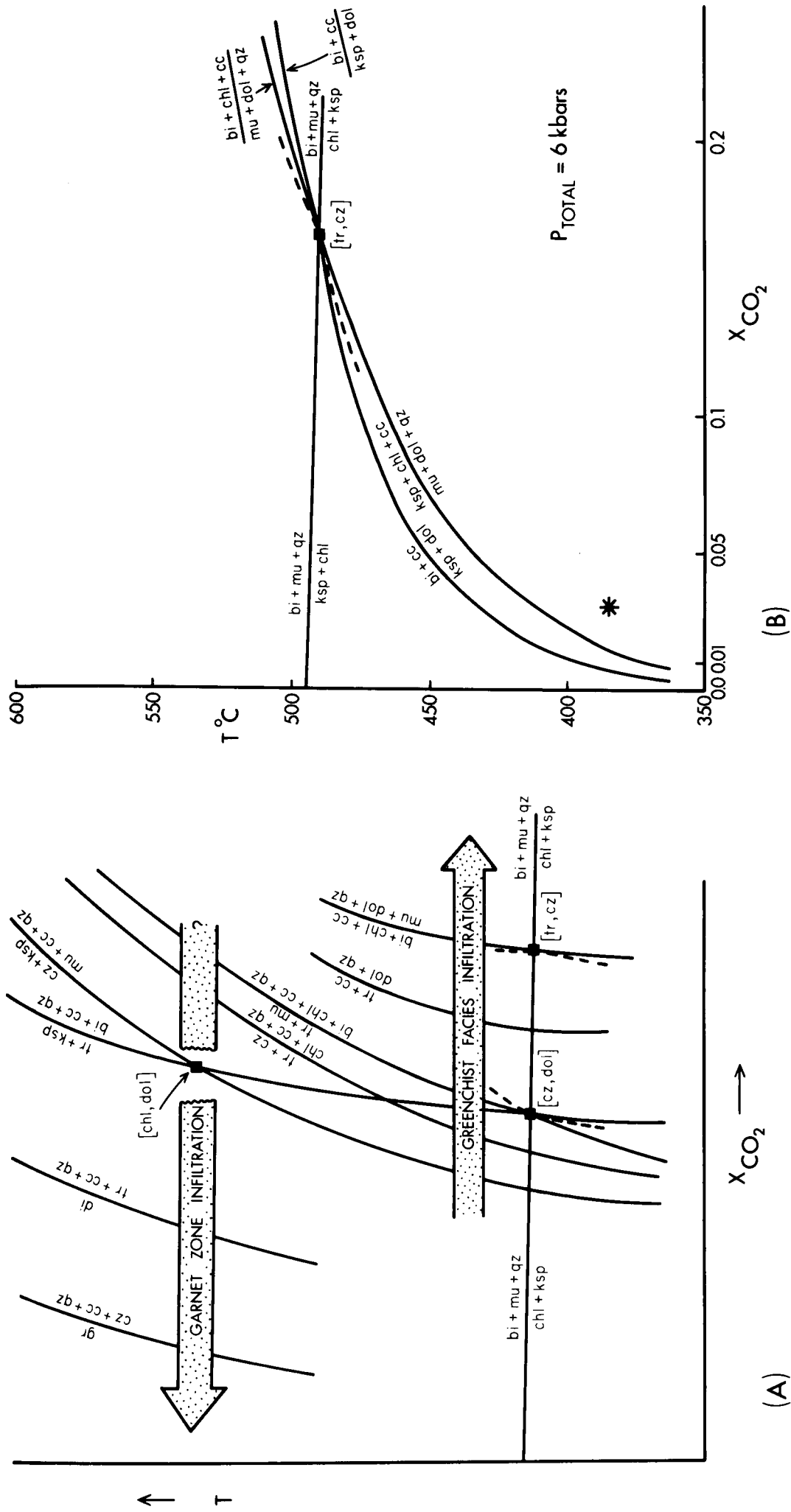


FIG. 7. Sketches of bounding T-X_{CO2} conditions for (A) prograde greenschist-facies assemblages in metabasic sills and adjacent metasediments (e.g. Fig. 5) and high-temperature hydrous assemblages (e.g. Fig. 6), and (B) low-temperature retrograde dolomite-bearing assemblages at locality 1 (Fig. 2) (e.g. Fig. 6). Prograde greenschist-facies assemblages in sills and metasediments and high-temperature hydrous assemblages define paths of increasing X_{CO2} and X_{H2O} respectively during fluid infiltration, as shown by shaded arrows. Reactions are in order observed in real assemblages (Fig. 4; cf. Fig. 3), so that reaction $tr + 3cc + 2qz = 5di + H_2O + 3CO_2$ lies to the H₂O-rich side of reactions (5) and (6). A is schematic, while B is calculated for real mineral assemblages and reactions around [tr, cz] at P_{total} = 6 kbar (appropriate to estimated conditions of low-temperature retrograde event) using mineral compositional data for assemblages 71-1 (Table 1) and activities for solid phases formulated in Table 2 in order to calculate limiting T-X_{CO2} conditions of retrograde fluid infiltration (in stability field shown by dashed lines are metastable in pure KCMASH-CO₂ system).

The very different $T-X_{CO_2}$ conditions of crystallization of the low temperature dolomite-bearing assemblages from the immediately adjacent high-temperature hydrous assemblages and garnet amphibolites within the same outcrop poses a considerable problem, unless the former assemblages represent zones of secondary, retrograde metamorphism and recrystallization of primary high-temperature hydrous calcareous rocks. There is textural evidence that this is the case. Small, low-birefringent, high relief grains of grossular or clinozoisite have been partly replaced by carbonate (assemblage 87, Fig. 6) and large rhombs of sphene have been replaced by rutile + dolomite in several assemblages. Occasionally, fresh, unaltered sphene is preserved as inclusions in quartz grains, and in one assemblage a relict high-temperature K-feldspar grain with ~20 mol% albite has been analysed.

We therefore conclude that at least a proportion, and probably all, of the calcareous rocks in the Loch Tay Limestones were originally high-temperature hydrous assemblages, as described above, which have been infiltrated over a range of *at least* tens of metres by water from dehydration reactions in metabasites. Subsequently, these calcareous rocks were re-infiltrated by a flux of hydrous but CO_2 -bearing fluid focused along broad zones or channelways in the high-temperature hydrous carbonate and calc-mica schist assemblages. The composition of this retrograde fluid was 'externally' controlled such that none of the low-temperature dolomite-bearing assemblages buffered the fluid composition. The timing and $T-X_{CO_2}$ conditions of this major retrograde event are discussed in more detail below. Some high-temperature hydrous assemblages experienced minor alteration, probably during this infiltration event, including alteration of sphene to rutile, and replacement of amphibole and biotite by chlorite and carbonate.

(iii) *Albite-porphyroblast schists*. In close proximity to the Loch Tay Limestones at locality 1, thin bands and lenses of conspicuous albite-porphyroblast schist up to 10–20 cm in thickness occur in association with garnetiferous psammites and mica schists. Albite porphyroblasts up to 2–3 mm or more in diameter are set in a fine-grained micaceous matrix in which secondary strain-slip crenulations or cleavages, associated with the Tarbert Monoform deformation are prominently developed. In thin section, the albite porphyroblasts attain their maximum size in micaceous bands. Inclusion trails of elongate quartz grains and specks of opaques are commonly crenulated, but the porphyroblasts are subsequently rotated relative to each other. We conclude that the albites grew during the later stages of the secondary Tarbert Monoform deformation event.

The dominant mineral assemblage of these schists is $qz + ab + mu + chl + ksp + gt + rut \pm bi \pm dol-ank \pm kaol \pm tourm$. Minerals preserved as inclusions

in albite porphyroblasts include garnet, celadonite-rich white mica, biotite, chlorite and sphene, the latter phase in large rhombs now replaced by rutile \pm dolomite-ankerite. Garnet inclusions in albites are euhedral and unaltered, while garnets in the micaceous matrix are typically partially or completely altered to chlorite. Dolomite-ankerite is rare and is restricted to sites of alteration of sphene to rutile. Na-free K-feldspar (Table 1) forms conspicuous rims of varying width around albite porphyroblasts, but only where albites are in contact with micaceous matrix, and the K-feldspar may in turn be rimmed or replaced by kaolinite. Thus K-feldspar growth appears to post-date albite growth, while kaolinite growth post-dates K-feldspar.

In micaceous schists where secondary strain-slip fabrics are most strongly developed, biotite is absent, garnet is largely altered to chlorite, K-feldspar rims are most extensively developed and rutile occurs in elongate rods rather than pseudomorphs after sphene.

We conclude that the albite porphyroblast schists originally crystallized as mica-rich garnet-mica-schists with the primary assemblage $qz + ab + gt + bi \pm chl + sph$. Subsequent recrystallization to the secondary assemblage $qz + ab + ksp + chl + rut \pm dol-ank \pm bi \pm kaol$ occurred at or below the temperature of reaction (7), under $T-X_{CO_2}$ conditions equivalent to those of crystallization of the low-temperature dolomite-bearing calcareous assemblages in the nearby Loch Tay Limestone (Figs. 6 & 7), and in response to infiltration of the same CO_2 -bearing fluid. This fluid/rock interaction is then associated in space and time with the secondary Tarbert Monoform deformation, and the deformation may be associated with the infiltration as cause and effect.

If biotite is assumed to be stable during this event, an approximate upper temperature limit and lower X_{CO_2} limit may be calculated using real mineral compositions in Table 1, and assuming hypothetical calcite of pure $CaCO_3$ composition. Calculations are based on reaction (7) and the reaction $mu + 5dol + 3qz + 3H_2O = chl + ksp + 5cc + 5CO_2$ (Fig. 7). A model upper pressure limit of 6 kbar was determined, as described earlier, from the celadonite content of white mica in equilibrium with biotite and chlorite (Powell & Evans 1983; Graham & Greig, unpubl. data) (Figs. 7 & 9). The calculated temperature of about 495°C (Fig. 5) is unrealistically high for the lower greenschist-facies temperatures at which this reaction is thought to occur (Mather 1970; Hoschek 1973, 1980), and a temperature between 350 and 400°C seems more realistic. Temperature uncertainties arise from inadequacies in the thermodynamic data set as discussed earlier. The temperature and pressure of reaction (7) are *upper* limits for the retrograde infiltration event as the primary status of biotite is open to question in these assemblages.

The calculated lower limit for the CO_2 content of

the equilibrium retrograde fluid phase is $X_{CO_2} \approx 0.01-0.02$ at 350–400°C (Fig. 7). These limiting X_{CO_2} conditions are very approximate, but indicate that the retrograde fluid of 'externally' controlled composition which infiltrated the garnet zone rocks along the axis of the secondary Tarbert Monoform may have been dominantly hydrous and need not have contained significantly greater amounts of CO₂ in solution than the prograde infiltrating hydrous fluids which controlled greenschist- and epidote-amphibolite-facies assemblages. The origin of this fluid is uncertain; it may be derived from dehydration and decarbonation reactions proceeding at much deeper levels in the metamorphic complex.

If kaolinite was a stable constituent of the retrograde assemblages, then biotite, like garnet, is probably a relict high temperature phase, since the maximum temperature of kaolinite stability at 6 kbar is 360–380°C (Thompson 1970; Perkins *et al.* 1979; Graham, unpubl. data). However, textural evidence indicates that much kaolinite growth post-dated crystallization of K-feldspar and celadonite-poor white mica.

Origins of CO₂ in the fluid phase during greenschist-facies metamorphism: stable isotope evidence

Carbonates, essentially calcites, have been isotopically analysed from the metabasites and their country rocks as part of a more general hydrogen, carbon and oxygen isotopic study of exchange processes during regional metamorphism (Turi *et al.* 1973). Country rock carbonates are of two principal types: (1) limestone formations of the Tayvallich and Loch Tay limestones (Fig. 1) of which some are dolomitic, and (2) calcite-bearing ($\leq 20\%$ calcite) phyllites which, in general, were sampled from within a few centimetres of metabasite sills. Calcites analysed from the metabasites constitute up to 21% of assemblages which were collected from the 20–30 cm wide marginal contact zones (Fig. 5).

Carbon dioxide for isotopic analysis was extracted from carbonate-bearing whole-rock samples with 100% H₃PO₄ at 25°C. The corrected carbon and oxygen isotopic data are given in the conventional δ notation in per mil relative to the PDB and SMOW standards respectively. The carbon isotope results which are of principal concern here are presented on Fig. 8 in such a way that data for carbonates from metabasites and their immediate country rocks can be readily compared. The measured carbonate yields in weight % are given in parentheses.

The carbonate isotope data ($\delta^{13}C$) fall into three

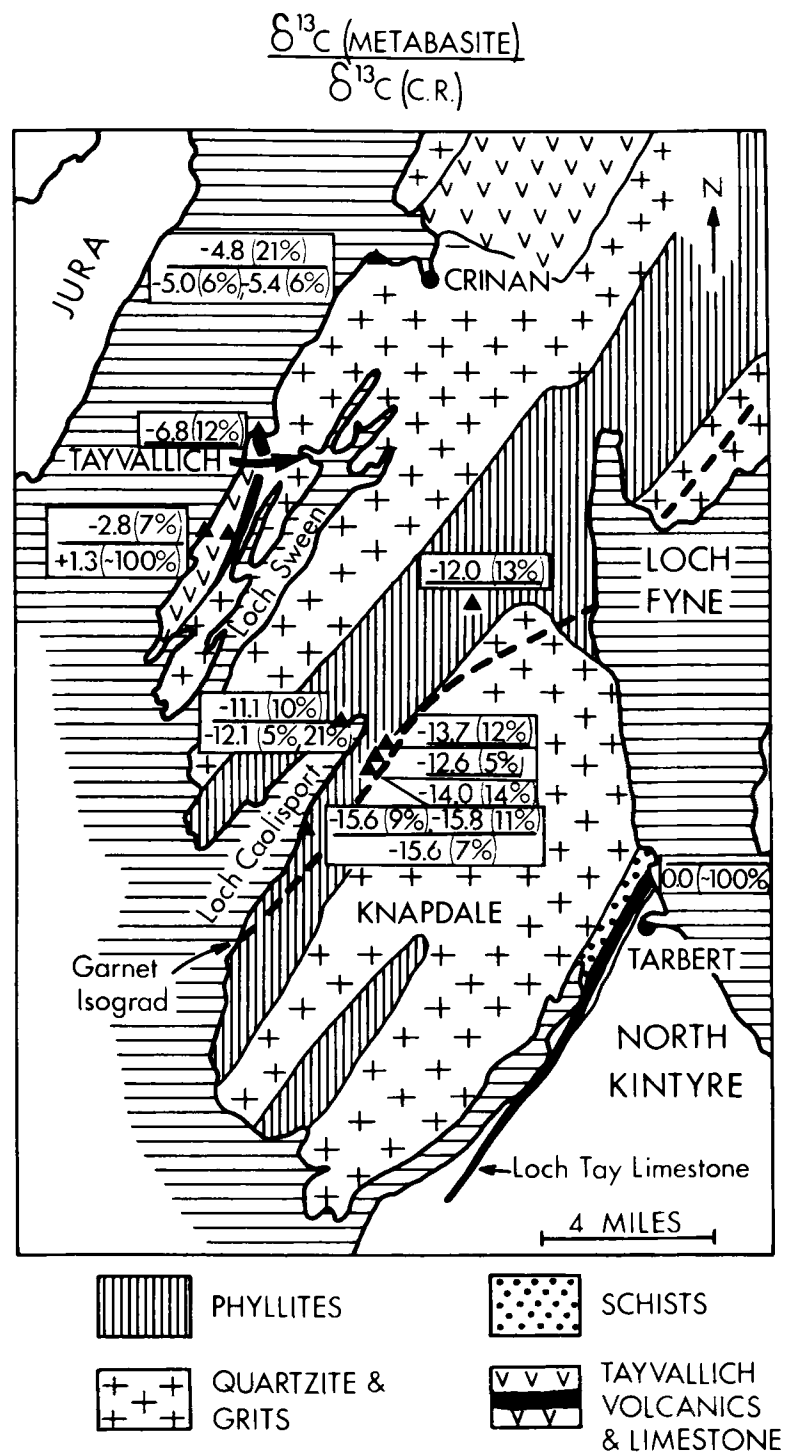


FIG. 8. Map of Knapdale showing carbon isotope data for carbonates from metabasites and adjacent country rocks ($\delta^{13}C$ in ‰ relative to PDB standard). For each locality carbonate $\delta^{13}C$ values for metabasites appear as 'numerator' values and $\delta^{13}C$ for country rocks (CR) appear as 'denominator' values. Measured carbonate yields in wt % appear in parentheses for each sample.

groups related to the character of the country rocks:

	Sills	Country rocks
Tayvallich Volcanics and Limestones	-2.8	+1.3 to -2.0
Crinan grits and quartzites	-4.8 to -6.8	
Phyllites	-11.1 to -15.6	-12.0 to -15.6

Thus, where carbonates occur both in the country rocks and metabasic sills, the carbon isotope compositions are very similar, but they vary from one host rock type to another.

The oxygen isotope values for carbonates are in the range +10.5 to +17‰, with the carbonates heavier than +15‰ coming from limestones intercalated with the Tayvallich volcanics. However, all of these values are 7–14‰ depleted in ^{18}O relative to diagenetically altered limestones and many low grade regionally metamorphosed limestones (Sheppard & Schwarcz 1970). Such values indicate isotope exchange with a volumetrically important lower- ^{18}O reservoir. The carbonate $\delta^{18}\text{O}$ values were thus externally buffered.

For the massive Tayvallich and Loch Tay Limestone either a lower- ^{18}O fluid was flushed through where fluid/rock ratios were large (such as the hydrous fluid which infiltrated metabasic sills), or a fluid phase, which need have been no more than a trace constituent, enabled exchange to take place between the limestones and the external lower- ^{18}O rock reservoir. Independent evidence from mineral assemblages cited elsewhere in this paper indicates very large time-averaged fluid/rock ratios of infiltrating fluids. An essentially aqueous fluid with no buffer capacity for carbon is also consistent with the observation that the $\delta^{13}\text{C}$ values of both the Tayvallich and Loch Tay limestones are comparable to those of sedimentary carbonates.

Internal buffering of $\delta^{13}\text{C}$ in the limestones contrasts with external buffering of $\delta^{18}\text{O}$. Contrasts in the scale of oxygen and carbon isotope exchange might be a general consequence of the infiltration of aqueous (i.e. oxygen-rich, carbon-poor) fluids with high time-averaged fluid/rock ratios during regional metamorphism. The scale of oxygen isotope exchange need not have been more than metric for two reasons: (1) the $\delta^{18}\text{O}$ values of +5 to +10‰ of the metabasites are low relative to sedimentary carbonate values, and (2) psammites and pelites have carbonate-free values of +9 to +16‰, values typical of such sedimentary rocks (Turi *et al.* 1973). For carbon isotopes, the similarity between the ratios for the metabasites and their country rocks must reflect a close approach to carbon isotope exchange equilibrium across the contact zones on at least a decimetric to metric scale. For the ^{13}C -rich Tayvallich Volcanics group, compositions within the metabasites are largely controlled by the Tayvallich Limestone values. The combined carbon and oxygen isotope results imply that communication occurred between different rock units but that the scale of isotope exchange may have been dominantly local (hectametric) rather than regional (kilometric).

Samples from the phyllites have $\delta^{13}\text{C}$ values which are markedly depleted relative to normal sedimentary carbonate values. These low- ^{13}C carbonates are interpreted to have derived a major part of their carbon

from an organic source which was formerly present in the phyllites. Unmetamorphosed residual organic matter typically has $\delta^{13}\text{C}$ values between -15 and -30‰ (e.g. Schwarcz 1969) and reduced carbon in phyllites from Islay (SW Highlands) has $\delta^{13}\text{C} = -17$ to -18‰ (Graham & R. S. Harmon, unpubl. data). Metamorphism of such organic matter in the presence of water can generate complex fluids, although CO_2 and CH_4 are commonly the dominant carbon-bearing species. The absence of graphite in assemblages in this study indicates that H_2O and CO_2 were overwhelmingly the dominant fluid species.

Similarly, ^{13}C -depleted carbonate could possibly be generated through decarbonation of sedimentary carbonates with Rayleigh-type distillation, since the CO_2 lost from the system during decarbonation is enriched in ^{13}C by about 2 to 3‰ relative to the residual carbonate over a wide range of metamorphic temperatures. The observed $\delta^{13}\text{C}$ value of -12 to -16‰ would require substantially greater than 95% decarbonation of carbonates which initially had sedimentary values. This mechanism is not considered responsible for the carbonate values in the phyllites, since with the possible exception of reaction (2), no major decarbonation reactions have been identified in greenschist-facies metasediments. Deposition of carbonates from CO_2 released from underlying granulite facies rocks is another possibility but at present there are too few isotopic analyses of such fluids (e.g. Pineau *et al.* 1981) to assess this hypothesis. Such CO_2 may also have been derived from an organic source.

Outside the limestone units the important role of oxidation-reduction reactions and dominant organic carbon sources, with possible variable contributions from sedimentary carbonates, are emphasized here because the isotopic data are consistent with this interpretation.

The presence of up to 15% carbonates both in the outer zones of the metabasite sills (Fig. 5) and the adjacent phyllites attests to the major mass transfer of carbon, at least on a local scale, and to the important role of the infiltrating fluid phase in this mass transfer. The influence of the nature of the country rocks—source of carbon dominantly in the form of (now oxidized) carbonaceous material in the phyllites or limestone in the volcanic sequence—on the carbon isotope composition of the metacarbonates is also demonstrated.

Discussion and conclusions

Fluid compositions

We have shown firstly that the presence of calcite and dolomite-ankerite carbonates in metabasic rocks and calcareous metasediments under the high-pressure-low-temperature conditions experienced by the Dalradian rocks of the SW Scottish Highlands does not

require the presence of significant proportions of CO₂ in the metamorphic fluid phase. Although reactions (1)–(6), which many calcareous and metabasic rocks have undergone at some stage during prograde greenschist and epidote-amphibolite facies metamorphism, all produce CO₂-rich fluids ($X_{\text{CO}_2} \geq 0.5$), the entire prograde metamorphic evolution occurred in the presence of exceedingly water-rich fluids which had composition X_{CO_2} less than (and usually *much* less than) ~ 0.06 .

Buffering, infiltration and fluid/rock ratios

Mineral assemblages containing both reactants and products of reactions such as (1)–(6), and which are therefore capable of buffering the pore fluid composition during metamorphism, are scarce in the area of study. Where 'buffered' assemblages do occur, they lie in zones adjacent to 'unbuffered' assemblages in situations where gradients of fluid composition (X_{CO_2}) have been preserved. Where internal buffering of pore fluid composition by mineral assemblages has occurred, we have shown that these occurrences do not imply lack of mass transport of the fluid species, but rather represent zones of pervasive reaction during infiltration of highly mobile hydrous fluids which are out of chemical equilibrium with the rocks through which they moved (Figs. 5–7).

The widespread absence of assemblages capable of buffering fluid composition over a range of temperature during prograde heating would suggest that, with the above exceptions, mineral assemblages have been controlled by fluid composition throughout the Knapdale area. The absence of assemblages containing both reactants and products of reaction (2) is perhaps surprising in this regard. It may be that such assemblages exist over small ranges of metamorphic grade but remain to be found by more detailed sampling, or that evidence of their existence at some stage in the metamorphic history has been destroyed by later infiltrative processes. As Greenwood (1975) emphasized, such small amounts of products may be generated during prograde buffering reactions in internally buffered systems that they remain undetected in rocks until invariant points are reached. In contrast, Ferry (1983) drew attention to the almost universal occurrence of buffering of fluid composition by mineral assemblages, based on the widespread recognition of reactants and products of buffering reactions over a range of metamorphic grade in various studies. The formation of products of isobarically univariant buffering reactions in substantial amounts is dependent on maintaining large fluid/rock ratios, and the maintenance of the buffering process may be viewed as a balance between CO₂-rich fluids generated by the buffering reactions themselves and H₂O-rich fluid being supplied to the reacting system by infiltration (Ferry, *op cit.*).

The capacity of metamorphic rocks to retain fluid, and therefore effectively buffer the composition of the fluid phase by internal-buffering processes alone, is dependent on both the porosities and the tensile strengths of rocks. If tensile strengths are vanishingly small at the pressures and temperatures of metamorphism in the SW Highlands, any internally-generated fluid will be lost along microcracks and only grain-surface monolayers of fluid will be retained (e.g. Walther & Orville 1982). Assuming that porosities of metamorphic rocks at these conditions are very small ($\ll 1\%$), it is likely that internal buffering of fluid composition by high pressure mineral assemblages would be sporadic and difficult to detect.

The evidence of metamorphic assemblages, and textural and field relationships in SW Highlands metabasic and metasedimentary rocks all indicate that metamorphic assemblages were controlled by infiltration of hydrous fluids, which also provided the driving force for a large number of observed metamorphic reactions. By comparison with the review of Ferry (1983), we infer that the absence of prograde buffering of fluid composition may be a consequence of maintaining *very* large time-averaged or cumulative fluid/rock ratios during infiltration. This conclusion has been supported by evidence presented above based on stable isotope studies and on mass balance constraints of precipitation of carbon (as carbonate) in metabasic sills and flows. Results of current quantitative studies of fluid/rock ratios in Knapdale metamorphic rocks will be presented elsewhere, but preliminary calculations outlined above for the CO₂-bearing fluid infiltrating type III metabasites in the greenschist facies indicate volumetric fluid/rock ratios of 6:1 to 20:1 or higher. These ratios are significantly higher than those recognized in other regional metamorphic examples (Rumble *et al.* 1982; Ferry 1983).

Fluid infiltration events in SW Highland rocks

We have distinguished 3 major infiltration events involving hydrous fluids in the SW Highland assemblages. In the greenschist-facies, metabasic sills and flows acted as sinks for CO₂-bearing hydrous fluid, which was actively generated within adjacent metasedimentary source rocks on a regional scale, probably at lower greenschist-facies temperatures. The source of CO₂ in this fluid was the oxidation of organic matter, probably graphite, within metasediments. In the epidote-amphibolite facies, and at least locally in the upper greenschist-facies, metabasic sills acted as a source of water generated by dehydration reactions involving the breakdown of chlorite. The resulting water-rich fluid drove reactions which destroyed carbonate in metabasic rocks on a regional scale and

infiltrated calcareous metasediments to produce hydrous assemblages containing grossular, diopside, clinozoisite, K-feldspar and amphibole. The full extent of this infiltration within the garnet zone remains to be established by further sampling. Finally, calcareous and micaceous metasediments in the epidote-amphibolite facies were, at least locally, infiltrated by CO₂-bearing hydrous fluid at lower greenschist-facies temperatures during uplift and cooling, producing assemblages containing K-feldspar + chlorite + dolomite-ankerite.

Ferry (1983) drew attention to the possibly acid nature of hydrous fluid infiltrating metacarbonate rocks in Maine. Evidence for infiltration of acid fluid during both the greenschist-facies prograde infiltration event and the retrograde infiltration event in the SW Highlands may be provided by textures indicating replacement of sphene by rutile in carbonate-free rocks. Calcium may have been removed in solution during progress of reactions such as (3). The replacement of K-feldspar and white mica by kaolinite during the later stages of the retrograde infiltration event may also be a result of hydrolysis reactions involving infiltrating hydrous fluid.

Pervasive versus focused fluid transport

Infiltration has been recognized only where the infiltrating fluid was out of chemical equilibrium with the rocks through which it passed. Therefore during prograde metamorphism pervasive reaction with the infiltrating fluids only occurred in Ca-rich lithologies, calcareous metasediments and metabasic rocks. Pervasive reaction during the retrograde infiltration event was also possible in micaceous lithologies, according to reaction (7). Other lithologies, such as psammites and non-calcareous mica schists, may also have been infiltrated pervasively, but usually preserve no record of the infiltration event because their mineral assemblages were stable over a range of fluid compositions at the temperatures of infiltration. However, it is also possible that in these 'unreactive' lithologies infiltration occurred by focused flow along discrete channelways (veins or microfractures) by hydraulic fracturing, leaving little or no record of their passage. Evidence for this mechanism could be sought by fluid inclusion or isotopic studies.

Walther & Orville (1982) calculated that progressive metamorphic devolatilization of an average pelite should generate about 5 wt% volatiles (~2.6 wt% of H₂O and ~2.4 wt% of CO₂) which, at 5 kbar and 500°C would occupy about 12 volume % of the rock. Such a hypothetical volumetric fluid/rock ratio is less to very much less than ratios calculated in this study and for other metamorphic terrains (e.g. Rumble *et al.* 1982; Ferry 1983). In order to attain such high ratios from metamorphic fluid generated by devolatilization reactions, it seems likely that

the infiltration of hydrous fluids may be focused through reactive (e.g. carbonate-bearing) lithologies.

Relationship of deformation and fluid transport

Mechanical strength is clearly an important factor in controlling the occurrence of pervasive reaction or discrete fluid transport during infiltration. 'Unreactive' lithologies are also commonly the more structurally competent lithologies, while 'reactive' lithologies containing carbonates are more likely to fail in a ductile manner. Indeed, deformation processes have demonstrably played an integral part in the transport, and possibly also the genesis, of the fluid phase. We have shown that in the absence of penetrative deformation grain-boundary diffusion by itself was not an important mechanism in the infiltration of CO₂-bearing fluid into statically recrystallized metabasic sills in the greenschist facies, and that infiltration occurred on a scale of at least tens of metres when accompanied by penetrative deformation. It is likely that the subsequent preservation of fluid composition gradients in these sills occurred because of cessation of penetrative deformation before reaction was complete.

The separation of cause and effect in the interaction between mechanisms of fluid transport and mechanisms of deformation may not be possible. The generation of large volumes of hydrous fluid may catalyse deformation by hydrolytic weakening processes, while the deformation itself may then control the subsequent infiltration and transport of the fluid. Subsequent loss of excess fluid may then terminate a particular deformation episode.

There is a close spatial and temporal association of the retrograde fluid infiltration event with genesis of the albite-porphyroblast schists and secondary deformation along the axis of the Tarbert Monofom. Albite schists are widely reported throughout the area of the Cowal Antiform, of which the Tarbert Monofom constitutes one component, and it seems likely that this retrograde infiltration event may be of regional significance in this part of the Dalradian, at least locally obscuring and overprinting primary prograde metamorphic mineralogy. The retrograde fluid infiltration is demonstrably not pervasive (Fig. 6), but is focused along zones or channelways which are most likely structurally controlled.

A mechanical mixing model for the origin of CO₂ in greenschist-facies fluids

An origin for CO₂ in the infiltrating hydrous fluid in the greenschist-facies by regional oxidation of graphite (or other organic precursors) is demonstrated by carbon isotope data, but is not well characterized. The nature of this oxidation reaction remains to be established, but one possible process is proposed here.

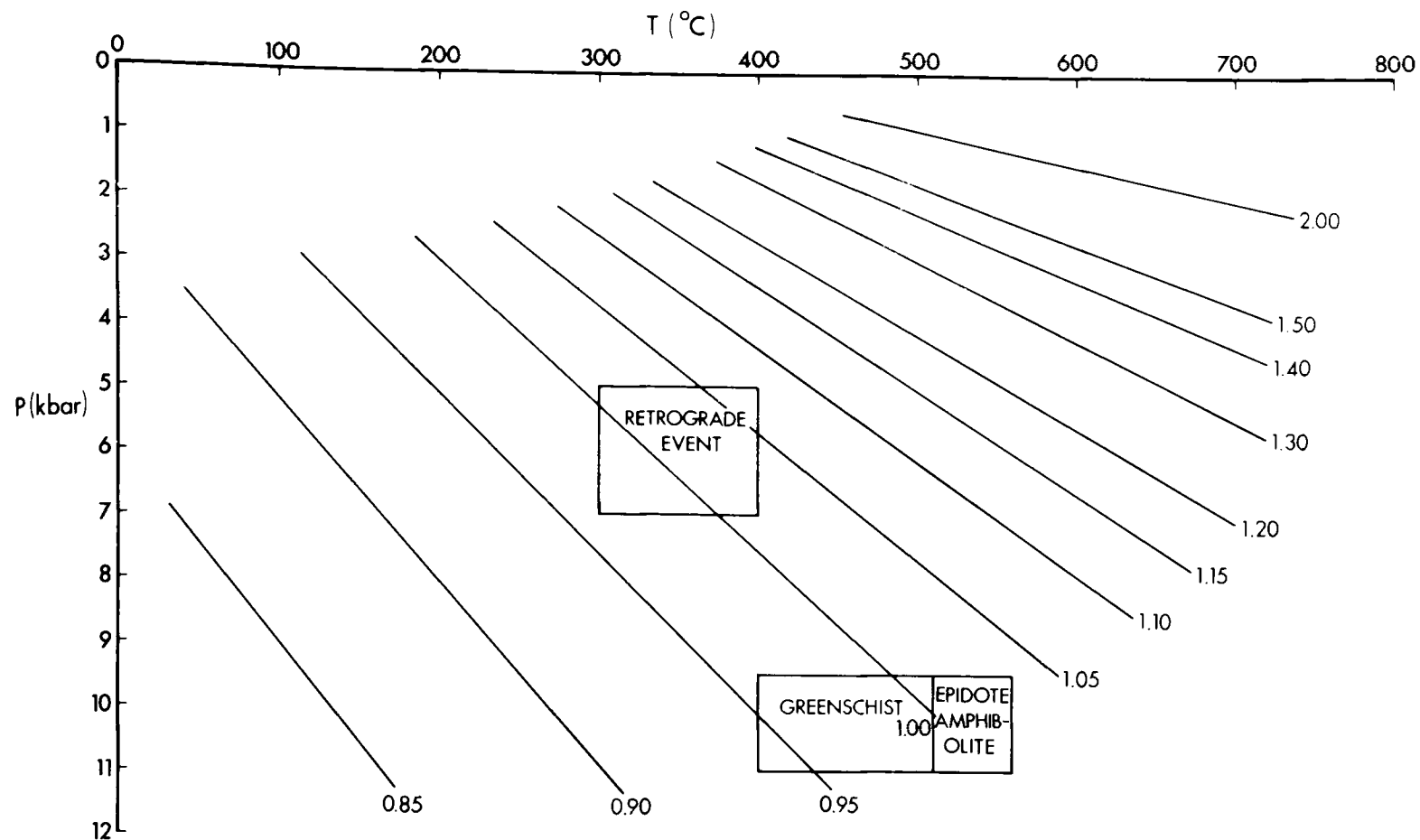


FIG. 9. P-T diagram showing estimated conditions of prograde and retrograde metamorphic crystallization of SW Highland metamorphic rocks. Estimates for retrograde event are probably upper limits calculated on the assumption of biotite stability in some retrograde assemblages (see discussion in text). Contours are for the specific volume of water after Norris & Henley (1976), using thermodynamic data of Burnham *et al.* (1969).

Norris & Henley (1976) pointed out that thermal expansion of water occurs during burial and heating along all geothermal gradients greater than about $12^\circ\text{C}/\text{km}$ (Fig. 9), and that when thermal expansion commences, the possibly vanishingly small tensile strength of the rock will be exceeded and hydraulic fracturing will commence. The Dalradian rocks in the SW Highlands have been metamorphosed at high pressures by deep burial (underneath a thick nappe pile?), and it is likely that during subsequent uplift and heating (e.g. England & Richardson 1977) thermal expansion of the fluid, with accompanying hydraulic fracturing, would commence under approximately lower greenschist-facies P-T conditions (Fig. 9). This process may have led to a general mechanical opening up of the fluid/rock system, which may have promoted mixing of low- f_{O_2} (CH_4 -bearing?) fluids in equilibrium with graphite with higher f_{O_2} hydrous fluids in graphite-free rocks. The estimated f_{O_2} of the fluid in equilibrium with a type III metabasite in the greenschist-facies ($\sim 10^{-21}$ bar) is outside the graphite stability field at the P-T conditions of metamorphism. Thus oxidation of graphite may possibly be explained by mixing of fluids of varying f_{O_2} and X_{CO_2} , and

consequent oxidation of the graphite by the resulting hydrous fluid during regional infiltration. The mechanisms proposed by Norris & Henley (1976) may play an important role in regional infiltration of hydrous fluid during metamorphism.

ACKNOWLEDGMENTS. We thank Giles Droop, John Ferry and Roger Powell for their careful reviews of this paper, and these people and other participants in the 'Fluids in Metamorphism' symposium in Glasgow for much stimulating discussion on fluid processes. We also thank Drs Ferry, Powell, Rumble and Wall, together with David Pattison and Nonie Ray, for accompaniment in the field to see Scottish fluids, and King Canute, in action. C.M.G. thanks Ben Harte and Steve Richardson for guidance during the early stages of this protracted study. K.M.G. acknowledges award of a N.E.R.C. studentship. Microprobe analyses were conducted with assistance of Peter Hill in the Edinburgh Microprobe Unit, which is supported by N.E.R.C. Stable isotope analyses were carried out at S.U.R.R.C., East Kilbride, which is supported by N.E.R.C. and the Scottish Universities. Jim Borthwick is thanked for laboratory assistance with stable isotope analyses, Andy Walker for assistance with computing problems, Mrs D. Baty for draughting figures, and Mrs H. Hooker for typing the manuscript.

References

- ANDERTON, R. 1979. Slopes, submarine fans, and syn-depositional faults: sedimentology of parts of the Middle and Upper Dalradian in the SW Highlands of Scotland. In: HARRIS, A. L., HOLLAND, C. H. & LEAKE, B. E. (eds.). *The Caledonides of the British Isles—Reviewed*. Spec. Publ. geol. Soc. London, **8**, 483–8.
- BEST, N. F. 1978. Mixed volatile equilibria in greenschist facies metabasalts. In: *Progress in Experimental Petrology, Fourth Report*. Natural Environment Research Council Publ. Ser. D, **11**, 159–62.
- BICKLE, M. J. & POWELL, R. 1977. Calcite-dolomite geothermometers for iron-bearing carbonates: the Glockner area of the Tauern Window, Austria. *Contrib. Mineral. Petrol.* **59**, 281–92.
- BURNHAM, C. W., HOLLOWAY, J. R. & DAVIS, N. F. 1969. Thermodynamic properties of water to 1000°C and 10,000 bars. *Spec. Pap. geol. Soc. Am.* **132**.
- ELLES, G. L. & TILLEY, C. E. 1930. Metamorphism in relation to structure in the Scottish Highlands. *Trans. R. Soc. Edinburgh*, **56**, 621–46.
- ENGLAND, P. C. & RICHARDSON, S. W. 1977. The influence of erosion upon the mineral facies of rocks from different metamorphic environments. *J. geol. Soc. London*, **134**, 202–13.
- FERRY, J. M. 1976a. P, T, f_{CO_2} , and $f_{\text{H}_2\text{O}}$ during metamorphism of calcareous sediments in the Waterville–Vassalboro area, South-Central Maine. *Contrib. Mineral. Petrol.* **57**, 119–43.
- 1976b. Metamorphism of calcareous sediments in the Waterville–Vassalboro area, South-Central Maine: mineral reactions and graphical analysis. *Am. J. Sci.* **276**, 841–82.
- 1980. A case study of the amount and distribution of heat and fluid during metamorphism. *Contrib. Mineral. Petrol.* **71**, 373–85.
- 1983. Regional metamorphism of the Vassalboro Formation, South-Central Maine, USA: a case study of the role of fluid in metamorphic petrogenesis. *J. geol. Soc. London*, **140**, 551–76.
- FINGER, L. W. & BURT, D. M. 1972. REACTION, a FORTRAN IV computer program to balance chemical reactions. *Yb. Carnegie Inst. Wash.* **71**, 616–20.
- GRAHAM, C. M. 1973. *Chemical petrology of metamorphosed basic rocks of the Dalradian series, with particular reference to the Knapdale area of Argyll*. Thesis, Ph.D. Univ. of Edinburgh (unpubl.).
- 1974. Metabasite amphiboles of the Scottish Dalradian. *Contrib. Mineral. Petrol.* **47**, 165–85.
- 1976. Petrochemistry and tectonic significance of Dalradian metabasaltic rocks of the SW Scottish Highlands. *J. geol. Soc. London*, **132**, 61–84.
- GRAPES, R. H. & GRAHAM, C. M. 1978. The actinolite-hornblende series in metabasites and the so-called miscibility gap: a review. *Lithos*, **11**, 85–97.
- GREENWOOD, H. J. 1975. Buffering of pore fluids by metamorphic reactions. *Am. J. Sci.* **275**, 573–93.
- HARRIS, A. L. & PITCHER, W. S. 1975. The Dalradian Supergroup. In: HARRIS, A. L., SHACKLETON, R. M., WATSON, J., DOWNIE, C., HARLAND, W. B. & MOORBATH, S. (eds.). *Spec. Rep. geol. Soc. London*, **6**, 52–75.
- HARTE, B. & GRAHAM, C. M. 1975. The graphical analysis of greenschist to amphibolite facies mineral assemblages in metabasites. *J. Petrol.* **16**, 347–70.
- HELGESON, H. C., DELANY, J. M., NESBITT, H. W. & BIRD, D. K. 1978. Summary and critique of the thermodynamic properties of rock forming minerals. *Am. J. Sci.* **278-A**, 1–229.
- HOSCHEK, G. 1973. Zur stabilität metamorpher biotitparagenesen. *Tschermaks Mineral. Petrol. Mitt.* **20**, 48–58.
- 1980. Phase relations of a simplified marly rock system with application to the Western Hohe Tauern (Austria). *Contrib. Mineral. Petrol.* **73**, 53–68.
- HSU, L. C. 1980. Hydration and phase relations of grossular-spessartine garnets at $P_{\text{H}_2\text{O}} = 2$ kb. *Contrib. Mineral. Petrol.* **71**, 407–15.
- JACOBS, G. K. & KERRICK, D. M. 1981a. APL and FORTRAN programs for a new equation of state for H_2O , CO_2 , and their mixtures at supercritical conditions. *Comput. Geosci.* **7**, 131–43.
- & — 1981b. Devolatilization equilibria in H_2O - CO_2 and H_2O - CO_2 -NaCl fluids: an experimental and thermodynamic evaluation at elevated pressures and temperatures. *Am. Mineral.* **66**, 1135–53.
- KERRICK, D. M. 1974. Review of metamorphic mixed-volatile (H_2O - CO_2) equilibria. *Am. Mineral.* **59**, 729–62.
- & JACOBS, G. K. 1981. A modified Redlich-Kwong equation for H_2O , CO_2 and H_2O - CO_2 mixture at elevated pressures and temperatures. *Am. J. Sci.* **281**, 735–67.
- KNILL, J. L. 1960. The tectonic pattern in the Dalradian of the Craginish–Kilmelfort district, Argyllshire. *J. geol. Soc. London*, **115**, 339–64.
- MATHER, J. D. 1970. The biotite isograd and the lower greenschist facies in the Dalradian rocks of Scotland. *J. Petrol.* **11**, 253–75.
- NORRIS, R. J. & HENLEY, R. W. 1976. Dewatering of a metamorphic pile. *Geology*, **4**, 33–6.
- PERKINS, D., ESSENE, E. J., WESTRUM, E. F. & WALL, V. J. 1979. New thermodynamic data for diasporite and their application to the system Al_2O_3 - SiO_2 - H_2O . *Am. Mineral.* **64**, 1080–90.
- PINEAU, F., JAVOY, M., BEHAR, F. & TOURET, J. 1981. La géochimie isotopique du faciès granulite du Bamble (Norvège) et l'origine des fluides carbonés dans la croûte profonde. *Bull. Minéral.* **104**, 630–41.
- POWELL, R. 1978. *Equilibrium thermodynamics in petrology: an introduction*. Harper & Row: London.
- & EVANS, J. 1983. A new geobarometer for the assemblage biotite-muscovite-chlorite-quartz. *Contrib. Mineral. Petrol.* (in press)
- & POWELL, M. 1977. Geothermometry and oxygen barometry using co-existing iron-titanium oxides: a reappraisal. *Mineralog. Mag.* **41**, 257–63.
- ROBERTS, J. L. 1966. Sedimentary affiliations and stratigraphic correlation of the Dalradian rocks in the southwest Highlands of Scotland. *Scott. J. Geol.* **2**, 200–23.
- 1974. The structure of the Dalradian rocks in the southwest Highlands of Scotland. *J. geol. Soc. London*, **130**, 93–124.
- 1977. The Dalradian rocks of Knapdale and North Kintyre. *Scott. J. geol.* **13**, 113–24.
- RUMBLE, D., FERRY, J. M., HOERING, T. C. & BOUCOT, A.

- J. 1982. Fluid flow during metamorphism at the Beaver Brook fossil locality, New Hampshire. *Am. J. Sci.* **282**, 886-919.
- RYE, R. O., SCHUILING, R. D., RYE, D. M. & HANSEN, J. B. H. 1976. Carbon, hydrogen and oxygen isotope studies of the regional metamorphic complex at Naxos, Greece. *Geochim. cosmochim. Acta* **40**, 1031-49.
- SCHIFFMAN, P. & LIOU, J. G. 1980. Synthesis and stability relations of Mg-Al pumpellyite, Ca₄Al₅MgSi₆O₂₁(OH)₇. *J. Petrol.* **21**, 44-74.
- SCHWARCZ, H. P. 1969. The stable isotopes of carbon. In: WEDEPOHL, K. H. (ed.). *Handbook of Geochemistry Vol. III*. Springer Verlag, Berlin.
- SHEPPARD, S. M. F. & SCHWARCZ, H. P. 1970. Fractionation of carbon and oxygen isotopes and magnesium between coexisting metamorphic calcite and dolomite. *Contrib. Mineral. Petrol.* **26**, 161-98.
- THOMPSON, A. B. 1970. A note on the kaolinite-pyrophyllite equilibrium. *Am. J. Sci.* **268**, 454-8.
- TOURET, J. 1977. The significance of fluid inclusions in metamorphic rocks. In: FRASER, D. G. (ed.). *Thermodynamics in Geology*, 203-27. D. Reidel: Dordrecht-Holland.
- TURI, B., GRAHAM, C. M. & SHEPPARD, S. M. F. 1973. Carbon and oxygen isotope studies of the Dalradian metabasic rocks, and the role of pore fluid during regional metamorphism. *Third European Colloquium of Geochronology, Cosmochronology and Isotope Geology, Oxford*. p. 69.
- WALTHER, J. V. & ORVILLE, P. M. 1982. Volatile production and transport in regional metamorphism. *Contrib. Mineral. Petrol.* **79**, 252-7.
- WISEMAN, J. D. H. 1934. The central and south highland epidiorites: a study in progressive metamorphism. *Q. J. geol. Soc. London*, **90**, 354-417.

Received 27 October 1982; revised typescript received 25 February 1983.

COLIN M. GRAHAM & KENNETH M. GREIG, Department of Geology, Edinburgh University, Edinburgh EH9 3JW, Scotland.

SIMON M. F. SHEPPARD, C.N.R.S.-C.R.P.G., B.P. 20, 54501 Vandoeuvre-les-Nancy, France.

BRUNO TURI, Istituto di Geochimica, Universita di Roma, 00100 Rome, Italy.



GREIG, K.M.
Ph.D. 1986

APPENDIX C: PROBE ANALYSES

Mineral analyses from Rock Nos: X1N, X12W, X6NA, X19N, CA62, CA88,
CA74, CA21, CA22 and CA41.

Mineral analysis numbers are coded, in that numbers which end in zero imply that the analyses is from a new grain. Numbers which do not end in zero mean that the analysis is from a different part of the preceding grain. Within any rock, minerals which have the same analysis number are adjacent.

Rock No: X1N

Catalogue No: 66,148

Location: South Bay, Barmore. Limestone B (see Fig 4.7)

Mineral Assemblage: CC-QZ-CZO-BT-AMPH-KSP Code: E

Petrography: no grossular, patchy alteration of amphibole to chlorite, possible amphibole to biotite reaction textures.

Mineral Analyses: 6 clinzoisites, 2 calcites, 3 biotites, 3 kfeldspars, 3 chlorites, 1 amphibole which is mix of amph and biotite.

	EP10		EP30		EP40		EP50	
	wt%	O=13	wt%	O=13	wt%	O=13	wt%	O=13
SiO2	38.29	3.18	38.38	3.19	41.25	3.36	38.81	3.20
TiO2	0.21	0.01	0.11	0.00	0.63	0.03	0.18	0.01
Al2O3	27.09	2.66	27.45	2.69	26.42	2.54	27.59	2.68
FeO	7.19	0.50	6.50	0.45	5.32	0.36	6.02	0.41
MnO	0.06	0.00	0.02	0.00	0.09	0.00	0.00	0.00
MgO	0.05	0.00	0.02	0.00	0.08	0.01	0.07	0.01
CaO	23.47	2.09	23.69	2.11	22.79	1.99	23.82	2.10
Na2O	0.02	0.00	0.01	0.00	0.02	0.00	0.03	0.00
K2O	0.00	0.00	0.00	0.00	0.00	0.00	0.00	0.00
total	96.41	8.47	96.22	8.46	96.64	8.33	96.55	8.44

	EP60		EP90		CC10		CC20	
	wt%	O=13	wt%	O=13	wt%	O=3	wt%	O=3
SiO2	39.57	3.27	38.55	3.19	0.05	0.00	0.10	0.00
TiO2	0.08	0.00	0.05	0.00	0.00	0.00	0.00	0.00
Al2O3	27.33	2.66	28.14	2.75	0.00	0.00	0.00	0.00
FeO	5.75	0.39	4.89	0.34	0.74	0.02	1.54	0.05
MnO	0.02	0.00	0.00	0.00	0.39	0.01	0.45	0.01
MgO	0.04	0.00	0.04	0.00	0.54	0.03	0.75	0.05
CaO	23.17	2.05	24.01	2.13	58.25	2.90	58.99	2.85
Na2O	0.01	0.00	0.03	0.00	0.00	0.00	0.00	0.00
K2O	0.00	0.00	0.00	0.00	0.00	0.00	0.00	0.00
total	96.01	8.40	95.74	8.43	60.20	3.00	62.10	2.99

	BI10		BI20		BI30 (CH6)		KSP10 (CH1)	
	wt%	O=23	wt%	O=23	wt%	O=28	wt%	O=28
SiO2	37.24	5.92	37.26	5.93	37.06	7.19	64.98	10.44
TiO2	1.03	0.12	1.16	0.13	0.99	0.14	0.03	0.00
Al2O3	16.77	3.14	16.57	3.11	16.43	3.76	18.31	3.46
FeO	16.18	2.15	16.28	2.16	16.75	2.72	0.88	0.12
MnO	0.13	0.01	0.13	0.01	0.16	0.02	0.01	0.00
MgO	13.05	3.09	12.95	3.07	13.29	3.84	0.74	0.17
CaO	0.00	0.00	0.02	0.00	0.03	0.00	0.04	0.00
Na2O	0.07	0.02	0.12	0.03	0.07	0.02	0.02	0.00
K2O	8.86	1.80	8.88	1.80	8.63	2.13	15.60	3.19
total	93.72	16.47	93.83	16.51	93.44	19.86	100.7	17.43

	KSP20 (CH2)		KSP30 (CH3)		KSP40 (CH7)		CH40	
	wt%	O=28	wt%	O=28	wt%	O=28	wt%	O=28
SiO2	64.78	10.54	65.56	10.51	57.82	9.74	26.17	5.58
TiO2	0.00	0.00	0.00	0.00	0.24	0.03	0.01	0.00
Al2O3	18.01	3.45	18.39	3.47	18.36	3.64	19.51	4.91
FeO	0.14	0.02	0.46	0.06	4.78	0.67	22.83	4.07
MnO	0.02	0.00	0.04	0.00	0.05	0.00	0.52	0.09
MgO	0.01	0.00	0.13	0.03	2.99	0.75	16.52	5.25
CaO	0.02	0.00	0.01	0.00	0.00	0.00	0.04	0.01
Na2O	0.03	0.01	0.02	0.00	0.04	0.01	0.00	0.00
K2O	16.31	3.38	16.23	3.31	14.31	3.07	0.05	0.01
total	99.36	17.43	100.9	17.42	98.62	17.95	85.69	19.96

	CH50		CH80		AM10	
	wt%	O=28	wt%	O=28	wt%	O=23
SiO2	26.54	5.70	25.50	5.44	37.02	6.05
TiO2	0.01	0.00	0.01	0.00	0.05	0.00
Al2O3	18.57	4.70	20.23	5.09	13.25	2.55
FeO	23.93	4.30	23.50	4.19	15.47	2.11
MnO	0.44	0.08	0.47	0.08	0.01	0.00
MgO	15.99	5.12	16.19	5.15	18.51	4.51
CaO	0.04	0.01	0.07	0.01	0.76	0.13
Na2O	0.00	0.00	0.00	0.00	0.14	0.04
K2O	0.02	0.00	0.02	0.00	2.50	0.52
total	85.58	19.94	86.03	20.01	87.86	16.01

Rock No: X12W Catalogue No: 66,157
 Location: South Bay, Barmore. Limestone B
 Mineral Assemblage: CC-QZ-GROSS-CZO-TREM-KSP Code: F
 Petrography: no micas, grossular - clinozoisite reaction textures.

Mineral Analyses: 2 grossulars, 1 mix of grossular and clinozoisite, 1 Kfeldspar.

	EP10		EP30		EP40		AF10	
	wt%	O=13	wt%	O=13	wt%	O=13	wt%	O=32
SiO2	41.51	3.37	39.16	3.28	36.04	3.20	63.28	11.92
TiO2	1.54	0.09	0.15	0.01	1.83	0.12	0.00	0.00
Al2O3	20.20	1.93	20.89	2.06	16.47	1.72	18.33	4.07
FeO	0.63	0.04	0.91	0.06	2.35	0.17	0.10	0.01
MnO	0.01	0.00	0.00	0.00	0.07	0.00	0.00	0.00
MgO	0.01	0.00	0.00	0.00	1.75	0.23	0.02	0.00
CaO	35.51	3.09	36.21	3.25	34.52	3.29	0.29	0.05
Na2O	0.05	0.01	0.05	0.00	0.47	0.08	0.13	0.04
K2O	0.00	0.00	0.00	0.00	0.00	0.00	15.87	3.81
total	99.51	8.56	97.40	8.68	93.54	8.85	98.41	19.97

Rock No: CASS Catalogue No: 66,081
 Location: South Bay, Barmore. Limestone D.
 Mineral Assemblage: CC-QZ-CZO-TREM-KSP-BT Code: E
 Petrography: common alteration of tremolite to secondary chlorite, no grossular.

Mineral Analyses: 3 biotites, 3 clinzoisites, 1 calcite, 2 altered biotites, 20 amphiboles, 2 chlorites.

	BI100		BI101		BI102		EP990 (MU101)	
	wt%	O=23	wt%	O=23	wt%	O=23	wt%	O=22
SiO2	36.92	5.86	37.33	5.92	37.37	5.91	39.66	5.56
TiO2	0.06	0.10	0.93	0.11	0.82	0.09	0.18	0.02
Al2O3	17.03	3.18	16.88	3.15	16.96	3.16	27.13	4.48
FeO	16.06	2.13	15.77	2.09	15.78	2.09	8.23	0.96
MnO	0.01	0.00	0.00	0.00	0.01	0.00	0.03	0.00
MgO	13.65	3.23	13.30	3.14	13.34	3.15	2.31	0.48
CaO	0.15	0.02	0.15	0.02	0.30	0.05	17.06	2.56
Na2O	0.07	0.02	0.09	0.03	0.07	0.02	0.04	0.01
K2O	8.79	1.78	8.90	1.80	9.04	1.82	0.79	0.14
total	93.96	16.53	93.75	16.48	94.09	16.51	95.47	14.25

	EP100		EP101		CC99 (MU102)		MU103	
	wt%	O=13	wt%	O=13	wt%	O=22	wt%	O=22
SiO2	41.36	3.25	40.38	3.20	0.00	0.00	54.90	7.53
TiO2	0.01	0.00	0.00	0.00	0.00	0.00	0.05	0.00
Al2O3	31.54	2.92	31.51	2.94	0.01	0.00	17.37	2.81
FeO	1.50	0.10	1.70	0.11	0.86	0.24	5.03	0.57
MnO	0.00	0.00	0.00	0.00	0.14	0.04	0.00	0.00
MgO	0.02	0.00	0.03	0.00	0.66	0.33	6.60	1.35
CaO	23.83	2.00	24.17	2.05	59.98	21.37	0.25	0.03
Na2O	0.01	0.00	0.02	0.00	0.00	0.00	0.03	0.01
K2O	0.00	0.00	0.00	0.00	0.00	0.00	8.33	1.45
total	98.30	8.29	97.83	8.33	61.68	22.00	92.61	13.79

	MU105		AM100		AM101		AM310	
	wt%	O=22	wt%	O=23	wt%	O=23	wt%	O=23
SiO2	56.77	7.51	53.50	7.70	53.92	7.74	56.36	7.64
TiO2	0.03	0.00	0.00	0.00	0.00	0.00	0.07	0.00
Al2O3	20.89	3.26	3.29	0.56	4.61	0.78	5.08	0.85
FeO	3.54	0.39	9.91	1.19	9.92	1.19	10.15	1.21
MnO	0.00	0.00	0.00	0.00	0.00	0.00	0.06	0.00
MgO	5.09	1.00	16.59	3.56	15.30	3.27	15.22	3.23
CaO	0.69	0.09	12.42	1.91	11.03	1.70	12.13	1.85
Na2O	0.03	0.01	0.43	0.12	0.42	0.11	0.68	0.18
K2O	6.80	1.14	0.12	0.02	1.23	0.22	0.15	0.02
total	93.89	13.43	96.36	15.12	96.48	15.05	97.20	15.03

	AM311		AM320		AM330		AM340	
	wt%	O=23	wt%	O=23	wt%	O=23	wt%	O=23
SiO2	52.45	7.58	51.55	7.42	55.62	7.82	55.54	7.85
TiO2	0.04	0.00	0.09	0.01	0.01	0.00	0.00	0.00
Al2O3	4.63	0.79	6.44	1.09	2.92	0.48	2.64	0.44
FeO	10.56	1.27	11.57	1.39	8.55	1.00	9.73	1.15
MnO	0.04	0.00	0.07	0.01	0.15	0.01	0.09	0.01
MgO	15.72	3.38	14.35	3.07	17.45	3.65	16.76	3.53
CaO	12.03	1.86	12.12	1.87	12.36	1.86	12.27	1.86
Na2O	0.63	0.18	0.91	0.26	0.45	0.12	0.40	0.11
K2O	0.14	0.02	0.19	0.03	0.17	0.03	0.11	0.02
total	96.28	15.12	97.34	15.17	97.72	15.01	97.58	14.99

	AM361		AM362		AM370		AM371	
	wt%	O=23	wt%	O=23	wt%	O=23	wt%	O=23
SiO2	55.11	7.74	55.14	7.76	53.32	7.65	54.65	7.73
TiO2	0.00	0.00	0.01	0.00	0.02	0.00	0.01	0.00
Al2O3	3.55	0.59	3.29	0.54	3.98	0.67	3.62	0.60
FeO	9.01	1.06	8.94	1.05	9.56	1.14	9.68	1.14
MnO	0.16	0.02	0.13	0.01	0.16	0.02	0.13	0.01
MgO	17.19	3.60	17.37	3.64	16.45	3.52	16.71	3.52
CaO	12.23	1.84	12.25	1.84	12.26	1.88	12.17	1.84
Na2O	0.55	0.15	0.52	0.14	0.58	0.16	0.51	0.14
K2O	0.19	0.03	0.17	0.03	0.24	0.04	0.15	0.02
total	98.03	15.05	97.87	15.05	96.60	15.11	97.66	15.05

	AM372		AM3120		AM3130		AM3140	
	wt%	O=23	wt%	O=23	wt%	O=23	wt%	O=23
SiO2	53.52	7.61	53.07	7.59	46.55	7.29	53.27	7.65
TiO2	0.04	0.00	0.03	0.00	0.00	0.00	0.00	0.00
Al2O3	4.77	0.80	4.34	0.73	3.01	0.55	3.53	0.59
FeO	10.75	1.28	10.74	1.28	8.32	1.09	8.72	1.04
MnO	0.04	0.00	0.06	0.00	0.08	0.01	0.13	0.01
MgO	15.69	3.32	16.11	3.43	14.11	3.29	17.37	3.72
CaO	12.09	1.84	12.31	1.88	18.27	3.06	12.42	1.91
Na2O	0.69	0.19	0.60	0.16	0.34	0.10	0.55	0.15
K2O	0.16	0.03	0.15	0.02	0.64	0.13	0.17	0.03
total	97.78	15.09	97.43	15.14	91.35	15.55	96.21	15.14

	AM3141		AM3142		AM3143		AM3144	
	wt%	O=23	wt%	O=23	wt%	O=23	wt%	O=23
SiO2	53.30	7.68	53.32	7.66	53.69	7.71	53.88	7.74
TiO2	0.00	0.00	0.01	0.00	0.00	0.00	0.00	0.00
Al2O3	3.54	0.60	3.61	0.61	3.18	0.53	3.26	0.55
FeO	8.91	1.07	8.78	1.05	8.53	1.02	8.73	1.05
MnO	0.11	0.01	0.14	0.01	0.12	0.01	0.12	0.01
MgO	16.97	3.64	17.19	3.68	17.40	3.72	17.08	3.66
CaO	12.31	1.90	12.18	1.87	12.41	1.91	12.10	1.86
Na2O	0.58	0.16	0.59	0.16	0.50	0.14	0.52	0.14
K2O	0.22	0.04	0.26	0.05	0.22	0.04	0.22	0.04
total	95.97	15.12	96.12	15.13	96.09	15.11	95.94	15.07

	AM3145		CH3143		CH3144	
	wt%	O=23	wt%	O=28	wt%	O=28
SiO2	54.00	7.71	45.23	9.38	51.87	9.21
TiO2	0.00	0.00	0.07	0.01	0.08	0.01
Al2O3	3.28	0.55	12.79	3.12	15.17	3.17
FeO	8.72	1.04	8.21	1.42	11.37	1.69
MnO	0.13	0.01	0.04	0.00	0.10	0.01
MgO	17.52	3.73	6.37	1.97	8.13	2.15
CaO	12.28	1.88	0.97	0.21	1.41	0.27
Na2O	0.50	0.14	0.10	0.04	0.13	0.04
K2O	0.16	0.03	6.67	1.76	5.67	1.28
total	96.62	15.10	80.49	17.95	93.97	17.86

Rock No: X19N Catalogue No: 66,164
 Location: South Bay, Barmore. Limestone B.
 Mineral Assemblage: CC-QZ-CZO-KSP-MS-BT Code: D
 Petrography: quartz-rich, common kfeldspar, no amphibole.

Mineral Analyses: 2 muscovites, 2 biotites, 2 Kfeldspars, 1 albite.

	MU10		MU20		BI10		BI20	
	wt%	O=22	wt%	O=22	wt%	O=23	wt%	O=23
SiO2	51.01	6.85	52.06	6.96	39.90	6.16	40.00	6.17
TiO2	0.07	0.00	0.09	0.01	0.48	0.05	0.42	0.04
Al2O3	26.91	4.26	25.75	4.05	14.84	2.70	14.78	2.69
FeO	1.91	0.21	2.38	0.26	11.53	1.49	12.15	1.57
MnO	0.00	0.00	0.01	0.00	0.01	0.00	0.02	0.00
MgO	3.49	0.70	3.67	0.73	17.74	4.08	17.39	4.00
CaO	0.17	0.02	0.37	0.05	0.14	0.02	0.15	0.02
Na2O	0.11	0.02	0.07	0.02	0.05	0.01	0.03	0.01
K2O	10.70	1.83	10.64	1.81	9.11	1.79	9.20	1.81
total	94.39	13.93	95.09	13.92	94.80	16.81	95.28	16.88

	AF10		AF20		PL10	
	wt%	O=32	wt%	O=32	wt%	O=32
SiO2	65.85	12.04	65.92	12.02	69.69	12.04
TiO2	0.00	0.00	0.00	0.00	0.01	0.00
Al2O3	18.31	3.94	18.48	3.97	19.34	3.94
FeO	0.07	0.01	0.11	0.01	0.00	0.00
MnO	0.00	0.00	0.00	0.00	0.00	0.00
MgO	0.02	0.00	0.02	0.00	0.00	0.00
CaO	0.06	0.01	0.05	0.01	0.00	0.00
Na2O	0.54	0.19	0.51	0.18	11.86	3.97
K2O	15.91	3.71	15.82	3.68	0.07	0.01
total	100.9	19.94	101.1	19.92	101.0	19.98

Rock No: X6NA Catalogue No: 66,152
 Location: South Bay, Barmore. Limestone B.
 Mineral Assemblage: CC-QZ-CZO-TREM-KSP-MS-BT Code: D and E
 Petrography: no grossular, two assemblages present with no obvious reaction boundary.

Mineral Analyses: 3 muscovites, 1 clinzoisite, 1 amphibole.

	MU10		MU20		MU30		EP10	
	wt%	O=22	wt%	O=22	wt%	O=22	wt%	O=13
SiO2	50.40	6.77	49.01	6.63	50.37	6.75	39.71	3.18
TiO2	0.19	0.02	0.27	0.02	0.08	0.00	0.01	0.00
Al2O3	27.79	4.40	28.90	4.60	28.00	4.43	31.57	2.98
FeO	1.83	0.20	1.85	0.21	1.82	0.20	1.50	0.10
MnO	0.00	0.00	0.00	0.00	0.00	0.00	0.00	0.00
MgO	3.31	0.66	3.17	0.64	3.42	0.68	0.01	0.00
CaO	0.00	0.00	0.04	0.00	0.01	0.00	23.84	2.04
Na2O	0.17	0.04	0.22	0.06	0.16	0.04	0.03	0.00
K2O	10.58	1.81	10.26	1.77	10.60	1.81	0.00	0.00
total	94.30	13.93	93.76	13.95	94.50	13.95	96.70	8.33

	AM10	
	wt%	O=23
SiO2	55.02	7.83
TiO2	0.06	0.00
Al2O3	1.94	0.32
FeO	8.49	1.01
MnO	0.14	0.01
MgO	18.05	3.83
CaO	12.55	1.91
Na2O	0.35	0.09
K2O	0.08	0.01
total	96.89	15.13

Rock No: CA74 Catalogue No: 66,067
 Location: South Bay, Barmore. Limestone B.
 Mineral Assemblage: CC-QZ-CZO-TREM-KSP-BT Code: E
 Petrography: common clinozoisite, biotite - amphibole reaction textures.

Mineral Analyses: 3 biotites, 8 clinozoisites, 6 calcites, 12 amphiboles, 2 chlorites.

	BI120		BI130		BI131		EP120	
	wt%	O=23	wt%	O=23	wt%	=230	wt%	O=13
SiO2	34.56	5.80	35.15	5.83	34.58	5.74	37.98	3.20
TiO2	1.22	0.15	1.28	0.16	1.27	0.16	0.13	0.00
Al2O3	16.48	3.26	16.38	3.20	16.75	3.28	26.39	2.62
FeO	18.64	2.62	18.76	2.60	19.06	2.64	6.75	0.47
MnO	0.15	0.02	0.12	0.01	0.14	0.02	0.08	0.00
MgO	10.31	2.58	10.58	2.61	10.56	2.61	0.03	0.00
CaO	0.00	0.00	0.12	0.02	0.06	0.01	23.72	2.14
Na2O	0.07	0.02	0.19	0.06	0.10	0.03	0.02	0.00
K2O	8.74	1.87	8.71	1.84	8.98	1.90	0.00	0.00
total	90.50	16.51	91.58	16.49	91.87	16.60	95.14	8.48

	EP130		EP140		EP161		EP162	
	wt%	O=13	wt%	O=13	wt%	O=13	wt%	O=13
SiO2	37.11	3.18	39.11	3.23	38.58	3.21	35.98	3.14
TiO2	0.07	0.00	0.07	0.00	0.09	0.00	0.05	0.00
Al2O3	25.61	2.59	27.62	2.69	27.11	2.66	23.39	2.41
FeO	7.66	0.55	5.86	0.40	6.10	0.42	11.07	0.81
MnO	0.18	0.01	0.08	0.00	0.11	0.00	0.12	0.00
MgO	0.04	0.00	0.03	0.00	0.51	0.06	4.77	0.62
CaO	23.54	2.16	22.85	2.02	23.33	2.08	17.56	1.64
Na2O	0.01	0.00	0.55	0.08	0.01	0.00	0.07	0.01
K2O	0.00	0.00	0.00	0.00	0.00	0.00	0.00	0.00
total	94.25	8.52	96.21	8.46	95.87	8.45	93.04	8.65

	EP170		EP171		EP200	
	wt%	O=13	wt%	O=13	wt%	O=13
SiO2	36.28	3.07	36.91	3.13	38.83	3.24
TiO2	0.09	0.00	0.09	0.00	0.08	0.00
Al2O3	28.22	2.82	27.13	2.71	26.57	2.61
FeO	5.78	0.41	6.45	0.45	6.71	0.46
MnO	0.09	0.00	0.13	0.01	0.08	0.00
MgO	0.04	0.00	0.11	0.01	0.04	0.00
CaO	23.94	2.17	23.70	2.15	23.52	2.10
Na2O	0.01	0.00	0.01	0.00	0.01	0.00
K2O	0.00	0.00	0.00	0.00	0.00	0.00
total	94.48	8.51	94.57	8.50	95.87	8.45

	CC101		CC110		CC200		CC210	
	wt%	O=3	wt%	O=3	wt%	O=3	wt%	O=3
SiO2	0.02	0.00	5.45	0.24	0.01	0.00	0.01	0.00
TiO2	0.00	0.00	0.00	0.00	0.00	0.00	0.00	0.00
Al2O3	0.00	0.00	0.00	0.00	0.00	0.00	0.00	0.00
FeO	1.37	0.05	4.82	0.17	0.93	0.03	1.18	0.05
MnO	0.38	0.01	0.10	0.00	0.23	0.01	0.22	0.01
MgO	0.69	0.05	1.89	0.12	0.51	0.03	0.60	0.04
CaO	55.02	2.87	46.39	2.20	55.12	2.90	53.71	2.89
Na2O	0.00	0.00	0.00	0.00	0.00	0.00	0.00	0.00
K2O	0.00	0.00	0.00	0.00	0.00	0.00	0.00	0.00
total	57.68	3.00	58.74	2.76	57.08	3.00	55.92	3.00

	CC220		CC230		AM200		AM210	
	wt%	O=3	wt%	O=3	wt%	O=23	wt%	O=23
SiO2	0.04	0.00	0.00	0.00	40.50	6.79	47.48	7.27
TiO2	0.00	0.00	0.00	0.00	0.18	0.02	0.09	0.01
Al2O3	0.00	0.00	0.00	0.00	6.95	1.37	6.88	1.24
FeO	1.12	0.04	1.00	0.04	15.80	2.21	15.92	2.04
MnO	0.20	0.00	0.20	0.00	0.27	0.04	0.12	0.01
MgO	0.58	0.04	0.51	0.03	8.76	2.19	11.10	2.53
CaO	53.51	2.88	53.48	2.90	14.70	2.64	10.59	1.74
Na2O	0.00	0.00	0.00	0.00	1.13	0.37	1.13	0.33
K2O	0.00	0.00	0.00	0.00	0.28	0.06	0.57	0.11
total	55.76	3.00	55.54	3.00	88.63	15.71	93.92	15.32

	AM220		AM240		AM250		AM270	
	wt%	O=23	wt%	O=23	wt%	O=23	wt%	O=23
SiO2	46.57	7.28	46.68	7.19	47.56	7.33	44.82	7.31
TiO2	0.09	0.01	0.12	0.01	0.07	0.01	0.06	0.00
Al2O3	6.32	1.16	7.99	1.45	7.49	1.36	9.04	1.74
FeO	17.15	2.24	18.49	2.38	16.42	2.11	13.70	1.87
MnO	0.20	0.02	0.11	0.01	0.07	0.00	0.10	0.01
MgO	10.23	2.38	9.58	2.20	10.68	2.45	7.67	1.86
CaO	10.58	1.77	9.38	1.55	8.86	1.46	9.08	1.58
Na2O	1.21	0.36	1.31	0.39	0.87	0.26	0.56	0.17
K2O	0.33	0.06	0.56	0.11	0.88	0.17	2.95	0.61
total	92.71	15.33	94.25	15.32	92.93	15.19	88.02	15.20

	AM280		AM290		Am2110		AM2160	
	wt%	O=23	wt%	O=23	wt%	O=23	wt%	O=23
SiO2	48.81	7.55	46.09	7.19	43.01	6.91	46.86	7.32
TiO2	0.07	0.01	0.12	0.01	0.03	0.00	0.07	0.00
Al2O3	11.24	2.05	6.89	1.26	9.25	1.75	5.94	1.09
FeO	12.35	1.59	17.30	2.25	16.55	2.22	16.63	2.17
MnO	0.05	0.00	0.12	0.01	0.08	0.01	0.10	0.01
MgO	7.28	1.68	11.06	2.57	12.12	2.90	10.94	2.54
CaO	5.99	0.99	9.94	1.66	7.15	1.23	10.51	1.76
Na2O	0.45	0.13	0.94	0.28	0.61	0.19	1.14	0.34
K2O	4.59	0.90	0.24	0.04	0.73	0.15	0.26	0.05
total	90.87	14.93	92.74	15.32	89.57	15.38	92.48	15.32

	AM2170		AM2180		CH200		CH220	
	wt%	O=23	wt%	O=23	wt%	O=28	wt%	O=28
SiO2	50.64	7.61	49.49	7.52	32.31	6.88	31.11	6.75
TiO2	0.03	0.00	0.05	0.00	0.05	0.00	0.07	0.01
Al2O3	4.11	0.73	4.41	0.79	13.88	3.48	13.54	3.46
FeO	15.03	1.88	15.61	1.98	19.26	3.43	19.45	3.53
MnO	0.09	0.01	0.10	0.01	0.08	0.01	0.08	0.01
MgO	12.81	2.87	12.11	2.74	16.93	5.37	17.31	5.60
CaO	11.03	1.77	11.64	1.89	0.28	0.06	0.18	0.04
Na2O	0.77	0.22	0.60	0.18	0.13	0.05	0.19	0.08
K2O	0.15	0.03	0.16	0.03	0.48	0.13	0.17	0.05
total	94.70	15.15	94.23	15.18	83.43	19.46	82.15	19.56

Rock No: CA62 Catalogue No: 66,057
 Location: South Bay, Barmore. Limestone A.
 Mineral Assemblage: CC-QZ-CZO-TREM-KSP-BT Code: E
 Petrography: quartz-rich, patchy calcite, common amphibole to chlorite
 reaction textures.

Mineral Analyses: 6 clinzoisites, 2 chlorites, 2 biotites, 1 amphibole.

	EP120		EP210		EP310		EP410	
	wt%	O=25	wt%	O=25	wt%	O=25	wt%	O=25
SiO2	43.25	6.66	39.36	6.05	38.88	6.05	63.76	9.03
TiO2	0.00	0.00	0.00	0.00	0.00	0.00	0.00	0.00
Al2O3	30.38	5.52	31.76	5.76	31.71	5.81	19.19	3.20
FeO	1.97	0.25	1.82	0.23	1.48	0.19	0.98	0.11
MnO	0.00	0.00	0.00	0.00	0.00	0.00	0.00	0.00
MgO	0.37	0.08	0.00	0.00	0.00	0.00	0.00	0.00
CaO	18.42	3.04	24.27	4.00	23.82	3.97	13.21	2.00
Na2O	0.00	0.00	0.00	0.00	0.00	0.00	0.00	0.00
K2O	0.00	0.00	0.00	0.00	0.00	0.00	0.00	0.00
total	94.41	15.57	97.23	16.06	95.91	16.04	97.15	14.36

	EP510		EP610		CH510		CH610	
	wt%	Q=25	wt%	Q=25	wt%	Q=28	wt%	Q=28
SiO2	39.53	6.05	39.41	6.01	35.85	7.17	44.30	8.13
TiO2	0.00	0.00	0.00	0.00	0.00	0.00	0.00	0.00
Al2O3	32.30	5.83	32.30	5.81	14.62	3.45	28.42	6.15
FeO	1.23	0.15	1.52	0.19	17.65	2.95	6.14	0.94
MnO	0.00	0.00	0.00	0.00	0.00	0.00	0.00	0.00
MgO	0.00	0.00	0.00	0.00	18.52	5.52	5.70	1.56
CaO	24.18	3.96	24.86	4.06	0.00	0.00	0.00	0.00
Na2O	0.00	0.00	0.00	0.00	0.00	0.00	0.00	0.00
K2O	0.00	0.00	0.00	0.00	0.00	0.00	0.00	0.00
total	97.39	16.02	98.11	16.08	86.66	19.10	84.57	16.79

	BI610		BI710		AM10 (UN6)	
	wt%	Q=23	wt%	Q=23	wt%	Q=1
SiO2	50.33	7.54	57.54	8.09	36.53	0.25
TiO2	0.00	0.00	0.15	0.01	0.29	0.00
Al2O3	15.69	2.77	17.02	2.82	16.68	0.13
FeO	10.37	1.30	4.83	0.57	20.57	0.12
MnO	0.00	0.00	0.00	0.00	0.00	0.00
MgO	6.54	1.46	3.34	0.70	13.49	0.14
CaO	0.82	0.13	1.95	0.29	0.68	0.00
Na2O	0.00	0.00	0.00	0.00	0.00	0.00
K2O	9.12	1.74	11.03	1.97	0.79	0.00
total	93.01	14.98	95.89	14.47	89.05	0.68

Rock No: CA21 Catalogue No: 66,020
 Location: South Bay, Barmore. Albite schist (see Fig 2.12)
 Mineral assemblage: QZ-CC-GT-MS-BT-CHL Code: pelite
 Petrography: Q- and M- zones (see section 2.4.2)

Mineral analyses: 1 muscovite, 5 albites, 4 Kfeldspars, 2 garnets, 2 biotites.

	MU10		PL100		PL101		PL200	
	wt%	Q=22	wt%	Q=32	wt%	Q=32	wt%	Q=32
SiO2	48.53	6.61	70.76	12.01	68.19	11.92	67.68	11.95
TiO2	0.33	0.03	0.00	0.00	0.00	0.00	0.00	0.00
Al2O3	28.75	4.61	20.07	4.01	19.75	4.07	19.44	4.04
FeO	3.64	0.41	0.00	0.00	0.03	0.00	0.01	0.00
MnO	0.00	0.00	0.00	0.00	0.00	0.00	0.00	0.00
MgO	2.12	0.43	0.00	0.00	0.00	0.00	0.01	0.00
CaO	0.00	0.00	0.37	0.06	0.65	0.12	0.13	0.02
Na2O	0.43	0.11	11.33	3.73	11.32	3.83	11.57	3.96
K2O	10.15	1.76	0.06	0.01	0.07	0.01	0.05	0.01
total	93.98	13.99	102.6	19.85	100.0	19.97	98.91	20.01

	PL201		PL202		AF100		AF101	
	wt%	O=32	wt%	O=32	wt%	O=32	wt%	O=32
SiO2	68.17	11.97	67.57	11.87	63.72	12.01	63.66	11.95
TiO2	0.00	0.00	0.00	0.00	0.00	0.00	0.00	0.00
Al2O3	19.37	4.01	19.82	4.10	17.83	3.96	18.03	3.99
FeO	0.00	0.00	0.03	0.00	0.03	0.00	0.65	0.10
MnO	0.00	0.00	0.00	0.00	0.00	0.00	0.00	0.00
MgO	0.00	0.00	0.01	0.00	0.01	0.00	0.01	0.00
CaO	0.12	0.02	0.75	0.14	0.00	0.00	0.00	0.00
Na2O	11.68	3.98	11.27	3.84	0.03	0.01	0.31	0.11
K2O	0.05	0.01	0.08	0.02	16.59	3.99	16.20	3.88
total	99.42	20.01	99.56	20.00	98.28	20.00	98.91	20.05

	AF200		AF210		GT200		GT400	
	wt%	O=32	wt%	O=32	wt%	O=24	wt%	O=24
SiO2	62.93	11.93	63.34	11.95	37.20	5.98	36.80	5.94
TiO2	0.00	0.00	0.00	0.00	0.09	0.01	0.10	0.01
Al2O3	18.13	4.05	18.14	4.03	21.11	4.00	21.13	4.02
FeO	0.09	0.01	0.06	0.01	32.69	4.39	31.89	4.30
MnO	0.00	0.00	0.00	0.00	1.68	0.22	3.02	0.41
MgO	0.01	0.00	0.01	0.00	0.95	0.22	0.88	0.21
CaO	0.00	0.00	0.00	0.00	6.67	1.15	6.48	1.12
Na2O	0.07	0.02	0.04	0.01	0.00	0.00	0.00	0.00
K2O	16.70	4.04	16.69	4.02	0.00	0.00	0.00	0.00
total	98.00	20.08	98.35	20.04	100.4	16.00	100.3	16.03

	BI300		BI400	
	wt%	O=23	wt%	O=23
SiO2	34.99	5.75	34.40	5.68
TiO2	1.91	0.23	1.67	0.20
Al2O3	17.35	3.36	17.62	3.43
FeO	23.23	3.19	23.97	3.31
MnO	0.14	0.02	0.16	0.02
MgO	7.38	1.81	7.38	1.81
CaO	0.00	0.00	0.01	0.00
Na2O	0.11	0.03	0.08	0.02
K2O	8.80	1.84	8.53	1.79
total	93.93	16.27	93.86	16.31

Rock No: CA22 Catalogue No: 66,021
 Location: South Bay, Barmore. Albite schist
 Mineral Assemblage: QZ-CC-GT-MS-BT-CHL Code: pelite
 Petrography: Q- and M- zones

Mineral Analyses: 2 garnets, 3 chlorites, 4 biotites, 2 muscovites, 4 Kfeldspars, 1 plagioclase.

	GT10		GT11		CH10		CH20	
	wt%	O=24	wt%	O=24	wt%	O=28	wt%	O=1
SiO2	37.85	6.04	38.24	6.01	20.71	5.39	30.01	0.22
TiO2	0.00	0.00	0.27	0.03	0.00	0.00	0.00	0.00
Al2O3	21.10	3.97	21.18	3.92	17.84	5.48	24.22	0.21
FeO	33.00	4.41	31.03	4.08	27.88	6.07	24.25	0.15
MnO	0.89	0.12	2.86	0.38	0.18	4.00	0.20	0.00
MgO	0.77	0.18	0.58	0.13	7.39	2.87	7.98	0.08
CaO	7.18	1.23	8.40	1.41	0.00	0.00	0.00	0.00
Na2O	0.00	0.00	0.00	0.00	0.00	0.00	0.00	0.00
K2O	0.00	0.00	0.00	0.00	0.00	0.00	0.00	0.00
total	100.8	15.97	102.5	15.99	74.03	19.86	86.68	0.67

	CH40		BI10		BI11		BI20	
	wt%	O=28	wt%	O=23	wt%	O=23	wt%	O=23
SiO2	23.58	5.20	33.25	5.52	37.10	5.86	36.27	5.80
TiO2	0.00	0.00	0.89	0.11	1.93	0.23	2.17	0.26
Al2O3	21.44	5.58	18.72	3.67	17.53	3.26	17.88	3.37
FeO	30.81	5.68	26.38	3.66	23.91	3.16	24.15	3.23
MnO	0.32	0.06	0.19	0.02	0.17	0.02	0.00	0.00
MgO	10.53	3.46	7.43	1.84	7.60	1.79	7.08	1.68
CaO	0.00	0.00	0.00	0.00	0.00	0.00	0.00	0.00
Na2O	0.00	0.00	0.00	0.00	0.00	0.00	0.00	0.00
K2O	0.00	0.00	6.38	1.35	9.21	1.85	8.86	1.80
total	86.70	20.00	93.33	16.22	97.47	16.20	96.44	16.16

	BI40		MU10		MU40		AF10	
	wt%	O=23	wt%	O=22	wt%	O=22	wt%	O=1
SiO2	35.49	5.78	47.01	6.35	46.96	6.37	65.26	0.37
TiO2	2.04	0.25	0.58	0.06	0.57	0.05	0.00	0.00
Al2O3	17.53	3.37	32.20	5.13	31.61	5.05	17.86	0.12
FeO	23.66	3.22	2.61	0.29	2.85	0.32	0.27	0.00
MnO	0.16	0.02	0.00	0.00	0.00	0.00	0.00	0.00
MgO	6.92	1.68	1.21	0.24	1.30	0.26	0.00	0.00
CaO	0.00	0.00	0.00	0.00	0.08	0.01	0.00	0.00
Na2O	0.00	0.00	0.53	0.14	0.65	0.17	0.00	0.00
K2O	9.00	1.87	9.92	1.71	10.11	1.75	16.53	0.12
total	94.84	16.20	94.10	13.94	94.14	14.01	99.94	0.62

	AF11		AF20 (UN1A)		AF30 (UN1C)		PL10	
	wt%	O=32	wt%	O=1	wt%	O=1	wt%	O=32
SiO2	65.62	12.05	65.34	0.37	65.85	0.37	68.42	11.96
TiO2	0.00	0.00	0.00	0.00	0.00	0.00	0.00	0.00
Al2O3	18.15	3.93	18.01	0.12	18.27	0.12	19.69	4.05
FeO	0.00	0.00	0.00	0.00	0.00	0.00	0.00	0.00
MnO	0.00	0.00	0.00	0.00	0.00	0.00	0.00	0.00
MgO	0.00	0.00	0.00	0.00	0.00	0.00	0.00	0.00
CaO	0.13	0.02	0.00	0.00	0.00	0.00	0.33	0.06
Na2O	0.00	0.00	0.00	0.00	0.00	0.00	11.34	3.84
K2O	16.78	3.93	16.57	0.12	16.60	0.12	0.00	0.00
total	100.7	19.95	99.94	0.62	100.7	0.62	99.80	19.93

Rock No: CA41 Catalogue No: 66,039
 Location: South Bay, Barmore. Albite schist
 Mineral Assemblage: QZ-CC-GT-MS-BT-CHL Code: psammite
 Petrography: no Q- and M- zones (see section 2.4.2)

Mineral Analyses: 2 garnets, 3 chlorites, 3 biotites.

	GT21		GT22		CH31		CH32	
	wt%	O=1	wt%	O=1	wt%	O=28	wt%	O=28
SiO2	38.25	0.25	38.26	0.25	25.20	5.35	25.27	5.38
TiO2	0.29	0.00	0.00	0.00	0.00	0.00	0.00	0.00
Al2O3	21.07	0.16	21.06	0.16	21.44	5.36	21.05	5.29
FeO	24.42	0.13	26.41	0.14	28.33	5.03	28.00	4.99
MnO	6.46	0.03	4.32	0.02	0.27	0.05	0.26	0.04
MgO	0.66	0.00	0.72	0.00	13.15	4.16	13.38	4.25
CaO	10.31	0.07	10.21	0.07	0.00	0.00	0.00	0.00
Na2O	0.00	0.00	0.00	0.00	0.00	0.00	0.00	0.00
K2O	0.00	0.00	0.00	0.00	0.00	0.00	0.00	0.00
total	101.4	0.67	101.0	0.67	88.41	19.96	87.99	19.97

	CH41		BI21		BI31		BI41	
	wt%	O=28	wt%	O=23	wt%	O=23	wt%	O=23
SiO2	24.92	5.32	36.96	5.89	36.81	5.84	36.67	5.84
TiO2	0.00	0.00	1.47	0.17	1.66	0.19	1.73	0.20
Al2O3	21.59	5.44	17.21	3.23	17.57	3.28	17.17	3.22
FeO	27.92	4.99	21.80	2.91	21.91	2.90	21.53	2.87
MnO	0.12	0.02	0.13	0.01	0.00	0.00	0.17	0.02
MgO	13.08	4.16	8.90	2.11	8.99	2.12	9.23	2.19
CaO	0.00	0.00	0.00	0.00	0.00	0.00	0.00	0.00
Na2O	0.00	0.00	0.00	0.00	0.00	0.00	0.00	0.00
K2O	0.00	0.00	9.31	1.89	9.44	1.91	9.53	1.93
total	87.64	19.95	95.86	16.27	96.40	16.27	96.05	16.30